

JAN 1992
87134

TITLE PAGE

CRANFIELD INSTITUTE OF TECHNOLOGY

SCHOOL OF AERONAUTICAL ENGINEERING

PhD

Academic Years 1989 - 1992

N P RICHARDS

Integration of Global Positioning and
Inertial Reference System data inside a
Flight Management Computer

Supervisor:

P THOMASSON

January 1992

ProQuest Number: 10820952

All rights reserved

INFORMATION TO ALL USERS

The quality of this reproduction is dependent upon the quality of the copy submitted.

In the unlikely event that the author did not send a complete manuscript and there are missing pages, these will be noted. Also, if material had to be removed, a note will indicate the deletion.



ProQuest 10820952

Published by ProQuest LLC (2019). Copyright of the Dissertation is held by Cranfield University.

All rights reserved.

This work is protected against unauthorized copying under Title 17, United States Code
Microform Edition © ProQuest LLC.

ProQuest LLC.
789 East Eisenhower Parkway
P.O. Box 1346
Ann Arbor, MI 48106 – 1346

ACKNOWLEDGMENTS

Firstly, I wish to thank Smiths Industries for allowing the work presented in this thesis to be submitted.

Secondly, I want to acknowledge the valuable time and considerable effort provided by Professor Mike Sanderson, Mr Pete Thomasson and Dr Tony Millman of the Cranfield Institute of Technology, and Dr Jim Meredith of Smiths Industries, who made up the Total Technology panel.

I am also extremely grateful for the valuable assistance given to me by many of my Smiths colleagues during the course of the work, particularly Mr Roy Griffin, Mr Tony Dymock and Mr John Ward.

Lastly, I want to thank my wife Norma and two children Luke and Steffan for their considerable patience and understanding during the course of the work.

ABSTRACT

A Kalman filter is used to integrate the outputs from a Global Positioning System and an Inertial Reference System inside a Flight Management Computer.

To initialise the Kalman filter, account is taken of the IRS errors that get set up during alignment.

Algorithms are developed that allow the Kalman filter to be initialised to several IRS specific alignment conditions.

CONTENTS

CHAPTER 1

INTRODUCTION

1.1	THESIS OVERVIEW	1
1.2	LITERATURE SURVEY	2
1.3	CHAPTER SUMMARY	10

CHAPTER 2

INERTIAL REFERENCE SYSTEM

2.1	INTRODUCTION	13
2.2	INERTIAL REFERENCE SYSTEM DESCRIPTION	17
2.3	GENERAL IRS ERROR MODEL EQUATIONS	24
2.4	IRS SPECIFIC POSITION AND ATTITUDE ERROR EQUATIONS	35
2.5	IRS VELOCITY EQUATIONS	39
2.6	GENERAL IRS VELOCITY ERROR EQUATION	43
2.7	IRS SPECIFIC VELOCITY ERROR EQUATION	46
2.8	BARO INERTIAL LOOP	49
2.9	INERTIAL REFERENCE SYSTEM SENSORS	52
2.10	COMMENTS	53

CHAPTER 3

GLOBAL POSITIONING SYSTEM

3.1	INTRODUCTION	54
3.2	BASIC GPS RECEIVER OPERATION	55
3.3	ROCKWELL COLLINS GPS RECEIVER	59
3.4	COMMENTS	59

CHAPTER 4

KALMAN FILTER

4.1	INTRODUCTION	60
4.2	KALMAN FILTER THEORY	61
4.3	SELECTING THE KALMAN FILTER STATE MODEL	63
4.4	TRANSITION MATRIX EQUATION	66
4.5	KALMAN FILTER MEASUREMENT PROCESSING	71
4.6	DEVELOPMENT OF THE KALMAN FILTER INSTRUMENT ERROR MODELS	74
4.7	COMMENTS	80

CHAPTER 5

SIMULATION PROGRAM

5.1	INTRODUCTION	81
5.2	SIMULATION ACCURACY	83
5.3	EXECUTIVE MODULE	83
5.4	RWORLD MODULE	84
5.5	INERTIAL REFERENCE SYSTEM MODULE	93
5.6	GLOBAL POSITIONING SYSTEM MODULE	98
5.7	KALMAN FILTER MODULE	100
5.8	CDU MODULE	103
5.9	FIX MODULE	104
5.10	REMAINING MODULES	104

CHAPTER 6

METHODS TO EVALUATE NAVIGATION SYSTEM PERFORMANCE

6.1	INTRODUCTION	105
6.2	95% CIRCULAR ERROR	106
6.3	CIRCULAR ERROR PROBABILITY	107
6.4	DISTANCE ROOT MEAN SQUARED ERROR	107
6.5	NAVIGATION PERFORMANCE ANALYSIS TECHNIQUES	108
6.6	COMPARISON OF RESULTS	114
6.7	COMMENTS	116

CHAPTER 7

INVESTIGATION INTO KALMAN FILTER PERFORMANCE

7.1	INTRODUCTION	117
7.2	INVESTIGATION INTO THE KALMAN FILTER TESTING METHOD	122
7.3	VERIFICATION OF THE KALMAN FILTER TESTING METHOD	123
7.4	A SECOND INVESTIGATION INTO KALMAN FILTER PERFORMANCE	125
7.5	INVESTIGATION INTO DIFFERENT PERIODS OF GPS COVERAGE	127
7.6	COMMENTS	133

CHAPTER 8

KALMAN FILTER MODIFICATION TECHNIQUES

8.1	INTRODUCTION	134
8.2	INERTIAL REFERENCE SYSTEM ALIGNMENT DESCRIPTION	135
8.3	MATCHING THE KALMAN FILTER TO THE ALIGNMENT CONDITION	142
8.4	KALMAN FILTER MATCHING WITH THE Z GYRO BIAS	151
8.5	COMPARISON OF RESULTS FOR A MATCHED AND UNMATCHED KF	155
8.6	DEVELOPMENT OF A GENERAL KALMAN FILTER MATCHING ALGORITHM	159
8.7	FURTHER INVESTIGATION WORK	168

CHAPTER 9

MARKET ANALYSIS

9.1	INTRODUCTION	182
9.2	SMITHS INDUSTRIES	183
9.3	KEY COMPETITORS	184
9.4	KEY CUSTOMERS	187
9.5	MARKET ANALYSIS	187
9.6	SCENARIO ANALYSIS	192
9.7	SUMMARY	197
9.8	COMMENT	197

CHAPTER 10

CONCLUSIONS

10.1	TECHNICAL WORK	198
10.2	NON TECHNICAL WORK	200

BIBLIOGRAPHY	201
---------------------	------------

APPENDIX A	206
-------------------	------------

APPENDIX B	220
-------------------	------------

APPENDIX C	221
-------------------	------------

APPENDIX D	222
-------------------	------------

TABLES	223
---------------	------------

FIGURES	228
----------------	------------

TABLES

4-1	Kalman Filter Initialisation Parameters	223
9-1	Large Commercial Aircraft Production Figures	224
9-2	Medium Commercial Aircraft Production Figures	225
9-3	Distribution of FMC and IRS Equipment	226
9-4	Estimated Market Share	227
9-5	IRS/FMC Combinations	227
9-6	Options For Future Sales	227

FIGURES

2-1	Strapdown Inertial Reference system block diagram	228
2-2	Relationship between coordinate systems	229
2-3	Relationship between body axis and wander azimuth axis	230
2-4	Baro inertial loop	231
2-5	Baro inertial loop error model	232
2-6	IRS error model system matrix	233
3-1	Global Positioning System	234
4-1	Kalman Filter block diagram	235
4-2	Kalman Filter system matrix	236
4-3	Optimal v sub optimal IRS state vector	237
4-4	Kalman filter state estimates for a KF iteration time of 30 seconds	238
4-5	Kalman filter state estimates for a KF iteration time of 5 seconds	239
4-6	Accelerometer noise power spectral density plot	240
5-1	Simulation program modules	241
5-2	Simulation program executive calling routines	242
5-3a	Level flight	243
5-3b	Non level flight	243
5-4	Quaternion representation of position	244
5-5a	Single sided power spectral density plot	245
5-5b	Gyro random walk simulation module	245
5-6	Correlated noise models	246
5-7	Accel correlated noise simulation model	247
5-8	Kalman filter implementation	248
6-1	Bivariate normal distribution	249
6-2	Flight profile 1	250
6-3	Monte Carlo simulation result for latitude	251
6-4	Monte Carlo simulation result for longitude	252
6-5	Method to combine results for sensitivity analysis	253
6-6	Method to combine results for covariance analysis	254
6-7	Comparison of results for the irs error state dthx	255
6-8	Comparison of results for the irs error state dthy	256
6-9	Sensitivity analysis v covariance analysis for the irs y gyro bias error source	257
6-10	Sensitivity analysis v covariance analysis for the irs z gyro bias error source	258
6-11	Method to compare sensitivity analysis and covariance analysis results for time series errors only	259

7-1	Overlay of irs latitude errors	260
7-2	Overlay of kalman filter latitude errors	261
7-3	Monte Carlo v sensitivity analysis for for Kalman filter latitude error	262
7-4	Monte Carlo v sensitivity analysis for for Kalman filter longitude error	263
7-5	Flight profile 2	264
7-6	KF covariance plots for different periods of GPS coverage	265
7-7	Overlay of IRS latitude errors	266
7-8	Overlay of Kalman filter latitude errors 42 minute case	267
7-9	Overlay of Kalman filter latitude errors 60 minute case	268
7-10	Overlay of Kalman filter latitude errors 3 hour case	269
7-11	Contribution of random constants to overall latitude error 42 minute case	270
7-12	Contribution of random constants to overall latitude error 60 minute case	271
8-1	Extended alignment axis set	272
8-2	Single channel inertial system gyro model	273
8-3	Comparison of IRS error sources	274
8-4	Z platform axis tilt affect on local level axis	275
8-5	Sub optimal Kalman filter covariance plots	276
8-6	Optimal IRS v sub optimal KF result	277
8-7	Sub optimal Kalman filter covariance plots	278
8-8	Sub optimal Kalman filter covariance plots	279
8-9	Optimal IRS v sub optimal Kalman filter	280
8-10	Sub optimal Kalman filter covariance plots	281
8-11	Optimal IRS v sub optimal Kalman filter	282
8-12	Optimal IRS v sub optimal Kalman filter	283
8-13	Optimal IRS v sub optimal Kalman filter	284
8-14	Comparison of Kalman filter covariance plots	285
8-15	A Seattle based flight profile	286
8-16	Comparison of IRS radial error v Kalman filter prediction of radial error	287
8-17	Comparison of IRS and KF radial errors for matched and unmatched Kalman filters	288
8-18	Comparison of KF radial errors for matched and unmatched Kalman filters	289
8-19	Sub optimal Kalman filter covariance plots	290
8-20	Sub optimal Kalman filter covariance plots	291
8-21	Accelerometer single channel inertial system model	292
8-22	Comparison of IRS error sources	293
8-23	Comparison of IRS error sources	294
8-24	Y channel inertial system model	295
8-25	Sub optimal Kalman filter covariance plots	296
8-26	Optimal IRS v sub optimal Kalman filter	297

NOTATION

A list of principal symbols used within the thesis is given and is intended to supplement the definitions given within the text.

\underline{a}	Measured accelerometer output
C_p^b	Platform axis to body axis direction cosine matrix
C_p^c	Platform axis to earth axis direction cosine matrix
$C_{x,y}$	Direction cosine elements where $x,y = 1,2,3$
C_b	GPS receiver clock bias error
e^2	Earth eccentricity
F	Continuous time system matrix
g	Gravity vector
g_m	Mass attraction gravity vector
h	Inertial altitude
h_{ref}	Air Data Computer indicated altitude
\underline{H}_k	Kalman filter measurement vector
K_k	Kalman filter gain matrix
$K_{1,2,3}$	Baro inertial loop gains
$M(t, t_0)$	Observability matrix
P_k	Discrete Kalman filter covariance matrix
Q_k	Process noise strength matrix
q	Quaternion
$q_{1,2,3,4}$	Quaternion components
\underline{r}	Position vector
r_1	GPS pseudo range

R_k	Measurement noise strength matrix
R	Spherical earth radius
R_x	Radius of curvature of the earth for the x platform axis direction
R_y	Radius of curvature of the earth for the y platform axis direction
s	Laplace operator
\underline{S}_1	GPS satellite position vector
t	Time
\underline{U}	GPS receiver host vehicle position
\underline{v}^b	Velocity vector expressed in the body axis frame of reference
\underline{v}^p	Velocity vector expressed in the platform axis frame of reference
$V_{x,y,z}^{p,p,p}$	Velocity components expressed in the platform axis
V_T	True airspeed
\underline{W}_{cp}^p	Angular velocity vector from platform axis to earth axis expressed in the platform axis
$W_{x,y,z}^{p,p,p}$	Angular velocity components expressed in the platform axis
$W(t)$	Continuous time white noise
ω	Frequency
\underline{W}	Continuous time noise vector
W_x	Spatial rate component expressed in terms of the x platform axis
W_y	Spatial rate component expressed in terms of the y platform axis
u, v, w	Aircraft body velocities
\underline{X}	n dimensional continuous time state vector
\underline{X}_k	n dimensional discrete time state vector

$\nabla_{x,y,z}$	X,Y,Z accelerometer bias error
\mathbf{X}	Vector cross product
X,Y,Z	Earth Centered Earth Fixed (ECEF) axis set
\underline{Z}_k	Kalman filter measurement data

GREEK SYMBOLS

α	Alpha angle
γ	Flight path angle
$\underline{\Delta V}^b$	Acceleration measurement expressed in the body axis frame of reference
Δt	Simulation iteration rate
$\delta(\text{prefix})$	Error term for the prefixed variable
$\epsilon_{x,y,z}$	X,Y,Z gyro bias components
$\underline{\delta V}$	Velocity error vector
$\underline{\delta \theta}$	Position error vector
$\underline{\delta \phi}$	Attitude error vector
$\delta \theta_{x,y}$	x and y platform axis position error components
$\delta \phi_{x,y,z}$	x,y,z platform axis tilt error components
θ	Pitch
ξ	Meridian convergence
λ	Latitude
$\sigma_{x,y}$	Rms values for x and y variable
σ^2	Variance
τ	Time constant

Φ_k	Transition matrix associated with the plant equation
Φ	Longitude
ϕ	Roll
ψ	Azimuth
Ω	Earth rate
Ω_x	Earth rate component expressed in terms of the x platform axis
Ω_y	Earth rate component expressed in terms of the y platform axis

SUPERSCRIPTS

b	Body axis frame of reference
e	Earth axis frame of reference
i	Inertial axis frame of reference
k	Skew symmetric
p	Platform axis frame of reference
T	Transpose

SUBSCRIPTS

b	Body axis frame of reference
c	Computed variable
e	Earth axis frame of reference
i	Inertial axis frame of reference
m	Measured variable
p	Platform axis frame of reference
x, y, z	Component values

CHAPTER 1.0

INTRODUCTION

1.1 THESIS OVERVIEW

The work presented in this thesis was carried out as part of a Smiths Industries / Boeing Aerospace contract to integrate a Global Positioning System and an Inertial Reference System inside a Flight Management Computer. The Flight Management Computer is produced by Smiths Industries and is fitted to a United States Navy Command and Control aircraft called the E6. The Global Positioning System is produced by Rockwell Collins and the Inertial Reference System is produced by Litton Aeroproducts.

The thesis contains a technical and a non technical content. The technical content is covered by chapters 2 to 8, the non technical work is the subject of chapter 9, while Chapter 10 gives the conclusion for both the technical and the non technical work.

The main body of original work is contained in chapter 8, where the subject of matching the Kalman filter to meet specific IRS alignment conditions is considered.

1.2 LITERATURE REVIEW

The integration of the global positioning system with an inertial navigation system via the technique of Kalman filtering is now the accepted way of combining such navigation systems. The specific techniques of integrating the two systems are varied however, with each offering its own advantages and disadvantages.

Barckley (1987) discusses three possible vehicle integration schemes. The first and simplest scheme described is to use the GPS position as a precise fix to which the inertial navigation system indicated position is periodically initialized. The resulting navigation performance should be almost as good as the GPS assuming that the GPS is working normally. The scheme has the disadvantage that in-flight alignment of the inertial navigation system is not possible. Alignment of the inertial navigation system is the process whereby the system gets ready to start navigating. Normally this alignment process is carried out on the ground when the inertial navigation system is stationary. There are techniques however, where the alignment can be performed when in motion where the term in air alignment is used to describe the process. In air alignments normally require the use of some source of information that is provided external to the inertial navigation system, the global positioning system is one such source of information.

Scheme two uses both position and velocity information as fixes to periodically re-initialize the inertial navigation system outputs. The paper states that for this scheme as for scheme one, no in air alignment is possible. The advantage of scheme two over scheme one is that scheme two uses velocity information from the GPS and therefore the inertial navigation system velocity is corrected and bounded. Scheme three uses GPS position and velocity as measurements in a navigation filter to estimate inertial navigation system errors. The estimates of error are then fed back to the inertial navigation system so that it can correct for the errors. This scheme has the advantage that it offers the possibility of in air alignment. Its disadvantage compared with the other two schemes is that it is much more complicated to implement as a solution in a practical system.

The techniques discussed in this paper have all assumed that the outputs from the inertial navigation system and the global positioning system are combined and processed in a separate avionics computer, which could be a flight management computer in the case of a commercial airline application.

Napier (1989) discusses several different methods of integrating GPS and INS data. The simplest approach discussed is a cascaded Kalman filter method, which can be described as a system consisting of a GPS subsystem with associated GPS kalman filter, and an inertial navigation subsystem with associated INS Kalman filter. The output from the GPS subsystem is GPS position and velocity, which is fed into the inertial navigation system Kalman filter. The other input to the inertial navigation system Kalman filter is the raw ie uncorrected inertial system outputs. The resultant output from the inertial system Kalman filter is then an estimate of the error in the raw inertial system data. The error in the inertial system can then be accounted for in some way. The advantages stated for this scheme are those of redundancy and easy implementation, since in the event of a single failure the non failed system can continue to navigate. The main disadvantage given is the fact that the output from the GPS receiver has already been passed through its own Kalman filter, which means that special care must be taken when using the GPS output measurements in the inertial system Kalman filter, to ensure that the GPS measurements used are not correlated.

The next approach discussed is that of full integration. Here there is no Kalman filter dedicated to processing the GPS data, since the outputs from the global positioning system are no longer position and velocity but range and range rate measurements. The range and range rate measurements are fed directly into the inertial navigation system Kalman filter, with the function of the filter being to estimate errors in both the inertial system and the global positioning system. In this scheme velocity information is fed back to the GPS module to facilitate better GPS code tracking. The disadvantage of this integration approach is that the technical task is much greater due to consideration of implementation of the GPS equations being required.

For both the integration schemes discussed, there is the option of operating either in an open loop or closed loop configuration.

In the closed loop configuration the estimate of the inertial system errors are fed back to the inertial system so that the system can correct its inherent errors. In the open loop configuration the inertial errors are not fed back to the system for correction, but they are used to modify the raw inertial system output.

Frazier (1987) discusses the flight test of a GPS aided inertial navigation system. The stated objective of the flight test was to assess the performance of a single channel GPS receiver, integrated with a high accuracy gimballed inertial navigation system. The flight test was carried out at the Yuma proving ground, where a laser tracking facility was available. A cascaded integration scheme was used to combine GPS with the inertial system. The GPS Kalman filter has 8 states, and the inertial system Kalman filter has 15 states (note throughout this thesis the word state is used to mean state variables). Velocity aiding data is provided from the inertial system to the GPS, to assist the GPS during periods of satellite outages. The GPS receiver provides measurements of position to the inertial system Kalman filter. The possibility of instability due to the use of two separate Kalman filters has been evaluated and found not to be a problem. In processing the GPS data, the inertial system Kalman filter takes account of the figure of merit provided by the GPS, which is an indication of the accuracy of its measurements.

The inertial system sub optimal Kalman filter was designed using a covariance analysis computer program, where a 60 state truth model was used as a reference for the design. An error model is used for GPS fixes, which is based on errors in the GPS range. Equations are stated which give the GPS error in terms of circular error probability (CEP). General details are given of the 10 flight tests carried out at the Yuma proving ground. An examination of one set of typical results obtained indicates, that predicted and measured values of GPS were in close agreement. For the inertial navigation system, the errors recorded show that the INS performance was better than the GPS stand alone performance for some parts of the flight test. This result was explained by the fact that the inertial system under evaluation was a high accuracy gimballed system which was calibrated in flight by the GPS.

Dayton (1989) describes the results obtained from a flight test of two different INS/GPS integration techniques of the types discussed by Napier (1989).

The stated objective of the flight test is to compare the navigational performance of the two integration techniques. It is stated that there is some controversy over which is the best method of integration for a given application. A brief history of the design of the two integration schemes is given. The technique of covariance analysis is used to develop the implemented Kalman filter. For the cascaded design a 12 state Kalman filter is used, and for the integrated approach, a 14 state solution is used.

For the cascaded filter the problem of using GPS data that may be correlated is overcome by processing the GPS measurements every 12 seconds. The flight tests carried out were typically of two to three hours duration. A total of nine flights in all were carried out. The basic method used to evaluate the navigation performance of the system was to difference the position data obtained from the filters with a reference GPS position. Results for north position error and east position error for the two integration techniques are provided from a sample of the results. The results recorded were post processed to evaluate the root mean square of the position errors of the ensemble of runs for both filters. The results obtained show that the performance of the integrated approach is better than that obtained by the cascaded filter.

Hartman (1989) discusses an integration system for GPS/INS that is intended for civilian aircraft use, and is currently under development with the system due to be certificated by the aviation authorities in 1990. The total navigation system consists of two main components an inertial navigation system and a global positioning system. The global positioning system can act as a stand alone GPS where it provides position and velocity information, or it can function in an integrated form, where its outputs of range and range rate are fed as inputs into an integrated Kalman filter, where the role of the integrated filter is to predict both INS and GPS errors. The integration function is open loop because no attempt is made to feedback the inertial corrections to the INS. A brief discussion of the results obtained from van and lab testing are given.

The situation is investigated where the global positioning system is operating with four satellites for a period of time and then reduces to three satellite operation. During three satellite operation the GPS solution drifts.

The inertial system considered is classified as being a 2 knot system. When the two systems were combined, the results obtained showed that the errors due to both the GPS and the INS were reduced. Two dimensional plots of latitude error against longitude error were used to observe this fact.

Mickelson (1989) discusses the development and flight evaluation of an integrated GPS/INS navigation system. The integration scheme uses two Kalman filters, one for the GPS and one for the INS. The input to the INS Kalman filter is range and range rate from the GPS set. In-flight alignment of the inertial system is also mechanized. The inertial system Kalman filter is referred to as an INS/GPS filter because it predicts GPS clock bias and clock drift errors, which allows processed GPS data to be turned into raw GPS data, as it is raw GPS data that the GPS/INS Kalman filter requires. The data output from the GPS is pre-processed because the GPS has its own 8 state Kalman filter. A discussion of inertial navigation and global positioning system errors is given, with statistical values for each error source provided. A brief mention of a special design feature is given, where the covariance terms relating to position error in the Kalman filter are modified as a function of the GPS satellite coverage, to overcome the problem of unwanted biases that can occur when new satellites are initially used in the GPS solution. Results from lab tests, van tests and flight tests are given. From the flight test results the recorded data was processed to obtain a circular error figure of performance. The figure achieved from flight tests for the navigation system performance was compared to a predicted value obtained by the method of covariance analysis. The two results were in close agreement. It is concluded from the flight tests that the integrated system provides a navigation solution that is more accurate than a stand alone GPS solution.

Griffiths (1984) discusses the results of an assessment of integrated navigation system accuracy, for two flight trajectories via the technique of covariance analysis. The investigation considers what is likely to happen in terms of navigation performance if one inertial navigation system is substituted for another, without making any changes to the integrating Kalman filter to account for the exact characteristics of the substituted inertial system. The inertial navigation systems considered are referred to as standard, a concept developed by the United States Air Force Aeronautical Systems Division, whereby certain parameters of an INS such as size, shape, weight, position and velocity accuracy are standardized.

A covariance analysis is carried out to predict the system accuracy for various integrated combinations. There are three basic components used in the covariance analysis, these being a trajectory generator which provides values for true parameters such as latitude, longitude, velocity etc. An INS error model which has 45 states, although the states do not relate to any particular manufacturer's inertial system. The third component is a 17 state Kalman filter, which models the inertial system and the doppler radar error. From the results of a Covariance simulation it is concluded that with very accurate GPS, and with the system operating in an aided mode, (this being when GPS measurements are valid and being used by the Kalman filter), performance is independent of the INS and Kalman filter configuration. For periods of unaided INS operation however, the mismatch between INS and Kalman filter was found to be significant.

Graham (1986) provides the results of further related work to that discussed by Griffiths (1984). The paper discusses the idea of a standardized integration Kalman filter, such that different types of avionics equipment can be interchanged with the minimum of cost. Several areas where a standardized approach to Kalman filter design could result in a significant reduction in cost and technical risk are discussed. A covariance analysis type evaluation is carried out to formulate and tune the proposed standard Kalman filter. The basic technique applied in the design of the standard filter was to first develop an optimal filter, and then from the optimal solution develop a standard model which is sub optimal. A description of the error sources used for the inertial system model is given together with statistical values for the various terms.

To test the sub optimal Kalman filter, several different flight profiles were investigated. The subsequent results were evaluated for the inertial system level axis and vertical axis errors separately. For the level axis results it is stated that the sub optimal Kalman filter was found to operate to within 10% of the optimal Kalman filter. For the vertical axis performance the sub optimal filter was found to operate to within 5% of the optimal filter, this lower figure being partly explained by the fact that the vertical channel operates in an aided mode ie, it has an external source of reference information provided by a barometric altimeter.

From the results obtained it is concluded that the sub optimal standard filter developed is suitable to integrate all variants of the standard inertial navigation system with GPS.

The integration of GPS with other navigation sensors is not limited to inertial navigation systems, attitude and heading reference systems (AHRS) can also benefit from such techniques.

Brown (1984) discusses the integration of GPS and AHRS. An AHRS system is discussed as having low quality inertial instruments compared with those used in an inertial navigation system such that the navigational accuracy is lower than would be obtained from an inertial system. The advantage of the AHRS system over an inertial system is one of cost. By using an integrated GPS/AHRS solution improved navigation accuracy can be obtained at a much lower cost than that offered by an equivalent inertial system. The integration of GPS and AHRS is carried out using a Kalman filter in much the same way as for an inertial system is integrated. Two integration techniques are discussed these being described as a GPS-aided AHRS system and an integrated GPS/AHRS system.

In the GPS-aided AHRS system, both the GPS subsystem and the AHRS have an associated Kalman filter. In the integrated approach only one combined Kalman filter is used to predict errors in both the AHRS and the GPS. The filter contains 18 states. Inputs to the Kalman filter are GPS measured range and range rate which can be processed directly. For the GPS aided AHRS the GPS Kalman filter has 12 states and the AHRS Kalman filter has 14 states. The AHRS instrument error states are feed back from the filter to the AHRS so that it can compensate for these unwanted errors. To simulate the performance of the two integration schemes a covariance analysis technique is employed. Brief details of the flight profile used in the simulation are given, this being a racetrack type scenario. The GPS coverage is simulated as being initially perfect and then degrading due to the loss of one satellite. From the results obtained it is concluded that the best performance is achieved from the integrated system where better position and velocity accuracy was obtained. The improved accuracy from the integrated system compared with the GPS-aided AHRS solution was most noticeable during the period of degraded GPS coverage. Both integration schemes were found to offer improved performance over stand alone operation.

Cunningham (1988) discusses the problem of instability that can occur with some GPS/INS integration methods. The main theme of the paper is the investigation into the behaviour of inertial navigation system errors under high dynamic conditions. It is stated that whereas the instabilities in the vertical channel of an inertial system are understood, instabilities that can occur as the result of high dynamic manoeuvres have not been characterized. It is also stated that the accuracy and stability limitations of a sub optimally integrated INS/GPS in a dynamically manoeuvring vehicle are not understood.

The paper sets out to investigate that when two sub optimal Kalman filters are used for the cascaded filter integration approach, interaction of the two sub optimal filters during high dynamic manoeuvres may result in a rapid degradation of navigational accuracy, with the degree of accuracy being strongly linked to the degree of departure from the sub optimal model to the optimal Kalman filter model. The investigation is carried out using two techniques. A covariance analysis is carried out where the performance of two filters are compared, one filter containing the optimal truth model solution and the other the sub optimal solution.

The second method used is that of evaluating the system eigenvalues. Eigenvalues are given first for a non manoeuvring inertial system where a brief explanation of how the nine eigenvalues obtained, relate to the classical inertial theoretical results is given. Eigenvalues are then computed for a manoeuvring fighter aircraft where 9g turns are simulated. The results obtained for the 9g level turn indicate the presence of an unstable complex pair of eigenvalues. The magnitude of the positive real parts of both the complex pairs is greater than the magnitude of the eigenvalues associated with the known instability that occurs in the unaided vertical channel.

Turns at 3g were simulated, and also showed instability but of smaller magnitude compared with the 9g case. A brief discussion of the results obtained from the covariance analysis is given. A covariance analysis is carried out for a joint solution Kalman filter using 36 states, this being the same number of states as the truth model. Results for the degradation of position error and velocity error during a constant g turn are given. The results show no degradation of position error over three complete turns.

For velocity a large transient which rapidly subsides to zero was observed. It is concluded that if this velocity error exceeds the linear region of the code loop operation, loss of GPS lock may occur which could destabilize the closed loop operation of the system. Results for the covariance analysis of the two sub optimal Kalman filters is not given as the performance investigation of this scheme is deferred to a future study.

The literature survey considered here is specific to the subject of GPS/IRS integration. Appendix A gives details of a further survey that was carried out to review some further issues associated with the subject.

1.3 CHAPTER SUMMARY

The objective of the technical part of this thesis is the development by simulation of a Kalman filter that can be used inside a flight management computer to combine the position and velocity outputs from two external aircraft navigation systems, for the purpose of improving navigation performance. The two navigation systems are a ring laser gyro strapdown inertial reference system and a global positioning system.

An inertial reference system is an autonomous navigation system providing position and velocity on a continuous basis. The two instruments used in an inertial system are gyros and accelerometers. Both instruments suffer from errors and cause therefore, a resultant error in the inertial system output. The inertial reference system errors can be modelled mathematically, in chapter 2 an error model of the customer inertial reference system is developed. This error model is then used in a computer program to simulate the outputs generated by the customer inertial system. The IRS simulation module is just one of several modules that make up the simulation program. The simulation program is the main tool that is used to develop the Kalman filter. The simulation program is discussed in detail in chapter 5.

The global positioning system is discussed in chapter 3. GPS is a space based radio navigation system which provides position and velocity on a continuous basis. The system works by receiving radio signals transmitted by orbiting satellites whose position relative to the earth is known.

By measuring the distance to the orbiting satellites the GPS receiver can determine its own position relative to the earth. Although the GPS system also suffers from errors, its navigation accuracy is very much greater than the IRS, it is ideal therefore, for use as a source of reference in a Kalman filter.

The Kalman filter is discussed in chapter 4, it is the means by which the inertial reference system and the global positioning system outputs are combined inside the flight management computer. The reason for using a Kalman filter to combine IRS and GPS data is to gain improved navigation system performance when operating in the IRS only mode, this being when the GPS signal is lost.

The navigation techniques that are needed to measure the IRS and Kalman filter navigation performance are developed in chapter 6. In chapter 7, these techniques are used to assess the performance of the Kalman filter.

The results obtained from chapter 7 provide an understanding of the limitations of the Kalman filter design. From this understanding some original Kalman filter work is carried out, this being the subject of chapter 8. In this further work, the general Kalman filter initialization parameters that were first thought to be adequate, are modified to become instrument specific values that take account of particular IRS alignment conditions. A general algorithm is developed that can be used by the Kalman filter to meet the specific alignment conditions of the customer IRS. It is shown how the specific Kalman filter initialization parameters produce an improvement in the Kalman filter navigation performance compared with the general parameters that were used for the analysis carried out in chapter 7. The selection of the Kalman filter initialization parameters to take account of specific IRS alignment conditions is referred to as Kalman filter matching. Although the major part of the work in chapter 8 deals with matching the Kalman filter to the specific alignment conditions of the customer IRS, consideration is also given to applying the matching technique to other types of alignment conditions that can occur in other IRS systems.

From the simulations carried out in chapter 8 it is concluded that to obtain the best Kalman filter performance, the filter must be matched to the IRS alignment condition. This requirement has implications on the methods that can be used to simulate the IRS navigation performance when developing the Kalman filter.

In chapter 6, three techniques to simulate IRS navigation performance are developed, these being Monte Carlo analysis, Sensitivity Analysis and Covariance Analysis. The results obtained from chapter 8 show that the Monte Carlo and sensitivity analysis techniques cannot easily be applied to deal with the IRS alignment condition, the technique of covariance analysis is therefore recommended as the best method to use to develop the Kalman filter.

The topic to be investigated for the non technical aspect of the thesis is the marketing of GPS/IRS technology. This subject is covered in chapter 9 where, a new trend in the market for the integration of GPS/IRS is identified and the possible impact of this new market on the Smiths Industries Flight Management Computer is investigated.

A conclusion for the technical and non technical work is given in chapter 10.

CHAPTER 2.0

INERTIAL REFERENCE SYSTEM

2.1 INTRODUCTION

The type of navigation system being considered in this work is a strapdown ring laser gyro inertial reference system. One of the major tasks involved in integrating a global positioning system and an inertial reference system, using a Kalman filter, is the development of the Kalman filter error model for the specific inertial system being integrated.

There are several different ways of developing an inertial reference system error model. Friedland (1978) discusses the development of an inertial error model using the technique of quaternions. In this present work the approach taken is based on vectors.

The error model to be developed in this chapter is in the form of a state transition matrix, where the states represent position, attitude, velocity and instrument errors. For the position, attitude and velocity errors the approach taken is to first develop the IRS equations, then to form general error equations, and then finally to apply specific conditions to these general error equations to generate the IRS specific error model. The conditions that are applied to the general error equations to form the IRS specific error model, have been supplied by the customer.

The final error model to be developed has 17 states and is referred to as an optimal IRS error model as shown in figure 2.6.

2.1.1 NOTATION

Before the development of the strapdown ring laser gyro inertial reference system error model is discussed, the notation to be used in this section is reviewed and some background mathematics discussed.

Vectors are represented by a bold letter with an underscore, and a superscript denoting the coordinate frame in which the vector is expressed. For example $\underline{\mathbf{v}}^e$ is the velocity vector consisting of three components expressed in the e frame.

Angular velocity vectors will additionally have two subscripts denoting the two reference frames between which the angular velocity exists.

Components of vector quantities are denoted by the same letter but without the underscoring and the bold notation. Also components have a subscript x, y or z. For example w_{epx}^p is the x axis angular velocity component.

A direction cosine matrix that transforms a vector from one coordinate frame to another is denoted by a bold letter but without an underscore. The lack of underscoring makes a matrix distinct from a vector. The letter will have a subscript denoting the original frame of reference, and a superscript for the new frame of reference.

A skew symmetric matrix is indicated by the addition of a superscript k for example, the skew form of the vector $\underline{\mathbf{w}}_{ep}^p$ which will form a 3 x 3 matrix is indicated as $\underline{\mathbf{W}}_{ep}^{pk}$ where the underscore has been dropped, because a matrix is being considered.

In this chapter IRS error models are developed, and the concept of true and computed values are used. Terms will therefore be bracketed to allow a subscript to be placed outside the bracket to indicate a computed value, for example $[\mathbf{C}_e^p]_c$ is the computed value of the direction cosine matrix. A measured value will be indicated by a subscript m outside the bracket, and a true value will be shown by a lack of subscript outside the bracket, for example $[\mathbf{C}_e^p]$ is the true value of the direction cosine matrix. When an error term is being considered then brackets will not be used, for example $\delta\mathbf{C}_e^p$.

2.1.2 MATHEMATICAL BACKGROUND

The development of the theory for the strapdown inertial reference system is heavily based on the mathematical concept of frames of reference. Before considering the development of the IRS specific frames of reference, some basic mathematics will be reviewed.

A 3 x 3 direction cosine matrix transforms a vector from one coordinate frame of reference to another. For instance C_b^p is the matrix that transforms a vector from the b frame to the p frame as :

$$\underline{V}^p = C_b^p \underline{V}^b \quad (2.1)$$

The 3 x 3 direction cosine matrix is updated from the following differential equation :

$$\dot{C}_b^p = W_{bp}^{pk} C_b^p \quad (2.2)$$

Where :

$$W_{bp}^{pk} = \begin{bmatrix} 0 & -W_z^p & W_y^p \\ W_z^p & 0 & -W_x^p \\ -W_y^p & W_x^p & 0 \end{bmatrix} \quad (2.3)$$

Here W_{bpk}^p represents the skew symmetric form of the vector \underline{W}_{bp}^p which represents the angular velocity between the p and b frames expressed in terms of the p frame.

The transpose of the direction cosine given by equation 2.2 can be written as :

$$\dot{C}_b^{pT} = \dot{C}_p^b \quad (2.4)$$

The update equation for the transposed direction cosine matrix is then given by :

$$\dot{C}_p^b = C_p^b W_{bp}^{pk} \quad (2.5)$$

Which can be written as :

$$\dot{C}_p^b = C_p^b (-W_{pb}^{pk}) \quad (2.6)$$

Where the following relationship has been assumed :

$$\underline{W}_{bp}^p = -\underline{W}_{pb}^p \quad (2.7)$$

2.2 INERTIAL REFERENCE SYSTEM DESCRIPTION

A block diagram showing the major functions of a general strapdown inertial reference system is given in figure 2-1. Acceleration measurements expressed in the body axis frame of reference $\underline{\Delta V}^b$, are transposed into equivalent components in the local level platform axis $\underline{\Delta V}^p$, by the body to platform direction cosine matrix C_b^p . The components of the body to platform direction cosine matrix can be used to obtain the following aircraft attitude values, pitch (θ), roll (ϕ) and azimuth (ψ).

The acceleration vector in the platform axis is then integrated to obtain platform velocity. Components of the platform axis velocities, are used to generate the angular rate vector \underline{W}_{ep}^p , commonly referred to as transport rate, which is used to update the earth to platform axis direction cosine matrix C_e^p . The components of the matrix C_e^p can be used to form the following aircraft position values, latitude (λ), longitude (ϕ), and alpha angle (α). An alpha angle is required because the strapdown system being considered is a wander azimuth system, the platform axis is therefore referred to as the local level wander azimuth axis.

The angular rate vector \underline{W}_{ep}^p is combined with the earth rate vector \underline{W}_{ie}^p to form the spatial rate vector \underline{W}_{ip}^p . The transpose of the body to platform direction cosine matrix C_p^b , is used to transform the components of the spatial rate vector from platform axis to body axis. The body referenced spatial vector \underline{W}_{ip}^b is then combined with the angular rate term \underline{W}_{ib}^b to form the angular rate vector \underline{W}_{pb}^b , which is used to update the matrix C_b^p . The angular rate term \underline{W}_{ib}^b is obtained from the raw gyro measurements $\underline{\Delta \theta}_{ib}^b$, where the gyros being considered in this strapdown system are rate integrating gyros.

Now that the functionality of the strapdown inertial reference system has been reviewed, the body to platform and earth to platform direction cosine matrices will be developed. These equations will then allow general IRS error equations for position and attitude to be developed.

2.2.1 EARTH AXIS TO WANDER AZIMUTH AXIS RELATIONSHIP

Consider the earth axis and the local level wander azimuth axis as shown in figure 2-2. The direction cosine matrix that transforms a vector from the platform axis to the earth axis will now be developed by considering the product of individual rotation matrices, where for the initial condition the earth axis and platform axis are aligned.

A positive rotation about Y^e gives :

$$\begin{bmatrix} V_x^e \\ V_y^e \\ V_z^e \end{bmatrix} = \begin{bmatrix} \cos\phi & 0 & \sin\phi \\ 0 & 1 & 0 \\ -\sin\phi & 0 & \cos\phi \end{bmatrix} \begin{bmatrix} V_x' \\ V_y' \\ V_z' \end{bmatrix} \quad (2.8)$$

A negative rotation about the displaced X' axis gives :

$$\begin{bmatrix} V_x^e \\ V_y^e \\ V_z^e \end{bmatrix} = \begin{bmatrix} \cos\phi & 0 & \sin\phi \\ 0 & 1 & 0 \\ -\sin\phi & 0 & \cos\phi \end{bmatrix} \begin{bmatrix} 1 & 0 & 0 \\ 0 & \cos\lambda & \sin\lambda \\ 0 & -\sin\lambda & \cos\lambda \end{bmatrix} \begin{bmatrix} V_x'' \\ V_y'' \\ V_z'' \end{bmatrix} \quad (2.9)$$

A positive rotation about the displaced Z'' axis gives :

$$\begin{bmatrix} V_x^e \\ V_y^e \\ V_z^e \end{bmatrix} = \begin{bmatrix} \cos\phi & 0 & \sin\phi \\ 0 & 1 & 0 \\ -\sin\phi & 0 & \cos\phi \end{bmatrix} \begin{bmatrix} 1 & 0 & 0 \\ 0 & \cos\lambda & \sin\lambda \\ 0 & -\sin\lambda & \cos\lambda \end{bmatrix} \begin{bmatrix} \cos\alpha & -\sin\alpha & 0 \\ \sin\alpha & \cos\alpha & 0 \\ 0 & 0 & 1 \end{bmatrix} \begin{bmatrix} V_x''' \\ V_y''' \\ V_z''' \end{bmatrix} \quad (2.10)$$

The final displaced triple axis set is equal to the wander azimuth local level frame of reference.

Carrying out the matrix multiplication gives the final relationship :

$$\begin{bmatrix} V_x^e \\ V_y^e \\ V_z^e \end{bmatrix} = \begin{bmatrix} \cos\phi\cos\alpha & -\sin\alpha\cos\phi & \sin\phi\cos\lambda \\ -\sin\lambda\sin\alpha\sin\phi & -\sin\phi\sin\lambda\cos\alpha & \\ \cos\lambda\sin\alpha & \cos\lambda\cos\alpha & \sin\lambda \\ -\sin\phi\cos\alpha & \sin\alpha\sin\phi & \\ -\sin\lambda\sin\alpha\cos\phi & -\cos\phi\sin\lambda\cos\alpha & \cos\phi\cos\lambda \end{bmatrix} \begin{bmatrix} V_X^P \\ V_Y^P \\ V_Z^P \end{bmatrix} \quad (2.11)$$

This equation expresses components of the wander azimuth local level frame into equivalent components in the earth frame.

In vector notation the equation is :

$$\underline{V}^e = \underline{C}_p^e \underline{V}^P \quad (2.12)$$

From the direction cosine matrix \underline{C}_p^e values for wander angle, geodetic latitude and longitude can be evaluated as follows :

For wander angle

$$\alpha = \tan^{-1}\left(\frac{C_{12}}{C_{22}}\right) \quad (2.13)$$

For latitude

$$\lambda = \sin^{-1}(C_{22}) \quad (2.14)$$

For longitude

$$\phi = \tan^{-1}\left(\frac{C_{31}}{C_{11}C_{22} - C_{12}C_{21}}\right) \quad (2.15)$$

The direction cosine matrix C_e^p can be updated using the following angular velocity vector whose components are expressed in terms of the platform axis velocities.

$$\dot{C}_e^p = W_{ep}^{pk} C_e^p \quad (2.16)$$

Where :

$$W_{ep}^{pk} = \begin{bmatrix} 0 & -W_z^p & W_y^p \\ W_z^p & 0 & -W_x^p \\ -W_y^p & W_x^p & 0 \end{bmatrix} \quad (2.17)$$

And the matrix components are given by :

$$W_x^p = -\frac{V_y^p}{R_y} \quad (2.18)$$

$$W_y^p = \frac{V_x^p}{R_x} \quad (2.19)$$

$$W_z^p = 0 \quad (2.20)$$

The z component is zero for a wander azimuth system.

2.2.2 WANDER AZIMUTH AXIS TO BODY AXIS RELATIONSHIP

Consider the local level wander azimuth axis and the aircraft body axis as shown in figure 2-3. The direction cosine matrix that transforms a vector from the platform axis to the body axis will now be developed by considering the product of individual rotation matrices, where for the initial condition the platform axis and body axis are aligned.

A positive rotation about Z^P gives :

$$\begin{bmatrix} V_x' \\ V_y' \\ V_z' \end{bmatrix} = \begin{bmatrix} \cos\psi & \sin\psi & 0 \\ -\sin\psi & \cos\psi & 0 \\ 0 & 0 & 1 \end{bmatrix} \begin{bmatrix} V_x^P \\ V_y^P \\ V_z^P \end{bmatrix} \quad (2.21)$$

A positive rotation about the displaced X' axis gives :

$$\begin{bmatrix} V_x'' \\ V_y'' \\ V_z'' \end{bmatrix} = \begin{bmatrix} 1 & 0 & 0 \\ 0 & \cos\theta & \sin\theta \\ 0 & -\sin\theta & \cos\theta \end{bmatrix} \begin{bmatrix} \cos\psi & \sin\psi & 0 \\ -\sin\psi & \cos\psi & 0 \\ 0 & 0 & 1 \end{bmatrix} \begin{bmatrix} V_x^P \\ V_y^P \\ V_z^P \end{bmatrix} \quad (2.22)$$

A positive rotation about the displaced Y'' axis gives :

$$\begin{bmatrix} V_x''' \\ V_y''' \\ V_z''' \end{bmatrix} = \begin{bmatrix} \cos\phi & 0 & -\sin\phi \\ 0 & 1 & 0 \\ \sin\phi & 0 & \cos\phi \end{bmatrix} \begin{bmatrix} 1 & 0 & 0 \\ 0 & \cos\theta & \sin\theta \\ 0 & -\sin\theta & \cos\theta \end{bmatrix} \begin{bmatrix} \cos\psi & \sin\psi & 0 \\ -\sin\psi & \cos\psi & 0 \\ 0 & 0 & 1 \end{bmatrix} \begin{bmatrix} V_x^P \\ V_y^P \\ V_z^P \end{bmatrix} \quad (2.23)$$

The final displaced triple axis set is equal to the body axis frame of reference.

Carrying out the matrix multiplication gives the final relationship :

$$\begin{bmatrix} V_x^b \\ V_y^b \\ V_z^b \end{bmatrix} = \begin{bmatrix} \cos\phi\cos\psi - \sin\psi\cos\phi + & \sin\psi\cos\phi + & -\sin\phi\cos\theta \\ \sin\phi\sin\theta\sin\psi, \sin\phi\sin\theta\cos\psi, & \sin\phi\sin\theta\cos\psi, & \\ -\cos\theta\sin\psi, & \cos\theta\cos\psi, & \sin\theta \\ \sin\phi\cos\psi + & \sin\phi\sin\psi - & \\ \sin\theta\sin\psi\cos\phi, \cos\phi\sin\theta\cos\psi, & \cos\phi\sin\theta\cos\psi, & \cos\theta\cos\phi \end{bmatrix} \begin{bmatrix} V_X^P \\ V_Y^P \\ V_Z^P \end{bmatrix} \quad (2.24)$$

This equation expresses components of the wander azimuth local level frame into equivalent components in the body frame.

In vector notation the equation is :

$$\underline{V}^b = C_p^b \underline{V}^p \quad (2.25)$$

From the direction cosine matrix C_p^b , which is the transpose of C_p^b , values for pitch, roll and azimuth can be evaluated as follows :

For pitch

$$\theta = \sin^{-1}(c_{32}) \quad (2.26)$$

For roll

$$\phi = \tan^{-1}\left(-\frac{c_{31}}{c_{33}}\right) \quad (2.27)$$

For azimuth

$$\psi = \tan^{-1}\left(\frac{-c_{12}}{c_{22}}\right) \quad (2.28)$$

The direction cosine matrix C_b^p which represents attitude can be updated using the following equation :

$$\dot{C}_b^p = -W_{pb}^{pk} C_b^p \quad (2.29)$$

The components for the angular velocity vector are not directly related to the gyro output measurements, because the gyro measures angle between the aircraft body axis and inertial space. An angular velocity vector expressed in terms of the body axis can be computed using the following relationship :

$$\underline{W}_{pb}^b = \underline{W}_{ib}^b - \underline{W}_{ip}^b \quad (2.30)$$

Where \underline{W}_{ip}^b is a computed rate vector expressing the angular rate between the inertial and wander azimuth frames, and \underline{W}_{ib}^b is a measured rate vector consisting of the x,y and z gyro measurements expressed in the body axis frame of reference.

2.3 GENERAL IRS ERROR MODEL EQUATIONS

The development of general IRS error model equations for attitude and position will now be considered.

2.3.1 DEVELOPMENT OF A DIRECTION COSINE MATRIX ERROR

To develop the IRS error model equations, error equations for the direction cosine matrices C_e^p and C_e^c are required. In section 2.2.1 the direction cosine matrix that transposes a vector from the platform axis to the earth axis was developed. By introducing a true and a computed value of earth to platform direction cosine matrix, then an error direction cosine matrix can be defined as the difference between the computed direction cosine matrix and true matrix as shown below :

$$\delta C_e^p = [C_e^p]_c - [C_e^p] \quad (2.31)$$

Consider element C_{11} (see equation 2.11) of the earth to platform direction cosine matrix :

$$C_{11} = \cos\phi \cos\alpha - \sin\lambda \sin\alpha \sin\phi \quad (2.32)$$

An increment in C_{11} can be formed from small increment theory where terms to first order only are considered :

$$\delta C_{11} = \frac{\partial C_{11}}{\partial \phi} \delta \phi + \frac{\partial C_{11}}{\partial \alpha} \delta \alpha + \frac{\partial C_{11}}{\partial \lambda} \delta \lambda \quad (2.33)$$

This gives :

$$\begin{aligned} \delta C_{11} = & \delta \phi (-\sin\phi \cos\alpha - \sin\lambda \sin\alpha \cos\phi) \\ & + \delta \alpha (-\cos\phi \sin\alpha - \sin\lambda \sin\phi \cos\alpha) \\ & + \delta \lambda (-\sin\alpha \sin\phi \cos\lambda) \end{aligned} \quad (2.34)$$

Here the equation for δC_{11} is expressed in terms of latitude, longitude and alpha angle. However, because the IRS error model equations being developed are required to be expressed in terms of the IRS platform axis frame of reference, an alternative approach to developing error direction cosine matrices is sought.

An alternative development can be obtained by considering the earth to platform direction cosine matrix update given by equation 2.16. Consider the term C_{11} :

$$\dot{C}_{11} = w_z^p C_{21} - w_y^p C_{31} \quad (2.35)$$

This equation can be written as :

$$\frac{C_{11}(t + \Delta t) - C_{11}(t)}{\Delta t} = w_z^p C_{21} - w_y^p C_{31} \quad (2.36)$$

Expressing the angular rate as an angle increment over time, and cancelling the Δt components gives the following alternative form of equation for δC_{11} :

$$\delta C_{11} = \delta \theta_z^p C_{21} - \delta \theta_y^p C_{31} \quad (2.37)$$

A similar procedure can now be repeated for the remaining 8 direction cosine components. A summary of the final results for the error terms is given below :

$$\delta C_{12} = \delta \theta_z^p C_{22} - \delta \theta_y^p C_{32} \quad (2.38)$$

$$\delta C_{13} = \delta \theta_z^p C_{23} - \delta \theta_y^p C_{33} \quad (2.39)$$

$$\delta C_{21} = \delta \theta_x^p C_{31} - \delta \theta_z^p C_{11} \quad (2.40)$$

$$\delta C_{22} = \delta \theta_x^p C_{32} - \delta \theta_z^p C_{12} \quad (2.41)$$

$$\delta C_{23} = \delta \theta_x^p C_{33} - \delta \theta_z^p C_{13} \quad (2.42)$$

$$\delta C_{31} = \delta \theta_y^p C_{11} - \delta \theta_x^p C_{21} \quad (2.43)$$

$$\delta C_{32} = \delta \theta_y^p C_{12} - \delta \theta_x^p C_{22} \quad (2.44)$$

$$\delta C_{33} = \delta \theta_y^p C_{13} - \delta \theta_x^p C_{23} \quad (2.45)$$

The nine equations can be written in the following matrix form :

$$\delta C_e^p = \delta \theta^p [C_e^p] \quad (2.46)$$

Where $[C_e^p]$ is the true value earth to platform direction cosine matrix and $\delta \theta^p$ is a position error expressed in terms of the platform axes.

An error equation for the body to platform direction cosine matrix can be formed in a similar manner to equation 2.46 above, the final result only is shown below :

$$\delta C_b^p = \delta \phi^p [C_b^p] \quad (2.47)$$

Where $[C_b^p]$ is the true body to platform direction cosine matrix and $\delta \phi^p$ is an attitude error expressed in terms of the platform axes.

2.3.2 DEVELOPMENT OF THE ATTITUDE ERROR EQUATION

The attitude error vector equation will now be developed where the various parts of the equation are coordinated in terms of the platform axis. The final form of the equation to be developed is shown below :

$$\underline{\delta \dot{\phi}}^p = \underline{\delta W}_{ip}^p + \underline{\delta \phi}^p \times \underline{W}_{ip}^p \quad (2.48)$$

Consider a perfect alignment, then the computed value of the body to platform direction cosine matrix will equal the true value as shown below :

$$[\underline{C}_b^p]_c = [\underline{C}_b^p] \quad (2.49)$$

The update equation for the direction cosine matrix is given by equation 2.29. On entering navigation mode, errors that existed in the alignment but were forced to zero, start to propagate. The computed value for the update equation for the body to platform direction cosine matrix then becomes :

$$[\underline{\dot{C}}_b^p]_c = ([\underline{W}_{bp}^{pk}] + \underline{\delta W}_{bp}^{pk}) ([\underline{C}_b^p] + \underline{\delta C}_b^p) \quad (2.50)$$

Where the following error terms are assumed

$$\underline{\delta C}_b^p = [\underline{C}_b^p]_c - [\underline{C}_b^p] \quad (2.51)$$

$$\underline{\delta W}_{bp}^{pk} = [\underline{W}_{bp}^{pk}]_c - [\underline{W}_{bp}^{pk}] \quad (2.52)$$

Carrying out the multiplication for equation 2.50, and substituting for the body to platform direction cosine matrix error term given by equation 2.47 gives :

$$\underline{\delta \dot{C}}_b^p = ([\underline{W}_{bp}^{pk}] \underline{\delta \phi}^p + \underline{\delta W}_{bp}^{pk}) [\underline{C}_b^p] \quad (2.53)$$

Now consider the development of an alternative form for equation 2.53 obtained by differentiation of equation 2.47 as shown below :

Differentiation of equation 2.47 gives :

$$\delta \dot{C}_b^p = \delta \dot{\phi}^p [C_b^p] + \delta \phi^p [\dot{C}_b^p] \quad (2.54)$$

Equation 2.47 be combined with equation 2.53 to give :

$$\delta \dot{\phi}^p [C_b^p] + \delta \phi^p [\dot{C}_b^p] = [W_{bp}^{pk}] \delta \phi^p [C_b^p] + \delta W_{bp}^{pk} [C_b^p] \quad (2.55)$$

Re-arranging and making use of equation 2.29 gives :

$$\delta \dot{\phi}^p [C_b^p] = [W_{bp}^{pk}] \delta \phi^p [C_b^p] + \delta W_{bp}^{pk} [C_b^p] - \delta \phi^p [W_{bp}^{pk}] [C_b^p] \quad (2.56)$$

The term $[C_b^p]$ can now be eliminated to give :

$$\delta \dot{\phi}^p = [W_{bp}^{pk}] \delta \phi^p + \delta W_{bp}^{pk} - \delta \phi^p [W_{bp}^{pk}] \quad (2.57)$$

Equation 2.57 can be written in vector form using the following relationship, where the symmetric matrix is expressed in terms of a vector :

$$[W_{bp}^{pk}] \delta \phi^p - \delta \phi^p [W_{bp}^{pk}] = -[W_{bp}^p] \times \underline{\delta \phi}^p \quad (2.58)$$

The vector equation equivalent to equation 2.57 is then :

$$\delta \dot{\phi}^p = \underline{\delta W}_{bp}^p - [W_{bp}^p] \times \underline{\delta \phi}^p \quad (2.59)$$

The final stage of the development of equation 2.48, is to arrange for the angular vectors in equation 2.59 to be expressed in terms of the angular rate between inertial and platform frames of reference, as opposed to the present body and platform axis set.

The transforming of the coordinate frames of reference from body and platform to inertial and platform will now be examined :

Consider the following two equations :

$$[\underline{W}_{bp}^p] = [C_b^p][\underline{W}_{bp}^b] \quad (2.60)$$

And

$$[\underline{W}_{bp}^b] = [\underline{W}_{ip}^b] - [\underline{W}_{ib}^b] \quad (2.61)$$

Combining the two equations gives :

$$[\underline{W}_{bp}^p] = [\underline{W}_{ip}^p] - [C_b^p][\underline{W}_{ib}^b] \quad (2.62)$$

Now the error angular vector can be expressed in terms of a computed and a true value as :

$$\underline{\delta W}_{bp}^p = [\underline{W}_{bp}^p]_c - [\underline{W}_{bp}^p] \quad (2.63)$$

Substituting the value for equation 2.62 gives :

$$\underline{\delta W}_{bp}^p = ([\underline{W}_{ip}^p]_c - [C_b^p]_c[\underline{W}_{ib}^b]_m) - ([\underline{W}_{ip}^p] - [C_b^p][\underline{W}_{ib}^b]_m) \quad (2.64)$$

By combining true and error terms this can be re-written as :

$$\underline{\delta W}_{bp}^p = \underline{\delta W}_{ip}^p - ([C_b^p]_c[\underline{W}_{ib}^b]_m - [C_b^p][\underline{W}_{ib}^b]_m) \quad (2.65)$$

Expressing the true body to platform direction cosine matrix in terms of a computed value, and an error value gives :

$$\underline{\delta W}_{bp}^p = \underline{\delta W}_{ip}^p - ([C_b^p]_c [\underline{W}_{ib}^b]_m - [C_b^p]_c [\underline{W}_{ib}^b]_m + \delta C_b^p [\underline{W}_{ib}^b]_m) \quad (2.66)$$

By cancelling terms and applying the result of equation 2.47 the result becomes :

$$\underline{\delta W}_{bp}^p = \underline{\delta W}_{ip}^p - \delta \phi^p [C_b^p] [\underline{W}_{ib}^b]_m \quad (2.67)$$

The final form of equation 2.48 can now be obtained by substituting equation 2.67 and 2.62 into equation 2.59 to give after some processing :

$$\underline{\delta \dot{\phi}}^p = \underline{\delta W}_{ip}^p + \underline{\delta \phi}^p \times \underline{W}_{ip}^p \quad (2.68)$$

This is the desired result where the angular velocity vectors will be seen to represent the angular velocity between the platform and inertial frames of reference with the values expressed in the platform axis. For the purposes of simulation, the angular error vector $\underline{\delta W}_{ip}^p$ needs to be expressed in terms of an earth rate and a transport rate error term as follows :

Expressing the angular error vector in terms of a transport rate and an earth rate error gives :

$$\underline{\delta W}_{ip}^p = \underline{\delta W}_{ep}^p + \underline{\delta W}_{ie}^p \quad (2.69)$$

The components of the earth rate error vector $\underline{\delta W}_{ie}^p$ can be developed by considering equation 2.70 below :

$$[\underline{W}_{ie}^p] = [C_e^p] [\underline{W}_{ie}^e] \quad (2.70)$$

Where the angular vector representing the rotation of the earth with respect to inertial space and expressed in terms of the earths' axes is :

$$[\underline{W}_{ie}^e] = \begin{bmatrix} 0 \\ \Omega \\ 0 \end{bmatrix}$$

An error in the direction cosine matrix will cause a resultant error in the earth rate vector. The computed value of earth rate in terms of the platform axis can therefore be expressed as :

$$[\underline{W}_{ie}^p]_c = [C_e^p] [\underline{W}_{ie}^e] + \delta C_e^p [\underline{W}_{ie}^e] \quad (2.72)$$

Using equation 2.46 this becomes :

$$\underline{\delta W}_{ie}^p = \delta \theta^p [C_e^p] [\underline{W}_{ie}^e] \quad (2.73)$$

Which reduces to :

$$\underline{\delta W}_{ie}^p = \delta \theta^p [\underline{W}_{ie}^p] \quad (2.74)$$

Where

$$\delta \theta^p = \begin{bmatrix} 0 & \delta \theta_z^p & -\delta \theta_y^p \\ -\delta \theta_z^p & 0 & \delta \theta_x^p \\ \delta \theta_y^p & -\delta \theta_x^p & 0 \end{bmatrix} \quad (2.75)$$

Finally, substituting equations 2.69 and 2.74 into equation 2.68, allows the attitude error vector to be written in the following component form that is suitable for simulation.

$$\delta \dot{\phi}_x^p = \delta W_{epx}^p + \delta \theta_z^p W_{iey}^p - \delta \theta_y^p W_{iez}^p + \delta \phi_y^p W_{ipz}^p - \delta \phi_z^p W_{ipy}^p \quad (2.76)$$

$$\delta \dot{\phi}_y^p = \delta W_{epy}^p + \delta \theta_x^p W_{iez}^p - \delta \theta_z^p W_{iex}^p + \delta \phi_z^p W_{ipx}^p - \delta \phi_x^p W_{ipz}^p \quad (2.77)$$

$$\delta \dot{\phi}_z^p = \delta W_{epz}^p + \delta \theta_y^p W_{iex}^p - \delta \theta_x^p W_{iey}^p + \delta \phi_x^p W_{ipy}^p - \delta \phi_y^p W_{ipx}^p \quad (2.78)$$

These equations can be used to simulate the attitude error for a general inertial system. These general equations will be developed into customer specific equations in section 2.4.2.

2.3.3 DEVELOPMENT OF THE POSITION ERROR EQUATION

A position error vector equation can be developed along the same lines as for the attitude error vector equation of the last section.

The final form of the equation to be developed is shown below :

$$\underline{\delta \theta}^p = \underline{\delta W}_{ep}^p - \underline{W}_{ep}^p \times \underline{\delta \theta}^p \quad (2.79)$$

The starting point is to consider the computed value for the update equation for the earth to local level direction cosine matrix. Assuming an error in the transport rate vector then the computed value for the direction cosine matrix update equation can be expressed as :

$$[\dot{C}_e^p]_c = ([W_{ep}^{pk}] + \delta W_{ep}^{pk}) [C_e^p] \quad (2.80)$$

Where

$$\delta W_{ep}^{pk} = [W_{ep}^{pk}]_c - [W_{ep}^{pk}] \quad (2.81)$$

This leads to the following equation :

$$\delta \dot{C}_e^p = \delta W_{ep}^{pk} [C_e^p] + [W_{ep}^{pk}] \delta \theta^p [C_e^p] \quad (2.82)$$

An alternative equation can be developed for the direction cosine matrix error differential. Consider equation 2.46, differentiation gives :

$$\delta \dot{C}_e^p = \delta \dot{\theta}^p [C_e^p] + \delta \theta^p [\dot{C}_e^p] \quad (2.83)$$

Combining equations 2.82 and 2.83 gives :

$$\delta \dot{\theta}^p = \delta W_{ep}^{pk} + [W_{ep}^{pk}] \delta \theta^p - \delta \theta^p [W_{ep}^{pk}] \quad (2.84)$$

Using the following relationship :

$$[W_{ep}^{pk}] \delta \theta^P - \delta \theta^P [W_{ep}^{pk}] = -[W_{ep}^P] \times \underline{\delta \theta^P} \quad (2.85)$$

Equation 2.84 can be re-written to give the final form of equation 2.79.

In component form the general position error equations are :

$$\delta \dot{\theta}_x^P = \delta W_{epx}^P + W_{epz}^P \delta \theta_y^P - W_{epy}^P \delta \theta_z^P \quad (2.86)$$

$$\delta \dot{\theta}_y^P = \delta W_{epy}^P + W_{epx}^P \delta \theta_z^P - W_{epz}^P \delta \theta_x^P \quad (2.87)$$

$$\delta \dot{\theta}_z^P = \delta W_{epz}^P + W_{epy}^P \delta \theta_x^P - W_{epx}^P \delta \theta_y^P \quad (2.88)$$

In the next section these general error equations will be further developed to give IRS specific error equations.

2.4 IRS SPECIFIC POSITION AND ATTITUDE ERROR EQUATIONS

General IRS error equations have been developed for position and attitude. These general equations will now be further developed to provide a customer specific instrument error model.

2.4.1 IRS SPECIFIC POSITION ERROR EQUATION

The fundamental step in developing the instrument specific error equation is to apply the condition of equations 2.89 and 2.90 below to the general position error equations developed in the last section :

$$\delta \dot{\theta}_z^P = 0 \quad (2.89)$$

$$W_{epz}^P = -\delta W_{epz}^P \quad (2.90)$$

These conditions that allow the general position and attitude error equations to be developed into IRS specific error equations, have been supplied by the customer. The conditions define the true IRS alpha angle and the computed IRS alpha angle to be equal. Applying these results to equation 2.88 gives :

$$\delta W_{epz}^P = (W_{epx}^P \delta \theta_y^P - W_{epy}^P \delta \theta_x^P) \quad (2.91)$$

Applying the condition of equation 2.91 to the x component position error given by equation 2.86 gives :

$$\delta \dot{\theta}_x^P = \delta W_{epx}^P + (W_{epx}^P \delta \theta_y^P - W_{epy}^P \delta \theta_x^P) \delta \theta_y^P \quad (2.92)$$

Ignoring the product of error terms gives :

$$\delta \dot{\theta}_x^P = \delta W_{epx}^P \quad (2.93)$$

Where

$$\delta W_{epx}^P = -\frac{\delta V_y}{R_y} - W_{epx}^P \frac{\delta R_y}{R_y} \quad (2.94)$$

A similar development follows for the y component position error component. Applying the condition of equation 2.91 to equation 2.87 gives :

$$\delta \dot{\theta}_y^p = \delta W_{epy}^p - (W_{epx}^p \delta \theta_y^p - W_{epy}^p \delta \theta_x^p) \delta \theta_x^p \quad (2.95)$$

Ignoring the product of error terms gives :

$$\delta \dot{\theta}_y^p = \delta W_{epy}^p \quad (2.96)$$

Where

$$\delta W_{epy}^p = \frac{\delta V_x}{R_x} - W_{epy}^p \frac{\delta R_x}{R_x} \quad (2.97)$$

Applying the instrument specific conditions of equations 2.89 and 2.90 to the general error equations for position, has removed the need for the z position error state. The remaining x and y position error equations are modelled as two states in the optimal IRS state transition matrix as shown in figure 2-6.

2.4.2 IRS SPECIFIC ATTITUDE ERROR EQUATION

The IRS specific attitude error equations can be developed by applying the conditions of equations 2.89, 2.90 and 2.91 to the general attitude error equations developed in section 2.3.2.

Substituting for equation 2.91 into equation 2.78 gives :

$$\delta\dot{\phi}_z^P = W_{epx}^P \delta\theta_y^P - W_{epy}^P \delta\theta_x^P + \delta\theta_y^P W_{iey}^P - \delta\theta_x^P W_{iey}^P + \delta\phi_x^P W_{iey}^P - \delta\phi_y^P W_{ipx}^P \quad (2.98)$$

Now Using

$$[\underline{W}_{ip}^P] = [\underline{W}_{ie}^P] + [\underline{W}_{ep}^P] \quad (2.99)$$

The final form of the instrument specific attitude error equation for the z component is obtained by substituting for equation 2.99 into equation 2.98 above, to give :

$$\delta\dot{\phi}_z^P = W_{ipx}^P \delta\theta_y^P - W_{ipy}^P \delta\theta_x^P + \delta\theta_y^P W_{iey}^P - \delta\theta_x^P W_{iey}^P \quad (2.100)$$

Having developed the z component, the x component will now be considered. Applying the condition of equation 2.89 to equation 2.76 gives :

$$\delta\dot{\phi}_x^P = \delta W_{epx}^P - \delta\theta_y^P W_{iey}^P + \delta\phi_y^P W_{ipz}^P - \delta\phi_z^P W_{ipy}^P \quad (2.101)$$

Now from equation 2.99, the z angular component for earth rate can be written as :

$$W_{iez}^P = W_{ipz}^P - W_{epz}^P \quad (2.102)$$

And from equation 2.90

$$W_{epz}^p = -W_{epx}^p \delta \theta_y^p + W_{epy}^p \delta \theta_x^p \quad (2.103)$$

Substituting equations 2.90 into equation 2.102, and applying the result of equation 2.101 gives :

$$\delta \dot{\phi}_x^p = \delta W_{epx}^p - \delta \theta_y^p W_{ipz}^p + \delta \phi_y^p W_{ipz}^p - \delta \phi_z^p W_{ipy}^p \quad (2.104)$$

The final form of the instrument specific attitude error equation for x component can be written by substituting for the value of δW_{epx}^p provided by equation 2.94 to give :

$$\delta \dot{\phi}_x^p = -\frac{\delta V_y}{R_y} - W_{epx}^p \frac{\delta R_y}{R_y} - \delta \theta_y^p W_{ipz}^p + \delta \phi_y^p W_{ipz}^p - \delta \phi_z^p W_{ipy}^p \quad (2.105)$$

The development of the y instrument specific equation follows the same pattern as for the x case, so only the final result is shown below :

$$\delta \dot{\phi}_y^p = -\frac{\delta V_x}{R_x} - W_{epy}^p \frac{\delta R_x}{R_x} - \delta \theta_x^p W_{ipz}^p + \delta \phi_z^p W_{ipx}^p - \delta \phi_x^p W_{ipz}^p \quad (2.106)$$

The final instrument specific attitude error equations for the x, y and z axis are modelled as states in the optimal IRS state transition matrix as given in figure 2-6.

2.5 IRS VELOCITY EQUATIONS

2.5.1 DEVELOPMENT OF THE IRS VELOCITY EQUATIONS

Each of the body mounted accelerometers measures a component of acceleration along its sensitive axis according to the laws of Newtonian Mechanics. Using vector notation, the accelerometer output is given by :

$$\underline{a} = \frac{d^2 \underline{r}^i}{dt^2} - \underline{gm} \quad (2.107)$$

where \underline{gm} is the mass attraction gravity vector, and $d^2 \underline{r}^i / dt^2$ is the second rate of change of the position vector expressed in terms of an inertial frame of reference. From the accelerometer output and using a computed value of \underline{gm} the navigation computer is able to solve for \underline{r} , the vector indicating the position of the vehicle. The actual equation that will be developed here, is the rate of change of the velocity vector as seen by the wander azimuth frame of reference.

The mass attraction gravity vector can be written as :

$$\underline{gm} = \underline{g} + \underline{W}_{ie} \times (\underline{W}_{ie} \times \underline{r}) \quad (2.108)$$

Where

\underline{g} is the gravity vector

and

\underline{W}_{ie} is the earth rate vector

Combining equations 2.107 and 2.108 gives :

$$\frac{d^2 \underline{r}^i}{dt^2} = \underline{a} + \underline{g} + \underline{W}_{ie} \times (\underline{W}_{ie} \times \underline{r}) \quad (2.109)$$

Having arrived at this equation using Newtonian Mechanics, a similar equation can be derived using the theorem of Coriolis.

By the theorem of Coriolis

$$\frac{d \underline{r}^i}{dt} = \frac{d \underline{r}^e}{dt} + \underline{W}_{ie} \times \underline{r} \quad (2.110)$$

Which gives:

$$\frac{d \underline{r}^i}{dt} = \underline{v} + \underline{W}_{ie} \times \underline{r} \quad (2.111)$$

By differentiating equation 2.111 the second derivative for the rate of change of the position vector expressed in terms of the inertial frame of reference can be found :

$$\frac{d^2 \underline{r}^i}{dt^2} = \frac{d \underline{v}^i}{dt} + \underline{W}_{ie} \times \underline{v} + \underline{W}_{ie} \times \underline{W}_{ie} \times \underline{r} \quad (2.112)$$

We Can now equate equation 2.112 to the previous equation for $d^2 \underline{r}^i / dt^2$ obtained from Newtonian Mechanics, to give :

$$\frac{d \underline{v}^i}{dt} = \underline{a} + \underline{g} - \underline{W}_{ie} \times \underline{v} \quad (2.113)$$

Having obtained the rate of change of the velocity vector \underline{v} in terms of the inertial frame of reference, an equation can be formed for the rate of change of the velocity vector in terms of the wander azimuth frame of reference.

From the theorem of coriolis :

$$\frac{d\underline{v}^i}{dt} = \frac{d\underline{v}^p}{dt} + \underline{W}_{ip} \times \underline{V} \quad (2.114)$$

Which gives :

$$\frac{d\underline{v}^p}{dt} = \frac{d\underline{v}^i}{dt} - \underline{W}_{ip} \times \underline{V} \quad (2.115)$$

Combining equations 2.113 and 2.115 gives :

$$\frac{d\underline{v}^p}{dt} = \underline{a} + \underline{g} - \underline{W}_{ie} \times \underline{V} - \underline{W}_{ip} \times \underline{V} \quad (2.116)$$

Which can be written in final form as :

$$\frac{d\underline{v}^p}{dt} = \underline{a} + \underline{g} - (2\underline{W}_{ie} + \underline{W}_{ep}) \times \underline{V} \quad (2.117)$$

Where the relationship from equation 2.99 has been used, and the final vector equation has been expressed in terms of components of the wander azimuth frame. Writing the final vector equation in component form gives :

$$\dot{V}_x^p = a_x^p + g_x^p + V_y^p 2W_{iez}^p + V_y^p W_{epy}^p - V_z^p 2W_{iey}^p - V_z^p W_{epy}^p \quad (2.118)$$

$$\dot{V}_y^p = a_y^p + g_y^p + V_z^p 2W_{iez}^p + V_z^p W_{epx}^p - V_x^p 2W_{iez}^p - V_x^p W_{epz}^p \quad (2.119)$$

$$\dot{V}_z^p = a_z^p + g_z^p + V_x^p 2W_{iey}^p + V_x^p W_{epy}^p - V_y^p 2W_{iey}^p - V_y^p W_{epx}^p \quad (2.120)$$

Equations 2.118 to 2.120 are general equations in that they can be modified for application with either a Gimballed or a Strapdown Inertial Navigation System. For the specific Strapdown Inertial System of interest in this work the component equations become :

$$\dot{V}_x^p = a_x^p + g_x^p + V_y^p 2W_{iez}^p - V_z^p 2W_{iey}^p - V_z^p W_{epy}^p \quad (2.121)$$

$$\dot{V}_y^p = a_y^p + g_y^p + V_z^p 2W_{iey}^p + V_z^p W_{epx}^p - V_x^p 2W_{iez}^p \quad (2.122)$$

$$\dot{V}_z^p = a_z^p + g_z^p + V_x^p 2W_{iey}^p + V_x^p W_{epy}^p - V_y^p 2W_{iez}^p - V_y^p W_{epx}^p \quad (2.123)$$

Where

$$\underline{g}^p = [0, 0, -g_z^p]^T \quad (2.124)$$

And

$$W_{epz}^p = 0 \quad (2.125)$$

For the gravity vector \underline{g}^p the effects of gravity anomaly and deviations of the vertical are ignored. The Z axis gravity component has a negative value, this is due to the non standard axis set used in the customer IRS for the wander azimuth frame of reference, ie the Z axis is positive up. The term W_{epz}^p equal to zero corresponds to a wander azimuth mechanization.

2.6 GENERAL IRS VELOCITY ERROR EQUATION

Equation 2.117 gives the rate of change of the velocity vector expressed in components of the wander azimuth axis with the component form of the equation being given by 2.118 to 2.220. An error equation for the rate of change of velocity coordinated in the wander azimuth axis can be formed by considering the difference between the computed (subscript c) and true value (no subscript) of the various terms of the velocity equation as follows :

$$\underline{\delta V}^P = [\underline{V}^P]_c - [\underline{V}^P] \quad (2.126)$$

From equation 2.117 this gives :

$$\begin{aligned} \underline{\delta V}^P = & [\underline{a}^P]_c + [\underline{q}^P]_c - ([2\underline{W}_{ie}^P]_c + [\underline{W}_{ep}^P]_c) \times [\underline{V}^P]_c \\ & - ([\underline{a}^P] + [\underline{q}^P]_c - ([2\underline{W}_{ie}^P] + [\underline{W}_{ep}^P])) \times [\underline{V}^P] \end{aligned} \quad (2.127)$$

To proceed with the development of the vector velocity error equation the cross product terms can be replaced by their skew symmetric matrix equivalent form to give :

$$\begin{aligned} \underline{\delta V}^P = & [\underline{a}^P]_c + [\underline{q}^P]_c + ([2\underline{W}_{ie}^{Pk}]_c + [\underline{W}_{ep}^{Pk}]_c) [\underline{V}^P]_c \\ & - ([\underline{a}^P] + [\underline{q}^P]_c - ([2\underline{W}_{ie}^{Pk}] + [\underline{W}_{ep}^{Pk}])) [\underline{V}^P] \end{aligned} \quad (2.128)$$

Now introducing the error terms :-

$$\delta (2\underline{W}_{ie}^P + \underline{W}_{ep}^P) = ([2\underline{W}_{ie}^P]_c + [\underline{W}_{ep}^P]_c) - ([2\underline{W}_{ie}^P] + [\underline{W}_{ep}^P]) \quad (2.129)$$

$$\underline{\delta V}^P = [\underline{V}^P]_c - [\underline{V}^P] \quad (2.130)$$

$$\underline{\delta a}^P = [\underline{a}^P]_c - [\underline{a}^P] \quad (2.131)$$

$$\underline{\delta q}^P = [\underline{q}^P]_c - [\underline{q}^P] \quad (2.132)$$

Ignoring products of error terms which are small, the above result can now be used to re-write the equation for $\underline{\delta V}^P$ in its final form :

$$\underline{\delta V}^P = \underline{\delta a}^P + \underline{\delta g} + ([2\underline{W}_{ie}^P] + [\underline{W}_{ep}^P]) \underline{\delta V}^P + \delta([2\underline{W}_{ie}^P] + [\underline{W}_{ep}^P]) [\underline{V}^P] \quad (2.133)$$

This is a general velocity error vector equation which can be applied to Strapdown Inertial Reference Systems.

The Component form of the general velocity error vector equation is :

$$\begin{aligned} \delta \dot{V}_x^P = & \delta a_x^P + \delta g_x^P + (2W_{iez}^P + W_{epz}^P) \delta V_y^P - (2W_{iey}^P + W_{epy}^P) \delta V_z^P \\ & + (2\delta W_{iez}^P + \delta W_{epz}^P) V_y^P - (2\delta W_{iey}^P + \delta W_{epy}^P) V_z^P \end{aligned} \quad (2.134)$$

$$\begin{aligned} \delta \dot{V}_y^P = & \delta a_y^P + \delta g_y^P - (2W_{iez}^P + W_{epz}^P) \delta V_x^P + (2W_{iey}^P + W_{epy}^P) \delta V_z^P \\ & - (2\delta W_{iez}^P + \delta W_{epz}^P) V_x^P - (2\delta W_{iey}^P + \delta W_{epy}^P) V_z^P \end{aligned} \quad (2.135)$$

$$\begin{aligned} \delta \dot{V}_z^P = & \delta a_z^P + \delta g_z^P - (2W_{iey}^P + W_{epy}^P) \delta V_x^P - (2W_{iey}^P + W_{epy}^P) \delta V_y^P \\ & + (2\delta W_{iey}^P + \delta W_{epy}^P) V_x^P - (2\delta W_{iey}^P + \delta W_{epy}^P) V_y^P \end{aligned} \quad (2.136)$$

Where the values for the acceleration and gravity error components are given as follows. For the acceleration error components :

$$\delta a_x^P = \delta \phi_z^P a_y^P - \delta \phi_y^P a_z^P \quad (2.137)$$

$$\delta a_y^P = \delta \phi_x^P a_z^P - \delta \phi_z^P a_x^P \quad (2.138)$$

$$\delta a_z^p = \delta \phi_y^p a_x^p - \delta \phi_x^p a_y^p \quad (2.139)$$

The components of the gravity error equation can be developed from equation 2.124 and shown to be :

$$\delta g_x^p = 0 \quad (2.140)$$

$$\delta g_y^p = 0 \quad (2.141)$$

$$\delta g_z^p = -\left(\frac{2g}{R}\right) \delta h \quad (2.142)$$

2.7 IRS SPECIFIC VELOCITY ERROR EQUATION

The instrument specific velocity error equations are obtained by applying the assumptions of equations 2.89 and 2.90 to the general velocity error equations developed in the last section.

Consider first the x axis general velocity error equation given by 2.134. The various terms that make up the total velocity equation will now be examined and the conditions of equations 2.89 and 2.90 applied.

Applying the instrument specific conditions to the third term from equation 2.134 gives :

$$(2W_{iez}^p + W_{epz}^p) \delta V_y^p = 2W_{iez}^p \delta V_y^p - (W_{epx}^p \delta \theta_y^p - W_{epy}^p \delta \theta_x^p) \delta V_y^p \quad (2.143)$$

Ignoring the small product of error terms gives :

$$(2W_{iez}^p + W_{epz}^p) \delta V_y^p = 2W_{iez}^p \delta V_y^p \quad (2.144)$$

The fourth term of equation 2.134 is not affected by the instrument specific equations, but using equation 2.19 it can be written as :

$$(2W_{iey}^p + W_{epy}^p) \delta V_z^p = 2W_{iey}^p \delta V_z^p + \frac{V_x^p}{R_x} \delta V_z^p \quad (2.145)$$

Considering the fifth term of equation 2.134 and applying the instrument specific condition of equation 2.91 and the component result from equation 2.74 gives :

$$(2\delta W_{iez}^p + \delta W_{epz}^p) V_y^p = 2(W_{iey}^p V_y^p + W_{epx}^p V_y^p) \delta \theta_y^p - (2W_{iey}^p V_y^p + W_{epy}^p V_y^p) \delta \theta_x^p \quad (2.146)$$

Considering the sixth term of equation 2.134 and applying equations 2.74 and 2.97 gives :

$$(2\delta W_{iey}^P + \delta W_{epy}^P) \delta V_z^P = (2\delta\theta_x^P W_{iez}^P - 2\delta\theta_z^P W_{iex}^P + \frac{1}{R_x} \delta V_x^P - W_{epy}^P \frac{\delta R_x}{R_x}) V_z^P \quad (2.147)$$

Using equation 2.89 this reduces to :

$$(2\delta W_{iey}^P + \delta W_{epy}^P) \delta V_z^P = (2\delta\theta_x^P W_{iez}^P + \frac{1}{R_x} \delta V_x^P - W_{epy}^P \frac{\delta R_x}{R_x}) V_z^P \quad (2.148)$$

These four terms can now be combined with the first and second terms from equation 2.134 to give the final instrument specific error equation for the x component of velocity :

$$\begin{aligned} \delta \dot{V}_x^P = & \delta a_x^P + 2W_{iez}^P \delta V_z^P - \frac{V_x^P}{R_x} \delta V_z^P + (2W_{iex}^P V_y^P + W_{epx}^P V_y^P) \delta \theta^P \\ & - (2W_{iey}^P V_y^P + W_{epy}^P V_y^P) \delta \theta_x^P - 2\delta\theta_x^P W_{iez}^P V_z^P \\ & - \frac{V_z^P}{R_x} \delta V_x^P + W_{epy}^P \frac{V_z^P}{R_x} \delta R_x^P \end{aligned} \quad (2.149)$$

The development of the equations for the y and z velocity error components follows the same method as for the x case above, so only the final result for the y and z components are shown :

$$\begin{aligned} \delta \dot{V}_y^P = & \delta a_y^P - 2W_{iez}^P \delta V_x^P + \frac{V_y^P}{R_y} \delta V_z^P - (2W_{iex}^P V_x^P + W_{epx}^P V_x^P) \delta \theta_y^P \\ & + (2W_{iey}^P V_x^P + W_{epy}^P V_x^P) \delta \theta_x^P - 2\delta\theta_y^P W_{iez}^P V_z^P \\ & - \frac{V_z^P}{R_y} \delta V_y^P - W_{epx}^P \frac{V_z^P}{R_y} \delta R_y^P \end{aligned} \quad (2.150)$$

$$\begin{aligned}
\delta \dot{V}_z^P &= \delta a_z^P + \delta g_z^P + (2W_{iey}^P + 2W_{epy}^P) \delta V_x^P - (2W_{iey}^P + 2W_{epy}^P) \delta V_y^P \\
&+ 2\delta\theta_x^P W_{iez}^P V_x^P - W_{epy}^P \frac{V_x^P}{R_x} \delta R_x \\
&+ 2\delta\theta_y^P W_{iez}^P V_y^P + W_{epx}^P \frac{V_y^P}{R_y} \delta R_y
\end{aligned} \tag{2.151}$$

The x and y velocity error equations above are mechanized as states in the optimal IRS state transition matrix as shown by figure 2-6. The z velocity error equation given by 2.151 above, requires further processing as it is unstable in its present form. The next section deals with the further processing required for the z velocity error equation.

2.8 BARO INERTIAL LOOP

The gravity term in the Inertial Reference system unaided velocity equation (see eq 2.151) is the source of potential instability, as it is a function of position and altitude. The altitude term used in the evaluation of the gravity value will potentially be in error due to any vertical accelerometer bias. The vertical channel velocity equation is therefore unstable.

To overcome the problem of instability, measurements from an outside reference source are combined with the inertial system vertical channel information, to form a stable system. The external reference source used in this instance is a barometric altimeter, which provides a measurement of barometric altitude. The barometric altitude is combined with the inertial system data by using a third order filter as shown in figure 2-4.

Ignoring the effect of transients, in a stationary condition the damped inertial altitude will follow the baro reference altitude, which is supplied from an air data computer system.

2.8.1 BARO INERTIAL LOOP ERROR MODEL DEVELOPMENT

The inertial reference system vertical channel unaided velocity equation is given by 2.123 as :

$$A_z^P = \dot{V}_z^P - g_z^P + (2W_{iey}^P + W_{epy}^P)V_x^P - (2W_{ieux}^P + W_{epx}^P)V_y^P \quad (2.152)$$

Where the equation used for the computed gravity value is :

$$g_z^P = 32.087448 + 0.1697\sin^2(\lambda) - 64.613 \frac{h}{R} \quad (2.153)$$

A baro inertial error model can be formed by assuming error components for the calculated gravity, rate of change of vertical velocity and coriolis terms. Figure 2-5 shows a block diagram of the baro loop error model.

The term δh_{ref} represents the error term from the baro inertial reference source. In practice there is often a lag effect associated with the baro inertial instrument.

The term DVZ represents the error value for the IRS rate of change of vertical velocity and computed coriolis terms as shown below :

$$\begin{aligned}
 DVZ = & \delta a_z^P + (2W_{iey}^P + 2W_{epy}^P) \delta V_x^P - (2W_{ieux}^P + 2W_{epx}^P) \delta V_y^P \\
 & + 2\delta\theta_x^P W_{iez}^P V_x^P - W_{epy}^P \frac{V_x^P}{R_x} \delta R_x + 2\delta\theta_y^P W_{iez}^P V_y^P + W_{epx}^P \frac{V_y^P}{R_y} \delta R_y
 \end{aligned} \tag{2.155}$$

The computed gravity error term δg in figure 2-5 is a function of altitude and is given by equation 2.142. The terms K_1 , K_2 and K_3 in figure 2.5 are gain terms chosen as follows :

$$K_1 = \frac{3}{\tau} \tag{2.156}$$

$$K_2 = \frac{3}{\tau^2} \tag{2.157}$$

$$K_3 = \frac{1}{\tau^3} \tag{2.158}$$

Where tau is the filter time constant which has been chosen to be 100 seconds.

The following state space equations can be applied to the error model :

$$\begin{bmatrix} \delta \dot{h} \\ \delta \dot{V} \\ \delta \dot{X} \end{bmatrix} = \begin{bmatrix} -K_1 & 1 & 0 \\ \left(\frac{2g}{a} - K_2\right) & 0 & -1 \\ K_3 & 0 & 0 \end{bmatrix} \begin{bmatrix} \delta h \\ \delta V \\ \delta X \end{bmatrix} + \begin{bmatrix} K_1 \\ K_2 \\ -K_3 \end{bmatrix} \delta h_{ref} + \begin{bmatrix} 0 \\ DVZ \\ 0 \end{bmatrix} \quad (2.154)$$

The states used to represent the baro inertial error model are mechanized to form part of the overall IRS error model state transition matrix, as shown in figure 2-6.

Now that specific IRS error model equations for position, attitude and velocity have been developed, the form of the model to be used for the two IRS sensors will be examined.

2.9 INERTIAL REFERENCE SYSTEM SENSORS

The strapdown inertial reference system has two sensors, gyros and accelerometers. Information about the specific errors associated with these instruments has been provided by the customer in the form of an IRS error budget table. Since it will be referred to in several other chapters of this thesis, the customer IRS error budget table is shown in appendix B.

2.9.1 RING LASER GYRO

The ring laser gyro measures rate, which is then integrated to get angle, thus it is a rate integrating gyro. The inertial reference system contains three ring laser gyros for the three input axes X^b , Y^b and Z^b (see figure 2-3). The error budget table (see appendix B) shows that the ring laser gyro has two sources of error, a random walk error, and a fixed gyro bias error.

The random walk is an error source that varies randomly with time. The term random walk refers to random walk in angle which is caused by integrating white noise in rate. To represent random walk in the IRS error model no states are required. The fixed bias error is a random constant error, that remains constant with time. The error budget table shows that the fixed bias values for the local level X and Y gyros have a lower value than for the Z gyro, this is due to the fact that the Z gyro quality does not need to be as good as the local level gyros as its impact on the resultant IRS performance is not as great. Three states are required to represent the three gyro bias errors. The states are shown in figure 2-6 by the terms ϵ_x , ϵ_y and ϵ_z .

2.9.2 ACCELEROMETER

The inertial reference system consists of three accelerometers for the three input axes (see figure 2-3). The accelerometers are single degree of freedom devices that use a proof mass suspended in a pendulous manner to measure acceleration. The error budget table shows that the accelerometer has three sources of error, a fixed bias, a wide band noise and a gravity anomaly error. The error values for all three accelerometers are the same. To represent the accelerometer correlated noise no states are required. To represent the accelerometer bias errors, three states are used, as shown by the terms ∇_x , ∇_y , and ∇_z in figure 2-6.

2.10 COMMENTS

The customer specific IRS error model has been developed in this chapter. It is in the form of a state vector matrix differential equation consisting of 17 states. The IRS error model is used as the basis for an IRS simulation module, which forms part of a total simulation program that is used to develop the Kalman filter.

The simulation program is discussed in chapter 5, where details are given of the method used to implement the IRS error model.

CHAPTER 3

GLOBAL POSITIONING SYSTEM

3.1 INTRODUCTION

The Navstar Global Positioning System (GPS) is a space based radio navigation system which provides position, velocity and time both globally and continuously. The GPS system comprises three major segments Space, Control, and User. The GPS development and production program for all three segments is managed by the US Air Force System Command, Space Division, Navstar GPS Joint Program Office at Los Angeles Air Force Station, California.

3.1.1 SPACE SEGMENT

The GPS space segment when fully operational will consist of 18 operational satellites and 3 active spares. The satellites will be placed in 6 orbital planes with 3 operational satellites in each plane and an active spare in every other plane to provide continuous 4 satellite coverage. The satellite orbital planes will have an inclination relative to the equator of 55 degrees and the orbit height will be 10,900 miles. The satellites will complete an orbit in approximately 12 hours. An observer on the ground will observe the same satellite ground track each day however, the satellite will become visible 4 minutes earlier each day due to a 4 minute / day difference between the satellite orbit time and the rotation of the earth.

The satellites radiate two spread spectrum pseudo random noise radio signals, at the following frequencies : $L_1 = 1575.42 \text{ MHz}$ and $L_2 = 1227.6 \text{ MHz}$. Both frequencies are derived from a highly stable on-board atomic clock. The spread spectrum techniques used are a Coarse / Acquisition code (C/A code) and a Precise code (P code). The L_1 frequency is sent using a C/A code and a P code, while the L_2 frequency is sent using only a P code. The C/A code is available to any GPS user either military or civilian, but the P code is only available to US Military users, NATO military users and other military users as determined by the US Department of Defense.

Both the P code and C/A code enable a receiver to determine the range between the satellite and the user. Since only the P code is on both frequencies, military users can make a dual frequency comparison to compensate for ionospheric propagation delay in the different transmission times.

The C/A code user must use a model for the ionosphere which results in a lesser navigation accuracy being obtained when compared to the P code user. Ananda (1988) reviews the navigation accuracy that can be achieved using GPS, by defining the concept of a user range error. Both the Space Segment, Control Segment and User Segments are analyzed.

3.1.2 CONTROL SEGMENT

The control segment consists of one Master Control Station (MCS) at Falcon Air force Station in Colorado Springs, USA plus monitor stations at Hawaii, Kwajalein, Diego Garcia and Ascencion. The monitor stations passively track all GPS satellites in view, collecting ranging data and satellite clock data from each satellite. This information is passed on to the MCS where the satellite future ephemeris and clock drift are predicted. Updated ephemeris and clock data are up-loaded to each satellite for later transmission to users. The control segment is also responsible for maintaining the health of the satellites.

3.1.3 USER SEGMENT

Navstar GPS can be used for different purposes including navigation for space, air, sea and land vehicles. The user segment consists of equipment with antenna, receiver, signal processing and data processing capabilities. Due to the large variety of users, several different types of GPS receivers are required.

3.2 BASIC GPS RECEIVER OPERATION

Satellite signals from each of the orbiting satellites can be received by the GPS receiver. Each satellite transmits a Navigation Message (NAV MSG) via almanac and ephemeris data. Almanac data contains information about all satellites in the constellation, whereas ephemeris data is specific to a single satellite. Before the Nav Msg can be read, the receiver has to track the carrier frequency being transmitted by the satellite, this is achieved via a carrier tracking loop.

Also the receiver has to track the C/A code and P code signals, this is achieved with a code tracking loop. The carrier tracking loop provides a measurement of relative velocity between the GPS receiver and the satellite being tracked. This measurement is commonly referred to as a delta range measurement. By using the relative velocity to four satellites the GPS receiver can determine its velocity relative to the earth.

Once the carrier tracking loop and the code tracking loop have locked on to the received signal the Nav Msg can be demodulated and the resultant satellite information processed. Contained within the Nav Msg is the time of transmission of the satellite signal, the GPS set can use this information together with the time it received the signal to make a measurement of range to the satellite.

To make an accurate measurement of range using time, the GPS receiver time source needs to be referenced to the GPS system time. This can be achieved by using an atomic time standard in the GPS receiver, however this type of time standard is expensive and not normally considered. Instead a cheaper crystal oscillator is used and the GPS receiver corrects its offset from GPS system time before calculating position. Because the GPS receiver clock introduces a bias to the true range to the satellite, the range measurement made is referred to as a pseudo range. By making four pseudo range measurements, the GPS receiver can estimate its position and GPS system time.

The GPS receiver calculates its position relative to the earth by using pseudo range measurements, and satellite position information which it obtains by decoding the Nav Msg. Consider figure 3-1. it shows the GPS receiver and satellite position (S_1) relative to the earth. The Earth Centred Earth Fixed (ECEF) frame of reference is shown by the axis set XYZ. The ECEF frame is defined as a frame which is fixed to the earth with its centre at the earths centre. Its X axis is defined as passing through the Greenwich meridian and the equator and the Z axis passing through the North pole. The frame of reference rotates about the Z axis with respect to inertial space at earth rate (Ω).

The satellite position in terms of ECEF coordinates is :

$$\underline{S}_1 = (S_{1x}, S_{1y}, S_{1z}) \quad (3.1)$$

Similarly the receiver position in terms of ECEF coordinates is:

$$\underline{U} = (U_x, U_y, U_z) \quad (3.2)$$

The satellite position relative to the earth is obtained by decoding the Nav Msg from satellite S_1 . The user position relative to the earth is computed using the pseudo range information from a total of four satellites, one of which is shown in figure 3-1. The actual range of satellite S_1 to the user is given by the distance r_1 however, because of the GPS receiver clock bias, the actual pseudo range measured is $(r_1 - c_b)$ where c_b is the user clock bias.

Thus an equation for the pseudo range measurement from satellite S_1 can be formed as follows :

$$(r_1 - c_b)^2 = (S_{1x} - U_x)^2 + (S_{1y} - U_y)^2 + (S_{1z} - U_z)^2 \quad (3.3)$$

This equation contains three unknowns relating to the user position, and one unknown relating to the receiver clock bias. Although the pseudo range measurement from each satellite is different, the user clock bias c_b , is the same. To solve for these four unknowns, three additional satellite equations are needed.

Once a value for user position has been evaluated, it will be in terms of ECEF coordinates. It will then have to be transformed into geodetic coordinates to provide latitude, longitude and altitude information. The transformation from ECEF to geodetic coordinates must be carried out by iteration or direct approximation, as an exact solution does not exist. Olson (1988) reviews several possible methods of calculating geodetic coordinates from ECEF coordinates.

The inverse transformation from geodetic to ECEF coordinates is exact, the transformation is shown below :

$$X = (R_c + h) \cos(\lambda) \cos(\Phi) \quad (3.4)$$

$$Y = (R_c + h) \cos(\lambda) \sin(\Phi) \quad (3.5)$$

$$Z = ((1 - e^2)R_c + h) \sin(\lambda) \quad (3.6)$$

Where the earth radius value R_c is given by :

$$R = \frac{R}{(1 - e^2 \sin^2 \lambda)^{\frac{1}{2}}} \quad (3.7)$$

In most GPS receivers, the measurement equations for position and velocity are implemented in a Kalman filter. For position, an estimate of pseudo range is made which is then used to update a state vector. The choice of GPS states chosen for the state vector generally includes position, velocity, clock bias and clock bias rate. Acceleration states can also be included to provide a smoother velocity estimate when operating in a dynamic environment.

No attempt is made here to discuss GPS Kalman filter design, as this information is not needed to understand the GPS error model used in this thesis. However, it is important to be aware of the GPS Kalman filter as it can have an impact on the IRS/GPS integration.

Two measurements have been discussed above, delta range relating to velocity and pseudo range relating to position. If these two raw measurements are output by the GPS receiver, then GPS position and velocity can be calculated by an external processor. Alternatively the GPS receiver can output its calculated position in terms of latitude/longitude and its velocity in terms of velocity north/east. Techniques to integrate GPS and IRS can utilize both types of GPS output, although the actual implementation is very dependant on which of the two possible GPS outputs is being used. Dayton (1989) discusses the advantages and disadvantages of both schemes.

3.3 ROCKWELL COLLINS 5 CHANNEL GPS RECEIVER

The type of GPS system being considered in this thesis is the Rockwell Collins 5 channel Receiver. This is a military system capable of tracking both C/A code and P code signals. It has a dedicated Control Display Unit (CDU) to allow the user to communicate with the system. Data is output to the Flight Management Computer via a MIL STD 1553 Communications Bus. This bus can also be used to control the GPS receiver, thus replacing the need for a dedicated CDU.

3.4 COMMENTS

A GPS simulation module is implemented as part of the overall simulation program used to develop the Kalman filter. Details of the GPS simulation module are given in chapter 5, where the simulation program is discussed.

The next chapter deals with the Kalman filter.

CHAPTER 4

KALMAN FILTER

4.1 INTRODUCTION

The Kalman filter is the means by which the outputs from the inertial reference system and the global positioning system are combined inside the flight management computer. In this chapter the theory relating to the Kalman filter is reviewed but not derived.

The IRS was discussed in chapter 2 where details were given for the development of an inertial reference system error model. From the IRS error model a Kalman filter error model can be developed. The development of the Kalman filter error model is discussed in this chapter.

The final part of the chapter deals with specific issues relating to the implementation of the Kalman filter in the flight management computer. Firstly, the solution of the Kalman filter transition matrix is discussed. This leads to the development of a fast/slow loop mechanization. Then, the technique used by the Kalman filter to model the IRS gyro and accelerometer errors is described.

4.2 KALMAN FILTER THEORY

Figure 4-1 shows a block diagram of a Kalman filter. The discrete Kalman filter equations relating to the diagram can be summarized as follows (reference Gelb 1987) :

System Model And Measurement Model Equations

$$\underline{X}_k = \underline{\Phi}_k \underline{X}_{k-1} + \underline{W}_{k-1} \quad (4.1)$$

$$\underline{\Phi}_k = \underline{\Phi}(t_k, t_{k-1}) \quad (4.2)$$

$$\underline{Z}_k = \underline{H}_k \underline{X}_k + \underline{V}_k \quad (4.3)$$

Where

\underline{W}_k is process noise of strength Q_k

\underline{V}_k is measurement noise of strength R_k

State Estimate And Error Covariance Extrapolation

$$\underline{\hat{X}}_k(-) = \underline{\Phi}_k \underline{\hat{X}}_{k-1}(+) \quad (4.4)$$

$$P_k(-) = \underline{\Phi}_k P_{k-1}(+) \underline{\Phi}_k^T + Q_{k-1} \quad (4.5)$$

State Estimate And Error Covariance Update

$$\underline{\hat{X}}_k(+) = \underline{\hat{X}}_k(-) + K_k [Z_k - H_k \underline{\hat{X}}_k(-)] \quad (4.6)$$

$$P_k(+) = [I - K_k H_k] P_k(-) \quad (4.7)$$

Kalman Gain Matrix

$$K_k = P_k(-) H_k^T [H_k P_k(-) H_k^T + R_k]^{-1} \quad (4.8)$$

The Kalman filter incorporates a system model in the form of a state transition matrix as shown by equation 4.1. Identification of the system model is one of the most difficult aspects in designing a Kalman filter. The form of the Kalman filter transition matrix used to represent the IRS error model is discussed in this chapter in section 4.3, and is shown to consist of 12x 12 matrix.

The Kalman filter takes a measurement \underline{Z}_k and subtracts from it the best prediction of its value before the actual measurement is made. In this work the measurements take the form of two position values, latitude and longitude, and two velocity values, velocity north and velocity east. These four data values are formed as the difference between IRS and GPS outputs. The measurement difference is then passed through an optimal weighting matrix \underline{K}_k and used to correct the best estimate of the state equation at the time instant before the measurement is taken. The optimal gain matrix \underline{K}_k is computed from the covariance prediction provided by equation 4.5, which can be interpreted as the Kalman filter uncertainty in its estimate of the system states. The gain matrix can be computed off line where the gain values can then be stored in a look up table for future use. In this application however, the gain matrix is computed in real time.

4.2.1 OBSERVABILITY

Observability is an important part of Kalman filter theory. Gelb (1986) gives the following statement for the observability condition for a continuous system :- A system is observable at time $t_1 > t_0$ if it is possible to determine the state $\underline{X}(t_0)$ by observing $\underline{Z}(t)$ in the interval (t_0, t_1) . If all states $\underline{X}(t)$ corresponding to all $\underline{Z}(t)$ are observable, the system is completely observable. A necessary and sufficient condition that the system defined by equations 4.1 and 4.2 be completely observable is that the observability matrix shown below be positive definite for some $t > t_0$ (reference Sorenson 1970).

$$M(t_0, t) = \int_{t_0}^t \Phi^T(t, t_0) H^T(t) H(t) \Phi(t, t_0) dt \quad (4.9)$$

The observability matrix can be seen to be dependant in part on the system state transition matrix. For the Kalman filter developed in this work the transition matrix is of order 12 x 12. The analytic computation of the observability matrix can only realistically be applied therefore using a computer.

When applying equation 4.9, the observability of the system is indicated by the fact that the resultant matrix is positive definite. In chapter 7 and 8 of this work the Kalman filters ability to observe states is discussed, no attempt is made however to apply equation 4.9.

4.3 SELECTING THE KALMAN FILTER STATE MODEL

In the chapter 2 an IRS error model suitable for modelling the customer inertial reference system was developed. In its final form the model contained 17 states, this being the total number of states thought necessary to accurately represent the inertial system behaviour for the proposed application. This 17 state IRS error model can be used as the basis for a Kalman filter error model, by making the Kalman filter state vector \underline{X} and system matrix F , equal to the IRS state vector and system matrix. In this form the Kalman filter is referred to as being an optimal Kalman filter because it contains the same number of states as the IRS error model. Although the Kalman filter should be able to accurately represent the IRS error performance using an optimal model, it is not often practical to implement the Kalman filter with such a large number of states, and therefore an alternative Kalman filter solution with a reduced number of states is developed. This reduced order filter is referred to as a sub optimal Kalman filter.

One method of producing a sub optimal Kalman filter is to use the technique of sensitivity analysis. Here the covariance equations of the optimal and sub optimal Kalman filters are compared in a systematic way, to determine the best choice of states that meet the requirements of the sub optimal design while still being representative of the real world system. One sub optimal design requirement may be for example that no more than 10 states can be accommodated in the state vector equation, as this is the maximum number of states that the real time software can process. Assume that the total number of states in the optimal Kalman filter model is 20, then in attempting to meet this sub optimal system requirement the Kalman filter designer would need to carry out a sensitivity analysis, where various states were selected for inclusion into the sub optimal Kalman filter model, and the filter performance for each selection of states, examined against the optimal filter performance.

No mention has yet been made of how the sub optimal states are initially selected. One method is for the filter designer to choose states based on some physical understanding of the system. Alternatively the "observability" test can be applied to the states being modelled. Here the observation matrix equation given by equation 4.9 could be used to determine how many state variables in the proposed sub optimal model can be separately estimated. If certain states cannot be estimated, then alternative states must be found.

The sensitivity analysis design process is time consuming and can lead to serious difficulties that affect the resultant sub optimal filter performance. One such difficulty is that of Kalman filter divergence. Because the sub optimal filter uses a reduced set of states when compared to the optimal filter, the covariance settings attributed to each state need to be carefully chosen, to avoid the situation where the sub optimal filter "thinks" it has learnt a particular state well, when in fact it has actually not learnt the state at all, because it was unable to distinguish between the modelled state and an un-modelled state, that just happened to be the true cause of the system error. The divergence of the Kalman filter in this way can cause the system to become unstable, therefore designing for stability is one of the main objectives of the sub optimal development process.

Another potential difficulty in the sub optimal design process is that of defining all of the real world situations that the system is likely to encounter. It is important that as many of these situations as is possible are simulated so that the performance of the sub optimal Kalman filter under these conditions is examined, to ensure correct system operation.

Identifying all of real world situations in this particular project would mean identifying all of the possible flight profiles for the customer aircraft. An alternative approach is to examine the individual optimal and sub optimal system states in detail to gain an understanding of what processes simulate the states and thus cause a system error. This understanding can then be used to design a series of flight profiles so that all of the states get exercised at least once during the series of flight simulations.

A general outline of the sub optimal Kalman filter design process has been discussed above. No attempt has been made to describe in detail the equations needed to implement the technique, because for this particular thesis the states necessary to form a sub optimal Kalman filter were provided by the customer, thus it was felt that because of this the lengthy process of sub optimal filter design was not needed. The philosophy behind this thinking was, that the states necessary to form a sub optimal Kalman filter have been provided, so the optimal IRS model could be used as a baseline with which to compare the sub optimal Kalman filter performance. Also, to circumvent the type of problems relating to filter divergence discussed above, the Kalman filter covariance initialisation parameters $P(0)$ and the noise matrix Q , could be used to tune the sub optimal filter to make its response to learning IRS errors slightly pessimistic.

The 12 states as supplied by the customer that make up the Kalman filter sub optimal model and the associated system matrix are shown in figure 4-2. The system matrix can be formed by taking the optimal IRS system matrix which consists of 17 x 17 states, and deleting those rows/columns that are not associated with the 12 sub optimal states. It is of interest to compare the optimal and sub optimal state vectors to gain an understanding of the reasons behind the choice of the 12 sub optimal states. The comparison of the IRS and Kalman filter state vectors is shown in figure 4-3, where it can be seen that all of the states that are included in the optimal state vector, but not the sub optimal state vector, can be associated with the IRS vertical channel. It was stated in chapter 2, section 2.8, that the inertial reference system vertical channel is unstable, and because of this a baro inertial loop is mechanized. As a result of using the baro inertial loop, the errors in the vertical channel are bounded, and have little affect on the local level axis errors. Therefore, the vertical channel effect can be ignored when choosing the states for the sub optimal Kalman filter. In some applications, the vertical channel is modelled in a separate filter. Graham (1986) discusses such a scheme intended for use in a standard integration filter.

Now that the form of the sub optimal Kalman filter system model is understood, issues relating to the implementation of the Kalman filter can be examined.

4.4 TRANSITION MATRIX EQUATION

The Kalman filter system matrix (F) used to represent the customer IRS error model has been shown to consist of a 12 x 12 matrix. The system matrix is needed to form the state transition matrix as used in equation 4.1. The solution of the transition matrix and its implementation in the Kalman filter will now be examined.

Consider a continuous system described by the linear stochastic vector differential equation as shown below :

$$\dot{\underline{X}} = F(t)\underline{X} + \underline{W} \quad (4.10)$$

Where :

\underline{X} is an $n \times 1$ state vector

$F(t)$ is an $n \times n$ system matrix whose elements are continuous functions of the independent variable t .

\underline{W} is an n dimensional gaussian white noise process with the following statistics :

$$E[\underline{W}] = 0 \quad (4.11)$$

$$E[\underline{W} \underline{W}^T] = Q(t) \delta(t - \tau) \quad (4.12)$$

Where $Q(t)$ is a $n \times n$ symmetric, non negative definite matrix and $\delta(t - \tau)$ is the dirac delta function.

The solution for equation 4.10 is given by :

$$\underline{X}(t) = \Phi(t, t_0)\underline{X}(t_0) + \int_{t_0}^t \Phi(t, \tau)\underline{W}(\tau) d\tau \quad (4.13)$$

Where $\Phi(t, \tau)$ is the transition matrix and is the solution of the matrix differential equation :

$$\frac{d\Phi(t, \tau)}{dt} = F(t)\Phi(t, \tau) \quad (4.14)$$

The transition matrix has the properties that :

$$\Phi(t_k, t_j) \Phi(t_j, t_i) = \Phi(t_k, t_i) \quad \text{for all } t_k, t_j, t_i \quad (4.15)$$

With

$$\Phi(0) = I$$

When implementing the Kalman filter a discrete form of the transition matrix equation is required. One possible solution for the transition matrix is the matrix exponential form as shown below :

$$\Phi(t, t_0) = e^{\int_{t_0}^t F(\tau) d\tau} \quad (4.16)$$

Which can be expanded to give the following solution for the transition matrix :

$$\Phi(t, t_0) = I + F\Delta t + F^2 \frac{\Delta t^2}{2} \quad (4.17)$$

Equation 4.17 is a solution for the transition matrix only if the following commutation property is valid :

$$F(t) \int_{t_0}^t F(\tau) d\tau = \int_{t_0}^t F(\tau) d\tau F(t) \quad (4.18)$$

For the Kalman filter implementation in this work, the exponential solution was not used, instead a Taylor series solution was implemented.

4.4.1 TAYLOR SERIES SOLUTION

The Taylor series solution for equation 4.14 is given by :

$$\Phi(t, t_0) = I + F\Delta t + \dot{F}\frac{\Delta t^2}{2} + F^2\frac{\Delta t^2}{2} \quad (4.19)$$

This equation shows that the Taylor series solution requires a value for the differential of the F matrix. One possible way of avoiding the need to generate the differential of the F matrix is to use a Runge Kutta method of integration, which requires a knowledge of certain functions ahead of time. For the implementation of the Kalman filter in the target system this information was not available, as the flight management computer which houses the Kalman filter only reads IRS and GPS measurements at certain times.

For the simulation program, generating the rate of change of the F matrix is not a problem, however for the actual Kalman filter implementation in the flight management computer, generation of the differential of the F matrix was considered to be a time intensive task, and therefore consideration was only given to a first order Taylor series solution.

For a first order solution the transition matrix takes the following discrete form :

$$\Phi(t_k, t_{k-1}) = I + F(t)\Delta t \quad (4.20)$$

The discrete transition matrix operates on the state vector as follows :

$$\underline{X}_k = \Phi(t_k, t_{k-1})\underline{X}_{k-1} \quad (4.21)$$

Thus the state transition matrix in this discrete form describes the influence of the state vector over one time period only, it does not provide the relationship between state vectors over all time.

4.4.2 KALMAN FILTER FAST LOOP SLOW LOOP MECHANISATION

The Kalman filter works on the assumption that its input measurements are un-correlated over time. In this implementation, to avoid any possibility of correlated measurements, the IRS and GPS measurements are processed by the Kalman filter every 30 seconds. The interval of 30 seconds was chosen by the fact that the GPS contains its own internal Kalman filter, which means that the GPS position and velocity outputs potentially become correlated with previous measurements if they are processed at too high a rate. Sturza (1984) also suggests a processing interval of 30 seconds.

As well as processing position and velocity information from the IRS, the Kalman filter also receives aircraft attitude information in the form of pitch, roll and azimuth. This data is used to form the Kalman filter F matrix, which in turn is used to compute the transition matrix. The fact that the IRS position and velocity information is required to be processed every 30 seconds, would normally mean that the computation of the F matrix would be carried out at the same rate. Consideration needs to be given to increasing the speed of computing the F matrix in this implementation however, because of the restriction that is placed on the transition matrix which is, that it can only be computed to first order.

An investigation was carried out to compare the results obtained from two Kalman filter modules, with the first module having the transition matrix coded using terms to first order, and the second module having the transition matrix coded using terms to second order. Using these two modules the results for different Kalman filter iteration times were investigated. A Taylor series expansion was used for the solution in both cases. The form of the transition matrix for each case is given below :

For 1st order :

$$\Phi(k+1,k) = I + F \Delta t \quad (4.22)$$

For 2nd order :

$$\Phi(k+1,k) = I + F \Delta t + (\dot{F} + F) \Delta t^2/2 \quad (4.23)$$

To investigate the effect of different Kalman filter iteration rates, runs for 30 seconds, 15 seconds, 5 seconds and 1 second were carried out for the two modules. The Kalman filter results for the two cases called at 30 seconds are shown in figure 4-4. The data shown in figure 4-4 is the first 8 states of the Kalman filter state vector \underline{X} . The result shows a noticeable difference between each of the 8 states. The result for the two filters being called at 15 seconds (result not shown) also showed a noticeable difference between states.

For the 5 second iteration rate the difference between the results for the two modules was very small as is shown by figure 4-5, indicating that at this rate the first order equation provides a similar result to the second order equation.

The 1 second results (not shown) were similar to the 5 second case. The Kalman filter design was therefore modified to include a fast loop and a slow loop. The fast loop being called at 5 seconds and the slow loop at 30 seconds. In the fast loop the Kalman filter state equation and the Kalman filter covariance extrapolation equation are computed.

The remainder of the Kalman filter equations are implemented in the slow loop. The 30 second slow loop is needed since the Kalman filter measurements need to be processed at this rate to avoid the effects of measurement correlation, as discussed. A summary of the Kalman filter equations implemented in the fast loop and slow loop are given below :

Fast loop

$$\underline{X}_k = \Phi_k \underline{X}_{k-1} + \underline{W}_{k-1} \quad (4.24)$$

$$P_k(-) = \Phi_k P_{k-1}(+) \Phi_k^T + Q_{k-1} \quad (4.25)$$

Slow loop

$$K_k = P_k(-)H_k^T[H_kP_k(-)H_k^T + R_k]^{-1} \quad (4.26)$$

$$P_k(+) = [I - K_kH_k]P_k(-) \quad (4.27)$$

$$\hat{X}_k(+) = \hat{X}_k(-) + K_k[Z_k - H_k\hat{X}_k(-)] \quad (4.28)$$

4.5 KALMAN FILTER MEASUREMENT PROCESSING

The Kalman filter state estimate equation 4.6, and the error covariance update equation 4.7, are all computed during the slow loop cycle as is the Kalman filter gain equation 4.8. The implementation of these equations will now be examined.

During the Kalman filter measurement process, four IRS and GPS measurements are made, these being two position measurements corresponding to the states X(1) and X(2) in the Kalman filter state vector, and two velocity measurements corresponding to the states X(3) and X(4) in the state vector. The GPS and IRS measurement residuals determine the form of the Kalman filter measurement matrix (H). Consider that initially a vector measurement is to be made such that the measurement matrix is required to be of order 4 x 12. The matrix order of the filter gain equation can now be examined. From equation 4.8 the gain matrix is given by :

$$K_k = P_k(-)H_k^T[H_kP_k(-)H_k^T + R_k]^{-1} \quad (4.29)$$

Which has the following matrix order :

$$K = [12 \times 12][12 \times 4]([4 \times 12][12 \times 12][12 \times 4] + [4 \times 4])^{-1} \quad (4.30)$$

This reduces to :

$$K = [12 \times 4] + [4 \times 4]^{-1} \quad (4.31)$$

From this equation it can be seen that to process the vector measurement an inversion of a 4 x 4 matrix is required which is a processor intensive activity. To avoid the need for a matrix inversion, a scalar form of measurement processing was implemented.

To implement a scalar measurement process, the gain equation is computed four times. The form of the measurement matrix H for the four measurements is given below :

For the position measurement associated with the state X(1)

$$H = [1, 0, 0, 0, 0, 0, 0, 0, 0, 0, 0, 0] \quad (4.32)$$

For the position measurement associated with the state X(2)

$$H = [0, 1, 0, 0, 0, 0, 0, 0, 0, 0, 0, 0] \quad (4.33)$$

For the velocity measurement associated with the state X(3)

$$H = [0, 0, 1, 0, 0, 0, 0, 0, 0, 0, 0, 0] \quad (4.34)$$

For the velocity measurement associated with the state X(4)

$$H = [0, 0, 0, 1, 0, 0, 0, 0, 0, 0, 0, 0] \quad (4.35)$$

The matrix form of the gain equation for the scalar measurement is:

$$K = [12 \times 1][1 \times 1]^{-1} \quad (4.36)$$

Establishing the form of the Kalman filter gain equation also establishes the form of the covariance update equation as shown below.

From equation 4.7 the Kalman filter update equation is :

$$P_k(+) = [I - K_k H_k] P_k(-) \quad (4.37)$$

Which has the following matrix order

$$P_k(+) = ([12 \times 12] - [12 \times 12][12 \times 1][1 \times 12][12 \times 12]) \quad (4.38)$$

In the implementation of the scalar measurement, equations 4.26, 4.27 and 4.28 need to be processed four times for each measurement. The Kalman filter covariance estimate equation as given by equation 4.25 is not dependant on the form of the measurement matrix, and therefore it only needs to be computed once during the scalar measurement scheme.

4.5.1 IMPLEMENTATION ISSUES

The implementation of the covariance update equation has some specific issues associated with it which need to be considered. The covariance update equation requires a long word length if it is to be calculated accurately, as the equation is often concerned with the small difference of large numbers. If implemented on a fixed word length computer, then the covariance update equation can lose its accuracy due to the accumulation of round off errors. This leads to numerical instability where the computed covariance matrices become non positive semi definite.

Potter (1963) aware of this potential problem in the conventional Kalman filter, formulated an alternative covariance algorithm in terms of a matrix square root which guarantees non negativity of the computed covariance matrix, whilst resulting in a stable update equation. Bierman (1976) produced a modified square root algorithm by use of a U-D factorization procedure. The Bierman U-D factorization approach achieves the same computational precision as the square root filter, but is computational more efficient, since it avoids any real time square root operations.

Since Potter and Bierman, there has been considerable work carried out in this area by various authors. Upadhyay (1979) discusses a solution to the processor loading problem that places a major constraint on the real time Kalman filter implementation, while Brown (1983) discusses how the U-D factorization algorithm which is normally associated with a scalar measurement scheme, can be extended to the more general vector measurement case, where the measurement noises are correlated.

The form of the covariance update equation implemented in this thesis is not based on the U-D factorization or the Potter square root approach. It is essentially the conventional Kalman filter equation, mechanized for a scalar measurement, carried out using double precision arithmetic. A trade study was not carried out to compare the accuracy of the U-D or Potter approaches against a double precision approach, because of development time limitations associated with the project. However, during the simulation development phase, a constant monitor was kept on the values of the covariance matrix diagonal terms to detect for negative values.

4.6 DEVELOPING THE KALMAN FILTER INSTRUMENT ERROR MODELS

Having established the form of the Kalman filter sub optimal system model, there is the need to develop the values required to initialize the Kalman filter covariance matrix $P(0)$ and the process noise matrix $Q(0)$. From the Kalman filter sub optimal state vector, two sources of instrument errors can be identified, gyro bias errors, and accelerometer bias errors. Associated with the gyro bias error is a gyro random walk. Associated with the accelerometer bias error is wide band noise, and a gravity anomaly error. The values needed to initialize the Kalman filter covariance matrix and the process noise matrix can be obtained by considering these instrument errors.

4.6.1 COVARIANCE MATRIX INITIALIZATION

The Kalman filter uncertainty of its estimate of the state vector \underline{X} is given by the values of the diagonal terms of the Kalman filter covariance matrix. The initial value given to the diagonal elements of the covariance matrix therefore represents the initial uncertainty of the Kalman filter states. Appendix C gives the relationship between the diagonal elements of the Kalman filter covariance matrix and the IRS states. The determination of the values needed to initialise the covariance matrix is often based on some a priori knowledge of the system. In this instance details of the gyro bias error values and the accelerometer bias error values are provided by the customer error budget table (see appendix B). For the remaining 7 states, engineering judgement was used. A summary of the 12 initialisation parameters for $P(0)$ is given in table 4-1.

This particular selection of the Kalman filter initialisation parameters does not take into account the various alignment conditions that may be encountered when operating with the customer inertial reference system. (In chapter 8, the topic of setting the Kalman filter covariance initialisation values to reflect a particular alignment condition is considered in detail. It is shown there, how the navigation performance of the Kalman filter can be improved by matching the initialisation values to the IRS alignment condition. The need to match the covariance parameters to the IRS alignment condition was only discovered as a result of the initial Kalman filter development work that was carried out in chapters 6 and 7. Therefore, for the Kalman filter work that is discussed in chapters 6 and 7 of this thesis, the general unmatched covariance values of table 4-1 are used.)

4.6.2 PROCESS NOISE MATRIX INITIALISATION

The values used in this matrix relate to gyro random walk and accelerometer correlated noise.

4.6.2.1 GYRO RANDOM WALK

The subject of gyro random walk was briefly discussed in chapter 2, where it was stated that gyro random walk is obtained by passing white rate noise through an integrator. To account for gyro random walk the elements of the 12×12 process noise matrix Q , that need to be initialized are those elements that correspond to the platform axis tilt states in the sub optimal state vector, these being $X(5)$, $X(6)$ and $X(7)$ see figure 4-2.

The process noise matrix is mechanized in terms of the body axis, therefore to obtain the correct value of process noise on elements that are mechanized in the platform axis, a similarity transformation is needed. The direction cosines that relate body axis to platform axis can be used to carry out the similarity transformation, as shown below :

$$Q_g^P = C_b^P Q_g^b C_P^b \quad (4.39)$$

The direction cosine matrix C_b^P was developed in chapter 2.

The elements of the process noise matrix Q_g^b that correspond to the three body mounted gyros are as follows :

$Q_g^b(1,1)$ - Relates to the x gyro random walk

$Q_g^b(2,2)$ - Relates to the y gyro random walk

$Q_g^b(3,3)$ - Relates to the z gyro random walk

The values used for the gyros to account for random walk are obtained from the customer error budget table (see appendix B). From the table the value for the X,Y and Z gyro random walk can be seen to be 0.002 deg/sqrt hr.

4.6.2.2 ACCELEROMETER CORRELATED NOISE

The customer error budget table given in appendix B lists the following two sources of accelerometer noise, wide band noise and gravity anomaly. Both of these noise sources need to be accounted for in the Kalman filter process noise matrix. An examination of the error budget table reveals that both of these noise sources are exponentially time correlated. For the wide band noise a correlation time is given, however for the gravity anomaly filter a spatial correlation distance is given as opposed to a correlation time. A correlation time of 225 seconds for example, can be obtained for the gravity anomaly filter by considering the correlation distance of 25 nm to be taken at a speed of 400 nm/hr.

Since the noise associated with the accelerometer is correlated, then a state is required if the correlated noise is to be modelled exactly.

One way of avoiding the need for additional states is to replace the exponentially time correlated noise with a white noise approximation, because white noise requires no states.

An equivalent equation will now be developed for the white noise approximation, to the accelerometer correlated noise. Consider an exponentially correlated error, it can be described by the following continuous state equation :

$$\dot{X}(t) = -\frac{1}{T_c}X(t) + W(t) \quad (4.40)$$

Where

T_c - correlation time

$W(t)$ - white noise

$X(t)$ - has variance σ^2

$$E\{ W(t) \cdot W(t + \tau) \} = [2 \sigma^2/T_c] \delta(\tau)$$

The steady process auto correlation function for the correlated error is given by :

$$\psi_{xx}(\tau) = \sigma^2 e^{-\frac{|\tau|}{T_c}} \quad (4.41)$$

The power spectral density function can be formed from the auto correlation function using the fourier transform pair equation shown below :

$$S_f(\omega) = 2 \int_{-\infty}^{+\infty} \sigma^2 e^{-\frac{|\tau|}{T_c}} \cos(\omega\tau) d\tau \quad (4.42)$$

Evaluating this equation gives the following power spectral density function :

$$S_f(\omega) = \frac{2 \frac{\sigma^2}{T_c}}{\omega^2 + \frac{1}{T_c^2}} \quad (4.43)$$

Figure 4-6 shows the power spectral density versus frequency plot for equation 4.43 . At zero frequency the amplitude of the power spectral density plot is given by :

$$S_f(\omega) = 2\sigma^2 T_c \quad (4.44)$$

This equation gives the required value of noise needed for the white noise approximation to the correlated model. The value of Q needed for the Kalman filter implementation can be calculated using the discrete equivalent form of equation 4.44 which is :

$$Q = 2\sigma^2 T_c G_0^2 \Delta t \quad (4.45)$$

Where

G_0 is the scaling term from g to nm/hr

And

Δt is the Kalman filter iteration time

To take account of the two accelerometer noises, the rms values for wide band noise and gravity anomaly are Rssed. The 1 sigma values used for the two noises are 30 ug for the gravity anomaly and 3 ug for the wide band noise, these values having been obtained from the customer error budget table (see appendix B).

The process noise values that account for the accelerometer correlated noise are placed on the elements of the Q matrix that corresponds to platform axis velocity, these states being X(3) and X(4). The value of process noise obtained from equation 4.45 is mechanized in terms of the body axis.

A similarity transformation is therefore needed to obtain the correct values of process noise in terms of the platform axis. The form of the similarity transformation needed is shown below :

$$Q_a^p = C_b^p Q_a^b C_p^b \quad (4.46)$$

Where

$Q_a^b(1,1)$ - Relates to the total x accelerometer process noise

$Q_a^b(2,2)$ - Relates to the total y accelerometer process noise

The similarity transformation for the accelerometer process noise, and the gyro process noise shown above consist of two separate 3 x 3 matrix processes. For the actual Kalman filter implementation a single Q matrix of order 12 x 12 is required, therefore the output from the two matrices Q_g^p and Q_a^p has to be mapped into a 12 x 12 result.

It has been stated that for the gyro random walk, the associated process noise gets placed on elements relating to the platform axis tilt states, the corresponding mapping needed to achieve this for the elements of the Q_g^p matrix is shown below, where the left matrix is part of the final 12 x 12 result.

$$\begin{bmatrix} Q(5,5) & Q(5,6) & Q(5,7) \\ Q(6,5) & Q(6,6) & Q(6,7) \\ Q(7,5) & Q(7,6) & Q(7,7) \end{bmatrix} = \begin{bmatrix} Q(1,1) & Q(1,2) & Q(1,3) \\ Q(2,1) & Q(2,2) & Q(2,3) \\ Q(3,1) & Q(3,2) & Q(3,3) \end{bmatrix} \quad (4.47)$$

Similarly the mapping for the x and y accelerometer elements from the Q_a^p matrix to the final 12 x 12 result is given by :

$$\begin{bmatrix} Q(3,3) & Q(3,4) \\ Q(4,3) & Q(4,4) \end{bmatrix} = \begin{bmatrix} Q(1,1) & Q(1,2) \\ Q(2,1) & Q(2,2) \end{bmatrix} \quad (4.48)$$

Although the mapping technique described above is not very elegant, and a more complete technique is certainly required for the final algorithm implemented in the target system, it was found to be useful during the simulation phases of development.

4.7 COMMENTS

In this chapter the Kalman filter error model for the customer inertial reference system has been developed. The Kalman filter error model consists of 12 states. In chapter 2, the IRS error model was developed which consists of 17 states. The Kalman filter error model is therefore referred to as a sub optimal error model, since it contains a smaller number of states than the IRS error model.

The Kalman filter is implemented in the simulation program in two modules. These two modules form just part of the total simulation program. The simulation program is discussed in detail in the next chapter, where, specific details are given on how the Kalman filter equations are implemented.

CHAPTER 5

SIMULATION PROGRAM

5.1 INTRODUCTION

The Kalman filter development work has been carried out using a Fortran simulation program running on a Vax computer system. The simulation program is of modular design consisting of 11 main modules as shown by figure 5-1. The IRS and GPS modules simulate the two instruments that the flight management computer interfaces to, while the Kalman filter module, the KFMUPD module, the FIX module and the CDU module all simulate functions that are carried out inside the flight management computer.

The executive module is the main program module that controls the calling rates of the other subroutines. The Executive module calls the Rig, Kalman Filter, CDU, Fix and Data Storage modules. The Rig module calls the IRS, GPS and Rworld modules, and accepts user inputs to the simulation.

The Rworld module is used to generate true aircraft parameters for position, velocity and attitude. The IRS module uses the outputs from the Rworld module to generate IRS parameters for position, velocity and attitude, by corrupting the true aircraft values with errors. The IRS errors are generated as outputs from the IRS error model equation. The GPS module is similar to the IRS module in that it accepts true aircraft parameters from the Rworld module, and then corrupts the parameters with errors, to form GPS position and velocity outputs.

The Kalman filter equations are split between the Kalman filter module and the KFMUPD module. The Kalman filter module uses outputs from the IRS routine to form the Kalman filter transition matrix equation. The transition matrix is then used to form estimates for the Kalman filter state vector, and covariance update equations. Outputs from the IRS and GPS modules are used by the Kalman filter module to form the Kalman filter input measurements. Once the input measurements have been formed, the Kalman filter calls the KFMUPD module, where the filter gain and update equations are implemented.

The Fix module is used to initialise the Kalman filter covariance matrix.

The CDU module takes outputs from the IRS, GPS and Kalman filter modules and computes values for FMC, IRS, GPS and Kalman filter position error.

The remaining modules are the Data Storage and Maths Routines. The Data Storage module controls the recording of all program parameters. The Maths module contains various matrix and vector routines as well as geometric routines, which are used by other program modules.

A full listing of the simulation program as used, is given in a separate document Smiths (1991). Before each simulation module is discussed in detail, the accuracy of the simulation program will be examined.

5.2 SIMULATION ACCURACY

A Vax 3100 satellite terminal linked to a Vax 780 mainframe was used as the host computer to carry out all of the simulation work. It is important particularly for the computation of the Kalman filter covariance matrix equations to be aware of the accuracy of numbers that are represented in single precision and double precision format. The accuracy of single and double precision numbers can be assessed in the following way.

Consider the machine unit of a digital device denoted by u_m , to be the smallest possible increment in a stored mantissa. The precision of such a digital device, which is defined as the maximum number of significant decimal digits that it can store accurately, is given by the integer value of k in the following formula (reference Maron 1987) :-

$$10^{-(k+1)} < u_m \leq 10^{-k} \quad (5.1)$$

For single precision numbers stored on the Vax, the mantissa is 23 bits, this gives k an integer value of 6 as shown below

$$10^{-7} < 2^{-23} \leq 10^{-6} \quad (5.2)$$

So numbers stored using single precision on the Vax are accurate to six decimal places. For double precision representation, the mantissa is 55 bits, which gives an accuracy of 2^{-55} . Double precision arithmetic is used for all of the simulation modules.

5.3 EXECUTIVE MODULE

The Executive module controls the calling rates for all of the program modules. An overview of the calling rates and the modules called by the Executive is given in figure 5-2. It can be seen from figure 5-2 that the Executive first calls a module called Rig, which in turn calls three other modules, Rworld, IRS and GPS. All of the other program modules are called directly from the Executive. As well as calling other modules, the Rig module is used to accept the user input values used by the simulation. The iteration rates used in the Kalman filter simulation module, correspond to the rates used in the actual flight management computer system.

5.4 RWORLD MODULE

The purpose of this module is to simulate a realistic aircraft and generate true aircraft parameters, which can then be passed as inputs to other modules. The Rworld module is specific in that it is designed for use with the customer Inertial Reference System, which has a non standard platform axis set, where the z axis is defined positive up. The Rworld simulation module consists of three parts, the velocity mechanization, the position mechanization and the turn mechanization. These three parts will now be examined.

5.4.1 AIRCRAFT VELOCITY MECHANIZATION

The simulation program generates values for the aircraft body axis velocities. These velocity components are then transposed via a direction cosine matrix into the IRS platform axis, before being finally resolved into North/South and East/West velocity.

Figure 5-3a shows the aircraft body axis velocity parameters u , v and w . The Rworld module does not simulate aircraft side slip, therefore the velocity parameter v is taken to be zero. The other aircraft velocities u and w can be formed from values of angle of attack (α) and true airspeed (V_T). The true airspeed parameter (V_T) is a user input to the program, while the angle of attack parameter (α) is calculated from an empirical relationship which is a function of true airspeed.

The following equations express the aircraft body velocities in terms of true airspeed and angle of attack:

$$w = -V_T \sin \alpha \quad (5.3)$$

$$u = -V_T \cos \alpha \quad (5.4)$$

For non level flight, the flight path angle (γ) also needs to be calculated. Figure 5-3b shows the relationship between flight path angle, angle of attack and pitch (θ) for an aircraft in non level flight.

The following equation expresses the relationship between these parameters.

$$\theta = \gamma + \alpha \quad (\phi = 0) \quad (5.5)$$

The flight path angle is calculated as follows :

$$\sin\gamma = \frac{v_z}{v_T} \quad (5.6)$$

Where the vertical speed v_z is a user input.

Once the aircraft body axis values have been obtained they are transformed into equivalent values in the IRS platform axis. A transformation from body axis to platform axis parameters can be made by using the direction cosine matrix C_b^p whose elements are functions of pitch (θ), roll (ϕ) and azimuth (ψ). The required transformation is shown below.

$$\begin{bmatrix} v_x^p \\ v_y^p \\ v_z^p \end{bmatrix} = C_b^p \begin{bmatrix} v \\ u \\ w \end{bmatrix} \quad (5.7)$$

Where C_b^p is given by :

$$\begin{bmatrix} \cos\psi\cos\theta - \sin\psi\sin\theta\sin\phi, & -\sin\psi\cos\theta, & \cos\psi\sin\theta + \sin\psi\sin\theta\cos\phi \\ \sin\psi\cos\theta + \cos\psi\sin\theta\sin\phi, & \cos\psi\cos\theta, & \sin\psi\sin\phi - \sin\theta\cos\phi\cos\psi \\ -\cos\theta\sin\phi, & \sin\theta, & \cos\theta\cos\phi \end{bmatrix}$$

The direction cosine matrix C_p^b is formed from the transpose of the matrix C_b^p which was developed in chapter 2, section 2.2.2.

Once the local level platform axis velocities are obtained, they can finally be resolved via the IRS alpha angle into true values of North/South and East/West velocity. Both platform axis velocity and geographic velocity are available as outputs to the other modules. Platform axis velocities are used by the IRS and GPS modules where they are corrupted with an error term to form IRS and GPS velocity values.

5.4.2 AIRCRAFT TURN MECHANIZATION

To mechanize a turn in the simulation program the following aircraft turn equation is implemented.

$$\psi = \frac{g \tan \phi}{v_T} \quad (5.8)$$

Where :

- ψ - rate of change of aircraft heading (rads/sec)
- g - gravity (ft/sec²)
- v_T - true airspeed (ft/sec)
- ϕ - roll (rads)

The user is required to input a desired aircraft heading (ψ). This desired heading value is then compared with the present aircraft heading, if the two heading values are different, then a roll (ϕ) is applied to turn the aircraft. During the turn the rate of change of aircraft heading is computed from equation 5-8, this allows the actual aircraft heading to be calculated. The desired aircraft heading and computed aircraft heading are compared, when the two values are equal the roll command is removed.

A roll delay, similar to that encountered in a conventional autopilot is also simulated using the equation shown below, where the time constant value (τ) has been chosen to be 2 seconds.

$$\phi = \frac{\phi_d}{1 + \tau s} \quad (5.9)$$

Where :

- ϕ - commanded roll
- ϕ_d - demanded roll
- τ - time constant

The computed value of aircraft pitch, roll, heading and rate of change of heading are available as outputs to the other modules.

5.4.3 AIRCRAFT POSITION

The Rworld module provides aircraft position in terms of latitude, longitude and alpha angle. These parameters are obtained from the direction cosine matrix C_e^p , which provides the relationship between the IRS platform axis and the earth geographic axis. This direction cosine was discussed in chapter 2, section 2.2.1, where it was shown how geodetic latitude, longitude and alpha angle could be derived from elements of the direction cosine matrix.

To simulate normal flight, the direction cosine matrix elements need to be constantly updated to keep track of the changing aircraft position. One possible method to update the direction cosine matrix is to use the following differential equation which was previously discussed in chapter 2, section 2.2.1 :

$$\dot{C}_e^p = W_{ep}^{pk} C_e^p \quad (5.10)$$

Where :

$$W_{ep}^{pk} = \begin{bmatrix} 0 & -w_z^p & w_y^p \\ w_z^p & 0 & -w_x^p \\ -w_y^p & w_x^p & 0 \end{bmatrix} \quad (5.11)$$

The terms w_x^p , w_y^p and w_z^p are angular rates which can be written in terms of the platform axis velocities as follows :

$$w_x^p = -\frac{V_y^p}{R_y} \quad (5.12)$$

$$w_y^p = \frac{V_x^p}{R_x} \quad (5.13)$$

$$w_z^p = 0 \quad (5.14)$$

The value of the rate term w_z^p is taken to be zero, because the IRS system being simulated is a wander azimuth system.

The above equations show how starting with the platform axis velocities, platform axis transport rates can be formed, which can then be used to update the direction cosine matrix, to provide updated values for latitude, longitude and alpha angle.

Although this direction cosine matrix update technique is valid, one of the requirements for the aircraft model is that it should be able to simulate flights in the polar regions, particularly the North pole. The direction cosine technique is not able to easily cope with polar region transitions because at the pole the value of some of the terms can become indeterminate. Because of this an alternative mechanization using quaternions was used. In the quaternion implementation, the direction cosine matrix is still used to form latitude, longitude and alpha angle values, the only difference is that the quaternion is updated from the platform axis velocities, and the direction cosine matrix elements are formed from the updated quaternion equation.

5.4.3.1 QUATERNION REPRESENTATION OF POSITION

Quaternions is a body of mathematics which is commonly used in the field of navigation to describe rigid body rotations. They were first developed by Sir William Rowan Hamilton. In this work Quaternions are used to represent position in the Rworld simulation module. Quaternions are also used in the actual customer inertial reference system where they transform measurements made by the gyro into components of the platform axis frame of reference. This use of quaternions in the IRS is discussed by Edwards (1971) and Bronkhorst (1978).

A quaternion (\mathbf{q}) is defined as a combination of a scalar (λ) and a vector (\mathbf{P}) with orthogonal components, the basic form of the quaternion is shown below :

$$\mathbf{q} = (\lambda, \underline{\mathbf{P}}) \quad (5.15)$$

Where λ is a scalar and $\underline{\mathbf{P}}$ is a vector.

The use of the quaternion to represent position in the Rworld module is shown in figure 5-4. Three quaternions \mathbf{q}_a , \mathbf{q}_b and \mathbf{q}_c can be formed for the three parameters latitude, longitude and alpha angle as follows :

For longitude

$$\mathbf{q}_a = (\cos \frac{\Phi}{2}, 0, \sin \frac{\Phi}{2}, 0) \quad (5.16)$$

For latitude

$$\mathbf{q}_b = (\cos \frac{\lambda}{2}, -\sin \frac{\lambda}{2}, 0, 0) \quad (5.17)$$

For alpha angle

$$\mathbf{q}_c = (\cos \frac{\alpha}{2}, 0, 0, \sin \frac{\alpha}{2}) \quad (5.18)$$

These three quaternions can be combined to form a final quaternion which transforms a vector with coordinates expressed in the platform frame of reference, into an equivalent vector expressed in components of the earth frame of reference. This quaternion operation is shown mathematically as :

$$\mathbf{q} \underline{\mathbf{v}}^p \mathbf{q}^* = \underline{\mathbf{v}}^e \quad (5.19)$$

The multiplication of the three quaternion elements representing latitude, longitude and alpha angle is carried out in the following order :

$$\mathbf{q}_{ab} = \mathbf{q}_a \cdot \mathbf{q}_b \quad (5.20a)$$

Followed by :

$$\mathbf{q}_{ac} = \mathbf{q}_{ab} \cdot \mathbf{q}_c \quad (5.20b)$$

The final quaternion result \mathbf{q}_{ac} is given by :

$$\mathbf{q} = (\cos\phi/2 \cos\lambda/2 \cos\alpha/2 - \sin\phi/2 \sin\lambda/2 \sin\alpha/2, \quad (5.20c)$$

$$-\cos\alpha/2 \cos\phi/2 \sin\lambda + \sin\phi/2 \cos\lambda/2 \sin\alpha/2,$$

$$\cos\alpha/2 \sin\phi/2 \cos\lambda/2 + \cos\phi/2 \sin\lambda/2 \sin\alpha/2,$$

$$\cos\phi/2 \cos\lambda/2 \sin\alpha/2 + \cos\alpha/2 \sin\phi/2 \sin\lambda/2)$$

This final result shows how the quaternion can be initialized to a particular starting position, when the latitude, longitude and alpha angle for the initial position are given.

Once the quaternion has been initialized, it needs to be updated to keep track of the changing aircraft position. A quaternion differential equation can be developed in terms of the platform axis velocities. The result is shown in its final form below :

$$\dot{\mathbf{q}} = \frac{1}{2} \mathbf{q} \mathbf{w} \quad (5.21)$$

Where the rotation vector \mathbf{w} has the components :

$$w_x^p = -\frac{v_y^p}{R_y} \quad (5.22)$$

$$w_y^p = \frac{v_x^p}{R_x} \quad (5.23)$$

$$w_z^p = 0 \quad (5.24)$$

The quaternion differential equation above (see eq 5.21) needs to be solved to give a discrete time solution that can be implemented in the simulation program. The discrete solution is :

$$q(t + \Delta t) = q(t) [(1, 0) + (0, \theta/2)] \quad (5.25)$$

The final stage in using the quaternion to represent position, is to generate from the updated quaternion a value for the direction cosine matrix C_c^p , from which, the final values for latitude and longitude and alpha angle can be formed.

The equations linking the quaternion and the direction cosine matrix C_c^p are shown in component form below :

$$c_{11} = q_1^2 - q_2^2 - q_3^2 + q_4^2 \quad (5.26)$$

$$c_{12} = 2(q_1q_2 + q_3q_4) \quad (5.27)$$

$$c_{13} = 2(q_1q_3 - q_2q_4) \quad (5.28)$$

$$c_{21} = 2(q_1q_2 - q_3q_4) \quad (5.29)$$

$$c_{22} = -q_1^2 + q_2^2 - q_3^2 + q_4^2 \quad (5.30)$$

$$c_{23} = 2(q_2q_3 + q_1q_4) \quad (5.31)$$

$$c_{31} = 2(q_1q_3 + q_2q_4) \quad (5.32)$$

$$c_{31} = 2(q_2q_3 - q_1q_4) \quad (5.33)$$

$$c_{33} = -q_1^2 - q_2^2 + q_3^2 + q_4^2 \quad (5.34)$$

The computed value of the true direction cosine matrix C_e^p is output to the IRS and GPS modules, where the value is corrupted to form the IRS and the GPS position parameters.

5.5 INERTIAL REFERENCE SYSTEM MODULE

The IRS module receives inputs from the Rworld module, these inputs can be considered to be true aircraft values which are then corrupted by error values to form the final IRS position and velocity outputs. The error values that are used to corrupt the true position and velocity parameters are generated as outputs from a state vector matrix differential equation. The state transition matrix for the customer IRS error model was developed in chapter 2 (see figure 2-6), where the IRS time state vector was shown to consist of 17 states. The discrete form of the state vector matrix differential equation which is implemented in the simulation program is shown below :-

$$\underline{X}_k = \Phi(t_k, t_{k-1}) \underline{X}_{k-1} \quad (5.35)$$

Where the following Taylor series solution is used for the transition matrix :-

$$\Phi(t_k, t_{k-1}) = I + F_k \Delta t + \dot{F}_k \frac{\Delta t^2}{2} + F_k^2 \frac{\Delta t^2}{2} \quad (5.36)$$

From the updated state vector the two position states $\delta \theta_x^p$ and $\delta \theta_y^p$ which correspond to the vector elements $x(1)$ and $x(2)$ are used to corrupt the true value of the earth to platform direction cosine matrix C_e^p . This is achieved using the following equation :-

$$[C_e^p]_{irs} = [C_e^p]_{true} + \delta C_e^p \quad (5.37)$$

With the value for the direction cosine error being given by :-

$$\delta C_e^p = \delta \theta^p [C_e^p]_{true} \quad (5.38)$$

This direction cosine matrix error equation was developed in chapter 2 (see equation 2-46).

Once the IRS direction cosine matrix update has been calculated, values for IRS latitude, longitude and alpha angle can be obtained. These values of IRS position are output to the Kalman filter module where they are combined with GPS position values, to form a Kalman filter position measurement.

IRS platform axis velocity parameters are formed by combining the true values of platform axis velocity, which are output by the Rworld module, with velocity error terms obtained from the IRS state vector.

The velocity equations implemented are shown below :-

$$[V_x^p]_{irs} = [V_x^p]_{true} + \delta V_x \quad (5.39)$$

$$[V_y^p]_{irs} = [V_y^p]_{true} + \delta V_y \quad (5.40)$$

Here, the velocity error terms δV_x^p and δV_y^p correspond to the state vector elements X(4) and X(5). The IRS platform axis velocities are finally resolved via the computed value of IRS alpha angle, into components of North and East velocity. The geographic velocity values are output to the Kalman filter module where they are combined with GPS velocity to form a velocity measurement input to the Kalman filter.

5.5.1 SIMULATION OF THE IRS GYRO ERRORS

The errors associated with the ring laser gyro are a gyro bias error and a random walk error. The ring laser gyro is a rate integrating device, so the random walk figure refers to a random walk in angle which is caused by integrating white rate noise.

To simulate gyro bias, an initial value is given to the appropriate gyro bias element in the state vector $\underline{x}(0)$. The elements of the state vector that correspond to the x,y and z gyro bias are X(10), X(11) and X(12).

To simulate random walk, an in-house computer module called Rgauss is used, which when called produces data with an RMS value of unity. Thus by scaling the output from the module, the rms value of the output data can be controlled.

The single sided power spectral density plot for the Rgauss module is given in figure 5-5a , and shows a cut off frequency of $1/2\Delta t$, where Δt is the rate that the Rgauss module is called.

A ring laser gyro with a specific value of angle random walk is simulated by the method shown in figure 5-5b . The constant k is chosen to give a value of rate white noise which when integrated, gives the desired angle random walk. The equation for choosing k is given below :

$$K = \sqrt{2(RW)^2 \frac{1}{2\Delta t}} \quad (5.41)$$

Where

RW - Gyro Random Walk value (deg/sqr root hr)
 Δt - IRS module iteration time (seconds)

5.5.2 SIMULATION OF THE IRS ACCELEROMETER ERRORS

The main sources of error associated with the accelerometers are a fixed bias error, and a random correlated error which is made up of two components, wide band noise and gravity anomaly.

To simulate accelerometer bias an initial value is given to the appropriate accelerometer bias element in the state vector. The elements of the state vector that correspond to the x,y and z accelerometer biases are X(13), X(14) and X(15).

To simulate accelerometer correlated noise, the model shown in figure 5-6a is used. This is a general model which will now be analyzed to develop the specific models that are used for the simulation of wide band noise and gravity anomaly. The transfer function for the model is given by :-

$$\frac{y(s)}{x(s)} = \frac{1}{1 + \tau s} \quad (5.42)$$

Where τ - Time Constant

The equivalent equation for the discrete model as shown by figure 5-6b is given by :

$$Y_k = Y_{k-1} + \frac{\Delta t}{\tau} (x_{k-1} - Y_{k-1}) \quad (5.43)$$

It is necessary for the purposes of the simulation to form an equation for the rms of the input in terms of the rms of the output. This relationship can be formed by taking the z transform of the discrete model above, where the term $\Delta t/\tau$ is not considered as it only a scaling term.

From the discrete equation can write

$$Y_k = (1 - \frac{\Delta t}{\tau})Y_{k-1} + x_{k-1} \quad (5.44)$$

Taking the z transform gives

$$y(z) = y(z)z^{-1}(1 - \frac{\Delta t}{\tau}) + x(z) \quad (5.45)$$

Which gives

$$y(z) = \frac{x(z)}{1 - (1 - \frac{\Delta t}{\tau})z^{-1}} \quad (5.46)$$

By using a binomial expansion the equation can be written as

$$y(z) = [1 + (1 - \frac{\Delta t}{\tau})z^{-1} + (1 - \frac{\Delta t}{\tau})^2 z^{-2} + \dots]x(z) \quad (5.47)$$

The equation can now be written in terms of variance as follows

$$\frac{\sigma_y^2}{\sigma_x^2} = 1 + (1 - \frac{\Delta t}{\tau})^2 + (1 - \frac{\Delta t}{\tau})^4 + \dots \quad (5.48)$$

Which can be written as

$$\frac{\sigma_y^2}{\sigma_x^2} = \frac{1}{1 - \left(1 - \frac{\Delta t}{\tau}\right)^2} \quad (5.49)$$

By expansions of the lower bracket the equation can finally be written as :

$$\sigma_x = \sqrt{\frac{2\Delta t}{\tau}} \sigma_y \quad (5.50)$$

Where

$$\frac{\Delta t^2}{\tau^2} \text{ is small} \quad (5.51)$$

This final equation gives the rms value of input noise that must be passed through the correlated model, to produce the desired value of output.

The form of the final simulation model for the two correlated noise sources is given by figure 5-7. The constants k_n and k_g are used to scale the white noise obtained from the Rgauss function, so that the correct value of input noise is generated in each case, to give the desired level of correlated output noise. The values of k for the two correlated noise sources is given below

For the wide band noise

$$K_n = \sqrt{\frac{2\Delta t}{0.5}} \quad 3 \times 10^{-6} \quad (5.52)$$

And for the Gravity Anomaly

$$K_g = \sqrt{\frac{2\Delta t}{225}} \quad 30 \times 10^{-6} \quad (5.53)$$

Where

Δt is the IRS module iteration rate.

5.6 GLOBAL POSITIONING SYSTEM MODULE

The methods used in the GPS simulation module to generate values of position and velocity are based on the same techniques as used for the IRS error model discussed above. The GPS error model simulation is therefore, not a sophisticated error model covering orbiting satellites, radio signal transmissions, GPS Kalman filter modelling etc. To generate values for GPS latitude and longitude, the true value of the earth to platform direction cosine matrix received from the Rworld module, is corrupted by an error direction cosine matrix to form a GPS direction cosine matrix. The equation used to form the GPS direction cosine matrix is shown below :

$$[C_e^P]_{GPS} = [C_e^P]_{TRUE} + \delta C_e^P \quad (5.54)$$

Where the direction cosine error (see eq 5.38) in its component form is :

$$\delta C_e^P = \begin{bmatrix} 0 & 0 & -\delta\theta_y^P \\ 0 & 0 & \delta\theta_x^P \\ \delta\theta_y^P & -\delta\theta_x^P & 0 \end{bmatrix} \begin{bmatrix} C_{11} & C_{12} & C_{13} \\ C_{21} & C_{22} & C_{23} \\ C_{31} & C_{32} & C_{33} \end{bmatrix} \quad (5.55)$$

In the IRS simulation module the X and Y platform axis tilts are obtained as states from a state vector matrix differential equation. This method cannot be applied to the GPS module however, as a GPS state vector matrix differential equation is not being simulated.

A simpler approach to generating the GPS X and Y tilt values is therefore taken as shown below :

$$\delta \theta_x^p = - \frac{R_{\text{gauss}} \times \text{Gps noise}}{r_e} \quad (5.56)$$

$$\delta \theta_y^p = - \frac{R_{\text{gauss}} \times \text{Gps noise}}{r_e} \quad (5.57)$$

The values chosen for the GPS noise are dependant on the type of GPS receiver being modelled. The simulation can model both P code and C/A code receiver noise. In this application the C/A code noise was chosen to be 10 times greater than the P code noise. The actual rms value used for the C/A code noise is 0.1 nm, and for the P code noise the value is 0.01 nm. To implement these noise values in the actual simulation program, a software module called Rgauss is used. The Rgauss module was previously discussed in section 5.5.1, where it was stated that the unscaled module produces data with an rms value of unity. By scaling the Rgauss output with either of the two values above, the desired value of rms position error in the platform axis is obtained.

Once the GPS earth to platform direction cosine matrix update has been formed, values for GPS latitude, longitude and alpha angle can be computed. These values of GPS position are then output to the Kalman filter module where they are combined with the IRS position values to form the Kalman filter measurement residuals.

The model for the GPS velocity error is formed by taking true values of velocity from the Rgauss module and adding on a component of velocity error. The rms value of north and east velocity error is taken to be 1 kt. To generate the velocity noise values in the simulation program, the Rgauss function discussed above is used. The actual GPS velocity equations implemented in the simulation are shown below :

$$[V_n]_{\text{GPS}} = [V_n]_{\text{TRUE}} + R_{\text{gauss}} \quad (5.58)$$

$$[V_e]_{GPS} = [V_e]_{TRUE} + R_{gauss} \quad (5.59)$$

The R_{gauss} function as discussed in section 5.5.1 has an rms output value of 1, since this is also the rms value chosen for the velocity noise then no scaling is needed for the R_{gauss} output data. Once formed, the GPS velocity values are output to the Kalman filter module.

5.7 KALMAN FILTER MODULE

The Kalman filter was discussed in detail in chapter 4, there, the system model that is used by the Kalman filter to represent the IRS errors was described. Figure 5-8 shows a block diagram of the Kalman filter as implemented in the simulation module. The Kalman filter receives position and velocity inputs from the IRS and GPS modules. These inputs are in the form of latitude and longitude, and velocity north and velocity east. To form a Kalman filter measurement, these inputs need to be transformed into components of the platform axis, this is because the Kalman filter error model of the IRS represents the position and velocity states in terms of the platform axis. The position and velocity transformation equations needed to form the Kalman filter measurement residuals are developed below.

5.7.1 POSITION MEASUREMENT

The Kalman filter receives IRS and GPS latitude and longitude values. These are first combined as follows :

$$X = XDISP(\lambda_{IRS}, \Phi_{IRS}, \lambda_{GPS}, \Phi_{GPS}) \quad (5.60)$$

$$Y = YDISP(\lambda_{IRS}, \Phi_{IRS}, \lambda_{GPS}, \Phi_{GPS}) \quad (5.61)$$

$XDISP$ is an in-house fortran routine that computes the distance (X) between the IRS and GPS in terms of nautical miles along the north geographic axis. $YDISP$ is a similar routine that computes the distance (Y) along the east geographic axis.

The north distance (X) and the east distance (Y) are then transposed into components of the platform axis via Kalman filter computed value of alpha angle (α_{kf}) as shown below:-

$$X_m = -(X \sin\alpha_{kf} + Y \cos\alpha_{kf}) \quad (5.62)$$

$$Y_m = -(X \cos\alpha_{kf} - Y \sin\alpha_{kf}) \quad (5.63)$$

The Kalman filter value for alpha angle is computed from the values of IRS platform heading ($\psi_{p\text{ irs}}$) and IRS true heading ($\psi_{\text{ irs}}$) as shown below :-

$$\alpha_{kf} = \psi_{p\text{ irs}} - \psi_{\text{ irs}} \quad (5.64)$$

In chapter 4, section 4.5, the measurement processing for the Kalman filter was discussed. There it was stated that a scalar measurement processing routine as opposed to a vector measurement processing routine is implemented, this means that the two Kalman filter measurement residuals are processed separately. The two measurement residuals are in units of nautical miles per hour, whilst the corresponding states in the Kalman filter state vector X(1) and X(2) are in units of radians. The Kalman filter measurement scalar H therefore contains the following scaling terms :

For X_m

$$H = R_0 \quad (5.65)$$

And for Y_m

$$H = -R_0 \quad (5.66)$$

Where R_0 is the value of earth radius in nautical miles. In the Kalman filter simulation module R_0 is taken to be a constant.

5.7.2 VELOCITY MEASUREMENT

The Kalman filter simulation module receives a velocity north value and a velocity east value from the IRS and GPS modules. These velocity values are then combined to form a difference value for velocity north (U) and a difference value for velocity east (V). To compute the velocity difference values, the GPS velocity is first resolved to the IRS position using a meridian convergence factor ξ , which is calculated as follows :

$$\xi = (\Phi_{GPS} - \Phi_{IRS}) \sin \lambda_{IRS} \quad (5.67)$$

Then the velocity difference values are computed as :

$$U = [V_n]_{IRS} - [V_n]_{GPS} \cos \xi - [V_e]_{GPS} \sin \xi \quad (5.68)$$

$$V = [V_e]_{IRS} - [V_e]_{GPS} \cos \xi + [V_n]_{GPS} \sin \xi \quad (5.69)$$

The north velocity difference value (U) and the east difference value (V) are then transposed into platform axis velocity values using the Kalman filter computed value of alpha angle as given by equation 5-64.

The two velocity equations implemented are shown below :

$$U_m = U \sin \alpha_{kf} + V \cos \alpha_{kf} \quad (5.70)$$

$$V_m = V \cos \alpha_{kf} - U \sin \alpha_{kf} \quad (5.71)$$

These two Kalman filter velocity values are in the same units as the corresponding states X(3) and X(4) in the state vector, therefore the value needed for the Kalman filter measurement scalar H is unity in each case.

5.7.3 KALMAN FILTER FAST LOOP / SLOW LOOP MECHANIZATION

In discussing the Kalman filter in chapter 4, details were given of a slow loop / fast loop mechanization that allows the Kalman filter state equations to be computed at a faster rate than the measurement processing equations. The fast loop iteration rate was chosen to be 5 seconds and the slow loop rate was chosen to be 30 seconds.

Implementing a fast loop allows the Kalman filter state vector matrix differential equation to be computed to first order. The form of the equation implemented in the Kalman filter simulation module is shown below :

$$\Phi(t_k, t_{k-1}) = I + F_k \Delta t \quad (5.72)$$

The terms needed to form the Kalman filter system matrix F_k are obtained as outputs from the IRS module. All of the slow loop equations are implemented in a module called KFMUPD. This module is called from the Kalman filter module four times during each 30 second Kalman filter measurement update cycle, the four calls correspond to the four scalar measurements.

Once computed, the values of the Kalman filter state vector and the covariance matrix are output to the CDU module for further processing.

5.8 CDU MODULE

The main tasks carried out by the CDU module is the evaluation of the Kalman filter performance figure and the computation of the flight management computer position output.

For the Kalman filter navigation performance figure, both the 95% circular error value and the radial error are computed (these parameters are for position error and are discussed in detail in chapter 6).

The CDU module computes the flight management computer position output by taking the two elements of the Kalman filter state vector that correspond to position, and computing a corresponding value of Kalman filter latitude error and longitude error. The Kalman filter latitude and longitude error is then added to the IRS latitude and longitude values to give the final flight management computer output.

The CDU also computes a value for the IRS position error by computing the difference between the true value of latitude and longitude received from the Rworld module and the IRS value of latitude and longitude. This allows the IRS position errors and the Kalman filter position errors to be compared.

5.9 FIX MODULE

The two main functions carried out by the Fix module are the initialization of the Kalman filter covariance parameters, and the computation of the alpha angle as used by the Kalman filter.

5.10 REMAINING MODULES

The remaining modules which all form part of a program library can be considered to carry out two main tasks, data storage and computation of the various geometric and matrix parameters required by the other program modules.

CHAPTER 6

METHODS TO EVALUATE NAVIGATION SYSTEM PERFORMANCE

6.1 INTRODUCTION

This thesis is concerned with the integration of GPS and IRS using a Kalman filter, to gain improved navigation system performance. In this chapter three techniques that can be used to assess the navigation performance of the customer inertial reference system and the Kalman filter are developed. These methods are monte carlo analysis, sensitivity analysis, and covariance analysis.

The method used to assess the Kalman filter navigation performance is to record and compare the position errors obtained from the Kalman filter and the IRS. The navigation specification of the IRS is such that it meets the IRS accuracy requirements of FAR 121, Appendix G, Para 6(a)(1) which states "For flights up to 10 hours duration, no greater than 2 nautical miles per hour of circular error on 95 percent of system flights completed is permitted". It should be noted that there are other FAR requirements relating to system accuracy that the IRS system is required to meet, although these will not be considered in this thesis. Thus, the first task that must be carried out before the Kalman filter performance can be assessed, is to simulate an IRS with a performance figure of 2 nm/hr.

Using the IRS accuracy figure of 2 nm/hr, the performance of the Kalman filter can then be specified in terms of a 95 percent circular error value. The exact performance figure for the Kalman filter as agreed by Boeing and Smiths Industries will not be discussed, as this information is confidential.

Before the IRS performance figure can be simulated, the specification "2 nm/hr, 95% circular error" needs to be understood. This specification is one of several that is used to measure navigation system performance. Other similar specifications include Circular Error Probability (CEP), and Distance Root Mean Squared (Drms) also referred to as radial error. These three specifications will now be considered, after which the three navigation performance analysis techniques will be developed.

6.2 95% CIRCULAR ERROR

To understand the meaning of the 95% circular error as it applies to the IRS and Kalman filter, the Bivariate Normal Distribution needs to be examined. The bivariate distribution is required, as opposed to the univariate distribution because the position measurements made for the IRS and Kalman filter are two dimensional, since they involve both latitude and longitude.

Figure 6-1 shows the bivariate normal distribution where the assumption has been made that the RMS values σ_x and σ_y are equal and also the correlation between the x axis and the y axis is zero. The probability density function equation for this specific case is given by (reference Leenhouts 1985) :

$$f(x,y) = \frac{1}{2\pi\sigma_x^2} \exp\left[-\frac{1}{2\sigma_x^2} [(x - \mu_x)^2 + (y - \mu_y)^2]\right] \quad (6.1)$$

Under these conditions, figure 6-1 shows that an area of constant probability is enclosed by a circle. If the rms values σ_x and σ_y were not equal, then a similar area would be traced out by an ellipse, with the values of σ_x and σ_y corresponding to the ellipse major and minor axis, depending on their ratio. Therefore making the assumption that the rms values σ_x and σ_y are equal has the effect of simplifying the distribution from an elliptical case to a circular case.

The 95% circular error figure assumes a circular distribution, therefore it requires the rms values to be equal and also the correlation coefficient to be zero. If these conditions do not hold, then the resultant 95% measurement will be slightly inaccurate. Valstar (1970) discusses a possible method of dealing with correlated errors. Leenhouts (1985) discusses the error that results from assuming a circular error probability, when the actual probability is described by an ellipse.

Leenhouts (1985) provides a solution, shown below, to equation 6-1 where the further assumption has been made that the mean values μ_x and μ_y are zero, this implies that the measurement observations are unbiased.

$$P(\sigma_x k) = 1 - \exp\left(-\frac{k^2\sigma_x^2}{2}\right) \quad (6.2)$$

Using this result, the radius of a circle (k) to give 95% probability can be evaluated, and found to be $k = 2.4477$. This leads to the following equation being used for 95% circular error.

$$95\% \text{ Err} = 2.4477 \frac{(\sigma_x + \sigma_y)}{2} \quad (6.3)$$

Where 95% Err is a quantitative measure of navigation performance.

6.3 CIRCULAR ERROR PROBABILITY

The circle of equal probability (CEP) implies that the probability of a point falling inside the circle is equal to it falling outside, this means that CEP is a 50% probability figure. Using equation 6.2, the radius value k , for a 50% probability is worked out to be $k = 1.1774$. This leads to the following equation being used for CEP :

$$CEP = 1.1774 \frac{(\sigma_x + \sigma_y)}{2} \quad (6.4)$$

Where CEP is another accepted measure of performance.

6.4 DISTANCE ROOT MEAN SQUARED ERROR

The Distance Root Mean Squared probability is computed as follows :

$$Drms = (\sigma_x^2 + \sigma_y^2)^{\frac{1}{2}} \quad (6.5)$$

For a circle with axis σ_x and σ_y , the Drms value equates to the radius of the circle, hence it is often referred to as a radial error. Drms is often confused with the one sigma probability of the univariate distribution, the two are not the same since the mean probability for Drms is 66.03%, and the probability for one sigma is 68%.

Although these three statistical probabilities are common there are still other measurements such as 2Drms, that are also used. One of the reason that performance is specified in so many different ways, is that various bodies choose to adopt different approaches. NATO documents are quoted at the 95% probability level as laid down by STANAG 4278 for example, while the United States DoD tends to use the 50% probability level.

6.5 NAVIGATION PERFORMANCE ANALYSIS TECHNIQUES

Each of the three probability measurements, 95% circular error, CEP and Drms requires an rms value of latitude and longitude to be generated. Three possible methods of generating rms position data will now be discussed, these are Monte Carlo simulation, sensitivity analysis and covariance analysis.

6.5.1 MONTE CARLO SIMULATION

The customer IRS error model was developed in chapter 2, there the gyro error model was shown to consist of a gyro random walk and a gyro bias, and the accelerometer error model was shown to consist of a correlated noise and an accelerometer bias. The gyro random walk and accelerometer correlated noise are both types of error sources that produce random data with time, and are referred to as random time series errors. The gyro bias and accelerometer bias are error sources that produce constant data with time, although their initial data value is random, they are therefore referred to as random constants. For the IRS state vector (see appendix D) there are six random constants comprising three gyro and three accelerometer terms.

In the simulation program, the IRS error model is implemented as a vector matrix differential equation of the form :

$$\dot{\underline{X}} = \underline{F}(t)\underline{X}(t) + \underline{W}(t) \quad (6.6)$$

Where :

- $\underline{X}(t)$ - is the system state vector (17 x 1)
- $\underline{F}(t)$ - is the system matrix (17 x 17)
- $\underline{W}(t)$ - is the a random forcing function (17 x 1)

The gyro random walk and accelerometer correlated noise are elements of the noise vector $\underline{W}(0)$, while the gyro bias and accelerometer bias are elements of the state vector $\underline{X}(0)$.

For a Monte Carlo simulation, a series of runs are carried out, 100 being a typical figure, where for each run, values for the random time series and random constant error sources are generated. The purpose of the simulation is to compute RMS values for IRS latitude and longitude error, and then to use equation 6.3 to evaluate the 95% performance figure.

The random constant and random time series error values are generated using a series of random number generators. Each individual error source has an associated random number generator which produces the required statistical data. For example, in the case of a random constant, for each 100 runs an initial random value is generated. If all 100 values for the random constant are processed to form an rms value, then the resultant value will equal the required statistical value given for the error source. The IRS error budget given in appendix B gives the statistical values needed for each error source for the customer IRS. Assuming the random constant and random time series errors are representative, recordings are made of the state vector \underline{x} over time for each of the 100 runs. The elements of the state vector relating to IRS position, $x(1)$ and $x(2)$, (see appendix D for a summary of the IRS states used in the state vector) can then be processed to compute rms values for IRS latitude and longitude error. The elements $X(1)$ and $X(2)$, give the IRS position error in terms of the platform axis. These two elements can be transformed into components of latitude and longitude, by first resolving the platform axis values into components of the north and east axis via the IRS alpha angle, and then using an appropriate value of radius to find latitude and longitude. Finally equation 6.3 can be used to compute the IRS 95% circular error figure.

6.5.1.1 SIMULATION RESULTS

using a suitable flight profile, a Monte Carlo simulation was carried out. Figure 6-2 shows the flight profile, which represents a typical long distance commercial flight, consisting of a great circle navigation route. The objective of the simulation was to evaluate the IRS navigational performance in terms of the 95% circular error. A total of 100 runs were carried out with each run consisting of a 10 hour simulation. For each run, values of latitude and longitude error were recorded every minute for the full 10 hours of the simulation. Values of rms latitude and longitude error were then calculated by taking each one minute sample across the ensemble of runs.

The resultant ensemble rms values for latitude and longitude error are shown in figure 6-3 and 6-4 respectively. From these two results, the 95% circular error value for the IRS was computed using equation 6.3 and found to be :

$$95\% \text{ Err} = 2.4477 \frac{[0.52 + 0.53]}{2} \text{ NM/HR} \quad (6.7)$$

$$95\% \text{ Err} = 1.285 \text{ NM/HR} \quad (6.8)$$

6.5.2 SENSITIVITY ANALYSIS

A sensitivity analysis is similar to a Monte Carlo simulation in that it is based on a vector matrix differential equation (see equation 6.6). The main difference between the two methods is the way that the sensitivity analysis uses the error sources during each run. In the Monte Carlo simulation, for each run, random samples are generated for all of the error sources of interest.

In a sensitivity analysis some runs are carried out based on single error sources. Consider as an example the x gyro bias random constant, if a single run is carried out with the value of the x gyro bias being set to its one sigma value, then assuming a linear system, the resultant latitude and longitude errors produced will be rms values. The rms latitude and longitude errors are obtained by the same method as discussed for the monte carlo simulation. Recordings of the position error states X(1) and X(2) which are in units of radians, are transformed via the IRS alpha angle into components of North and East axis, and then using a suitable value for earth radius, values of latitude and longitude error are computed. The simulation equation in this instance does not contain random time series errors. The simulation equation as shown below can be considered to be linear :

$$\dot{\underline{X}} = F(t)\underline{X}(t) \quad (6.9)$$

Having obtained rms values for latitude and longitude for the x gyro bias random constant error source, the process can be repeated for each of the other IRS random constant errors. Once all the random constant type runs are completed, the effect of the random time series errors can be investigated.

As with the random constant errors, the random time series error sources can be considered on an individual basis, although this requires a large series of runs to be carried out as explained. Consider the affect of the x gyro random walk on position, a series of runs, typically 100, needs to be carried out to calculate the rms affect of this error on latitude and longitude.

To produce the rms result, an ensemble of runs needs to be processed in a similar way to the method described for the Monte Carlo simulations, where one minute data points are combined across the 100 runs to form an ensemble rms value.

Since such a large number of runs are needed to evaluate the rms affect on position of a single random time series error source, it is usual to group together all random time series error sources, and just investigate their combined affect on position. This method was adopted in this work.

6.5.2.1 SIMULATION RESULTS

A sensitivity analysis was carried out using the same flight profile as for the Monte Carlo simulation (see figure 6-2). To investigate the effect of the random constant error sources, six runs were carried out, while 100 runs were carried out to investigate the effect of the random time series errors. Details of the 106 runs are given below :

RUN NUMBER	ERROR SOURCE	VALUE USED	NO OF RUNS
1	X GYRO BIAS	1σ	1
2	Y GYRO BIAS	1σ	1
3	Z GYRO BIAS	1σ	1
4	X ACCEL BIAS	1σ	1
5	Y ACCEL BIAS	1σ	1
6	Z ACCEL BIAS	1σ	1
7 - 106	X, Y, Z GYRO RANDOM WALK AND X, Y, Z ACCEL NOISE	RANDOM SAMPLES	100

Results for latitude and longitude error for each of the 106 runs were recorded and processed as follows :- For the random constant error sources, the six results produced were in rms form. For the random time series errors, the 100 results had to be processed to produce ensemble rms values, this then provided a total of seven rms values for latitude error and 7 rms values for longitude error. Final values for latitude and longitude error were then produced by Rssing the 7 rms values. The resultant Rssed values of latitude and longitude were then processed using equation 6.3, to compute the 95% circular error. Figure 6-5 summarizes the overall method of combining results for the sensitivity analysis method. The final 95% error value for the simulation was calculated to be 1.302 nm/hr.

6.5.3 COVARIANCE ANALYSIS

Covariance analysis is different from the Monte Carlo and sensitivity analysis methods, because it does not use the vector matrix differential equation (see eq 6.6). Instead, it is based on the Kalman filter covariance estimate equation. The Kalman filter was discussed in chapter 4, where the covariance estimate equation was shown to be of the following form :

$$P_k(-) = \Phi_k P_{k-1}(+) \Phi_k^T + Q_{k-1} \quad (6.10)$$

Using this equation random constant and random time series errors are considered on an individual basis. Random constants are accounted for in the P(0) matrix, while random time series errors use the Q matrix. For each of the two types of error source the one sigma value of the error source is used.

The covariance estimate equation is a statistical equation, and therefore its outputs are statistical predictions. Its diagonal elements corresponds to the states in the state vector \underline{X} . Appendix C gives the relationship between the Kalman filter covariance matrix diagonal elements and the Kalman filter states. Estimates of position error are given by the covariance elements P(1,1) and P(2,2) which correspond to the position states X(1) and X(2). The estimates are in terms of variance expressed in terms of the platform axis, so taking the square root enables the rms value to be calculated. Final rms values for latitude and longitude can be formed by transposing the platform axis components into equivalent values of north and east using the system alpha angle.

For the monte carlo and sensitivity analysis, simulations were carried out using the 17 state optimal IRS error model. To perform a covariance analysis using the same optimal model, then a covariance matrix equation of order 17 x 17 is required. In discussing the Kalman filter in chapter 4, the point was made that an optimal Kalman filter model was not going to be used to develop a sub optimal Kalman filter model, because a suitable sub optimal Kalman filter error model was being supplied by the customer. In this work therefore, a covariance analysis will refer to the 12 state sub optimal Kalman filter error model.

The results of the covariance analysis can be viewed as a Kalman filter prediction of IRS error performance. If the Kalman filter error model of the IRS is close to the actual optimal IRS error model, then the Kalman filter predictions of performance should be very close to the actual IRS performance. Therefore, if a covariance analysis is carried out using the same flight profile as a monte carlo or sensitivity analysis simulation, then a comparison of the Kalman filter performance compared to the IRS performance can be carried out.

6.5.3.1 SIMULATION RESULTS

A covariance analysis was carried out using the same flight profile as for the monte carlo and sensitivity analysis simulations (see figure 6-2). A series of 10 runs were made to examine the individual effect of the 10 error sources associated with the sup optimal Kalman filter. Details of the 10 runs are given below :

RUN NUMBER	ERROR SOURCE	VALUE USED	NO OF RUNS
1	X GYRO RW	1σ	1
2	Y GYRO RW	1σ	1
3	Z GYRO RW	1σ	1
4	X ACCEL NOISE	1σ	1
5	Y ACCEL NOISE	1σ	1
6	X GYRO BIAS	1σ	1
7	Y GYRO BIAS	1σ	1
8	Z GYRO BIAS	1σ	1
9	X ACCEL BIAS	1σ	1
10	Y ACCEL BIAS	1σ	1

Runs 1 to 5 relate to the random time series errors, these were carried out by placing the appropriate variance value in the $Q(0)$ matrix (see eq 6.10), with the $P(0)$ matrix initialized to zero.

Runs 6 to 10 relate to the random constants, these were carried out by placing the appropriate variance value in the $P(0)$ matrix, with the $Q(0)$ matrix set to zero. The 10 values used for the covariance error terms were obtained from the IRS error budget table given in appendix B, by computing the appropriate variance value from the one sigma values given. Values of latitude and longitude error were recorded at intervals of 1 minute throughout the 10 hour simulation. The values of latitude and longitude error produced from the 10 covariance runs are all rms values. They were combined by Rssing to give two final values of latitude and longitude error. An illustration of the overall method used to combine the results from the covariance analysis is given in figure 6-6. From the rms values of latitude and longitude error, a 95% circular error value was then calculated using equation 6-3 and found to be 1.26 nm/hr.

6.6 COMPARISON OF RESULTS

The covariance analysis 95% circular error value is a Kalman filter prediction of the navigation performance that is expected from the inertial reference system. The covariance result of 1.26 nm/hr is very close to the actual IRS values obtained from the monte carlo and sensitivity analysis which were 1.28 nm/hr and 1.3 nm/hr respectively. These results show that the covariance analysis carried out using the sub optimal Kalman filter model, produces a good estimate of the actual IRS error performance. Figures 6-7 and 6-8 show a comparison of position errors for the three methods, with the data being presented in terms of the x platform axis position error (see DTHX in figure 6-7), and the y platform axis position error (see DTHY in figure 6-8). The two results confirm the close agreement between the three methods.

In both the covariance analysis and sensitivity analysis techniques, the effect of individual error sources on position were examined. The results for the individual error sources obtained from the two methods can be compared to gain further useful information on the performance of the sub optimal Kalman filter. Two different methods of comparing results will now be examined. The two methods are a comparison of results which show the effect of a single random constant error source, and a comparison of results which show the effect of random time series error sources.

6.6.1 COMPARISON OF RESULTS FOR RANDOM CONSTANT ERRORS

When investigating the effect on position of a single random constant error, both the covariance analysis and sensitivity analysis methods produced a single rms result. The rms results from the two methods can therefore be directly compared. The covariance analysis did not consider the effect of the z accelerometer state because, this state is part of the optimal IRS error model, but not the sub optimal Kalman filter error model. Results for the z accelerometer state cannot be compared therefore. All of the other 5 instrument errors are common to both models, so their results can be examined.

Figure 6-9 shows a comparison of results for the y gyro bias random constant error source, where the position error is shown in terms of the x and y platform axis. The x platform axis position error is shown by DTHX in figure 6-9, and the y platform axis tilt by DTHY. For both position error terms, the result from covariance analysis and the sensitivity analysis are very close. Figure 6-10 shows a similar comparison for the z gyro bias random constant error source. Again the results for the two error terms show a close agreement for the covariance analysis and sensitivity analysis cases.

6.6.2 COMPARISON OF RESULTS FOR RANDOM TIME SERIES ERRORS

In the sensitivity analysis, the effect of the six time series errors relating to the optimal IRS error model were investigated by carrying out a series of 100 runs. It was explained that to reduce the amount of simulation runs from 600 to 100, the time series errors were considered together, rather than on an individual basis. A resultant rms value for the time series errors, was then computed by taking data samples across the ensemble at a specific time interval.

In the covariance analysis, the effect of the 5 individual time series error sources relating to the sub optimal IRS error model were investigated. A resultant rms value was not computed for the effect of only the time series errors, but rather a resultant rms value was computed for all of the 10 error sources of interest. Since the random time series results were considered on an individual basis and were separated from the random constant error sources, then an overall Rss value for the effect of the random time series results only, can be easily computed. This allows the random time series results from the covariance analysis, and the random time series results from the sensitivity analysis to be compared.

Figure 6-11 illustrates the process of combining and comparing the time series results for the covariance analysis and the sensitivity analysis methods. Actual results obtained from the simulations are not discussed.

6.7 COMMENTS

In this chapter three techniques have been discussed that are suitable to assess navigation system performance, Monte Carlo analysis, sensitivity analysis and covariance analysis. The monte carlo and sensitivity analysis techniques use the solution to the state vector matrix differential equation as the basis for the simulations. The covariance analysis uses the Kalman filter covariance estimate equation as the basis for the simulation. As well as providing a figure for overall navigation performance, the sensitivity analysis and covariance analysis techniques can also be used to provide information on the contribution of individual error sources to overall navigation performance.

In the introduction it was stated that the customer inertial reference system is a 2 nm/hr, 95% circular error system. The computed values of 95% circular error obtained from the three methods although all in close agreement were only in the range 1.2 nm/hr to 1.3 nm/hr. The performance figure of 2 nm/hr was therefore not been obtained. Since in all of the simulations, the error values used were obtained from the customer IRS error budget table (see appendix B), it was not clear at this time why a figure of 2 nm/hr 95% has not been achieved. This point will be further discussed in chapter 8, section 8.6.5, where the reason for not obtaining a performance figure of 2 nm/hr is explained.

In the next chapter the three techniques developed above are used to assess the navigation performance of the Kalman filter.

CHAPTER 7

INVESTIGATIONS INTO KALMAN FILTER PERFORMANCE

7.1 INTRODUCTION

In chapter 6, three different methods applicable to the investigation of navigation system performance were investigated, these were Monte carlo simulation, sensitivity analysis and covariance analysis. In this chapter, these methods are used to analyze the performance of the development Kalman filter.

To evaluate Kalman filter performance using the Monte carlo and sensitivity analysis techniques, then values of Kalman filter latitude and longitude error are needed. To generate these values, a similar method can be applied as used for the IRS in the last chapter (see section 6.5.2). That is, the Kalman filter x and y position error states which are in components of the platform axis, can be transformed into components of the latitude and longitude error by first, transforming the platform axis components into north and east axis using the Kalman filter alpha angle. Then, using a suitable value for earth radius, the north and east axis components can be transformed into Kalman filter latitude and longitude error.

7.1.1 SENSITIVITY ANALYSIS SIMULATION DETAILS

The Kalman filter was discussed in chapter 4, where details were given of the 12 state sub optimal IRS error model which the Kalman filter is implementing. Using the 10 hour flight profile of the previous chapter (see figure 6-2), a sensitivity analysis was carried out to investigate the Kalman filter performance.

Following the outline of the sensitivity analysis method discussed in the last chapter (see section 6.5.2), a total of 100 runs were carried out to simulate the effect of the IRS random time series error sources, with a further 6 runs to simulate the effect of the gyro and accelerometer random constant errors. For each run perfect GPS measurements were available for the first 4 hours of the flight, after which time GPS was switched out. This period of GPS coverage was purposely chosen, as it allows the Kalman filter a four hour period in which to observe IRS errors. After the 4 hour period, the Kalman filter reverts to IRS only operation, and therefore its ability to predict IRS errors can be examined.

Results were recorded at one minute intervals for IRS latitude and longitude error, and Kalman filter latitude and longitude error. The recorded data was then processed to obtain the following 3 sets of results, total error due to random time series and random constant error sources, partial error due to the combined effect of random time series errors only, partial error due to the combined effect of the random constants only.

Figure 7-1 shows the three sets of results for the IRS latitude error. The continuous line in figure 7-1 represents the overall latitude error due to random constant and random time series error sources. The dashed line shows the latitude error for random time series error sources only, while the dotted line gives the latitude error for random constant sources only. A similar set of results was obtained for the IRS longitude error, but is not shown. Figure 7-2 gives the corresponding result for the Kalman filter latitude error. A similar result was obtained for the Kalman filter longitude error but is not shown. Using the results for IRS latitude and longitude error, and Kalman filter latitude and longitude error, the 95% circular error for the three sets of results were evaluated using the equation developed in the last chapter (see eq 6.3).

7.1.2 EVALUATION OF OVERALL IRS AND KALMAN FILTER PERFORMANCE

The 95% circular error value for the IRS is given by :

$$95\% \text{ Err} = \frac{[0.5174 + 0.5467]}{2} \quad \text{NM/HR} \quad (7.1)$$

$$95\% \text{ Err} = 1.3023 \quad \text{NM/HR} \quad (7.2)$$

The 95% circular error for the Kalman filter is given by :

$$95\% \text{ Err} = \frac{[0.3866 + 0.3866]}{2} \quad \text{NM/HR} \quad (7.3)$$

$$95\% \text{ Err} = 0.94628 \quad \text{NM/HR} \quad (7.4)$$

7.1.2 EVALUATION OF PERFORMANCE DUE TO RANDOM TIME SERIES ERROR SOURCES

The results for random time series errors consisting of gyro random walk and accelerometer noise, are evaluated below :

The 95% circular error value for the IRS result due to random time series errors only is given by :

$$95\% \text{ Err} = \frac{[0.172 + 0.212]}{2} \quad \text{NM/HR} \quad (7.5)$$

$$95\% \text{ Err} = 0.46995 \quad \text{NM/HR} \quad (7.6)$$

The corresponding 95% circular error for the Kalman filter is given by :

$$95\% \text{ Err} = \frac{[0.362 + 0.354]}{2} \quad \text{NM/HR} \quad (7.7)$$

$$95\% \text{ Err} = 0.876 \quad \text{NM/HR} \quad (7.8)$$

7.1.4 EVALUATION OF PERFORMANCE DUE TO RANDOM CONSTANTS

The 95% circular error value for the IRS due to random constant errors only is given by :

$$95\% \text{ Err} = \frac{[0.488 + 0.504]}{2} \quad \text{NM/HR} \quad (7.9)$$

$$95\% \text{ Err} = 1.2140 \quad \text{NM/HR} \quad (7.10)$$

The corresponding 95% circular error for the Kalman filter is given by :

$$95\% \text{ Err} = \frac{[0.146 + 0.146]}{2} \quad \text{NM/HR} \quad (7.11)$$

$$95\% \text{ Err} = 0.3573 \quad \text{NM/HR} \quad (7.12)$$

7.1.5 DISCUSSION OF RESULTS

An examination of the IRS and Kalman filter results for the total position error due to random constants and random time series error sources shows, that the effect of the Kalman filter is to improve the overall system performance from a 1.3 nautical mile per hour system to a 0.95 nautical mile per hour system.

Considering the effect of the random time series errors only, the results show that the Kalman filter performance is no better than the IRS performance, in fact it is worse. An examination of the effect due to random constant error sources only, shows that the Kalman filter 95% performance figure is 0.36 nautical miles per hour compared with 1.2 nautical miles per hour for the IRS.

From the IRS results it is concluded that the random constant error sources make up the major proportion of the total IRS position error. From the Kalman filter results, it is concluded that the major contributor to the total Kalman filter position error is the random time series noise. From the results for the random constant error sources only, it is concluded that the Kalman filter is able to make a good estimate of the gyro and accelerometer random constants during the initial 4 hour period of GPS. During the subsequent 6 hour period of IRS only operation, the Kalman filter was able to make a good prediction of the IRS random constant errors.

7.2 INVESTIGATION INTO THE KALMAN FILTER TESTING METHOD

The Kalman Filter performance has been investigated by the technique of sensitivity analysis. Using this method the kalman filter performance was recorded for the effect of two different sets of IRS error sources, random time series errors and random constants. During the simulations no adjustments were made to the kalman filter design values the kalman filter covariance matrix was therefore initialised with values relating to random constants, and the filter noise matrix was initialised with values relating to the random time series errors. The values used to initialise the Kalman filter were discussed in chapter 4, section 4.6.1 (see table 4-1 for a list of the values used).

It is of interest to investigate an alternative configuration for initialising the kalman filter when carrying out the simulations for the random time series results. The alternative configuration is to set the Kalman filter covariance matrix $P(0)$ to zero at initialisation for each of the 100 runs, to account for the fact that the kalman filters initial uncertainty in the estimate of the random constant states is zero.

Using the flight profile of the last chapter (see figure 6-2) a series of 100 runs were carried out to investigate the kalman filter performance for the random time series errors with the kalman filter covariance matrix set to zero at initialisation.

Values of kalman filter latitude and longitude error were recorded at one minute intervals, and then processed to compute an ensemble rms value for latitude and longitude error. A 95% circular error value was then computed for the random time series error sources. The result is detailed below :-

$$95\% \text{ Err} = \frac{[0.213 + 0.235]}{2} \quad \text{NM/HR} \quad (7.13)$$

$$95\% \text{ Err} = 0.5482 \quad \text{NM/HR} \quad (7.14)$$

This 95% circular error result of 0.5482 nm/hr is an improvement over the previous case for the random time series error sources, which was shown to 0.876 nm/nr. It is concluded therefore, that setting the Kalman Filter covariance matrix to zero has a significant impact on the kalman filter performance.

7.3 VERIFICATION OF THE KALMAN FILTER TESTING METHOD

In applying the sensitivity analysis technique to measure the effect of the random time series errors on Kalman filter performance, two different methods of initialising the Kalman filter covariance matrix have been used. These two methods provided different results but without any indication of which technique is correct. To establish which of the two methods is correct, a Monte Carlo simulation was carried out.

The Monte Carlo technique is representative of the real world situation as it generates both random time series errors and random constant errors simultaneously. The selection of the Kalman filter initialisation parameters is straight forward for the Monte Carlo case, with both the covariance matrix $P(0)$, and noise matrix $Q(0)$, being initialised with the design values that are intended to be used in the final implementation. (The Kalman filter initialisation parameters were discussed in chapter 4, see section 4.6.1 and table 4-1).

A Monte Carlo simulation was carried out using the flight profile of the last chapter (see figure 6-2). Latitude and longitude error was recorded at one minute intervals for both the IRS and Kalman Filter for each of the 100 runs. The results from the IRS and Kalman Filter were then processed to produce a resultant rms value of latitude and longitude error. The final values obtained, give the rms latitude and longitude errors for the combined effect of random constant and random time series error sources.

Figure 7-3 shows the Kalman Filter result for the final rms latitude error for the Monte Carlo simulation, compared with the same results obtained from the two sensitivity analysis cases. The continuous line in figure 7-3 is for the Monte Carlo result, while the dashed line is for the sensitivity analysis case where the covariance matrix was not reset to zero. The figure shows that these two results are almost identical. The case for the alternate Kalman filter configuration where the covariance values were set to zero, is shown by the dotted line in figure 7-3. This sensitivity analysis result can be seen to be significantly different from the Monte Carlo case. The result for Kalman filter longitude error is shown by figure 7-4, where the same trend as for the latitude error case can be observed.

From these results it is concluded that when investigating the effect of random time series errors by the method of sensitivity analysis, the Kalman filter covariance matrix $P(0)$, should not be set to zero, but initialised with the Kalman filter design values.

7.4 A SECOND INVESTIGATION INTO KALMAN FILTER PERFORMANCE

Having established the correct technique for initialising the Kalman Filter covariance matrix when applying the sensitivity analysis technique, it was decided to repeat the investigation discussed in section 7.1 but under a slightly different alignment condition. The initial alignment heading was chosen to be 225 degree instead of 090 degree. The sensitivity analysis was carried out along the same lines as the investigation discussed in section 7.1.1, where 100 runs were carried out to simulate the effect of the random time series errors and a further 6 runs were carried out to investigate the effect of the random constant error sources. Results were recorded for latitude and longitude error at intervals of one minute throughout the 10 hour simulation period for each run. The results were processed into three sets in the same manner as described in section 7.1.1. Using the final processed values of rms latitude and rms longitude error, the 95% circular error for the IRS and kalman filter were computed and found to be as follows:-

7.4.1 IRS CIRCULAR ERROR PERFORMANCE

The 95% circular error value for the overall IRS error is evaluated as :

$$95\% \text{ Err} = \frac{[0.388 + 0.68]}{2} \quad \text{NM/HR} \quad (7.15)$$

$$95\% \text{ Err} = 1.3070 \quad \text{NM/HR} \quad (7.16)$$

The corresponding 95% circular value for the overall Kalman filter error is evaluated as :

$$95\% \text{ Err} = \frac{[0.2933 + 0.32]}{2} \quad \text{NM/HR} \quad (7.17)$$

$$95\% \text{ Err} = 0.7505 \quad \text{NM/HR} \quad (7.18)$$

7.4.2 DISCUSSION OF RESULTS

The 95% circular error performance figure for the overall IRS performance was found to be 1.3070 nautical miles per hour. This result which is for an alignment heading of 225 degree, is very close to the previous value achieved for the 090 degree alignment case (see section 7.1.2) which was 1.3023 nautical miles per hour.

For the kalman filter the result for the 225 degree alignment case was found to be 0.7505 nautical miles per hour compared with a value of 0.9462 nautical miles per hour for the 090 degree case. These results show that changing the alignment heading from 090 degree to 225 degree causes a reduction in the overall kalman filter performance of approximately 0.2 nautical miles per hour but does not significantly affect the resultant IRS error performance. By comparing the results for the random constant sources for the two alignment cases, it was noted that the kalman filters ability to learn the z gyro bias was quite different for the two runs, with the 225 degree alignment case providing the best result.

It is concluded therefore that the kalman filters ability to observe the z gyro bias is a function of vehicle heading.

7.5 INVESTIGATION INTO DIFFERENT PERIODS OF GPS COVERAGE

The previous investigations into Kalman filter performance were carried out using a suitable flight profile, where GPS measurements were available for the first four hours of a 10 hour flight. The amount of time that real GPS measurements will be available cannot be predicted. The intention is for GPS to be able to provide continuous coverage, although this will only be possible when the full constellation of GPS satellites are launched. At the present time GPS coverage is intermittent, and because of this it is of interest to examine the effect on the Kalman filter performance of different periods of GPS coverage.

Using the flight profile shown in figure 7-5, three separate sensitivity analysis simulations were carried out. For each simulation perfect GPS measurements were mechanized to provide the following periods of GPS coverage, 42 minutes, 60 minutes and 3 hours. After each of these times, the pattern for the remainder of the 3 runs was the same with GPS being switched out until the 5 hour point. At 5 hours GPS was again switched in for a period of 42 minutes before being finally switched out for the remainder of the 10 hour flights.

Results for the diagonal elements of the Kalman filter covariance matrix were also recorded for the three GPS cases, so that a covariance analysis could be carried out.

7.5.1 DISCUSSION OF RESULTS FROM THE COVARIANCE ANALYSIS

Figure 7-6 shows the result for an overlay of the various diagonal terms of the Kalman filter covariances matrix for the three cases. Appendix C gives the relationship between the diagonal elements of the Kalman filter covariance matrix and the corresponding IRS states. From the covariance terms associated with the X and Y accelerometer biases these being $sd(11)$ and $sd(12)$, it can be seen that the difference between the three plots for both accelerometers is small, compared with the initial value of uncertainty of the two states. Examination of the result for the 3 hour case (the dotted line on the graph) reveals that for both the X and Y accelerometer states, the plots reach a minimum value at a time of one and a half hours, which means that at this time, the Kalman filter has its best estimate of the two states.

For the gyro case, the covariance plots relating to the X,Y and Z gyro are shown by sd(8),sd(9) and sd(10) respectively. For the level axis gyros the trend that can be observed from the three cases is as follows :-

After 42 minutes the Kalman filter uncertainty is still high when compared to the initial value of uncertainty of the two states. The uncertainty reduces quite rapidly between the 42 minute and 60 minute intervals for both gyros, reaching a minimum value of uncertainty at approximately the one and a half hour point.

For the vertical axis gyro the trend is quite different. For the 42 minute and 60 minute case, the Kalman filter does not have time to estimate Z gyro bias (see SD(10)), thus the uncertainty in the state does not change from its initial value. For the 3 hour case, the filter is able to estimate the state, and as shown by the graph (see dotted line for plot SD(10)) the uncertainty reduces rapidly after approximately 1.2 hours to a minimum value at approximately 3 hours.

From the results obtained above for the gyro cases, it can be concluded that for the 42 minute case, the Kalman filter does a poor job of estimating the local level and vertical axis gyro biases. For the 60 minute case, the Kalman filter is able to make a reasonable estimate of the local level gyro biases, but is unable to make any estimate of the vertical axis gyro bias. For the 3 hour case, the Kalman filter is able to make a good estimate of all gyro bias errors.

7.5.2 DISCUSSION OF THE RESULTS FOR THE SENSITIVITY ANALYSIS

IRS latitude and longitude information that was recorded at one minute intervals was processed to produce 3 sets of results. Figure 7-7 shows the 3 results which are, overall IRS latitude error due to random constant and random time series error sources (continuous line), IRS latitude error due to random constants only (dashed line), and finally IRS latitude error due to random time series errors only (dotted line). Similar results were obtained for IRS longitude error but are not shown. From figure 7-7 it can be seen that the major contributor to the IRS latitude error is the random constant error source. This result is consistent with the findings of section 7.1.5.

The Corresponding results for the Kalman filter latitude error for the 42 minute GPS case is given by figure 7-8, figure 7-9 shows the result for the 60 minute case and figure 7-10 shows the result for the 3 hour case. Similar results were obtained for the Kalman filter longitude case but are not shown.

From the graph showing Kalman filter latitude error for the 60 minute case, figure 7-9, the following trend is observed :- After 60 minutes of continuous coverage, GPS is lost. With the loss of GPS the Kalman filter latitude error starts to increase, reaching a final value of 1.88 nm after 5 hours.

Also shown in figure 7-10, are the contributions of random noise and random constants to the overall error. It can be seen that the biggest contribution to the overall error comes from the random constants. At 5 hours, GPS provides coverage again for a period of 42 minutes, after which time it is switched off for the remainder of the test. After loss of GPS for the second time, the Kalman filter latitude error starts to increase once again, reaching a final value of 1.66 nm at the end of the 10 hour run. For this second phase however, the random noise error provides the largest contribution to the overall error. The pattern observed here can be explained by the fact that during the first period of unaided operation, the Kalman filter has not been able to observe the Z gyro bias, this fact being confirmed from the covariance analysis results discussed above. Further evidence that this is indeed the case is given from figure 7-12, which shows the contribution of each of the individual 5 random constant error sources, to the total random constant error. The dashed dotted line is the contribution of the Z gyro random constant which can be seen to be dominant.

Figure 7-8 shows the Kalman filter latitude error for the 42 minute case. After the initial loss of GPS the latitude error can be seen to increase to a final value of 2.2 nm after 5 hours. As observed in the 60 minute case, the random constant error is the major contributor to the overall latitude error. Figure 7-11 shows the breakdown of the 5 random constant error sources for the 42 minute case. It is apparent from this set of graphs, that the Z gyro random constant is the major contributor to the overall random constant error. By making a comparison of the results from figure 7-11 and figure 7-12, it can be seen, that for the 42 minute case, the magnitude of the X and Y gyro bias error for the first period after loss of GPS, is greater than the corresponding values observed in the 60 minute case.

This result confirms the conclusions made in the covariance analysis results, which was, that the Kalman filter does a good job of observing the local level gyro bias errors during the 60 minute period of GPS coverage, but not the 42 minute period.

Figures 7-10 shows the make up of the Kalman filter latitude error for the 3 hour case. The figure shows that the random noise is the major contributor to the Kalman filter error for both periods of GPS outage. This result confirms the conclusions drawn from the covariance analysis above about the 3 hour operation, which was, that the Kalman filter is able to make a good estimate of all three gyro biases after having this initial phase of GPS coverage.

7.5.3 95% CIRCULAR ERROR PERFORMANCE FIGURES

The overall 95% performance figure for the IRS is evaluated as follows :

$$95\% \text{ Err} = \frac{[0.712 + 0.365]}{2} \quad \text{NM/HR} \quad (7.19)$$

$$95\% \text{ Err} = 1.3180 \quad \text{NM/HR} \quad (7.20)$$

The corresponding 95% circular value for the overall Kalman filter error for the 42 minute GPS case is evaluated as :

$$95\% \text{ Err} = \frac{[0.712 + 0.3255]}{2} \quad \text{NM/HR} \quad (7.21)$$

$$95\% \text{ Err} = 1.26994 \quad \text{NM/HR} \quad (7.22)$$

Similarly, the 95% circular value for the overall Kalman filter error for the 60 minute GPS case is evaluated as :

$$95\% \text{ Err} = \frac{[0.46 + 0.2125]}{2} \quad \text{NM/HR} \quad (7.23)$$

$$95\% \text{ Err} = 0.8230 \quad \text{NM/HR} \quad (7.24)$$

Finally, the 95% circular value for the overall Kalman filter error for the 3 hour GPS case is evaluated as :

$$95\% \text{ Err} = \frac{[0.52 + 0.2]}{2} \quad \text{NM/HR} \quad (7.25)$$

$$95\% \text{ Err} = 0.8811 \quad \text{NM/HR} \quad (7.26)$$

7.5.4 DISCUSSION OF RESULTS FOR CIRCULAR ERROR PERFORMANCE

The 95% circular error performance figure for the effect of all of the IRS errors was computed to be 1.3180 nautical miles per hour. For the Kalman filter 42 minute GPS case, the 95% performance figure was computed to be 1.2699 nautical miles per hour, this figure relating to the first period of GPS outage. For the 60 minute and 3 hour cases the corresponding 95% performance figures were found to be 0.8230 nautical miles per hour and 0.8811 nautical miles per hour.

The Kalman filter result for the 60 minute case shows that there is an improvement in performance of approximately 0.4 nautical miles per hour when compared with the same result for the 42 minute case. This is explained by the fact that at 42 minutes the Kalman filter is still estimating the value of the x and y local level gyros. The Kalman filter uncertainty in its estimate of the local level gyros reaches a final minimum after one and a half hours, but between the 42 minute and 60 minute points, the uncertainty is rapidly decreasing.

The result for the Kalman filter performance for the 3 hour case is 0.8811 nautical miles per hour, which is slightly greater than the value for the 60 minute case. This can be explained by the fact that the Kalman filter's uncertainty in its estimate of the x and y gyro and accelerometer biases reaches a minimum at the one and a half hour point. After this time the Kalman filter uncertainty in these states starts to increase due to the presence of process noise. The fact that the filter uncertainty for a state starts to increase implies that the filter is no longer able to observe that state. Itzhack (1980) discusses the problem of observing IRS errors and provides details of several manoeuvres that enhance a Kalman filter's ability to observe certain IRS errors.

7.6 COMMENTS

In this chapter techniques that measure navigation system performance that were previously developed in chapter 6, have been applied to the inertial reference system and the Kalman filter, to assess the Kalman filter navigation performance.

The results obtained show that the Kalman filter provides a reduction in the FMC position error compared to the IRS position error. This improvement in the FMC result is achieved during the IRS/GPS and IRS only mode of operation. For the IRS/GPS mode of operation an improvement in the FMC performance against the IRS is expected, since accurate GPS measurements are being used in the form of position and velocity. The effect of using GPS position and velocity as measurement inputs to the Kalman filter is that the Kalman filter tracks the IRS position and velocity states very closely, with the result that a very accurate FMC position is obtained.

For the IRS only mode the results show how the Kalman filter provides an improvement in the FMC position compared to the IRS. In this mode of operation the Kalman filter is predicting the IRS errors. The result for the FMC position compared to the IRS position is therefore an indication of how well the Kalman filter has been able to observe the various IRS states. In the case of the z gyro bias error source, the results have shown the Kalman filters ability to observe this state is sensitive to heading.

At the end of chapter 6, the comment was made that although the customer inertial reference is quoted as being a 2 nm/hr 95% circular error system, results obtained from simulation only showed performance in the range 1.2 to 1.3 nm/hr, 95%. In this chapter, a similar set of results not demonstrating the IRS 2 nm/hr figure were obtained. Therefore, the Kalman filter performance figure could only be evaluated for a corresponding IRS performance figure which was, less than 2 nm/hr.

In reviewing the monte carlo analysis, sensitivity analysis and covariance analysis techniques, it was recognised that although the values used for the simulations were obtained from the customer error budget table (see appendix B), no consideration was given to the IRS alignment and the way that the alignment might affect the error values. Therefore, for all of the simulations carried out in chapter 6 and chapter 7, the error budget values used were assumed to be independent of each other. In the next chapter, the alignment process that is relevant to the customer inertial reference system is considered, and its impact on the Kalman filter assessed.

CHAPTER 8.0

KALMAN FILTER MODIFICATION TECHNIQUES

8.1 INTRODUCTION

The results from the study carried out in the last chapter, into the effects of different periods of GPS, has shown that not all of the IRS errors are observed at the same time, and as a consequence of this, the Kalman filter performance varies according to when GPS is lost. In particular, the results revealed that under certain circumstances the Kalman filter takes a considerable time to learn the Z gyro bias. Also it was noted that an IRS performance figure of 2 nm/hr was not able to be simulated, this value being the performance figure quoted for the customer IRS.

In this chapter, the IRS alignment which occurs in the customer inertial reference system is examined in detail. Consideration is given to the initialisation of the Kalman filter, so that it reflects the IRS alignment condition.

The first part of the work deals with alignment conditions which are specifically related to the customer inertial reference system. Covariance values are developed that can be used to initialize the Kalman filter so that the filter is matched to a specific IRS alignment condition. Then a more general alignment conditions not directly related to the customer IRS is investigated, and Kalman filter initialisation parameters developed.

8.2 INERTIAL REFERENCE SYSTEM ALIGNMENT DESCRIPTION

During the alignment and navigation phases of operation of the customer IRS, one of several different processes can take place which are dependent on real time conditions. There are two types of alignment modes referred to as a normal alignment and extended alignment. Normal alignment can be considered to take place, when the aircraft has been parked overnight and is switched on for the first flight of the day. Once normal alignment is completed which takes about 10 minutes, the system enters the navigate mode where the extended alignment phase is entered if the aircraft has not taxied for the first time. Assuming that an extended alignment has taken place, the resultant errors in the inertial system that remain uncorrected are a Z gyro bias and the components of the level axis gyro bias errors along the east axis. Whereas the normal alignment phase takes place when the inertial system is in alignment mode, the extended alignment solution takes place when the system is in the navigate mode.

This last point causes a potential design problem, which is where to start the integrated GPS/IRS Kalman filter solution. If the Kalman filter is started immediately the IRS system goes into navigate mode after completion of a normal alignment, then the Kalman filter will start to learn what it considers to be IRS errors. If at the same time, the IRS has entered extended alignment mode, then it will be trying to learn and thus reduce its own errors. The consequence of this being the Kalman filter will be trying to learn IRS errors that may not be present at the end of the extended alignment phase of operation. To gain a better understanding of the extended alignment process and the requirements it places on the Kalman filter design, the following investigations were carried out.

8.2.1 DESCRIPTION OF THE EXTENDED ALIGNMENT SOLUTION

In the extended alignment solution, estimates of X and Y platform axis tilt rates are made by the IRS, in an attempt to resolve system errors. The estimated tilt rates are resolved through the wander angle into equivalent rates about the north and east axis. The north axis tilt rate is assumed to be due to components of only level gyro bias error along the north axis, this component of level axis gyro bias error is therefore corrected. The equation for the north axis bias correction is developed below.

Consider the axis set shown in figure 8-1 where the platform axis is misaligned from the north / east axis set by an angle α . If the total gyro output is made up of a true value and an error value, then for the x and y gyros the total gyro outputs ϵ_x and ϵ_y , can be written in terms of the x and y platform axis as follows :

$$\epsilon_x = \text{Cos}(\lambda)\text{Sin}(\alpha)\Omega + \epsilon b_x \quad (8.1)$$

$$\epsilon_y = \text{Cos}(\lambda)\text{Cos}(\alpha)\Omega + \epsilon b_y \quad (8.2)$$

Resolving into the north axis gives :

$$\epsilon_N = \text{Cos}(\alpha)\epsilon_y + \text{Sin}(\alpha)\epsilon_x \quad (8.3)$$

Which becomes:

$$\begin{aligned} \epsilon_N = \text{Cos}(\lambda)\Omega(1 - \text{Sin}^2(\alpha)) + \text{Cos}(\alpha)\epsilon b_y \\ + \text{Sin}^2(\alpha)\text{Cos}(\lambda)\Omega + \text{Sin}(\alpha)\epsilon b_x \end{aligned} \quad (8.4)$$

This reduces to :

$$\epsilon_N = \text{Cos}(\lambda)\Omega + \text{Cos}(\alpha)\epsilon b_y + \text{Sin}(\alpha)\epsilon b_x \quad (8.5)$$

Finally the north axis tilt rate error becomes:

$$\epsilon b_N = \text{Cos}(\alpha)\epsilon b_y + \text{Sin}(\alpha)\epsilon b_x \quad (8.6)$$

Once a value for the north axis tilt rate error has been obtained, it is resolved back into components of x and y gyro bias in terms of platform axis via the angle α , and then into body axis components via platform heading. Once values for the gyro biases have been obtained in body axis, they are added to gyro bias terms from calibration.

After these bias corrections have been carried out, the gyro bias errors in the system that remain uncorrected are the Z gyro bias error which primarily causes azimuth gyro drift, and the component of level axis gyro bias along the east axis. The IRS state that accounts for the azimuth error is the Z platform axis tilt. The value of this error is related to the unknown component of east gyro bias by the following equation.

$$\phi_z = \frac{\epsilon b_E}{\Omega} \quad (8.7)$$

In terms of x and y gyro biases this becomes :

$$\phi_z = \frac{\cos(\alpha) \epsilon_X}{\Omega} + \frac{\sin(\alpha) \epsilon_Y}{\Omega} \quad (8.8)$$

8.2.2 IRS THEORETICAL ERROR MODEL FOR GYRO BIAS

It has been stated that at the end of the extended alignment solution there is a z platform axis tilt error associated with an unknown component of east gyro bias. These two error sources exist because they cancel each other out. To explain this point a single channel error model showing the effect of gyro bias on velocity will be developed using classical control theory. Consider the single channel inertial system model given in figure 8-2. The transfer function for this system can be obtained using the laplace transform operator as follows :

$$\frac{V(s)}{\epsilon b(s)} = \frac{\frac{g}{s^2}}{1 + \frac{g}{Rs^2}} \quad (8.9)$$

For a step input :

$$\epsilon b(s) = \frac{\epsilon}{s} \quad (8.10)$$

The equation then becomes :

$$V(s) = \epsilon g \frac{1}{s(s^2 + (\sqrt{\frac{g}{R}})^2)} \quad (8.11)$$

The inverse transform gives :

$$V(t) = R\epsilon(1 - \text{Cos} \sqrt{\frac{g}{R}} t) \quad (8.12)$$

Which can be written in convenient form as :

$$V(t) = 60.1 \epsilon(1 - \text{Cos}(4.46t)) \quad (8.13)$$

Where :

- v - Velocity (kts)
- ϵ - gyro bias (deg/hr)
- t - time (hours)

The transfer function shows that the effect of a gyro bias error on velocity, is to cause an error with a one minus cosine characteristic that repeats itself after 84 minutes, this being the Schuler period. The peak of the waveform therefore appears after 42 minutes. In the inertial system then an east gyro bias if it existed on its own, would cause a north velocity error in nav mode with the characteristic discussed above. At the end of the extended alignment there is a heading error associated with the east gyro bias error. If the heading error existed on its own, it would also cause a north velocity error in nav mode with the same characteristic as the gyro bias but of opposite sign, but because both errors exist together they cancel each other out because of their opposite signs.

If the inertial system is rotated through 180 degrees, then the two error sources no longer cancel, they become additive.

This is because the east gyro bias error is caused by gyros which are in the body axis of the system, and the body axis changes its orientation with respect to the platform axis when the inertial system is rotated. The heading error or azimuth error is in the platform axis, and its orientation does not change with heading.

This uncoupling of the balanced errors is peculiar to strapdown inertial navigation systems where the gyros are physically mounted to the body of the unit. In a gimballed system although the two error sources may exist the error sources do not become uncoupled, because for a gimballed system the gyros are space stable and therefore the platform orientation does not change as system heading changes.

8.2.3 SIMULATION DETAILS

Simulations for a non moving aircraft (stationary simulations) were set up to model the effect of the customer IRS extended alignment condition, using the optimal IRS error model simulation discussed in chapter 5. The simulation runs were carried out at latitude 0 degrees with an initial heading of 090 degrees, as this corresponds to an east alignment. Under this condition the unknown component of east gyro bias is equal to the full value of the y gyro bias, and the component of the north bias is the full value of the x gyro bias. Since the north gyro bias component is measured and removed during the extended alignment phase, then the value of the x gyro bias used in the simulation was taken as zero. The value for the y gyro bias was set equal to 1.398×10^{-4} rads/hr which is the equivalent rms value obtained from the customer IRS error budget as given in appendix B. The remaining z platform axis tilt error source value was determined using equation 8.8, and found to be 533×10^{-6} rads.

A theoretical value for peak velocity error which occurs at 42 minutes, was also computed using equation 8.13, and found to be 0.9615 kts. The theoretical model solution is useful in that it can produce theoretical predictions, which can be used to validate results obtained from simulation, where the simulation model is different from the theoretical model.

8.2.4 SIMULATION RESULTS

Three separate simulations were carried out to investigate the effects of the y gyro bias, and z platform axis tilt, error sources at alignment time. For the first simulation, a y gyro bias having a value of 0.008 deg/hr was used.

For the second simulation, a z platform axis tilt value was chosen from equation 8.8.

For the third simulation the y gyro bias and z platform axis errors were combined, so that the resultant effect of the two error sources could be examined.

Figure 8-3 shows the combined results for the three simulations all of which were run for a 2 hour period. For the case of the y gyro bias (EPSY), the continuous line shows that this error source causes a velocity error in the x platform axis (DEL VX) of approximately 1 knot at 42 minutes, with almost zero velocity error in the y platform axis (DEL VY). By using the theoretical result obtained from the single axis IRS model, the x platform axis velocity error was found to be 0.95046 kts. So there is a good agreement with the value observed from the simulation and the theoretical prediction.

The y platform axis velocity error is zero due to the fact that the system is simulated as being stationary with the values of latitude, longitude and alpha angle all chosen so that there is no cross coupling of errors in the local level IRS axis.

The dashed line in figure 8-3 shows the result for the z platform axis tilt error (PHIZ). Before considering the result, it is useful to examine the effect of a z platform axis tilt error on the x and y local level axis as shown in figure 8-4. The z tilt can be seen to cause the y platform axis to be displaced towards the south axis, and the x platform axis to be displaced towards the west axis. The value of the y platform axis tilt error (PHIY) will therefore be significant compared to the value of the x platform axis tilt error (PHIX), because the y axis is moved towards the south axis where the full value of earth rate is sensed.

Examination of figure 8-3 shows that the value of the y platform axis tilt error is significant when compared with the x platform axis tilt error. The plot for the y axis tilt error shows a sinusoidal type variation which can be explained as follows :

The y platform axis tilt error starts to build up due to the displacement of the y axis towards south. The y tilt error generated, causes the vertical component of acceleration which is gravity for this case, to be resolved into the x platform axis as a velocity error. This velocity error is then feedback to level the offset y axis, causing a Schuler related oscillation in the y platform axis tilt error term.

The result for the x platform axis velocity error can be seen to be of the form of a "1-cosine" graph, which is similar to the result obtained for the first simulation but of opposite sign.

The result for the y platform axis tilt error for the first simulation above (see continuous plot for PHIY) also shows an oscillation 180 degrees out of phase when compared with the same result for the second simulation.

The two previous results have shown the effects of the individual IRS error sources. The third simulation as shown by the dotted line in figure 8-3, gives the result for the combined effect of the two error sources. For the x platform axis velocity error, the result can be seen to be zero. Similarly for the x platform axis tilt error the result can be seen to be zero. For the case of the Y platform axis velocity error, and the x platform axis tilt, although the results are not zero, they are very small.

This third simulation has shown that the effect of combining the two IRS error sources is to produce a zero velocity error. This is the result expected from the extended alignment phase of operation.

The next phase of the work deals with the Kalman filter and how it can be set up to reflect the conditions of the IRS extended alignment.

8.3 MATCHING THE KALMAN FILTER TO THE ALIGNMENT CONDITION

The objective for this section of the work is to find a method whereby the Kalman filter covariance matrix can be initialised to reflect the particular conditions of the customer IRS extended alignment. When a suitable solution is found the Kalman filter will be referred to as being matched to the IRS extended alignment condition. The approach taken to find the Kalman filter matched parameters is based on the discrete Kalman filter equations which have been discussed in chapter 4 and are summarized below.

Kalman Filter Covariance Estimate Equation

$$P_k(-) = \Phi_k P_{k-1}(+) \Phi_k^T + Q_{k-1} \quad (8.14)$$

Kalman Filter Gain Equation

$$K_k = [P_k(-)H_k^T][H_k P_k(-)H_k^T + R_k]^{-1} \quad (8.15)$$

Kalman Filter Covariance Update Equation

$$P_k(+) = [I - K_k H_k] P_k(-) \quad (8.16)$$

The previous phase of work has dealt with the extended alignment condition, by considering one particular alignment heading and showing how the IRS functions at that heading. The particular heading of 090 degrees was specifically chosen because, on this heading the y gyro platform axis, and the east geographic axis are coincident, thus at the end of the extended alignment phase of operation, the unknown component of east gyro bias is simply equal to the total value of the y gyro bias. The x gyro bias is assumed to be removed for this particular alignment orientation, because the x platform axis is coincident with the north geographic axis, and the north gyro bias is measured and removed during extended alignment.

This initial development of the Kalman filter matched solution will assume the above extended alignment conditions for the IRS, and therefore the covariance initialisation parameters that are developed will be appropriate for only one specific heading. This solution will lay the framework however, for the more general case to be considered later.

The first task in the development of the covariance parameters for a matched Kalman filter solution, is to choose values to initialize the Kalman filter covariance matrix.

These values are chosen on the basis of what is known about the IRS system. In this instance because there are only two IRS error sources being considered, a y gyro bias in balance with a z platform axis tilt, then all of the off-diagonal elements of the 12 x 12 Kalman filter covariance matrix are taken as zero at initialization. All of the leading diagonal elements are set to unity, except for the two values relating to the IRS error sources. These two covariance parameters are $P_{7,7}(0)$ for the z platform axis tilt state and $P_{9,9}(0)$ for the y gyro bias state. Appendix C gives the relationship between the Kalman filter diagonal covariance elements and the IRS states.

Having set the values for the initial covariance matrix, the first and where necessary second iterations of the covariance estimate (see 8.14), Kalman filter gain (see 8.15) and covariance update equations (see 8.16) are worked out, so that the conditions that are required for a matched filter solution can be identified. The results for the first iteration of the Kalman filter covariance update equation for a stationary system will now be considered, where the initial value of the covariance matrix $P(0)$ is taken to be zero except for the two elements $P_{7,7}(0)$ and $P_{9,9}(0)$.

From the result for the first iteration of the covariance update equation $\underline{P}(+)$ it was found that the first five diagonal terms were zero. The sixth diagonal term which is the Kalman filter update for the y platform axis tilt was not zero and is discussed below.

8.3.1 Y PLATFORM AXIS TILT

The result for the covariance update equation for the Y platform axis tilt after the first iteration is :

$$P_{6,6}(+) = P_{6,6}(-) - K_{6,3}P_{3,6}(-) \quad (8.17)$$

Substituting in the value for the gain $K_{6,3}$ gives :

$$P_{6,6}(+) = P_{6,6}(-) - \frac{P_{6,3}(-)}{P_{3,3}(-) + R_{velx}} P_{3,6}(-) \quad (8.18)$$

where the Y tilt value obtained from the covariance estimate equation (8.14) is :

$$P_{6,6}(-) = P_{7,7}(0)W_x^2\Delta t^2 + P_{9,9}(0)C_{2,2}^2\Delta t^2 \quad (8.19)$$

Similarly, the cross correlation term relating the Y tilt and X platform axis velocity, obtained from the first iteration of the covariance estimate equation is :

$$P_{6,3}(-) = P_{3,3}(0)\frac{\Delta t}{R} - P_{6,6}(0)g\Delta t + P_{7,7}(0)A_yW_x\Delta t^2 \quad (8.20)$$

For the IRS extended alignment condition being considered here, the Y gyro bias and Z platform axis tilt errors are taken to be balanced, which means that the value of the IRS Y tilt error is zero. For the Kalman filter to be matched to this IRS condition then, the value of Kalman filter covariance update equation for the y axis tilt $P_{6,6}(+)$ must also be zero, since if it is not zero the Kalman filter will think it is uncertain of the Y tilt state and will try to learn the value of the tilt state. It will be unable to do this however, because in the IRS the value of the Y tilt state is zero due to the balancing effect of the Y gyro bias and the Z platform axis tilt.

For $P_{6,6}(+)$ to be zero, then $P_{6,6}(-)$ must be zero also. By examining equation 8.19 above, it can be seen that the equation for $P_{6,6}(-)$ can only be made equal to zero by the addition of extra terms. The terms needed to obtain a zero condition for $P_{6,6}(-)$ are developed in section 8.3.3.

8.3.2 Y GYRO BIAS

The result for the covariance update equation for the Y gyro bias after the first iteration is :

$$P_{9,9}(+) = P_{9,9}(-) - K_{9,3}P_{3,9}(-) \quad (8.21)$$

substituting in the value for the gain $K_{9,3}$ gives :

$$P_{9,9}(+) = P_{9,9}(-) - \frac{P_{9,3}(-)}{P_{3,3}(-) + R_{velx}} P_{3,9}(-) \quad (8.22)$$

where the Y gyro bias value obtained from the covariance estimate equation is given by :

$$P_{9,9}(-) = P_{9,9}(0) \quad (8.23)$$

Similarly, the cross correlation term relating the Y gyro bias and the X platform axis velocity obtained from the covariance estimate equation is :

$$P_{9,3}(-) = 0 \quad (8.24)$$

For the second iteration of the covariance update equation the value for the Y gyro bias becomes :

$$P_{9,9}(+) = P_{9,9}(-) - \frac{P_{9,9}(-)C_{2,2}g\Delta t^2}{P_{3,3}(-) + R_{velx}} P_{3,9}(-) \quad (8.25)$$

Expressing values in terms of the covariance matrix initialisation parameters gives :

$$P_{9,9}(+) = P_{9,9}(0) - \frac{(P_{9,9}(0)C_{2,2}g\Delta t^2)^2}{P_{3,3}(-) + R_{velx}} \quad (8.26)$$

This last equation shows how the Kalman filter uncertainty in the Y gyro bias estimate starts to decrease. The equation models the effect of the Y gyro bias first getting into the Y axis tilt, and then into the X velocity. Providing an X velocity measurement therefore allows the Kalman filter to estimate the Y gyro bias effect.

For the Kalman filter to be matched to the IRS condition, the value of the update equation $P_{9,9}(+)$ must be constant and equal to $P_{9,9}(0)$, since this is the initial uncertainty in the Kalman filter estimate of the Y gyro bias state. To achieve this condition, the term $P_{9,3}(-)$ must be zero. From equation 8.26 above the value for $P_{9,3}(-)$ after the second iteration can be seen to be :

$$P_{9,3}(-) = P_{9,9}(0)C_{2,2}g\Delta t^2 \quad (8.27)$$

This equation cannot be made equal to zero in its present form since $P_{9,9}(0)$ is non zero and $C_{2,2}$ is unity. The additional terms that are needed to make $P_{9,3}(-)$ zero are discussed in the next section.

8.3.3 SELECTING THE MATCHED KF INITIALISATION PARAMETERS

The analysis of the Kalman filter covariance equations has shown that if the Kalman filter is to be matched to IRS extended alignment condition, then additional terms are required. These parameters can be generated by choosing certain cross correlation terms to be non zero in the initial Kalman filter covariance matrix $P(0)$. Identifying which cross correlation terms to choose is the difficult task and is discussed below.

Based on the fact that the Y gyro bias and the Z platform axis tilt errors are balanced during the IRS extended alignment, the following set of cross correlation terms, $P_{7,9}$ and $P_{9,7}$, were chosen and found to satisfy the above requirements. The terms $P_{7,9}$ and $P_{9,7}$ are the cross correlations between the y gyro bias and the z platform axis tilt. The way that these cross correlation terms can be used to produce a balanced Kalman filter will now be examined.

Consider first the initial covariance matrix $P(0)$, it now has four non zero values which are :

- $P_{7,7}(0)$ - Value to be determined
- $P_{7,9}(0)$ - Value to be determined
- $P_{9,7}(0)$ - Value to be determined
- $P_{9,9}(0)$ - Value chosen according to the one sigma value of the y gyro bias given in the error budget table.

At this stage no attempt is made to consider possible numeric values for the first three unknown parameters above. Numeric values can be found once the relationships between the parameters has been established.

8.3.3.1 Y PLATFORM AXIS TILT ERROR

Using the four non zero values for the Kalman filter initial covariance matrix $P(0)$, the covariance estimate for the Y platform axis tilt and the covariance update for the Y gyro bias are recomputed.

The results for the first iteration of the covariance estimate equation for the y platform axis tilt becomes :

$$P_{6,6}(-) = P_{7,7}(0)W_x^2\Delta t^2 + P_{7,9}(0)W_xC_{2,2}\Delta t^2 + P_{9,9}(0)C_{2,2}^2\Delta t^2 + P_{9,7}(0)W_xC_{2,2}\Delta t^2 \quad (8.28)$$

To meet the balanced Kalman filter condition the value of $P_{6,6}(-)$ is required to be zero. A comparison of the equation with its previous form (see equation 8.19) shows that it now contains extra terms $P_{9,7}$ and $P_{7,9}$. Additional information is still needed however, before actual values for the parameters can be determined, so it is necessary to proceed with the analysis and examine the covariance update equations for the y gyro bias state.

8.3.3.2 Y GYRO BIAS STATE

The first iteration of the covariance update equation for the y gyro bias state is :

$$P_{9,9}(+) = P_{9,9}(0) \quad (8.29)$$

For the second iteration the update equation becomes :

$$P_{9,9}(+) = P_{9,9}(-) - \frac{P_{9,3}(-)}{P_{3,3}(-) + R_{velx}} P_{3,9}(-) \quad (8.30)$$

where

$$P_{9,3}(-) = P_{9,9}(0)C_{2,2}g\Delta t^2 - P_{9,7}(0)W_xg\Delta t^2 \quad (8.31)$$

And

$$P_{3,9}(-) = P_{9,9}(0)C_{2,2}g\Delta t^2 - P_{9,7}(0)W_xg\Delta t^2 \quad (8.32)$$

To meet the balanced Kalman filter condition, the uncertainty in the estimate of the y gyro bias is required to remain constant at its initialised value of $P_{9,9}(0)$.

This constant condition can be satisfied by choosing the value of $P_{9,7}(0)$ in the equation for $P_{9,3}(-)$ (see 8.31) above as follows :

$$P_{9,7}(0) = -\frac{P_{9,9}(0)}{W_x} \quad (8.33)$$

The value for the cross correlation term $P_{7,9}(0)$ must also be equal to $P_{9,7}(0)$ due to the fact the covariance matrix is symmetrical. If the covariance term $P_{7,9}(0)$ is chosen such that it is not equal to the value $P_{9,7}(0)$ then a covariance matrix may be set up that is not positive definite.

If the chosen values for $P_{9,7}(0)$ and $P_{7,9}(0)$ are now substituted into the equation for $P_{6,6}(-)$ (see 8.28), then the value for the final unknown term $P_{7,7}(0)$ can be found :

Substituting in values for $P_{9,7}(0)$ and $P_{7,9}(0)$ into equation 8.28 gives :

$$P_{6,6}(-) = P_{7,7}(0)W_x^2\Delta t^2 + P_{9,9}(0)C_{2,2}^2\Delta t^2 - 2P_{9,9}(0)C_{2,2}^2\Delta t^2 \quad (8.34)$$

The value for $P_{7,7}(0)$ that makes $P_{6,6}(-)$ equal is then found to be :

$$P_{7,7}(0) = \frac{P_{9,9}(0)}{W_x^2} \quad (8.35)$$

8.3.3.3 SUMMARY OF RESULTS

The analysis has shown how the Kalman filter can be matched to the IRS extended alignment condition by suitable choice of the parameters contained in the initial covariance matrix. The relationship between the four parameters has been developed and is summarized below.

$$P_{9,9}(0) = \sigma^2 \quad (8.36)$$

Where σ^2 is the variance of the Y gyro bias state obtained from the error budget table.

$$P_{9,7}(0) = -\frac{P_{9,9}(0)}{W_x} \quad (8.37)$$

$$P_{7,9}(0) = -\frac{P_{9,9}(0)}{W_x} \quad (8.38)$$

$$P_{7,7}(0) = \frac{P_{9,9}(0)}{W_x^2} \quad (8.39)$$

8.3.4 KALMAN FILTER SIMULATION RESULTS FOR THE MATCHED FILTER

Simulations for a non moving aircraft were carried out to investigate the performance of the Kalman filter where the Kalman filter covariance matrix was initialised with the design values developed above (see equations 8.36 to 8.39). Stationary simulations were carried out at two locations, latitude north 0 degrees and latitude north 45 degrees. For each location the effect on the Kalman filter of uncoupling the IRS errors with a 180 degree was investigated. In all cases the IRS alignment heading was taken to be 090 degrees ie an easterly alignment. The IRS error sources were chosen to be representative of the extended alignment condition where the Y gyro bias error is balanced by a Z platform axis tilt.

The actual value chosen for the Y gyro bias was 0.008 degs/hr this being the rms value for the Y gyro bias obtained from the customer IRS error budget (see appendix B). The corresponding value for the z platform axis tilt was determined using equation 8.8 where the value of the earth rate term (Ω) is 0.2618 rad/hr for the zero latitude case and 0.1851 rad/hr for the 45 degree latitude case.

Figure 8-5 shows the result for the Kalman filter covariances for a stationary simulation carried out at latitude north zero degrees, where a 180 degree rotation was applied after one hour to uncouple the IRS error sources. GPS was simulated as perfect for the two hour run.

The variables SD(1) to SD(12) in figure 8-5 are covariance values which correspond to the values of the Kalman filter covariance matrix diagonal terms. The IRS states corresponding to the covariance diagonal terms are summarized in appendix C. The result for the Kalman filter uncertainty for the Y gyro bias SD(9), and the Z platform axis tilt SD(7), can both be seen to be constant during the first hour of the two hour simulation. The fact that the two values are constant means the Kalman filter is not able to improve on its initial estimate of the two IRS states. The two states are therefore un-observable to the Kalman filter, and the filter can be considered to be correctly matched to the IRS condition.

For the second hour of the simulation the results show that the filter uncertainty in both states starts to decrease, reaching a final value of zero. This is due to the 180 degree rotation being applied at the one hour point, which causes the IRS error sources to become uncoupled, thus making the error states observable to the Kalman filter. The final value of the two covariances SD(7) and SD(9), reach a zero value because the process noise has been set to zero. A zero covariance value means that the Kalman filter is totally certain of its estimate. Figure 8-6 shows the result for the IRS states v Kalman filter estimates. It can be seen that the Kalman filter has been able to learn the full value of the IRS states for the Y gyro bias (EPSY) and for the Z platform axis tilt (PHIZ). Figure 8-7 shows the results for the Kalman filter covariances where the simulation was carried out at latitude north 45 degrees, with a 180 degree rotation applied after one hour.

The same trend in the Kalman filter covariances is noted as for the zero latitude case above, this being a constant value of covariance during the first hour of the simulation, followed by a decreasing value finally reaching zero, during the second hour. The constant value of covariance for the Z platform axis tilt state is different for the two latitude cases, as its value is a direct function of latitude.

The above results show, that the Kalman filter can be matched to a specific IRS post alignment condition by suitable selection of the Kalman filter initialization values for the covariance matrix. The results show that the technique is not limited to low latitudes. During the time that the IRS errors are in balance, the Kalman filter uncertainty remains constant. The un-balancing of the IRS errors by rotation, is correctly detected by the Kalman filter.

8.4 KALMAN FILTER MATCHING WITH THE Z GYRO BIAS

The last sections dealt with the general problem of matching the Kalman filter to the particular IRS post alignment conditions where the East gyro bias and Z platform axis tilt errors were balanced. Consideration is now given to the effects of including the Z gyro bias error source. Inclusion of the IRS z gyro bias error term does not affect the previously developed covariance parameters (equations 8.36 to 8.39), but it does mean that an additional term relating to the z gyro bias state is required when initialising the Kalman filter covariance matrix. This additional term is $P_{10,10}$ which is set equal to 7.7982×10^{-8} this being the variance of the Z gyro bias as given by the IRS error budget table (see appendix B).

8.4.1 SIMULATION DESCRIPTION

The results presented here are for simulations carried out under different latitude conditions. The first set of results follow the pattern described above where runs were carried out at latitude zero with and without a 180 degree rotation, followed by two similar cases carried out at latitude north 45 degrees. In each case the IRS alignment heading was taken to be an east heading of 090 degrees. The IRS error sources were chosen to be representative of the extended alignment condition as discussed above. The value for the z gyro bias error source used in the IRS error model was chosen to be equivalent its one sigma value as given by the error budget table.

8.4.2 DISCUSSION OF RESULTS FOR THE ZERO LATITUDE CASE

Figure 8-8 shows the result for the zero latitude case without a turn. The result shows that the Kalman filter uncertainty in its estimate of the IRS Y gyro bias error source (SD 9) remains virtually constant at its initialised value, due to the fact that the IRS Y gyro bias error source is balanced by a Z platform axis tilt, and is thus not observable to the Kalman filter. For the Z platform axis tilt the Kalman filter uncertainty in its estimate (SD 7) can be seen to increase from the initialised value reaching a peak value after approximately 30 minutes before decreasing again and finally settling out with a value equal to the initialization value.

The additional uncertainty in the filter estimate of the Z platform axis is due to the inclusion of the Z gyro bias. The Kalman filter uncertainty in this state (SD 10) starts decreasing from its initial value after a time of approximately 24 minutes, reaching a final value of zero approximately one hour later.

Figure 8-9 shows an overlay of the IRS and Kalman filter states for the same simulation. The plot for the Kalman filter estimate of the Z gyro bias (EPSZ) reveals how well the Kalman filter is able to estimate this constant IRS error, during the two hour simulation period, thus confirming the observations made above from the covariance matrix result, about the uncertainty of the Kalman filter estimate of the Z gyro bias.

The result for the Kalman filter estimate of the Z platform axis tilt error (PHIZ) shows how only part of the total IRS error source is learnt. This is due to the fact that the Z platform axis tilt error can be considered to be made up of two components, one part due to the Y gyro bias error and another part due to the direct integration of the Z gyro bias. The Kalman filter is able to estimate the first component of the Z tilt caused by the integration of the Z gyro bias, but not the second component, because this part of the error is in balance with the Y gyro bias and is therefore not observable to the Kalman filter as discussed above. The Kalman filter estimate of the Y gyro bias (EPSY) can be seen to be zero.

Figure 8-10 shows the result for a 180 degree turn applied after one hour. The Kalman filter uncertainty in the Y gyro bias (SD 9) and the Z platform axis tilt (SD 7) is constant during the first hour due to the fact that the two IRS error sources are balanced. During the second hour the Kalman filter uncertainty for the two states can be seen to decrease to a zero value, due to the fact that the applied rotation has caused the two IRS error sources to become unbalanced, making the individual errors observable to the Kalman filter. The Kalman filter covariance plot for the Z gyro bias (SD 10) starts to decrease from its constant value after a period of approximately 30 minutes, and reaches a final value of zero after approximately 1 hour 30 minutes. When this result is compared with the same result for the non turn case above (see figure 8-8) it is seen that the Kalman filter learns the Z gyro at the same rate for both cases.

For these two covariance results it has been shown how the 180 degree rotation allows the Kalman filter to learn the value of the Z gyro bias and the two unbalanced IRS error sources. Figure 8-11 (IRS v KF) shows the comparison of IRS and Kalman filter states for the turn case. The result shows how the Kalman filter is able to correctly predict the IRS values of the three states Y gyro bias (EPSY), Z platform axis tilt (PHIZ) and Z gyro bias error (EPSZ) as a result of the 180 degree turn.

The result for the Z platform axis tilt is of particular interest because it shows how the Kalman filter was first able to estimate part of the IRS state during the first hour of the simulation, which agrees with the previous result observed in figure 8-9 above, and then the full value of the error source once a 180 degree rotation was applied.

This set of results has shown how the Kalman filter can be matched to the customer IRS extended alignment condition when the alignment is carried out at the coordinates north 0 degrees / east 0 degrees. The next set of results considers the effect of an alignment carried out at the coordinates north 45 degrees / east 45 degrees. Both turn and non-turn cases are considered.

8.4.3 DISCUSSION OF RESULTS FOR THE NON ZERO LATITUDE CASE

The result for the comparison of IRS and Kalman filter states for the non turn case is shown in figure 8-12. The Kalman filter estimate of the Z platform axis tilt error (PHIZ) shows that only part of this IRS error has been observed due to the fact that the error source is made up of two components, one component due to the Y gyro bias and the other, the direct integration of the Z gyro bias. As discussed above for the zero latitude case (see figure 8-9), the IRS Y gyro bias error is balanced by a component of the Z platform axis tilt error making the Y gyro bias also unobservable to the Kalman filter. This fact can be seen by examination of figure 8-12 which shows that the Kalman filter estimate of the Y gyro bias error (EPSY) is zero.

Figure 8-13 shows the result for the comparison of IRS and Kalman filter states for the case where a 180 degree rotation was applied after one hour. The result for the Kalman filter estimate of the Y gyro bias, and the Z platform axis tilt, shows that the filter was able to estimate both of the error sources once they had been unbalanced by the 180 degree rotation. This result is similar to the one obtained for the zero latitude case above and proves that in respect to these error sources the Kalman filter is correctly matched to the IRS extended alignment condition. The result for the Z gyro bias (EPSZ) shows that the Kalman filter is only able to learn the Z gyro bias error to within 95% of its value during the two hour simulation period.

An examination of the two results for the turn case carried out at zero latitude (see figure 8-11) and the mid latitude case carried out at north 45 degrees (see figure 8-13), shows that the Kalman filter takes a shorter time to learn the Z gyro bias in the zero latitude case compared to the mid latitude case. The reason that the Kalman filter is able to learn the error source faster in the zero latitude case is due to the fact that there is no cross coupling between the local level axis at this latitude.

8.5 COMPARISON OF RESULTS FOR A MATCHED AND UNMATCHED KF

In this work the matched Kalman filter refers to the case where the covariance matrix $P(0)$ is initialized with specific diagonal and off diagonal elements as developed in section 8.3.3. The unmatched Kalman filter refers to the case discussed in chapter 4 section 4.6.1, where arbitrary non zero initialization values are chosen for all 12 of the diagonal covariance terms, and zero values are given to all of the off diagonal terms. The actual values used to initialise the Kalman filter to the unmatched condition are given in table 4-1.

8.5.1 A COMPARISON OF RESULTS FOR A MATCHED AND UNMATCHED KALMAN FILTER UNDER STATIONARY CONDITIONS

The above results have shown how the Kalman filter performs when it is matched to the IRS extended alignment condition. It is of interest to compare these results with similar results obtained from an unmatched Kalman filter, so that the improvement in performance for the matched filter over the unmatched filter can be seen.

Figure 8-14 shows a comparison of results for a matched and unmatched Kalman filters for the zero latitude alignment case carried out without a turn. Plots of Kalman filter covariances for the three states of interest are given, these states being the Y gyro bias (SD 9), the Z gyro bias (SD 10), and the Z platform axis tilt (SD 7). For the case of the matched Kalman filter, the covariance plots for the Y gyro bias, and the Z platform axis tilt, show a constant level of uncertainty during the two hour simulation. For the unmatched filter however, the Kalman filter uncertainty for the same states can be seen to decrease from their initial value after a period of approximately six minutes and finally settle out at a non zero value.

This result shows clearly the fact the Kalman filter is unmatched to the IRS condition because in the IRS simulation the Y gyro and Z platform axis tilt errors were chosen so that they balanced each other out which means the Kalman filter has no way of observing these errors and hence its uncertainty in its estimate of these errors should not decrease. From figure 8-14 it can also be seen that, compared to the matched Kalman filter, the unmatched Kalman filter takes a longer time to estimate the z gyro bias. This is a significant finding since in chapter 7, the fact that the Kalman filter was not easily able to estimate the Z gyro bias state was a major contributor to the limited performance obtained from the FMC.

8.5.2 RESULTS FOR A MATCHED AND UNMATCHED KALMAN FILTERS CARRIED OUT UNDER NON STATIONARY CONDITIONS

Here a comparison of results is given for a matched and unmatched Kalman filter for a non stationary case where the simulations have been carried out based on the details of the airfield at the Boeing company based in Seattle, whose coordinates are latitude north 47 degrees, longitude west 122 degree. As was the case for the stationary results, the alignment has been simulated for an initial heading of 090 degrees ie an east alignment. Details of the flight profile are given in figure 8-15. It consists of a 10 hour great circle flight with a 180 degree turn after takeoff to evaluate performance on a typical long range corridor flight. Normally the 180 degree turn would be carried out a few minutes after takeoff, but to provide some consistency with the previous results, the turn has been applied after 1 hour.

The IRS error sources are a Y gyro bias and an associated Z platform axis tilt, a Z gyro bias, and random noise consisting of gyro random walk and accelerometer correlated noise. The values of the IRS Y gyro bias and Z gyro bias have been set at one sigma from the error budget table. Since the simulation is for a non stationary case random noise has been included in the IRS simulation model, to account for this the Kalman filter Q matrix is also initialised to non zero.

8.5.2.1 ANALYSIS OF IRS ERRORS

Figure 8-16 shows a comparison of results for IRS and matched Kalman filter radial errors for the Boeing field. Details are given for the total radial error due to the combination of IRS error sources as well as for the radial errors due to the individual error sources. By examining the results in this way it is possible to see how the individual error sources contribute to the overall radial error. The results show that the major contributor to the total radial error during the first five hours of the flight is the Y gyro bias and associated Z platform axis tilt. At about the five hour point the effect of the Z gyro bias error sources on the total radial error starts to increase, and after 10 hours its effect on the radial error is as large as the effect of the Y gyro bias. The effect of the random noise on the total radial error can be seen to be small compared with the effect of the Y gyro bias.

8.5.2.2 KALMAN FILTER v IRS COMPARISON

Figure 8-16 also shows the result for the matched Kalman filter radial errors for the various IRS error sources. To obtain these results, the Kalman filter was run without a Gps measurement input. Also the Kalman filter covariance matrix was initialised with a single value which was dependant on the particular IRS source being investigated, the results obtained are therefore Kalman filter predictions of the radial error that a particular IRS error should cause.

For the Y gyro bias (and associated Z platform axis tilt) and Z gyro bias, the IRS and Kalman filter radial errors show a close agreement which is to be expected since the values chosen for the IRS error model were the 1 sigma values from the IRS error budget table. For the random noise there is also a close agreement between IRS and Kalman filter radial error even though for this simulation the IRS result is obtained from one run and cannot therefore be thought of as an 1 sigma result.

For the total IRS and Kalman filter radial errors, there is a close agreement up to the 5 hour point after which time the two results start to show a different trend. This result is expected since the total IRS radial error was also obtained from one run and is therefore not a 1 sigma value.

The above results have been produced using a combination of the covariance analysis and sensitivity analysis performance techniques. The results show that the matched Kalman filter predictions of radial error are closely related to the actual IRS radial errors. For the unmatched Kalman filter a similar simulation was carried out to predict the total IRS radial error due to all IRS error sources.

8.5.2.3 MATCHED v UNMATCHED KALMAN FILTER

Figure 8-17 shows the result for the comparison of total radial errors for the matched and unmatched Kalman filters, also shown is the IRS radial error from a single run. There is a large difference between the matched and unmatched Kalman filter radial error results. By examining the two results at time zero a clear difference can be seen between the two filter radial error values.

The matched filter value is zero, which is also the value of the IRS radial error. This is the expected value since during the extended alignment phase of operation the IRS system accepts a position input from the operator, and under normal circumstances this position input will be accurate. The value at time zero for the unmatched Kalman filter can be seen to be 1.45nm, this is because the covariance values SD(1) and SD(2) which relate to position have each been given an initial value of $9.0E-08 \text{ rads}^2$.

8.5.3 ASSESSING KF PERFORMANCE FOR VARYING PERIODS OF GPS

Figure 8-18 shows a comparison of radial error results for a matched and unmatched Kalman filter, for different periods of GPS coverage. For the 0.5 hr GPS case, the result for the matched filter (see dashed line) and for the unmatched filter (see dotted line) show a radial error difference at the end of the 10 hour simulation of 1.5 nm. Similarly for the one hour case, the radial error difference at the end of the 10 hour simulation is 1.5 nm. For the 2 hour GPS case, the radial error difference at the end of the 10 hour simulation is 0.8 nm. In each of the three cases the matched Kalman filter radial error at the end of 10 hours, is less than the corresponding value for the unmatched filter. This is clear evidence therefore of the benefits of matching the Kalman filter to the IRS extended alignment condition.

8.5.4 CONCLUSION OF RESULTS FOR THE MATCHED AND UNMATCHED KALMAN FILTER

The comparison of results for the matched and unmatched Kalman filter for the stationary case has shown that if the Kalman filter is not matched to the IRS alignment condition then the filter can start to miscalculate the value of some of the IRS states, namely the Y gyro bias and the Z platform axis tilt as seen in the results discussed in section 8.5.1. Also it has been shown that it takes the unmatched Kalman filter a longer time to observe the Z gyro bias error source.

For the non stationary case, the results show that over a 10 hour simulation period the radial error for the unmatched Kalman filter is significantly larger than the corresponding radial error for the matched filter.

The above results show that the FMC Kalman filter can be matched to the customer IRS extended alignment condition by use of the covariance initialisation values developed above, plus an additional term to take account of the Z gyro bias error. By using the matched Kalman filter initialization parameters a large improvement in navigation performance can be obtained compared to the unmatched filter.

8.6 DEVELOPMENT OF A GENERAL KALMAN FILTER MATCHING ALGORITHM

The last section dealt with matching the Kalman filter to a particular extended alignment condition. The alignment heading chosen for investigation was 090 degrees, because at this heading the unknown component of east gyro bias is due only to the y gyro bias, the x gyro bias having been corrected. Values to initialise the Kalman filter were developed for this particular condition, and via simulation these values were shown to provide a matched Kalman filter solution. In this section of work a similar analysis is carried out, to develop a general algorithm that can be used to initialise the Kalman filter for any heading.

8.6.1 THEORETICAL DEVELOPMENT

An alignment heading of 030 degrees has been chosen for investigation because at this particular heading the unknown component of east gyro bias is made up of both an x and a y gyro bias component. Because the y gyro bias is no longer coincident with the east axis as was the case for the 090 degree alignment above, there will be a non zero value of earth rate measured in both the y platform axis, and the x platform axis. The fact that there is a value of earth rate in both platform axis means, that both the x and y velocity measurements become important and need to be considered in the analysis of the discrete Kalman filter equations.

The previous work showed that where there was a y gyro bias error and an associated z platform axis tilt error, then it was necessary to include the Kalman filter covariance terms $P_{9,7}(0)$ and $P_{7,9}(0)$ to account for the cross correlation between the gyro and z platform axis tilt. For the 30 degree alignment case, there is an additional correlation between the x gyro and the z platform axis tilt, so as a first step in solving this case, the initial covariance terms $P_{8,7}(0)$ and $P_{7,8}(0)$ are included. In addition to the above four cross correlation terms the Kalman filter covariance matrix was initialised with non zero values for the y gyro bias $P_{9,9}(0)$, the x gyro bias $P_{8,8}(0)$ and the z platform axis tilt $P_{7,7}(0)$. All other covariance terms were set to zero.

The values used to initialise the covariance terms $P_{9,9}(0)$ and $P_{8,8}(0)$ are now a function of heading, as shown by the following equations :

$$P_{9,9}(0) = \text{Sin}^2(\alpha)\sigma^2 \quad (8.40)$$

$$P_{8,8}(0) = \text{Cos}^2(\alpha)\sigma^2 \quad (8.41)$$

Where :

α - system alpha angle

The result for the first iteration of the Kalman filter covariance estimate equation for the x and y platform axis tilts will now be evaluated. In the last section (see 8.3.3) only the value of the Y platform axis tilt was considered because there the alignment heading being considered was 090 degrees, which meant that only an east gyro bias or Y platform axis tilt needed to be examined. Now the alignment heading being considered is 030 degrees and therefore both an X and Y gyro bias and an X and Y platform axis tilt are needed.

8.6.1.1 X AND Y PLATFORM AXIS TILTS

For the x platform axis tilt the covariance estimate equation is :

$$\begin{aligned} P_{5,5}(-) = & P_{7,7}(0)W_y^2\Delta t^2 + P_{8,8}(0)C_{1,1}^2\Delta t^2 \\ & - P_{7,8}(0)C_{1,1}^2W_y\Delta t^2 - P_{8,7}C_{1,1}W_y\Delta t^2 \end{aligned} \quad (8.42)$$

For the y platform axis tilt the covariance estimate equation is :

$$\begin{aligned} P_{6,6}(-) = & P_{7,7}(0)W_x^2\Delta t^2 + P_{9,9}(0)C_{2,2}^2\Delta t^2 \\ & - P_{7,9}(0)C_{2,2}^2W_x\Delta t^2 - P_{9,7}C_{2,2}W_x\Delta t^2 \end{aligned} \quad (8.43)$$

For the Kalman filter to be matched to the 30 degree alignment condition, then the value of the filter covariances for the x and y platform axis tilt states must be zero, and remain at zero assuming no turns.

8.6.1.2 Y GYRO BIAS

The result for the second iteration of the Kalman filter covariance update equations for the y gyro bias state is considered next.

$$P_{9,9}(+) = P_{9,9}(0) - \frac{(P_{9,9}(0)C_{2,2}^2g\Delta t^2 - P_{9,7}(0)gW_x\Delta t^2)^2}{P_{3,3}(-) + R_{velx}} \quad (8.44)$$

This is the equation for the y gyro covariance update due to an x velocity measurement, it is identical to the equation developed previously for the 90 degree alignment case.

Similarly :

$$P_{9,9}(+) = P_{9,9}(0) - \frac{(P_{9,9}(0)C_{1,2}^2g\Delta t^2 - P_{9,7}(0)gW_y\Delta t^2)^2}{P_{4,4}(-) + R_{vely}} \quad (8.45)$$

This is the equation for the y gyro covariance update due to a y velocity measurement. Previously this equation had not been considered, as the y platform axis earth rate variable W_y was zero as a result of the alignment heading being 090 degrees, and also the direction cosine term C_{12} was zero, due to the platform axis frame of reference, and the body axis frame of reference being coincident at alignment time.

For the Kalman filter to be matched to this present extended alignment condition, where the alignment heading is 030 degrees, then the Kalman filter uncertainty in its estimate of the y gyro bias needs to remain constant at its initialised value, $P_{9,9}(0)$. To achieve this condition the sum of the bracketed terms must equal zero, in equations 8.44 and 8.45 above.

For equation 8.44 this can be achieved by choosing the initial value of $P_{9,7}(0)$ as follows :

$$P_{9,7}(0) = - \frac{P_{9,9}(0)}{\Omega_x} \quad (8.46)$$

To maintain the symmetry of the Kalman filter covariance matrix the term $P_{7,9}(0)$ must be set equal to $P_{9,7}(0)$.

Since the value of $P_{9,7}(0)$ has now been fixed, and the value of the direction cosine term $C_{1,2}$ in equation 8.45 is zero at alignment time, then the bracketed terms in equation 8.45 cannot be made equal to zero without the introduction of additional terms. The additional terms needed are developed in section 8.6.2.

8.6.1.3 X GYRO BIAS

The equation for the covariance update relating to the x gyro bias will now be considered. In the previous work where the initial heading was 090 degrees, this equation was not required, because at this heading the alignment process was able to detect and thus remove the full value of the x gyro bias error.

The result for the second iteration of the Kalman filter covariance update equation for the x gyro bias due to an x velocity measurement is :

$$P_{8,8}(+) = P_{8,8}(0) - \frac{(-P_{8,8}(0)C_{2,1}^2g\Delta t^2 + P_{8,7}(0)gW_x\Delta t^2)^2}{P_{3,3}(-) + R_{velx}} \quad (8.47)$$

Similarly the result for a y velocity measurement is :

$$P_{8,8}(+) = P_{8,8}(0) - \frac{(P_{8,8}(0)C_{1,1}^2g\Delta t^2 - P_{8,7}(0)gW_y\Delta t^2)^2}{P_{4,4}(-) + R_{vely}} \quad (8.48)$$

For a matched Kalman filter condition, the filter uncertainty in its estimate of the x gyro bias needs to remain constant at its initialised value of $P_{8,8}(0)$.

To meet this conditions the sum of the two bracketed terms in equation 8.47 and 8.48 need to be zero. For equation 8.48 this can be achieved by setting $P_{8,7}(0)$ as follows :

$$P_{8,7}(0) = \frac{P_{8,8}(0)}{W_y} \quad (8.49)$$

To maintain symmetry of the Kalman filter covariance matrix $P_{7,8}(0)$ is set equal to $P_{8,7}(0)$.

Since the value of $P_{8,7}(0)$ has now been fixed, and the value of the direction cosine term $C_{2,1}$ in equation 8.47 is zero at alignment time, then the bracketed terms in equation 8.47 cannot be made equal to zero without the introduction of additional terms. The additional terms needed are developed in the next section.

8.6.2 SELECTION OF THE MATCHED KALMAN FILTER PARAMETERS

Using engineering judgement and after a certain amount of experimentation, the extra Kalman filter covariance terms that are needed to satisfy the conditions for a matched Kalman filter were found to be $P_{9,8}(0)$ and $P_{8,9}(0)$. These are cross correlation terms which provide a relationship between the X and the Y body axis gyro biases. The results for the Kalman filter covariance update equations relating to the x and y gyro bias states, where these two new cross correlation terms have been included, is given below.

8.6.2.1 X AND Y GYRO BIAS

The second iteration of the x gyro bias covariance update equation due to an x velocity measurement is given by :

$$P_{8,8}(+) = P_{8,8}(0) - \frac{((-P_{8,8}(0)C_{2,1}^2g + P_{8,7}(0)gW_x - P_{8,9}(0)gC_{2,2})\Delta t^2)^2}{P_{3,3}(-) + R_{velx}} \quad (8.50)$$

The second iteration of the y gyro bias covariance update equation due to an y velocity measurement is given by :

$$P_{9,9}(+) = P_{9,9}(0) - \frac{((P_{9,9}(0)C_{1,2}^2g - P_{9,7}(0)gW_y - P_{9,8}(0)gC_{2,2})\Delta t^2)^2}{P_{4,4}(-) + R_{vely}} \quad (8.51)$$

For a matched Kalman filter condition, the sum of the bracketed terms in equations 8.50 and 8.51 are both required to be zero.

For equation 8.50 this can be achieved by choosing the value for $P_{8,9}(0)$ as follows :

$$P_{8,9}(0) = -P_{8,7}(0)\Omega_x \quad (8.52)$$

Similarly for equation 8.51, the value of $P_{9,8}(0)$ is chosen to be :

$$P_{9,8}(0) = P_{9,7}(0)\Omega_y \quad (8.53)$$

Equations 8.52 and 8.53 represent the final terms needed to initialise the Kalman filter so that, it can be matched the IRS extended alignment condition where the alignment heading can take on any general value.

A summary of the equations necessary to meet the general extended alignment condition is given below :

$$P_{9,9}(0) = \text{Sin}^2(\alpha)\sigma^2 \quad (8.54)$$

$$P_{8,8}(0) = \text{Cos}^2(\alpha)\sigma^2 \quad (8.55)$$

$$P_{7,7}(0) = \frac{P_{8,8}(0) + P_{9,9}(0)}{\Omega_n^2} \quad (8.56)$$

$$P_{9,7}(0) = -\frac{P_{9,9}(0)}{\Omega_x} \quad (8.57)$$

$$P_{9,8}(0) = P_{9,7}(0)\Omega_y \quad (8.58)$$

$$P_{8,7}(0) = \frac{P_{8,8}(0)}{\Omega_y} \quad (8.59)$$

$$P_{8,9}(0) = -P_{8,7}(0)\Omega_x \quad (8.60)$$

Where :

σ^2 Gyro bias covariance value obtained from the IRS error budget table.

Ω_x X axis earth rate value.

Ω_y Y axis earth rate value.

All other terms in the Kalman filter covariance matrix are set to zero.

Due to the symmetric nature of the Kalman filter covariance matrix, the terms $P_{8,9}(0)$ and $P_{9,8}(0)$ will be equal, so equations 8.58 and 8.60 above could have been formed into a single equation. Leaving the equation in the above form, will provide a useful way of checking for inconsistencies or errors.

Simulations were carried out to evaluate the performance of the Kalman filter, where the covariance matrix $P(0)$ was initialised with theoretical values above, and the initial alignment heading was taken to be 030 degrees.

8.6.3 DISCUSSION OF RESULTS OBTAINED FROM SIMULATION

Figure 8-19 shows the result for the Kalman filter covariances for a stationary simulation that was carried out based on the coordinates of the Boeing company airfield in Seattle, where the coordinates are north 47 degrees, west 122 degrees. A 180 degree rotation was applied after 1 hour of the simulation to show the effect of a turn on the Kalman filter result.

The Kalman filter uncertainty for the x gyro bias SD(8), the y gyro bias SD(9), and the z platform axis tilt SD(7), can all be seen to be constant during the first hour of the two hour simulation. The fact that the three values are constant during this time, means the Kalman filter is not able to improve on its initial estimate of these states. The three states are therefore not observable to the Kalman filter, and the filter can be considered to be correctly matched to the IRS extended alignment condition during this period.

During the second hour of the simulation the results show, that the Kalman filter uncertainty for all three of the states starts to decrease, and approaches a value of zero at the two hour point. The 180 degree rotation has uncoupled the error sources, thus making the error states observable to the Kalman filter.

Figure 8-20 shows the Kalman filter covariance results for the non zero latitude case. Up to the time the turn is applied the results for the x gyro, y gyro and z platform axis tilt can be seen to be constant. Applying the 180 degree rotation, causes the Kalman filter covariances to decrease towards a zero value.

8.6.4 CONCLUSION OF RESULTS FOR THE GENERAL KALMAN FILTER MATCHING ALGORITHM

These results show that the Kalman filter covariance matrix can be initialised using equations 8.54 to 8.60 so that its operation is correctly matched to the IRS extended alignment condition. The developed equations are general and can be applied for any alignment heading, and any latitude.

8.6.5 COMMENTS

At the end of chapter 6 and 7, the comment was made that although the customer inertial reference system navigation performance is quoted as being 2 nm/hr (95% circular error figure), the results obtained from the simulations carried out in these chapters only showed an IRS performance figure in the range 1.25 to 1.3 nm/hr. Three different methods of simulation were used to compute the results, Monte Carlo analysis, sensitivity analysis and covariance analysis. For each method the values used in simulations were obtained from the IRS error budget table as supplied by the customer (see appendix B).

The fact that the navigation performance figures was not observed to be 2 nm/hr was therefore a puzzling result that could not be explained at the time.

In this chapter, where consideration has been given to the effect of alignment errors when simulating navigation performance, results showing a 95% circular error figure of approximately 2 nm/hr have been observed. Consider figure 8-16 as discussed in section 8.5.2.1, the continuous line shows the IRS radial error for a 10 hour flight. The computed value of radial error is approximately 1 nm/hr for this simulation, which corresponds to a 95% circular error value of approximately 2 nm/hr.

It is concluded therefore that the effect of the IRS alignment needs to be taken into account when simulating navigation performance. This requirement has an affect on the type of simulation technique that can be used to simulate navigation performance as the Monte Carlo and sensitivity analysis techniques cannot be easily applied to take account of the alignment conditions. The covariance analysis technique is therefore recommended as the best method to use to develop the Kalman filter as it can be easily applied to take account of the alignment condition as shown in this chapter.

One of the reasons for not initially considering the alignment conditions when simulating the navigation performance of the customer IRS, was the fact that the IRS error budget table as supplied by the customer made no mention of any alignment related errors. Obtaining information from the customer about the performance of the inertial reference system was a very sensitive issue during this project, as the inertial reference system is supplied by a third party who were not engaged in the Smiths Industries / Boeing contract. So, although it has been mentioned that the IRS error budget table was supplied by the customer (Boeing), it was more a case of Smiths Industries drawing up the error budget table and Boeing confirming the choice of values. Fortunately enough information was available from the technical description of the inertial reference system to allow the alignment details as discussed in this chapter to be worked out.

For future work it is recommended that any alignment details that need to be considered when developing the Kalman filter should be included in the IRS error budget table.

8.7 FURTHER INVESTIGATION WORK

The previous work dealt with matching the Kalman filter to a particular extended alignment conditions encountered when operating with the customer inertial reference system. Different manufacturers mechanize their inertial systems in different ways, and although the overall objective of the alignment phase of operation may be the same for each system, the means by which this objective is achieved will be entirely different. Itzack (1983) discusses another type of inertial error source which is not encountered during the extended alignment phase of operation in the customer inertial system, but may occur in other inertial systems where different alignment techniques are used. The IRS error sources considered by Itzack is an accelerometer bias error and an associated platform axis tilt error.

These sources of error will now be investigated, and suitable values to initialise a Kalman filter covariance matrix will be developed, so that the filter is matched to the IRS alignment condition.

8.7.1 IRS THEORETICAL CONSIDERATIONS

It is possible to develop a control model for a single axis strapdown inertial system using conventional control techniques, to show the effect of an accelerometer error on velocity. The theoretical model is useful in that it can produce theoretical predictions, which can be used to validate results obtained from simulation, where the simulation model is different from the theoretical model.

Figure 8-21 shows a block diagram of a single axis inertial reference system. The system transfer function can be written in terms of velocity output over acceleration input as follows

$$\frac{V(s)}{A(s)} = \frac{1}{\sqrt{\frac{g}{R}}} \frac{s}{s^2 + \left(\sqrt{\frac{g}{R}}\right)^2} \quad (8.61)$$

Where

R - Earth radius (ft)
g - Gravity (ft/sec²)

For a step input $\frac{A_o}{s}$ (8.62)

The output velocity becomes

$$V(s) = \frac{1}{\sqrt{\frac{g}{R}}} \frac{A_o}{s^2 + \left(\sqrt{\frac{g}{R}}\right)^2} \quad (8.63)$$

The inverse laplace transform gives

$$V(t) = A_o \sqrt{\frac{R}{g}} \sin\left(\sqrt{\frac{g}{R}} t\right) \quad (8.64)$$

And finally

$$V(t) = 15.35 A_o \sin(4.46t) \quad (8.65)$$

Where

A_o - Acceleration bias (mg's)

t - Time (hours)

V - Velocity (kts)

The final equation shows that the velocity error due to a acceleration bias term is sinusoidal in nature having a period of 84 minutes this being the Schuler period.

Now consider that an inertial system which is aligned on a cardinal heading of 090 degrees, has a y accelerometer bias error. If the accelerometer bias is the only error source present, then it will cause an east velocity error output which will be sinusoidal in nature. Alternatively, If the only error source in the inertial system was an x platform axis tilt error, it would also cause an east velocity output which would be sinusoidal in nature but of opposite sign to the error caused by the acceleration bias.

In a real alignment situation both of these error sources are present, but they combine to cancel each other out, so the resultant velocity error output is zero. The error sources will continue to cancel each other out as long as there is no change in system heading, when there is a change in system heading the error sources will start to uncouple. The error sources start to uncouple because the accelerometer is fixed to the body of the system and therefore rotates with the system. If the system is rotated through 180 degrees for example, then the velocity output caused by the acceleration bias will change sign, due to the fact that the accelerometer input axis has been physically rotated.

In the case of the platform axis tilt error, rotation of the system by 180 degrees, does not effect the sign of the resultant velocity output, because the tilt error source is mechanized to exist in the platform axis frame of reference, which does not rotate when system heading changes.

8.7.1.1 DISCUSSION OF RESULTS OBTAINED FROM SIMULATION

Figure 8-22 shows the results for three stationary simulations that were carried using an alignment heading of 090 degrees, at a latitude of zero degrees. The IRS error sources used in each case were :- 1) A single y axis acceleration bias of 40 micro g's. 2) An x platform axis tilt of -4×10^{-5} rads. 3) A combination of 1 and 2.

The continuous line in figure 8-22 shows how the y acceleration bias error effects the IRS system states. For the case of the y platform axis velocity (DVELY), the results show that the acceleration bias error causes a sinusoidal velocity output with a peak of 0.6 kts at 21 minutes. Using the equation developed from the single axis theoretical IRS model above, the value of the velocity output at 21 minutes was also found to be 0.6 kts, so there is good agreement between the theoretical model and the simulation model in this instance. The simulation details were purposely chosen to allow a direct comparison to be made of the theoretical and simulation results. Carrying out the simulation at a latitude of north 47 degrees for example, would result in the simulation and theoretical values not being exactly equal, because of the fact that the theoretical model assumes a single axis IRS and does not account for any cross coupling effects that can occur at high latitudes.

The dashed line in figure 8-22 shows how the x platform axis tilt error (PHIX) effects the IRS states. The result for the y platform axis velocity shows how the tilt error has caused a sinusoidal oscillation in its output. The peak value of the velocity occurs at 21 minutes and has a value of 0.6 kts. This result is very similar to the one obtained above for the acceleration case, the only difference being, the opposite sign observed for the two waveforms.

It is now possible having seen the effect of these two separate error sources on velocity, to postulate that the value of the y platform axis velocity output if the two error sources were to be combined, would be a zero, assuming the system is linear, and the superposition theorem holds true. The dotted line in figure 8-22 shows the result on the IRS system states for the two error sources combined. The y platform axis velocity plot, shows a zero velocity output as predicted.

In a real alignment situation, these two error sources will cancel each other out, as long as the alignment heading is not changed. If the alignment heading is changed, then the two error sources will start to uncouple. Figure 8-23 shows the effect of uncoupling the two balanced error sources, by applying a turn of 180 degrees at a time of 12 minutes. The result has been overlaid with the previous result above for comparison. The case for the y platform axis velocity is shown by the dashed line in plot DELVY. During the first twelve minute interval the velocity output can be seen to be zero. After the application of the turn, the velocity error starts to build up, and reaches a peak negative value of -1.25 kts after a period of approximately 21 minutes. The value of -1.25 kts can be recognized as being twice the value of the peak velocity error caused by the individual error sources, and illustrates how the two error sources combine as a result of the turn.

These simulations have demonstrated the process whereby the y acceleration bias and x platform axis tilt error sources, are able to combine to form a zero velocity output, and then as a result of a single rotation, they become uncoupled and cause a sinusoidal velocity output. Now that this process which takes place in the IRS is understood, Kalman filter initialisation parameters can be developed, so that the filter can be matched to this particular IRS alignment condition.

8.7.2 SELECTION OF THE MATCHED KALMAN FILTER PARAMETERS

This section of work deals with the development of the parameters that are needed to initialise the Kalman filter covariance matrix so that, the filter can be correctly matched to the IRS alignment condition where, the Y acceleration bias and the X platform axis tilt errors are balanced. The approach taken to develop the initialised Kalman filter parameters, is, to consider only a single axis IRS error model, by ignoring the effect of the other two IRS channels.

Figure 8-24 shows a Kalman filter error model for the IRS y channel axis. The model shows how the y channel interacts with the x and z platform axes. To develop the Kalman filter covariance parameters, the interaction between the x and the z axes are ignored by taking the z platform axis tilt (ϕ_z) and the y platform axis tilt (ϕ_y) to be zero.

A single axis IRS error model can then be formed using states for velocity error, attitude error and position error as shown below :

$$\begin{bmatrix} \delta V \\ \phi \\ \nabla \end{bmatrix}_{k+1} = \begin{bmatrix} 1 & g\Delta t & c_{2,2}g\Delta t \\ -\frac{\Delta t}{R} & 1 & 0 \\ 0 & 0 & 1 \end{bmatrix} \begin{bmatrix} \delta V \\ \phi \\ \nabla \end{bmatrix}_k \quad (8.66)$$

Using this state transition matrix, the parameters used to initialise the Kalman filter covariance matrix $P(0)$ are chosen to be :

$$P(0) = \begin{bmatrix} 0 & 0 & 0 \\ 0 & P_{2,2}(0) & 0 \\ 0 & 0 & P_{3,3}(0) \end{bmatrix} \quad (8.67)$$

These values have been chosen to reflect the specific alignment condition where the tilt and accelerometer errors are balanced resulting in a zero velocity output. Thus the variance of the velocity state $P_{1,1}(0)$ is set to zero.

The variance of the accelerometer bias state $P_{3,3}(0)$ is chosen from the system error budget (see appendix B), its value is $1.6 \times 10^{-9} g^2$. It has been stated that in the extended alignment mode of operation, the customer inertial reference system does not suffer from this particular type of alignment error. The customer IRS error budget table has been used however, to select a value for the accelerometer bias state since it provides a realistic value for the magnitude of the error.

The variance of the tilt state $P_{2,2}(0)$ is not available from the system error budget as this error is a function of the alignment condition, so obtaining a numerical value for $P_{2,2}(0)$ is one of the tasks that needs to be carried out before the Kalman filter can be hoped to be matched to the IRS alignment condition.

Using the initial covariance matrix equation $P(0)$, the Kalman filter covariance estimate equation for the first iteration can be shown to be :

$$P(-) = \begin{bmatrix} P_{2,2}(0)g^2\Delta t_2 + P_{3,3}(0)C_{2,2}g^2\Delta t^2 & P_{2,2}(0)g\Delta t & P_{3,3}(0)C_{2,2}g\Delta t \\ P_{2,2}(0)g\Delta t & P_{2,2}(0) & 0 \\ P_{3,3}(0)C_{2,2}g\Delta t & 0 & P_{3,3}(0) \end{bmatrix} \quad (8.68)$$

Similarly, the Kalman filter gain matrix after the 1st iteration can be shown to be :

$$K = \frac{\begin{bmatrix} P_{2,2}(0)g^2\Delta t_2 + P_{3,3}(0)C_{2,2}g^2\Delta t^2 \\ P_{2,2}(0)g\Delta t \\ P_{3,3}(0)C_{2,2}g\Delta t \end{bmatrix}}{P_{2,2}(0)g^2\Delta t^2 + P_{3,3}(0)C_{2,2}^2g^2\Delta t^2 + R_{VEL}} \quad (8.69)$$

From the Kalman filter covariance estimate equation, and the Kalman filter gain equation above, the covariance update equation for the first iteration can be formed. The update equations for the three states are of particular interest and are shown below.

8.7.2.1 TILT STATE

The update equation for the platform axis velocity state is given by the covariance term $P_{1,1}(+)$ where :

$$P_{1,1}(+) = P_{2,2}(0)g^2\Delta t^2 + P_{3,3}(0)C_{2,2}^2g^2\Delta t^2 - \frac{(P_{2,2}(0)g^2\Delta t^2 + P_{3,3}(0)C_{2,2}^2g^2\Delta t^2)^2}{P_{2,2}(0)g^2\Delta t^2 + P_{3,3}(0)C_{2,2}^2g^2\Delta t^2 + R_{VEL}} \quad (8.70)$$

For a balanced Kalman filter condition the value of this update equation is required to be zero, to match the fact that the IRS velocity error is zero. In its present form the equation does not give a zero condition, this fact can be seen by examining the terms in $P_{1,1}(+)$ that relate to the covariance estimate these being :

$$P_{1,1}(-) = P_{2,2}(0)g^2\Delta t^2 + P_{3,3}(0)C_{2,2}^2g^2\Delta t^2 \quad (8.71)$$

The point has been discussed above that a numeric value for $P_{2,2}(0)$ has not yet been determined, however its value cannot be negative as this would lead to an illegal covariance matrix condition, so assuming $P_{2,2}(0)$ is positive, and $P_{3,3}(0)$ is non zero, the value of $P_{1,1}(-)$ will be non zero. If $P_{1,1}(-)$ is to be maintained at a zero value therefore, it will be necessary to introduce additional terms into the equation. From a practical point of view, equation 8.70 above is showing the fact that the Kalman filter uncertainty in its estimate of the velocity error is increasing due to the effect on velocity of the tilt error and the accelerometer bias error. The determination of the additional covariance terms is discussed in section 8.7.3.

8.7.2.2 VELOCITY STATE

The update equation for the platform axis tilt state is given by the covariance term $P_{2,2}(+)$ shown below :

$$P_{2,2}(+) = P_{2,2}(0) - \frac{(P_{2,2}(0)g\Delta t)^2}{P_{2,2}(0)g^2\Delta t^2 + p_{3,3}(0)C_{2,2}^2g^2\Delta t^2 + R_{VEL}} \quad (8.72)$$

For a matched Kalman filter condition the value of this covariance term is required to be constant and equal in value to the initial covariance term $P_{2,2}(0)$. This is because for a balanced condition the value of the covariance update term must reflect the fact that, at alignment time there is a tilt error in the IRS which is balanced by a corresponding accelerometer bias error, this means the IRS tilt error cannot be observed unless the system undergoes a rotation.

Examination of equation 8.72 shows that the equation $P_{2,2}(+)$ will not be constant due to the non zero value of the terms shown below :

$$[P_{2,2}(0)g\Delta t]^2 \neq 0 \quad (8.73)$$

In its present form the update equation $P_{2,2}(+)$ does not represent a balanced Kalman filter condition, so additional terms are needed.

8.7.2.3 ACCELEROMETER STATE

The update equation for the accelerometer bias state is given by the covariance term $P_{3,3}(+)$ shown below :

$$P_{3,3}(+) = P_{3,3}(0) - \frac{(P_{3,3}(0)C_{2,2}g\Delta t)^2}{P_{2,2}(0)g^2\Delta t^2 + p_{3,3}(0)C_{2,2}^2g^2\Delta t^2 + R_{VEL}} \quad (8.74)$$

The same comments made for equation 8.72 above apply to this case. The terms that cause the value of $P_{3,3}(+)$ not to be constant are given below :

$$[P_{3,3}(0)g\Delta t]^2 \neq 0 \quad (8.75)$$

8.7.3 SELECTION OF THE COVARIANCE CROSS CORRELATION TERMS

The analysis of the above covariance equations has shown that to achieve a matched Kalman filter condition, additional cross correlation terms are needed. The covariance matrix in this instance is a 3 by 3 matrix which means that the selection of possible combinations of cross correlation terms is small, so it is possible to work through all the various combinations in an attempt to find the set that provides the correct answer. This systematic approach of working through all the combinations is not ideal however, as it soon becomes a major task when higher order systems are involved. A better approach is to make some engineering judgement on the likely cross correlation terms that may be involved.

For this case the required cross correlation terms necessary to produce a balanced Kalman filter were found to be $P_{2,3}$ and $P_{3,2}$. These terms provide the cross correlation between the accelerometer bias and the platform axis tilt. A analysis will now be carried out to show how these cross correlation terms can be used to develop a balanced Kalman filter solution.

The initial value of the Kalman filter covariance matrix is chosen to be :

$$P(0) = \begin{bmatrix} 0 & 0 & 0 \\ 0 & P_{2,2}(0) & P_{2,3} \\ 0 & P_{3,2} & P_{3,3}(0) \end{bmatrix} \quad (8.76)$$

8.7.3.1 VELOCITY STATE

Using the initial covariance matrix equation $P(0)$, the estimate equation for the velocity state $P_{1,1}(-)$ becomes :

$$P_{1,1}(-) = P_{2,2}(0)g^2\Delta t^2 + P_{3,3}(0)C_{2,2}^2g^2\Delta t^2 + 2P_{2,3}(0)C_{2,2}g^2\Delta t^2 \quad (8.77)$$

For a balanced Kalman filter condition this equation is required to be zero. This gives :

$$2P_{2,3}(0)C_{2,2}g^2\Delta t^2 = - (P_{2,2}(0)g^2\Delta t^2 + P_{3,3}(0)C_{2,2}^2g^2\Delta t^2) \quad (8.78)$$

Where the value of $P_{2,2}(0)$ has not yet been chosen.

8.7.3.2 TILT STATE

The covariance update equation for the tilt state is :

$$P_{2,2}(+) = P_{2,2}(0) - \frac{(P_{2,2}(0)g\Delta t + P_{2,3}C_{2,2}g\Delta t)^2}{P_{1,1}(-) + R_{VEL}} \quad (8.79)$$

For a balanced Kalman filter condition, the update equation is required to be a constant.

This gives :

$$P_{2,3}(0)C_{2,2}g\Delta t = - P_{2,2}(0)g\Delta t \quad (8.80)$$

A solution for the value of the term $P_{2,2}(0)$ can now be found by combining this last result, with the solution from equation 8.78 to give :

$$P_{2,2}(0) = P_{3,3}(0) \quad (8.81)$$

8.7.3.3 ACCELEROMETER STATE

The covariance update equation for the accelerometer state is :

$$P_{3,3}(+) = P_{3,3}(0) - \frac{(P_{3,3}(0)C_{2,2}g\Delta t + P_{3,2}(0)g\Delta t)^2}{P_{1,1}(-) + R_{VEL}} \quad (8.82)$$

For a balanced Kalman filter condition, the update equation is required to be a constant. This gives :

$$P_{3,2}(0)g\Delta t = - P_{3,3}(0)C_{2,2}g\Delta t \quad (8.83)$$

This result is consistent with the previous findings for $P_{2,3}(0)$ and $P_{2,2}(0)$ above.

8.7.3.4 SUMMARY OF RESULTS

The parameters necessary to initialise the covariance matrix to produce a balanced Kalman filter condition have been evaluated and are summarized below.

$$P_{3,3}(0) = \sigma^2 \quad (8.84)$$

$$P_{2,2}(0) = P_{3,3}(0) \quad (8.85)$$

$$P_{2,3}(0) = - P_{2,2}(0) \quad (8.86)$$

$$P_{3,2}(0) = - P_{3,3}(0) \quad (8.87)$$

Where :

σ^2 is the accelerometer bias covariance value obtained from the IRS error budget table.

8.7.4 DISCUSSION OF RESULTS OBTAINED FROM SIMULATION

A stationary simulation was carried out to investigate the effect of running the Kalman filter using the covariance initialization values developed above and summarized in equations 8.84 to 8.87. The actual value of the covariance term for the y accelerometer bias $P_{12,12}(0)$ was chosen to be 1.6×10^{-9} g's. The run was carried out at coordinates north zero / east zero with a 180 degree rotation applied after one hour. The IRS alignment heading was taken to be 090 degree. The IRS error sources were a single y axis accelerometer bias of 40 micro g's and a corresponding x platform axis tilt of -4×10^{-5} radians, this being the value needed to set up a balanced IRS alignment condition.

Figure 8-25 shows the result for the diagonal terms of the 12x12 Kalman filter covariance matrix. (Appendix C gives the relationship between diagonal elements of the Kalman filter covariance matrix and the corresponding IRS states). From the results it can be seen that the covariance plots for the y accelerometer bias SD(9), and the x platform axis tilt SD(5), are constant during the first hour of the simulation. This means the Kalman filter's uncertainty in its estimate of these two states remains fixed. This result is the expected result because, during this period the two IRS error sources are balanced, the resulting IRS velocity error is zero, which means the Kalman filter is unable to observe either of the two balanced errors.

The effect of uncoupling the IRS errors by introducing a 180 degree rotation is detected by the Kalman filter. This is clearly shown from the step like response observed in the plots for the accelerometer bias SD(12), and the x platform axis tilt SD(5), at the time the turn is applied. It can be seen that as a result of the 180 degree rotation both plots rapidly decay from their initialized value to a final value of zero. The fact that both the covariance results reach a final value of zero is to be expected, and is explained by the fact that the simulation was carried out with the Kalman filter system noise matrix (Q matrix) set at zero to reflect the absence of random IRS noise.

Figure 8-26 shows an overlay of the IRS and Kalman filter states for the above case. The result shows that for the first hour of the simulation the IRS errors for velocity (DELVX and DELVY) and position (DTHX and DTHY) are approximately zero due to the balanced alignment condition. The Kalman filter estimate of the 12 IRS states as shown by the dotted line in figure 8-26, can also be seen to be zero over this initial period.

This result is in agreement with the observations made from the covariance plots above, confirming the fact that the Kalman filter is matched to the balanced IRS condition and cannot therefore learn the value of the y accelerometer bias (DELVY) or the x platform axis tilt (PHIX).

During the second hour of the simulation as a direct result of the 180 degree rotation, the plots in figure 8-26 show how the IRS errors build up. Similarly the plots for the Kalman filter show how the filter is able to correctly estimate the value of the y accelerometer state (DELAY) and the x platform axis tilt state (PHIX).

These results have shown how the theoretical values used to initialise the Kalman filter covariance matrix can produce a filter output that is matched to the IRS alignment condition.

8.7.5 CONCLUSION

In this further work a general type of alignment condition not encountered in the customer IRS system has been investigated. A single axis IRS theoretical model was used to simulate the IRS alignment condition. Using a single axis IRS error model, Kalman filter initialisation parameters were then developed to match the Kalman filter to the IRS alignment condition.

8.7.6 FURTHER WORK

During the development of the Kalman filter covariance parameters the analysis of the IRS alignment condition was limited to a y platform axis accelerometer error and an x platform axis tilt. Although this is a general result and not a function of a specific heading, it is quite likely that some component of x accelerometer error and y platform axis tilt may also be present during the alignment process. In this instance, to develop the matched Kalman filter initialisation values, then the single axis IRS error model would need to be developed to take account of the interaction between the three IRS axes.

No attempt has been made to pursue this area of work because the cross coupling between the IRS axes is dependant on the actual transition matrix and state vector being used to represent the IRS error model.

CHAPTER 9.0

MARKET ANALYSIS

9.1 INTRODUCTION

This chapter covers the non technical aspect of the thesis, the subject to be discussed is the marketing of GPS and IRS integration technology.

The integration of a global positioning system and an inertial reference system can be carried out by one of two main methods: in the first method the integration is performed inside the inertial reference system while in the second method the integration is carried out inside a flight management computer System. Recent trends in the market suggest that the FMC integration scheme is the one that is most attractive to the major customers. The main aim of this chapter is, therefore, to examine the market potential for a Smith's FMC product that provides GPS/IRS integration.

The total market for GPS and IRS integration covers both civilian and military aircraft. In this work, however, the main emphasis will be consideration of the commercial aircraft market. The main framework for analysis will be the "strategic triangle", comprising key customers, competitors and Smiths Industries.

9.1.1 SCHEMES FOR GPS/IRS INTEGRATION

Before considering the strategic triangle a general summary is given below of the various GPS/IRS integration schemes that can be applied.

SCHEME 1 Integration of the GPS/IRS inside the IRS where the GPS and IRS are separate systems which communicate over an ARINC 429 interface.

- SCHEME 2** Integration of the GPS/IRS inside the IRS where the GPS function is carried out on one or more cards that slot into the IRS.
- SCHEME 3** Integration of the GPS/IRS inside a flight management computer where the GPS, IRS and FMC are separate line replaceable units.
- SCHEME 4** Integration of the GPS/IRS inside a flight management computer where the IRS and GPS are separate line replaceable units, but where the FMC is part of a larger avionics functions.

The major products produced by Smiths Industries and its major competitors will now be examined.

9.2 SMITHS INDUSTRIES

Smiths has two main sites that are involved in the manufacture of flight management computer systems, these sites are Cheltenham in the United Kingdom and Grand Rapids in the United States.

9.2.1 SMITHS CHELTENHAM

Development of the flight management computer started at Cheltenham in 1980. Since that time Smiths has successfully manufactured and sold systems to 10 major airlines operating the Airbus A300-600 and A310 aircraft. Although the FMC can be considered to be a mature product, recent enhancements to the system has produced further sales with more sales expected.

With the success of the initial FMC on the Airbus A300/A310 aircraft, Smiths tendered for further Airbus work in 1989, by submitting proposals for the A330 /A340 FMC. The company was not successful with the bid, however, finally losing out to Honeywell.

Following successful development of the first FMC, Smiths (Cheltenham) were awarded a contract by Boeing to supply the flight management computer system for the United States Navy command and control (E6) aircraft.

This FMC was very similar to the original FMC developed for the Airbus aircraft except that the E6 aircraft did not require vertical guidance. The first completed E6 FMC was delivered to Boeing in 1987. Since that time Smiths has won a follow on contract to integrate GPS and IRS inside the flight management computer. The first enhancement to the E6 FMC providing GPS/IRS integration was delivered in 1991. Although the E6 aircraft is operated by the military, the inertial reference system that is used is a commercial type product. In fact, it is the same inertial product that is fitted to some variants of the airbus A300/A310 aircraft. Therefore, the expertise that Smiths has gained in the integration of GPS/IRS can be easily applied to the commercial aircraft market.

At the time of writing, Smiths (Cheltenham) does not have a commercial flight management computer system that can provide GPS/IRS integration, but it does have inhouse expertise that will allow such a product to be developed in a relatively short time scale and at relatively low cost, by producing an update to the existing Airbus flight management computer system.

9.2.2 SMITHS GRAND RAPIDS

Smiths Industries facility at Grand Rapids also produces a flight management computer system which was first developed in the early eighties. This FMC is a successful product as it is currently being used by over 50 airlines on the Boeing 737 aircraft. With the initial success of the FMC, Smiths bid for further work on the Boeing 747-400, and 777 aircraft. In each case however, the work was awarded to Honeywell.

In common with the Cheltenham site, Smiths at Grand Rapids has been involved in the integration of GPS/IRS on a military project. The Grand Rapids site has therefore gained expertise in the integration of GPS/IRS which it could easily apply to the commercial aircraft market.

9.3 KEY COMPETITORS

The two major competitors involved in the area of IRS/GPS integration are Honeywell, and Litton Aeroproducts. A comparison will now be made for the various IRS/GPS systems produced by the two companies.

9.3.1 LITTON v HONEYWELL

Honeywell and Litton have been developing ring laser gyro strapdown inertial reference systems for some considerable time. Indeed, the first generation Honeywell IRS systems began to fly as early as 1974, with certification being received on the HG1050 IRS in 1981. In the Litton case, the design and development of their first inertial reference system, the LTN 90, started in February 1979. In June 1980 the Litton LTN 90 system was selected by Aerospatiale for the Airbus A310 aircraft. The first production units were delivered to Aerospatiale in July 1981. In early 1982 the LTN 90 was flown for the first time on the A310 aircraft and in March 1983 full certification for the system was obtained.

The strapdown ring laser gyro inertial reference system has the advantage over the traditional gimballed gyro system in that it is more reliable and easier to maintain. The ring laser gyro comes housed in its own metal case. It is easily removed and replaced, unlike a gimballed gyro which is a complex mechanical instrument, requiring a skilled technician to maintain it.

Since the early developments, a series of successful civilian products has been produced and sold both by Honeywell and Litton to over 127 airlines worldwide. Today, both Litton and Honeywell supply a range of products.

Early inertial reference systems required an input from an air data computer system which was separately housed from the inertial system. Honeywell produces its own air data computer systems but Litton does not. About 8 years ago, a significant change occurred and the air data computer function was built into the inertial reference system. This offered the airlines the advantage of reduced weight and rack space and improved maintainability. This product is referred to as an Air Data Inertial Reference System (ADIRS). During the development of this product, both Honeywell with their HG1150 and Litton with their LTN 90-200 were targeting the Airbus A320 aircraft. Honeywell eventually won the A320 contract, probably because Honeywell was ahead of Litton with the development work when the contract was awarded.

The fact that Honeywell had a working ADIRS while Litton were still developing the system was due to Honeywell being able to develop and manufacture its own product, while Litton was reliant on an outside company to develop the air data module. That outside company was Smiths Industries.

As a result of Honeywells' success with the A320 aircraft, Litton effectively cancelled their LTN 90-200 ADIRS development program to concentrate their effort on their next generation inertial product which they call the Flagship.

The Litton Flagship or the LTN-101, is a global positioning air data inertial reference system. Thus the unit has an air data module housed within it which Litton eventually produced on their own.

The Litton Flagship is designed for a wide range of applications. It can be used in single, dual or triple installation as an IRS, IRS/GPS, ADIRS or ADIRS/GPS. To provide this flexibility the Flagship hardware consists of five components:- an air data inertial reference unit (ADIRU), an air data module (ADM), a global positioning system sensor unit (GPSSU), a mode select unit (MSU) and a control display unit (CDU).

The global positioning system sensor unit caters for both ARINC 743 configurations. The two configurations are a bay mounted avionics unit that uses a remote antenna and an internal preamplifier to produce GPS outputs of position and velocity, or a remote GPS sensor that is physically located near the passive antenna that also provides GPS position and velocity but via some form of connecting cable.

In both configurations the GPS sends information to the ADIRU where it is processed by a Kalman filter to provide improved position and velocity data, also IRS alignment during taxi or inflight is possible. If required the GPS can also provide raw position and velocity information in the form of pseudo range and delta range.

Honeywell produce a similar product to the Litton Flagship, the HG2001 IRU. The HG2001 accommodates air data integration in accordance with ARINC 738. It also has provision for GPS integration. The integration function is carried out within the existing IRU software. There is no need therefore for any additional cards or modules. As with the Litton system the integration of GPS also allows alignment to be carried out while in motion.

Functionally the Litton and Honeywell inertial products are the same, both systems use the same integration scheme where a Kalman filter inside the IRS is used to integrate the GPS and IRS signals. Since the Kalman filter models the IRS errors, this scheme is easily implemented by Litton and Honeywell since both companies are experts in this field.

To complement its range of inertial products Litton also produces global positioning systems. Litton have been developing GPS receivers for over nine years. The first generation product was the LTN 700 GPS which operates as a C/A code receiver. This system has been successfully flight tested by Boeing, Aeritalia, Dassault, Lockheed and the US Navy. The second and third generation products are the LTN 710 and the GPSSU. The GPSSU can easily be integrated with any ARINC 704 IRS and any ARINC 738 ADIRS. Litton is the only company in the world that has developed both inertial systems and GPS receivers.

The key competitors for Smiths Industries in the GPS/IRS integration market are Litton and Honeywell. The range of products produced by these two companies has been examined. In summary, both Litton and Honeywell have a history of producing successful products and supporting them. Each company has product support facilities at several locations worldwide. Both companies are well established in the market, and from their range of current products, it is concluded that both companies intend to stay in the market.

Having examined Smiths and the key competitors, the major customers will now be considered.

9.4 KEY CUSTOMERS

The main market segment being considered in this work is the commercial jet aircraft market consisting of large commercial jets with over 200,000 lbs take off weight, medium commercial jets with 110,000 - 200,000 lbs take off weight and small commercial jets with 80,000 - 110,000 lbs take off weight. For these markets there are three key manufacturers, Boeing and McDonnell Douglas in the USA, and Airbus Industries in Europe.

The range of present and future aircraft manufactured by these companies is listed in the tables 9-1 and 9-2 for the large and medium aircraft types.

9.5 MARKET ANALYSIS

Having introduced the major competitors and the key customers the present state of the market will now be examined.

9.5.1 MARKET SHARE

Table 9-3 shows the distribution of FMC equipment manufactured by Honeywell (H) and Smiths (S), and the IRS equipment manufactured by Honeywell (H) and Litton (L) for the various customer aircraft. The table shows that Honeywell dominates both the FMC and the IRS market with equipment distributed across all aircraft, except for, the Boeing 737 where Smiths supplies the FMC.

Table 9-4 shows the estimated market share of the FMC and IRS products for the three companies. In the case of Honeywell, its market share for the FMC is 69%, and for the IRS, 82%. In the case of Smiths, the market share for the FMC is 31%. Approximately 30% of this total figure is for FMC sales on the Boeing 737 series aircraft, with the remaining 1% representing Airbus A300/A310 sales.

9.5.2 CURRENT MARKET TRENDS

The civilian market for the integration of GPS/IRS can be considered in two broad segments. Firstly, there is the new aircraft market; and secondly, the retrofit market.

The decision over which type of integration scheme to adopt for the new aircraft market is influenced by the aircraft manufacturer and the airlines. In the case of Boeing for example, and the new 777 aircraft, two major airlines United Airlines and American Airlines approached Boeing early in 1991 expressing their views on GPS/IRS integration. Both airlines favour the integration scheme being carried out inside the flight management computer.

Since that time, a further meeting between Boeing and several other major airlines has taken place, with the consensus being that the airlines prefer the integration of GPS/IRS to be carried out inside the flight management computer. The airlines involved were Delta, Continental, North West, British Airways, Lufthansa, Quantas, Japan, Cathy Pacific, USA Air and All-Nippon airways. Several of these major airlines have already placed orders for the new Boeing 777 aircraft, including British Airways, United, American and All-Nippon.

In expressing their view on the new aircraft market, the airlines are also affecting the retrofit market. United airlines for example, are considering retrofitting their existing fleet of Boeing 737, 757, 767 and 747-400 aircraft with GPS.

If the integration scheme is to be carried out inside the IRS, then United will have to purchase a modified IRS, a GPS and update the existing software inside the flight management computer system to accommodate the new IRS outputs. If they choose the FMC integration scheme however, then they do not need to update the existing IRS. It is worth mentioning also that each aircraft has three IRS's, and two FMC's so there will be a substantial cost saving to the airlines.

To gain an understanding of the airlines reason for choosing the FMC integration scheme, consideration should be given to the advantages and disadvantages of the FMC scheme over the alternative IRS scheme.

9.5.2.1 ADVANTAGES OF CARRYING OUT THE GPS/IRS INTEGRATION INSIDE THE FMC.

There are some clear advantages to the FMC integration scheme particularly from the point of view of the airlines when retrofitting GPS. These advantages are summarized below:-

- No modification to the inertial reference unit required.
- Maintains interchangeability of IRU's if GPS is installed in only a few aircraft.
- GPS sensor will be interchangeable between FMS and non FMS aircraft.
- No hardware modification to the FMC required.
- Uses common FMC software package as integrated GPS/IRS, which can be certified by the airframe manufacturer.
- Provides position data comparison from 3 IRU's and dual GPS sensors for integrity monitoring.
- Allows GPS manufacturers to be competitive in the market place.
- Allows airlines to certify use of GPS.
- Simplified / lower installation cost.

9.5.2.2 DISADVANTAGES

- The benefit of IRS alignment while in motion cannot be achieved.
- Correction of IRS errors cannot be achieved.
- Development of the IRS error model to be used by the Kalman filter would require the cooperation of the IRS supplier.

In summarizing the present market, therefore, it is correct to say that Litton and Honeywell have been driving the new GPS/IRS technology by offering an inertial product that takes GPS as an input and performs the GPS/IRS integration. The market is now being influenced by the major airlines, however, as they have expressed their combined interest in the GPS/IRS integration being carried out inside the FMC.

9.5.3 THE THREAT FROM HONEYWELL FOR THE NEW AIRCRAFT MARKET

Assuming that the airlines are successful in their attempts to have the GPS/IRS integration carried out inside the flight management computer system then Honeywell will have a competitive advantage over Litton and Smiths in both the new aircraft market and the retrofit market since the company produces both inertial systems and flight management systems. Take as an example the new Boeing 777 aircraft, Honeywell has already been selected for both the flight management function and the inertial reference system which is an ADIRS.

The FMC on the Boeing 777 is different to previous systems as it is not a stand-alone unit but forms part of the Airplane Information Management System (AIMS). The AIMS function provides a major portion of the 777 avionics capability. These include display functions, onboard maintenance functions, flight management functions, engine data interface functions and communications management. This approach to the flight management function is very different to previous approaches where the FMC consisted of a plug in box. Since Honeywell produces both the inertial system and the flight management function for the 777, the company can easily accommodate the desires of the various airlines by carrying out the GPS/IRS integration inside the FMC.

9.5.4 THE THREAT FROM HONEYWELL FOR THE RETROFIT MARKET

Honeywells dominance of this new AIMS concept in the new aircraft market could also extend to part of the retrofit market. For example, the Boeing 737 is to have a major avionics update in 1998/99 and the AIMS concept is being considered.

For a non AIMS type GPS/IRS integration scheme where the FMC is a stand-alone line replaceable unit, then Litton and Smiths are also under threat from Honeywell, since Honeywell manufacture both FMC and IRS. This type of integration scheme is relevant to the Airbus A300/A310 aircraft and the Boeing 737 aircraft.

Littons IRS sales are under threat from Honeywell for this aircraft despite the fact that one of the advantages to the airlines of carrying out the GPS/IRS integration in the FMC is thought to be that there is no need to change the existing inertial system. The fact that the IRS system may need to be changed when carrying out the GPS/IRS integration inside the FMC is discussed later in section 9.6.

If Smiths and Litton are to compete effectively against Honeywell then they need to combine forces. The strengths and weaknesses of the two companies are considered next.

9.5.5 STRENGTHS AND WEAKNESSES

Both Smiths and Litton have strengths and weaknesses as far as this GPS/IRS technology is concerned. For Litton the major weakness is that they do not manufacture flight management systems or any of the other major AIMS functions such as the display function and the engine interface function. Littons strength lies in its inertial system experience and its global positioning experience.

For Smiths the weakness is the lack of inertial systems experience while its strengths are its flight management experience and also its experience in cockpit displays, engine instruments and auto throttles, since this experience could be used to advantage in developing an AIMS type function.

If Smiths is to combat the threat from Honeywell and remain in the flight management business then it needs to link up with a major manufacturer of inertial systems and Litton Aeroproducts is the obvious choice. Some of the key reasons are listed below :

- Smiths and Litton already have a successful track record of working together on the development of the air data computer card for the Litton 90-200 inertial air data system.
- Smiths (Cheltenham) has already successfully carried out the integration of a Litton IRS and a GPS inside their FMC. Although this scheme did not include vertical guidance, the major technical risks associated with such a project are well understood. The technical expertise needed to carry out such a task already exists in house. It is just a matter of applying it. To perform the GPS/IRS integration inside the FMC for a non AIMS type function, then only minor hardware changes are needed with the major effort being in software.
- Together Litton and Smiths possess the breadth of engineering experience needed to implement an AIMS type function.
- Litton could benefit by the sale of GPS systems if they were offered as part of the Smiths/Litton GPS/IRS integration scheme.

9.6 SCENARIO ANALYSIS

The second point listed above raises a very important issue which emphasises the opportunities that would come from, a union of Smiths and Litton and also explains why Littons share of the IRS market is under threat from Honeywell. During the integration of the Litton IRS and a GPS inside the Smiths FMC, Smiths discovered that particular attention must be paid to the inertial reference system error model particularly its alignment characteristics, if a successful integration is to be carried out. Such information can only be obtained from the inertial manufacturer because of the highly theoretical and specific nature of the data. Also, data that is relevant to one manufacturer's inertial product is not compatible with another manufacturer's systems, (ie each inertial system error model is unique). It is doubtful if the airlines are aware of this fact but its consequences affect both the FMC and the IRS.

In view of the above statement that the error model for each inertial system is unique, it is of interest to consider each of the combinations of FMC and IRS in terms of Smiths, Litton and Honeywell and consider the cases for an AIMS type FMC and a non AIMS type FMC. The various combinations are given in table 9-5.

9.6.1 AIRCRAFT INSTALLATION TYPE 1

This type covers the case where Smiths supplies the FMC and Litton the IRS, and is found on the Boeing 737 and A300-600 / A310 aircraft.

9.6.1.1 AIMS

Consider the airline required an AIMS type update with the GPS/IRS integration to be carried out inside the flight management function then this is a worst case scenario for Litton and Smiths since in this situation Smiths would lose the FMC because of the requirement for an FMC within AIMS, and Litton would also lose because Honeywell could not carry out the GPS/IRS integration in the FMC using the Litton IRS.

Table 9-3 shows that it is on the Boeing 737 series aircraft that Litton and Smiths share the IRS and the FMC slots and where Smiths make their major sales accounting for 30% of the total 31% of the their current market. It is on this aircraft, therefore, that the greatest threat to Smiths exists.

To combat this threat, Litton and Smiths could combine to produce an equivalent AIMS function. Mechanization of the GPS/IRS inside the FMC would be a relatively easy and risk free exercise, the major effort being in the development of the other AIMS functions.

9.6.1.2 NON AIMS

Smiths and Litton are in a strong position to defend their market share for a standard FMC update offering GPS/IRS integration. For the Boeing 737 aircraft, Smiths Grand Rapids could work with Litton to provide the required enhancement, while for the A300-600 / A310 Smiths Cheltenham could work with Litton. The Cheltenham site has the advantage that it has already carried out a successful GPS/IRS integration inside the FMC using a Litton inertial system. Although the major volume of sales for the Smiths FMC are gained from the 737 aircraft, it is still viable for the Cheltenham site to offer an FMC with GPS/IRS integration for the low volume A300-600 / A310 market, since the development costs associated with updating the existing product would be very low because of the inhouse expertise that already exists and the fact that a similar type of integration has already been carried out.

9.6.2 AIRCRAFT INSTALLATION TYPE 2

This type covers the case where Smiths supplies the FMC and Honeywell the IRS, and is found on the Boeing 737 and A300-600 / A310 aircraft.

9.6.2.1 AIMS

Assuming an AIMS type flight management function is required, then Smiths would be under direct threat from Honeywell on the Boeing 737 aircraft because Smiths does not produce an AIMS. Also Honeywell supplies the IRS for the aircraft so a GPS/IRS integration could be easily carried out. Even if Litton/Smiths could produce and offer an AIMS, Honeywell would still have the advantage of supplying the inertial systems.

9.6.2.2 NON AIMS

For the standard flight management function Smiths could not provide the GPS/IRS integration without the assistance of Honeywell. For this situation there are at least three possible scenarios that can be considered :

Firstly there is the case where Honeywell may provide Smiths with the technical data needed to carry out the GPS/IRS integration, although it is doubtful if Honeywell would volunteer this information. Since the combination of Smiths and Honeywell exists on the largest portion of the aircraft, the airlines could force Honeywell to cooperate. As Honeywell does not supply any of the 737 aircraft with flight management systems, then their FMC sales are not under threat.

There would be a technical risk here for Smiths because to be sure of success with the minimum of cost Smiths would probably require some engineering assistance from Honeywell as well as the technical data relating to the IRS error model.

As a second scenario Honeywell could refuse to supply the technical data preferring to offer the GPS/IRS solution to be carried out inside the IRS. The airlines have already indicated that they do not favour this approach because it is not the most cost effective solution. However, it is not clear at this time if the Airlines are aware of all of the technical risks involved in performing the GPS/IRS integration inside the FMC.

For a third scenario, Litton and Smiths could combine to offer an FMC that was capable of providing the GPS/IRS integration using the Litton IRS. This combination could encourage further sales of the Litton IRS for future 737 aircraft, particularly to those airlines that might already have Litton equipment on other aircraft.

Both the Type 1 and the Type 2 installation are found on the Boeing 737 and A300-600 / A310 aircraft, but as far as the AIMS is concerned only the Boeing 737 needs to be considered. It is evident from the analysis for the Type 1 and Type 2 schemes that Honeywell poses a real threat to Litton and Smiths, the size of the threat depending to a great extent on the ratio of Litton's IRS's to Honeywell's IRS's on the Boeing 737 aircraft. For the current market the ratio is Honeywell 99% and Litton the remaining 1%. This means Smiths is under a serious threat from Honeywell for future Boeing 737 FMC sales.

9.6.3 AIRCRAFT INSTALLATION TYPE 3

This type covers the case where Honeywell supplies the FMC and Litton the IRS, and is found on the A300-600 / A310 aircraft. The AIMS case is not discussed since at the present time AIMS is not being considered for the A300-600/A310.

9.6.3.1 NON AIMS

If the GPS/IRS integration is to be carried out inside the FMC then without access to the Litton inertial error model, Honeywell will not be able to offer a GPS/IRS solution.

It seems very unlikely that Litton would allow Honeywell access to their inertial system error model as this data could then be used by Honeywell to gain an in depth understanding of the performance limitations of the Litton IRS. This type of detailed information could then be used to advantage by Honeywell when competing with Litton for future IRS business. One option open to Honeywell would be to swap out at reduced cost the Litton IRS's recovering the cost on the sale of the enhanced FMC offering GPS/IRS integration and possible also a maintenance contract on the repair of the IRS's.

An alternative would be for Smiths/Litton to replace the Honeywell FMC since Smiths could easily offer the GPS/IRS integration for the Litton IRS. Smiths/Litton could offer an attractive alternative to the various airlines by offering the Litton GPS and the Smiths FMC as a combined package. Smiths has a small proportion of the A300-600/A310 FMC business compared to Honeywell, Litton however holds 80% of the IRS sales, so despite the fact that production of the aircraft is due to finish in 1997, there is still an attractive market for a Smiths (Cheltenham) FMC which can offer the GPS/IRS solution with the Litton IRS.

In summarizing this third scenario it is a case of Honeywell maintaining the FMC position and swapping out the Litton IRS or Litton maintaining the IRS and Smiths swapping out the Honeywell FMC. The airlines' decision on which option to select is clearly going to be influenced by the sales prices, and any further costs for certification. The reliability of the existing inertial system might also have a bearing on the decision process. Airlines have various maintenance agreements with inertial systems manufacturers which can range from the airline sending back the failed IRS to the manufacturer to the airline carrying out its own level one, two and 3 maintenance.

Airlines have become very sensitive to the failure rate of inertial systems which arise mainly due to the complex sensing instruments (strapdown ring laser gyros) that it uses. To repair an inertial system where a ring laser gyro has failed can typically take up to 10 hours because of the lengthy calibration process that is required. So, even if the cost of replacing an IRS ship set was made attractive, airlines would be very reluctant to consider replacing a manufacturers IRS that had a good record of reliability.

9.6.5 FUTURE BUSINESS

In terms of future Airbus business, Federal Express have recently announced an order for some 75 A300-600 aircraft to be purchased in three stages, with the first delivery being due in early 1994. From the airline point of view it makes sense to consider only two options for the IRS and FMC as shown in table 9-6.

For these options it is feasible for the GPS/IRS integration to be carried out in the FMC or the IRS. The second option assumes that Litton and Smiths will join forces. If they don't, then the airline might well consider that Honeywell offers the only cost effective solution as it will be the only company that can offer the GPS/IRS solution to be carried out inside the FMC or the IRS.

9.7 SUMMARY

The potential market for the Smiths industries flight management computer that offers GPS/IRS integration has been examined. The major customers and competitors have been considered with the conclusion that Honeywell dominates both the IRS and FMC market, except for the case of the Boeing 737 series aircraft where Smiths supplies the FMC and the Airbus A300-600/A310 aircraft where Litton hold 80% of the IRS sales. If the airlines demands for the GPS/IRS integration is to be carried out inside the FMC are to be met, then Smiths future position on the Boeing 737 aircraft is under serious threat from Honeywell because of two main reasons. Firstly, Honeywell supplies 99% of the inertial systems for the aircraft, and secondly Honeywell is the only company that can offer an AIMS. To counter the threat from Honeywell the possible scenario of Smiths and Litton combining forces has been examined.

Similarly on the Airbus A300-600/A310 Smiths and Litton face direct competition from Honeywell. The possibility of Litton and Smiths combining to counter the threat on this aircraft has been examined, with the conclusion that Smiths could win further business by being able to offer an FMC that provides GPS/IRS integration using the Litton IRS.

It is interesting to note that Litton has filed a law suit (see Interavia 1990) against Honeywell Inc alleging that Honeywell's Commercial flight systems group has monopolised the sale of inertial reference systems used in commercial aircraft. Litton alleges unlawful Honeywell tactics on several European aircraft sales, including the Airbus A330/A340 and the Fokker 100. Litton says that it is Honeywell's only competitor in the IRS market and estimates the value of the market at more than 1,000 million dollars over the next decade. In view of this action it is quite likely that Litton would welcome the chance of combining forces with Smiths industries to attack the Honeywell IRS/FMC market.

9.8 COMMENT

In this work, the topic of pricing, cost structure and return on investment has been considered but not included, as information on this subject is company confidential.

CHAPTER 10.0

CONCLUSIONS

This thesis has dealt with the integration of a global positioning system and an inertial reference system inside a Smiths Industries Flight Management Computer. Both technical and non technical aspects of the subject have been considered. The major findings from the technical and non technical work are summarized below :

10.1 TECHNICAL WORK

- 1) The navigation performance figure for the customer inertial reference system being considered in this work is given as 2 nm/hr circular error on 95% of system flights. To simulate an IRS with this navigation performance it is necessary to correctly model the effect of balanced IRS errors that get set up during alignment.

During alignment, certain sources of IRS error exist that can become balanced, so that the combined error sources do not affect the IRS output. The results obtained from simulation show that as long as the IRS heading is unchanged, then the IRS error sources remain balanced. A change of heading causes the error sources to become unbalanced, with the error sources becoming completely unbalanced when the IRS heading is changed by 180 degrees. Therefore, if an IRS simulation is carried out and the IRS heading is relatively unchanged, then the resultant IRS navigation performance figure measured as a position error drift, will be much less than the specified value for the IRS. If however, the aircraft heading is changed by 180 degrees, then the simulated IRS navigation performance figure will be optimal.

- 2) When initialising the Kalman filter, which combines the IRS and GPS information within the flight management computer, consideration must be given to the balanced IRS errors that get set up during alignment, if the Kalman filter is to be correctly matched to the IRS condition.

A Kalman filter matching technique has been developed that uses a series of equations to obtain initialisation values for the Kalman filter covariance matrix. The chosen covariance values account for the balanced errors that are set up during the alignment process of the IRS.

If the Kalman filter is not correctly matched to the IRS alignment condition, then the filter will start to incorrectly estimate the value of certain IRS states, with the result that, the navigation performance of the system is degraded.

The types of IRS error sources that exist, and the way that different error sources become balanced are particular to each IRS type. The covariance values necessary to match the Kalman filter to the IRS are therefore specific to the IRS type.

- 3) In developing the Kalman filter three analysis techniques were investigated, these being Monte Carlo simulation, covariance analysis and sensitivity analysis. Each of the three techniques can be used to measure overall navigation system performance. The sensitivity analysis and covariance analysis techniques can also provide data on individual error sources, so that the effect of single error sources on overall navigation performance can be examined.

To develop the necessary parameters for a matched Kalman filter the technique of covariance analysis was found to be the most suitable. This technique allows the Kalman filter uncertainty in its estimate of IRS errors to be observed. Using this method, the correct conditions for a matched Kalman filter can be clearly identified.

- 4) Results obtained from simulations showed that the Kalman filter's ability to estimate the Z gyro bias error source varies with heading. The Kalman filter's ability to estimate this IRS error is therefore a function of the vehicle's heading.

- 5) The Kalman filter equations can be coded using a fast/slow loop mechanization. To implement the Kalman filter equations, a discrete solution to the state vector matrix differential equation is needed. A first order solution can be used provided the iteration rate for the equation is suitably high. The equation can then be implemented in the Kalman filter fast loop.

When implementing the Kalman filter measurement equations, consideration must be given to the rate at which the IRS and GPS measurements are processed. If the rate chosen is too fast, then the Kalman filter measurement inputs may be correlated. Hence these equations need to be processed at a lower rate than the other Kalman filter equations. The measurement equations are therefore, implemented in the Kalman filter slow loop.

10.2 NON TECHNICAL WORK

Smiths Industries supplies Flight Management Computer Systems for the Boeing 737 series aircraft and the Airbus A300-600/A310 aircraft, while Honeywell Inc and Litton Aero Products supply the inertial reference systems. Since some of the major airlines have recently expressed an interest in a flight management computer that can provide GPS/IRS integration, the market potential for such a system being produced by Smiths Industries has been examined. The main conclusions are listed below :

- 1) The major customer threatening Smiths future FMC business on both the Boeing 737 series aircraft and the Airbus A300-600/A310 is Honeywell.
- 2) Smiths and Litton could collaborate in the development of a flight management system that provides GPS/IRS integration. This would provide direct competition for Honeywell, and improve the chances of Smiths and Litton gaining a future market share on the Boeing 737 series aircraft.
- 3) In meeting the airlines demands for an FMC that provide GPS/IRS integration, there is potential for Smiths to gain further sales on the Airbus A300-600/A310 series aircraft by collaborating with Litton, since on this aircraft Litton supplies 80% of the inertial systems.

BIBLIOGRAPHY

- Ananda M The Global Positioning System Accuracy, System Error Budget. Space And Control Segment Overview. AGARD Lecture Series No 161, The Navstar GPS System, 1988.
- Bierman J Measurement Updating using the U-D Factorization. Automatica, Vol 12, no 4, 1976.
- Brackley K D deDoes, P Sinha, Performance and Operation Of Selected Aspects of GPS/Host Vehicle Integration Schemes. The Institute Of Navigation Satellite Division, Colorado Springs, September 21-25, 1987.
- Brockstein A GPS-Kalman-Augmented Inertial Navigation System Performance. IEEE National Aerospace and Electronics Conference, NAECON 1976.
- Bronkhorst.A Agard Lecture series No.95 Strap-Down Inertial Systems, May 1978.
- Brown A W Bowles, Measurement Updating Using the U-D Factorization Method When The Measurement Noise is Correlated. IEEE National Aerospace and Electronics Conference, May 17-19, 1983.
- Brown A D Lottman, K Homb, Kalman Filter Implementation in the Litton LR-80 AHRS. NAECON Vol 1, 21-25 May 1984.
- Chen P Accuracy Requirement And Cost Effectiveness Of GPS-Aided INS For Tactical Fighters. IEEE National Aerospace and Electronics, May 16-18, Vol 3, 1978.
- Cunningham J Z Lewantowicz, Dynamic Interaction Of Separate INS/GPS Kalman Filters. The Institute of Navigation, Satellite Division's International Technical Meeting, Colorado Springs, September 19-23, 1988.
- Dayton R J Nielson, A Flight Test Comparison Of Two GPS/INS Integration Approaches. The Institute Of Navigation Satellite Division, Colorado Springs, 1989.

- Disel J GPS/INS Integration by Functional Partitioning. The Institute Of Navigation Satellite Division, Colorado Springs, September 19-23, 1988
- Edwards A The State Of Strapdown Inertial Guidance and Navigation. Journal of The Institute Of Navigation, vol 16, Number 4 Winter 1971-1972.
- Frazier D E Mickle, J Nielson, K Rigg, T-33 Aircraft Demonstration Of GPS Aided Inertial Navigation. The Institute Of Navigation Satellite Division, Colorado Springs, September 21-25, 1987
- Friedland A Analysis Strapdown Navigation Using Quaternions. IEEE Transactions on Aerospace and Electronic Systems Vol aes-14, 1978.
- Gelb A Applied Optimal Estimation. The Technical Analytic Sciences Corporation, M.I.T Press 1987.
- Graham W G Johnston, Standard Integration Filter (SIF) State Specification and Accuracy Projections. Journal of the Institute of Navigation Vol 33, No 4, Winter 1986-87.
- Griffiths B M Geyer, Interfacing Kalman Filters With The Standard INS. IEEE 1984.
- Ham F R Brown, Observability, Eigenvalues, and Kalman Filtering. IEEE Transactions on Aerospace and Electronic Systems, Vol aes-19, No 2, March 1983.
- Hartman R Integrated Laser Inertial/GPS Navigation. The Royal Institute Of Navigation NAV 89, 17-October 1989.
- Hoefener C R Van Wechel, Accuracy Considerations For GPS TSPI System Design. The Institute Of Navigation Satellite Division, Colorado Springs, September 19-23, 1988.
- Huddle J Inertial Navigation System Error Model Considerations In Kalman Filter Applications. Agard Control And Dynamic Systems, Vol 20, 1983.

- Interavia Legal Battle Between Litton and Honeywell. Interavia Air Letter, No 12,025, June 28th, 1990.
- Itzhack B D Meskin, In-Flight Inertial Guidance Alignment. 16th Congress of the International Council of the Aeronautical Sciences, Jerusalem, Israel, August 28-September 2, Vol 1, 1988.
- Itzhack B B Porat, Azimuth Observability Enhancement During Inertial Navigation System In-Flight Alignment. Journal Guidance and Control, Vol 3, No 4, July-August 1980.
- Itzhack B B Porat, Effects of Acceleration Switching During INS In-Flight Alignment. Journal of Guidance and control Vol 4, No 4, July-August 1981.
- Itzhack B Minimal Order Time Sharing Filters for INS In-Flight Alignment. Journal of Guidance and Control, Vol 5, No 4 1982.
- Itzhack B Modeling of Certain Strapdown Heading-Sensitive Errors in INS Error Models. Journal of Guidance and Control, Vol 8, NO 1 1983.
- Itzhack B N Berman, Control Theoretic Approach To Inertial Navigation Systems. AIAA Guidance, Navigation and Control Conference, Vol 2, Monterey, California August 17-19, 1987.
- Kalman R.E R S.Bucy, New Results In Linear Filtering and Prediction Theory. Journal Of Basic Engineering, March 1961.
- Killpatrick J The Laser Gyro. IEEE Spectrum 1967.
- Leenhouts P On The Computation Of Bi-Normal Radial Error. Journal of the Institute of Navigation, Vol 32, No 1, 1985.
- Maron M.J Numerical Analysis A Practical Approach. Macmillan Publishing Company, 1987.
- Maybeck P Performance Analysis Of A Particularly Simple Kalman Filter. Journal Guidance and Control, Vol 1, No 6, NOV-Dec, 1978.

- Mickelson W M Carrico, Development and Flight Evaluation of an Integrated GPS/INS Navigation System. AIAA Guidance, Navigation and Control Conference, August 14-16, 1989.
- Milliken A Zoller, Principles of Operation of Navstar and System Characteristics. Agard-AG-245 Principles and Operational Aspects of Precision Position Determination Systems, 1979.
- Napier M The Integration Of Satellite and Inertial Positioning Systems. The Royal Institute Of Navigation NAV 89, 17-19 October, 1989.
- Nuttal J.D Requirements For Gyroscopes For Inertial Navigation. IEE Proceedings, Vol 132, No 5, October 1985.
- Olson P Calculation Of Geodetic Coordinates From ECEF. Journal Guidance, Vol 2, March 1988.
- Potter J New Statistical Formulas. Space Guidance Analysis Memo, Charles Stark Draper Laboratory, 1963.
- Savage P M Ignagni, Honeywell Laser Inertial Navigation System Test Results. IEEE Proc NAECON 1975, Dayton Ohio.
- Schneider A.M Vector Principles Of Inertial Navigation. IRE Transactions on Aeronautical and Navigational Electronics, 1959.
- Smiths Ind Aircraft Production Forecast 1991-2005. Smiths Industries Marketing Department, Internal Document, March, 1991.
- Smiths Ind Simulation Listing For Kalman Filter Development, July, 1991.
- Sorenson H.W Linear Estimation Theory. AGARD 139, Theory And Applications Of Kalman Filtering, Feb 1970.
- Sturza M A Brown, J Kemp, GPS/AHRS A Synergistic Mix. IEEE National Aerospace and Electronics Conference, May 21-25, 1984.

- Tafel R D Krasnjanski, Rapid Alignment Of Aircraft Strapdown Inertial Navigation Systems Using Navstar Global Positioning System. Agard Conference Proceedings No 298, Precision Positioning and Inertial Guidance Sensors Technology and Operational Aspects, 1981.
- Tapley B J Peters, Sequential Estimation Algorithm Using A Continuous UDU Covariance Factorization. Journal Guidance and Control, Vol 3, No 4, 1978.
- Tucker S J Thacker, D Simpson, Analysis Of Inertial Platform Errors. WESCON 85, San Francisco, 1985.
- Upadhayay T J Damoulakis, A Real-Time Sequential Filtering Algorithm For GPS Low-Dynamics Navigation System. IEEE 1979.
- Valstar J The Fifty-Percent Coverage Problem of the General Bivariate Gaussian Distribution. IEEE National Aerospace and Electronics Conference, NAECON 1970.

APPENDIX A

INERTIAL NAVIGATION SYSTEMS

Inertial navigation systems have been used as a source of navigation information since the late 1950's. The fundamental principle of an inertial navigation system as discussed by Edwards (1971), is that accelerometers measure acceleration with respect to an inertial frame of reference. From the acceleration measurement, velocity and position can be derived. Gyro's are used to measure angular motion with respect to inertial space. In doing so, a frame of reference can be set up, such that the velocity and position evaluated from the acceleration measurement can be obtained relative to an earth frame of reference.

In the early developments of inertial navigation systems the type of gyro's used were of the mechanical spinning type, with the basic principle being that a spinning mass is space stable and does not rotate as the earth rotates. Navigation systems that used this type of gyro are called gimballed inertial navigation systems.

Gimballed gyros were then replaced by ring laser gyros. The basic principle of the ring laser gyro as discussed by Killpatrick (1967), is that two beams of light are passed in opposite directions around a fixed length cavity. The two beams of light are combined by use of a prism to form light and dark fringes. As the laser gyro is rotated, a change in the fringe occurs such that light and dark patterns can be detected by suitably placed photodiodes. The photodiodes provide a corresponding electrical output which can then be processed. The use of ring laser gyros in inertial navigation systems results in a special type of navigation system called a strapdown inertial navigation system (INS) since, the ring laser gyros are fixed to a base which moves with the aircraft body.

The use of ring laser gyros in inertial navigation systems has several advantages over gimballed gyro systems, as discussed by Edwards (1971). The main advantages being lower weight, lower cost and higher reliability. By the mid 1970's, development of ring laser gyro technology had progressed to the point where strapdown inertial navigation systems could be flight tested.

Since the early developments, ring laser gyro technology has improved, but the errors associated with such instruments remain. The fundamentals of ring laser gyros are very complex as explained by Killpatrick (1967).

The theory of inertial navigation systems is well known, but often the development of strapdown system algorithms is unique to a particular manufacturers system. Schneider (1959), gives an explanation of basic inertial navigation system theory. Bronkhorst (1978) gives a discussion of strapdown algorithms.

There is a direct relationship between gyro errors and the resultant navigation performance that can be expected from an inertial navigation system. Nuttall (1985) discusses gyro requirements for a navigation system to meet the performance of 1 nm/hr position error.

Due to instrument errors, strapdown inertial navigation systems are not perfect. Efforts have been made therefore to try and model such errors mathematically. Huddle (1983) describes the development of an inertial navigation system error model. The paper starts by discussing the frames of reference used in the error model development. A direction cosine approach is used to describe frames of reference. The errors in various parameters within the system are then discussed, and equations are developed that describe errors in terms of system position, velocity and attitude. The resultant overall error model is presented using state space theory. It is noted that the error model developed is suitable for use in a Kalman filter. Several possible versions of the derived error model suitable for use in a Kalman filter are discussed, with the merits of each method outlined.

There is a body of mathematics called quaternion algebra, which is widely used in the application of strapdown inertial navigation systems. Friedland (1978) discusses the use of quaternions to form the basic equations of a strapdown inertial navigation system. An inertial navigation system error model using quaternions is also formulated. The paper starts by developing the equations for position, velocity and angular velocity in terms of quaternions where the various parameters are expressed in terms of an inertial frame of reference. Via quaternion algebra, a special quaternion matrix is established, which is found useful in the development of the inertial system error model.

The concept of errors in the inertial system parameters are discussed. A set of 10 differential equations are then developed in terms of quaternions, that form the basis of the system error model. A brief discussion of the interpretation of the terms in the derived error model is given. The paper concludes by saying that the quaternion error model developed should be useful for system behaviour analysis.

KALMAN FILTERS

By using certain alternative navigation sources as a reference, and combining this reference data with the information provided by the inertial navigation system, the errors in the navigation system can be reduced. This offers the potential for improved navigation system performance. The technique of combining inertial navigation information with another source of navigation data is best carried out using a Kalman filter.

A Kalman filter is essentially a technique of determining an optimal estimate of some parameter that is corrupted by the effects of noise. The early equations that were developed were limited in that they could only be solved for certain problems. Kalman (1961) introduced the modern approach to the problem of filtering which had the advantage that the solution could be implemented on a digital computer, and thus offered a practical solution to the filtering problem as opposed to a pure analytical one. A nonlinear differential equation is derived for the covariance matrix of the optimal filtering error. The Solution of this Riccati type equation then specifies the optimal filter.

GLOBAL POSITIONING SYSTEM

For today's application, the Global Positioning System (GPS) provides an ideal source of navigation information that can be combined with inertial navigation system data via the technique of Kalman filtering, to improve the overall performance of the integrated navigation system. The Global Positioning System as discussed by Milliken (1979) is a satellite based radio navigation system intended to provide highly accurate three dimensional position, velocity and time on a continuous global basis.

The system is at present not fully operational, but when it is, it will consist of 18 satellites in 6 orbital planes inclined at 55 degrees. Two classes of GPS service are available. The first class is the standard positioning service which is available to the general public. The second class is the precise positioning service which is intended for military use, since its navigational accuracy will be much higher when the full system is operational.

Navigation using GPS is accomplished by using the satellites transmitted signals to an earth based receiver or a receiver installed in an aircraft. Part of the signal transmitted by each GPS satellite, contains information relating the position of each satellite to the earth. By processing the received satellite data from at least 4 different satellites, a user can determine the receiver position relative to the earth. In addition to position, GPS can provide velocity information in three dimensions. Although it is capable of providing precise navigation information, the global positioning system does have several limitations.

The main GPS limitations are :-

- 1) The radio signals that are used to communicate the satellite information to the ground based receiver are susceptible to jamming or interference.
- 2) It takes time for the GPS receiver to track and lock onto the satellite signals. This happens when the Gps is required to track and lock onto the satellite signal initially when it starts navigating, and also when it loses sight of one satellite and starts to track another.

KALMAN FILTER INSTABILITY

Although the Kalman filter has been proved to be a suitable way to integrate INS and GPS systems, care must be taken with the actual Kalman filter implementation equations to avoid the problems of filter instability. Instability in this context can be thought of as the Kalman filter producing an unexpected and unusable result. The problem of instability can be overcome by using a certain set of equations called, the Bierman U-D factorization equations. Bierman (1976) discusses the U-D equations. The paper suggests that some but not all of the original equations developed by Kalman can be written in an alternative form. Where the alternative equations are presented in the form of upper triangular matrices.

The paper acknowledges that there are other forms of possible mechanization, the square root covariance approach suggested by Potter (1963) is quoted. The paper also claims that the U-D factorization method is as accurate as Potters square root formulation, with the advantage that it is more efficient in terms of computation time.

The U-D factorization technique appears to be the preferred method of implementing Kalman filter algorithms. Upadhyay (1979) discusses the implementation of a U-D factorization in an extended Kalman filter as used in a GPS solution. The basic equations relating to the extended Kalman filter are described. The U-D factorization equations are given that are used to propagate the covariance matrix and to update the covariance matrix. The rest of the paper discusses the GPS system model used in the GPS Kalman filter, and the tests carried out to evaluate the performance of the filter. From the results obtained, it is concluded that by using the U-D factorization in the extended Kalman filter, a stable Kalman filter is achieved.

Efforts have continued since Bierman founded the initial U-D factorization algorithms to generate more efficient methods of solving for the Kalman filter instability problem. Tapley (1978) discusses a method of propagating an alternative U-D factorization method, which is claimed to be more efficient with respect to computer storage and computation time than the original Bierman U-D factorization method.

Brown (1983) discusses a method by which the Bierman U-D factorization algorithms can be extended to cope with a special case of Kalman filter implementation, where the filter measurement noise is correlated.

SPECIFYING NAVIGATION SYSTEM PERFORMANCE

For all navigation systems it is possible to specify navigation performance in several different ways. Leenhouts (1985) discusses in some detail the various ways of assessing performance. In introducing the topic, Leenhouts makes the point that the commonly adopted conventions for the computation of radial navigation error are not consistent in probability. This inconsistency is investigated and the bivariate normal distribution is discussed. Special cases of the equation that result in a circular distribution are considered. The probability circle is then introduced. A comparison is given of methods to measure circular error.

Distance root mean squared (Drms), circle of equal probability (CEP), and geometric dilution of precision are discussed. An equation for circle of error probability can be written in several different forms. The various commonly used formula are given.

The inconsistency mentioned above is described as being due to the fact that some methods of evaluating radial error make the assumption that navigation parameters (specifically latitude and longitude), are uncorrelated and have equal statistics to describe them thus leading to a circular distribution. If the two assumptions are not valid however, then the distribution obtained is not circular, but becomes elliptical. Thus applying the circular error theory to these elliptical cases will result in some error in the value of navigation performance. Graphs are given that show what error can be expected when circular theory is applied to elliptical responses.

Identifying the fact that the latitude and longitude errors are correlated is not an easy task in practice. Valstar (1970), discusses a method of uncorrelating latitude and longitude errors if they are correlated, so that the circular error theory can then be correctly applied to form a measure of navigation performance.

TECHNIQUES TO EVALUATE PERFORMANCE

One of the major tasks involved in the integration of inertial navigation systems with GPS via a Kalman filter, is that of evaluating system navigational performance. Tucker (1985) discusses the evaluation of navigation errors in inertial navigation systems. Three different types of evaluation technique are discussed, these being Monte Carlo analysis, error analysis and covariance analysis. Typical error sources expected from an inertial navigation system are summarized, amounting to some 29 individual sources. It is assumed that each error source is independent of all other error sources, which allows the combined effect of individual error sources to be investigated, this being the principle of the error method of analysis.

The Monte Carlo method of analysis is described as a statistical experiment, where the combined effect of all error sources is determined by generating random samples of each error source, and processing a large number of such experiments. The third method of analysis discussed is the technique of covariance analysis.

This method differs from the first two, as it deals with the dynamics of the errors themselves. The mathematical development of the error covariance equations is discussed. The use of the equations are restricted to a certain type of error referred to as random constant, although it is concluded that the equations could be extended to the more general type of application by including the effects of random noise. Results for all three methods of analysis as applied to the inertial system error model, are compared. It was found that all three methods provided results that were in close agreement.

Savage (1975) discusses the testing of a Laser Gyro Inertial Navigation System. Laboratory and flight tests are discussed. Statistical results are given of alignment tests carried out in the laboratory where the inertial system was first aligned to north and then east. The results quoted are for root mean squared (RMS) heading error versus alignment time.

The relationship between alignment time and gyro random walk is discussed, where it is implied that the lower the gyro random walk the faster the alignment time. This relationship was seen from the results, where the X gyro random walk and the Y gyro random walk had different values which resulted in different values of RMS heading error for the north and east cases. A total of 13 flight profiles were tested.

Brockstein (1976) discusses the performance of a 15 and a 22 state Kalman filter used for the integration of GPS/INS. The evaluation of the system is carried out by the method of Monte Carlo analysis. The integration scheme discussed is open loop since no attempt is made to feed back INS corrections to the actual IN system. Corrections to the raw INS data are used however in the computations of GPS range and range rate estimates. There is only one Kalman filter used to model both the INS and GPS errors. The measurement input into the Kalman filter is a range and range rate residual, which is the difference between the range and range rate measured by the GPS receiver, and the range and range rate estimates computed as a function of the corrected INS variables.

The truth model, which is a model of all known errors associated with GPS and INS is discussed. The total number of error sources used in the truth model is 106. A brief description of the 106 error sources is given. After an extensive period of simulation and study a 15 state Kalman filter was developed from the reference truth model.

A Monte Carlo simulation was carried out to investigate system performance. The results obtained showed that the 15 state Kalman filter with a 1 second update rate performed well as a sub optimal Kalman filter solution. It was noted that jamming of the GPS system affects level axis position and velocity, although its effect on vertical axis performance is not so great if a baro-inertial loop is implemented, this is to be expected since the barometric altimeter acts as an external source of information.

Maybeck (1978) also discusses the performance analysis of a Kalman filter where a strapdown inertial navigation system is integrated with a radiometric area correlator (RAC). The RAC provides a number of accurate fixes by correlating a radiometric picture of the terrain immediately below the vehicle with a pre-stored reference map of the region. The Kalman filter is used in a closed loop mode where the estimates of the INS errors are feed back to the INS for correction. The Kalman filter design consists of two decoupled level axis filters which are used to model the INS errors. It is stated that the common approach to this type of problem is to use a single coupled filter.

An explanation of how the two decoupled filters can be justified is given. Evaluation of the sub optimal Kalman filter is carried out via the technique of covariance analysis. A truth model is used which represents an ideal model of an inertial system. The truth model chosen has 46 states which are detailed. Using the covariance analysis technique the sub optimal Kalman filter was tuned by comparing its performance against the truth model. Once a suitable design was arrived at, its performance was assessed against the required specification, details of which are not given. The paper concludes that the performance of the sub optimal filter is within the required specification.

Chen (1978) discusses the accuracy requirements for GPS aided inertial navigation systems. The paper deals with an INS intended for use in a missile system. A covariance analysis program was used to investigate the performance of a GPS aided INS during enroot navigation. A 15 state INS error model is used in the inertial system Kalman filter which accepts GPS position. Estimates of inertial system errors obtained from the Kalman filter are fed back to the INS for calibration. A simulation was carried out to assess unaided inertial system performance after a one hour period of GPS coverage. The performance of the simulated INS before calibration is given as 1 nm/hr CEP. Results are given for the horizontal position error and velocity error obtained from the simulation.

A technique is then discussed that allows the one sigma velocity error obtained from the Kalman filter covariance analysis to be converted into a one sigma ensemble statistic that is suitable for use to describe weapon system performance. Conclusions are drawn about the accuracy required of an inertial navigation system such that a weapon system can meet its required specification.

INERTIAL NAVIGATION SYSTEM ALIGNMENT

Inertial navigation systems can generally be considered to have two basic modes of operation, these being alignment mode and navigate mode. The alignment mode is where the inertial system orientates itself with respect to the earth in preparation to start navigating, and also tries to estimate the errors in the inertial system and hence calibrate for them. The alignment is normally carried out via a Kalman filter. It is not always possible to detect all of the inertial system errors during the alignment phase because some of the errors may be unobservable.

Itzhack (1980) considers the observability of certain INS errors during the alignment phase of an inertial system. An in-air alignment is considered. A discussion is given on the observability of the azimuth error, which can be thought of as being an error in the inertial system heading. It is stated that the time to estimate the azimuth error can be reduced if certain manoeuvres are carried out such that accelerations are introduced into the system. It is possible to produce one of two types of acceleration, these being axial and lateral. The paper investigates the effect of both of these types of manoeuvre on the observability of the azimuth error source. The inertial system error model used to carry out the investigation consists of 5 states.

A simulation is carried out by considering the continuous time matrix Riccati equation which is solved for several cases of interest. Analytic solutions are also obtained to compare with the results obtained from simulation. Two manoeuvres are considered which simulate the generation of axial and lateral accelerations. For the first case of interest the 5 state error model is reduced to third order by making assumptions about the size of the azimuth gyro errors, the assumption being that the error is small. The analytic solution to the problem is given where it is noted that the solution depends on the stochastic observability matrix of the system.

Two solutions are generated, one where the accelerations are assumed to be axial, and one where they are assumed to be lateral. By examining the results for the two analytic solutions, it is concluded that the axial acceleration manoeuvre is superior to the lateral acceleration manoeuvre provided the condition assumed for the gyro holds. To account for the case when the gyro assumption cannot be made, a fourth order model is developed. Similar results are analyzed as for the third order model, from which it is again concluded that the axial acceleration is superior to the lateral acceleration in enhancing the observability of the azimuth error. A comparison of results for the analytic cases against the simulated cases also showed good agreement.

Itzack (1981) is a follow on paper from the work carried out in Itzack (1980). Simulations are carried out to investigate the effect on azimuth observability of two types of acceleration. A circular orbit as opposed to an S shaped manoeuvre is considered to examine the first type of acceleration, while for the second type a constant axial acceleration as opposed to an alternating one is considered. Simulation results are presented for the two types of acceleration from which it is concluded that for the constant axial acceleration case the azimuth misalignment estimation error reaches a smaller value than for the alternating axial acceleration case. Similarly for the circular manoeuvre the azimuth error is smaller than for the S shaped manoeuvre. Theoretical results are given for the azimuth estimation error as a function of time. Graphs were plotted using the theoretical results for the two cases above. A close agreement was observed between theoretical and simulation results. By examining the theoretical results it is concluded that when there is a change in the sign of the acceleration, the correlation coefficient that correlates the measured velocity error and the azimuth misalignment, changes sign and thus crosses zero which temporarily halts the estimation process.

Itzhack (1982) discusses a technique whereby the in-flight alignment of an Inertial Navigation System is carried out using a time sharing filter. The investigation is carried out using a covariance analysis simulation which is based on a 24 state truth model of an INS. The time sharing filter is based on the fact that the INS error behaviour can be described by simplified equations during certain manoeuvres. Three filters are given to be used with a base line S shape manoeuvre that is carried out during the in-flight alignment phase. Simulation results are presented for the time sharing filter.

It is concluded from these results that certain errors that are estimated namely the level misalignment errors, need to be fed back to the INS for correction if the overall filter is to function correctly.

Itzhack (1983) discusses the theory relating to heading sensitive errors in Inertial Navigation Systems. Results are quoted but not derived for INS errors in terms of position and velocity, and attitude. An additional equation describing velocity error is introduced. Using this equation an analysis is carried out to show how in a strapdown inertial system alignment errors can be uncoupled by rotation.

Itzhack (1988) discusses the observability carried out on a three channel inertial navigation system. The difficulties of applying classical observability theory to inertial navigation systems that are time varying are discussed. The paper reports on the use of a special technique that can be used to help determine the observability of INS parameters. The technique reported is referred to as a stepped observability matrix (SOM) which is where a special trajectory for in-flight alignment is considered, which allows a piecewise constant model to be used as the dynamics of the INS model.

The use of the SOM provides a simple way to analyze the change of observability that occurs with changes in trajectory. The SOM is applied to investigate the observability associated with a 12 state inertial system error model. A covariance simulation was carried out for the same 12 state INS error model as used in the SOM analysis. The two sets of results obtained from the SOM and the covariance analysis were found to be in close agreement.

Ham (1983) discusses the use of eigenvalues as applied to the covariance matrix of a Kalman filter, to help provide information on observability of the Kalman states being modelled. A mathematical development to obtain the eigenvalues and eigenvectors of the Kalman filter covariance matrix is discussed. It is stated that the largest eigenvalue relates to the state in the system that is least observable, while the smallest eigenvalue corresponds to the state that is most observable. Because of potential difficulties with the range of possible eigenvalues that could be encountered, a scheme to normalize the eigenvalues is suggested which takes into account the initial conditions of the system.

An example of applying the method to a 6 state inertial system is given, which illustrates the fact that the smallest eigenvalue corresponds to the state that is most observable.

Alignment of an inertial system can benefit from the use of GPS as an external source of information. Diesel (1988) discusses the use of GPS during the alignment phase of a strapdown inertial navigation system. The type of errors that are expected from a standalone inertial system after a typical alignment phase is complete are discussed. It is shown that the resultant inertial system performance is directly affected by the errors that remain after the alignment phase is complete.

The solution of a matrix Ricatti equation is given for certain types of instrument errors to illustrate this point. The use of GPS in the alignment phase is then discussed. The solution of a matrix Ricatti equation is again considered to show the improvement that might be expected in terms of navigation performance, if GPS is used. The paper considers that with the use of GPS, the error sources remaining after the alignment phase is complete, are mostly random walk type errors. For standalone INS operation, random constant errors are dominant.

Tafel (1981) discusses the use of GPS during the alignment phase of an inertial system. The study considers the increase in speed that can be obtained by the use of GPS during the alignment phase, over that achieved by a standalone alignment. The paper states that certain types of error source are only observable when the inertial system is experiencing an acceleration. Two types of acceleration, lateral and axial are discussed. It is concluded that to observe all the errors of interest during an in-flight alignment, certain types of manoeuvre (which are not specified), must be carried out so as to generate accelerations in the inertial system.

Itzhack (1987) discusses a control theory approach to the analysis of inertial navigation systems. The paper does not attempt to expose new features of inertial navigation systems, but to examine known features using modern control theory. A discussion is given on the type of error model used to represent an inertial system which is used throughout the paper. Two types of possible error model are considered for use, these being the perturbation approach and the psi-angle approach. It is stated that most of the published work on INS error models adopts the psi-angle approach, so this version is selected for use.

The vector form of the INS error model is given but not derived. From this set of vector equations, a resultant state space model is produced which contains nine states. Certain simplifying assumptions about the conditions under which the equations are to be analyzed are given. The main condition is that the system is considered to be at rest. Further simplifications are then made about the characteristics of the instrument errors, allowing the 9 state error model to be reformulated into a 10 state version. The eigenvalues of the corresponding 10 state model are then presented. Several of the eigenvalues relate to known inertial system characteristics, these are identified.

The concept of controllability and observability are examined. Observability is examined by considering the alignment and calibration phase of an inertial system. It is stated that the quality of the inertial system is related to the observability of the system errors. To investigate the topic of observability a linearity transformation is applied to the 10 state model to produce a corresponding model that contains a distinct observable and non-observable part. The matrices required to perform the transformation are detailed. The transformation matrices relate to the physics of the system. The physical reasoning behind the transformation is discussed, where it is shown how the transformation are based on defining new states for the error model. The relationship between the new states and the old states used to represent the inertial model is seen to be surprisingly simple. Consideration is given to applying a Kalman filter to the transformed equations, where the expected results from the Kalman filter covariance matrix are briefly discussed.

RELATED PAPERS

Hoefenen (1988) considers accuracy aspects of GPS system design. The question "how accurate is GPS" is discussed. Four major sources of error that affect the accuracy of GPS are quoted. Three of the four sources given make up the user equivalent range error (UERE). The process whereby the UERE affects the final position error is given, this being the geometric dilution of precision (GDOP). GDOP is described as being a measure of how satellite geometry affects accuracy and can be thought of as the amplification or scaling of pseudorange measurement errors into user position error due to the effects of the three dimensional geometry of the satellite and user position. Techniques are discussed as to how the effects of the UERE error sources can be minimized.

The principles of differential GPS are described, since it offers a method to eliminate the space and control segment errors that effect the UERE. Brief details are given of how the use of the P or C/A code techniques can aid in reducing transmission time errors. Tropospheric errors and there relationships to satellite elevation are considered. The pseudosatellite, which is a ground based satellite, can be used to augment satellite coverage. Two graphs are given to illustrate this effect, where PDOP versus time is plotted. For the case with no pseudosatellite, a peak in the PDOP v time graph is observed at around 10 hours. For the corresponding pseudosatellite result, the peak is completely removed due to the augmented pseudosatellite. A table showing typical accuracies of various GPS receivers for several different error sources are given.

APPENDIX B

INERTIAL REFERENCE SYSTEM ERROR BUDGET TABLE

ERROR SOURCE	1 SIGMA	UNITS
X GYRO BIAS	0.008	DEG/HR
Y GYRO BIAS	0.008	DEG/HR
Z GYRO BIAS	0.016	DEG/HR
X ACCELEROMETER BIAS	40	MICRO G
Y ACCELEROMETER BIAS	40	MICRO G
Z ACCELEROMETER BIAS	40	MICRO G
GYRO RANDOM WALK	0.002	DEG SQRT HR
ACCELEROMETER NOISE CORRELATION TIME	3 30	MICRO G MINUTES
ACCELEROMETER GRAVITY ANOMOLY	6	ARC SECONDS
CORRELATION DISTANCE	25	NM

APPENDIX C

RELATIONSHIP BETWEEN THE KALMAN FILTER COVARIANCE MATRIX DIAGONAL ELEMENTS AND THE IRS STATES

IRS ERROR STATE	GRAPH NOTATION	COVARIANCE ELEMENT
x position	SD 1	P(1,1)
Y position	SD 2	p(2,2)
x velocity	SD 3	p(3,3)
y velocity	SD 4	p(4,4)
x tilt	SD 5	p(5,5)
y tilt	SD 6	p(6,6)
z tilt	SD 7	p(7,7)
x gyro bias	SD 8	p(8,8)
y gyro bias	SD 9	p(9,9)
z gyro bias	SD 10	p(10,10)
x accel bias	SD 11	p(11,11)
y accel bias	SD 12	p(12,12)

APPENDIX D

SUMMARY OF IRS STATES FOR THE OPTIMAL IRS ERROR MODEL

X(1)	X PLATFORM AXIS POSITION ERROR
X(2)	Y PLATFORM AXIS POSITION ERROR
X(3)	INERTIAL ALTITUDE ERROR
X(4)	X PLATFORM AXIS VELOCITY ERROR
X(5)	Y PLATFORM AXIS VELOCITY ERROR
X(6)	Z PLATFORM AXIS VELOCITY ERROR
X(7)	X PLATFORM AXIS TILT (OR ATTITUDE) ERROR
X(8)	Y PLATFORM AXIS TILT (OR ATTITUDE) ERROR
X(9)	Z PLATFORM AXIS TILT (OR ATTITUDE) ERROR
X(10)	X BODY AXIS GYRO BIAS ERROR
X(11)	Y BODY AXIS GYRO BIAS ERROR
X(12)	Z BODY AXIS GYRO BIAS ERROR
X(13)	X BODY AXIS ACCELEROMETER BIAS ERROR
X(14)	Y BODY AXIS ACCELEROMETER BIAS ERROR
X(15)	Z BODY AXIS ACCELEROMETER BIAS ERROR
X(16)	BARO INERTIAL LOOP ERROR
X(17)	BARO INERTIAL LOOP REFERENCE SOURCE ERROR

TABLES

Table 4-1 - Kalman Filter Initialisation Parameters

IRS ERROR STATE	COVARIANCE ELEMENT	VALUE	UNITS
x position	P(1,1)	9.0×10^{-12}	rads ²
Y position	p(2,2)	9.0×10^{-12}	rads ²
x velocity	p(3,3)	25.0	kts ²
y velocity	p(4,4)	25.0	kts ²
x tilt	p(5,5)	9.0×10^{-8}	rads ²
y tilt	p(6,6)	9.0×10^{-8}	rads ²
z tilt	p(7,7)	1.0×10^{-6}	rads ²
x gyro bias	p(8,8)	1.9×10^{-8}	rads ² /hr ²
y gyro bias	p(9,9)	1.9×10^{-8}	rads ² /hr ²
z gyro bias	p(10,10)	7.7×10^{-8}	rads ² /hr ²
x accel bias	p(11,11)	1.6×10^{-9}	g ²
y accel bias	p(12,12)	1.6×10^{-9}	g ²

Note : All other values of the covariance matrix are set to zero.

Table 9-1 - Large Commercial Aircraft Production Figures

CUSTOMER	AIRCRAFT	1990	91	92	93	94	95	96	97	98	99
BOEING	747-400/500	103	50	50	50	40	40	40	40	40	40
BOEING	757	332	70	60	60	50	50	40	40	40	40
BOEING	767	343	50	50	40	30	20	15	15	15	15
BOEING	777	-	-	-	-	1	24	48	48	48	60
AIRBUS	A300-600/ A310	272	40	40	40	33	25	20	5	-	-
AIRBUS	A330	-	-	2	10	27	35	35	35	35	30
AIRBUS	A340	-	2	11	20	23	20	20	22	25	25
AIRBUS	A350	-	-	-	-	-	-	-	-	1 IN	YEAR 2000
MCDONNELL DOUGLAS	MD-11	-	4	30	40	40	40	38	38	35	35
MCDONNELL DOUGLAS	MD-12X	-	-	-	-	-	-	2	12	20	25

Source of data - Smiths (1991)

Table 9-2 - Medium Commercial Aircraft Production Figures

CUSTOMER	AIRCRAFT	1990	91	92	93	94	95	96	97	98	99
AIRBUS	A320	132	100	100	100	85	80	80	80	80	80
BOEING	737-Series	833	200	200	100	150	140	110	100	90	90
MCDONNELL DOUGLAS	MD 80	821	140	100	80	75	50	-	-	-	-

Source of data - Smiths (1991)

Table 9-3 - Distribution Of FMC And IRS Equipment

CUSTOMER	AIRCRAFT TYPE	FMC	IRS
BOEING	737-300/400/500	S	L/H
BOEING	747-400	H	H
BOEING	757	H	H
BOEING	767	H	H
BOEING	777	H	H
AIRBUS	A300-600/A310	H/S	L/H
AIRBUS	A320/A321	H	H
AIRBUS	A330/A340	H	H/L
MCDONNELL DOUGLAS	MD-88	H	H
MCDONNELL DOUGLAS	MD-90	H	H
MCDONNELL DOUGLAS	MD-11	H	H

Source of data - Smiths (1991)

Table 9-4 - Estimated market share

CUSTOMER	FMC	IRS
SMITHS	31%	-
HONEYWELL	69%	82%
LITTON	-	18%

Table 9-5 - IRS/FMC Combinations

FMC	SMITHS	HONEYWELL	-
IRS	-	HONEYWELL	LITTON

Table 9-6 - Options For Future Sales

FMC	IRS
Honeywell	Honeywell
Smiths	Litton

Source of data for all tables - Smiths (1991)

STRAPDOWN INERTIAL REFERENCE SYSTEM BLOCK DIAGRAM

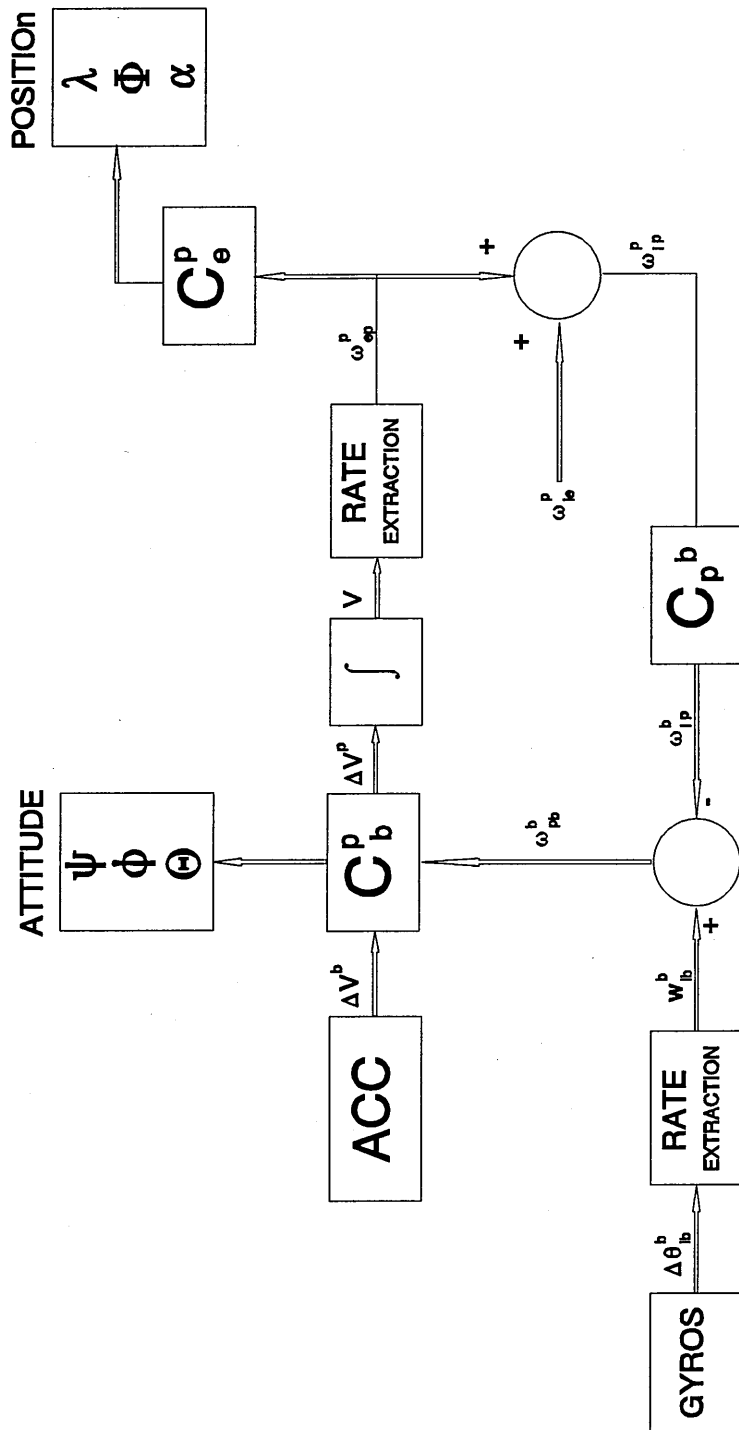


Figure 2-1

RELATIONSHIP BETWEEN COORDINATE SYSTEMS

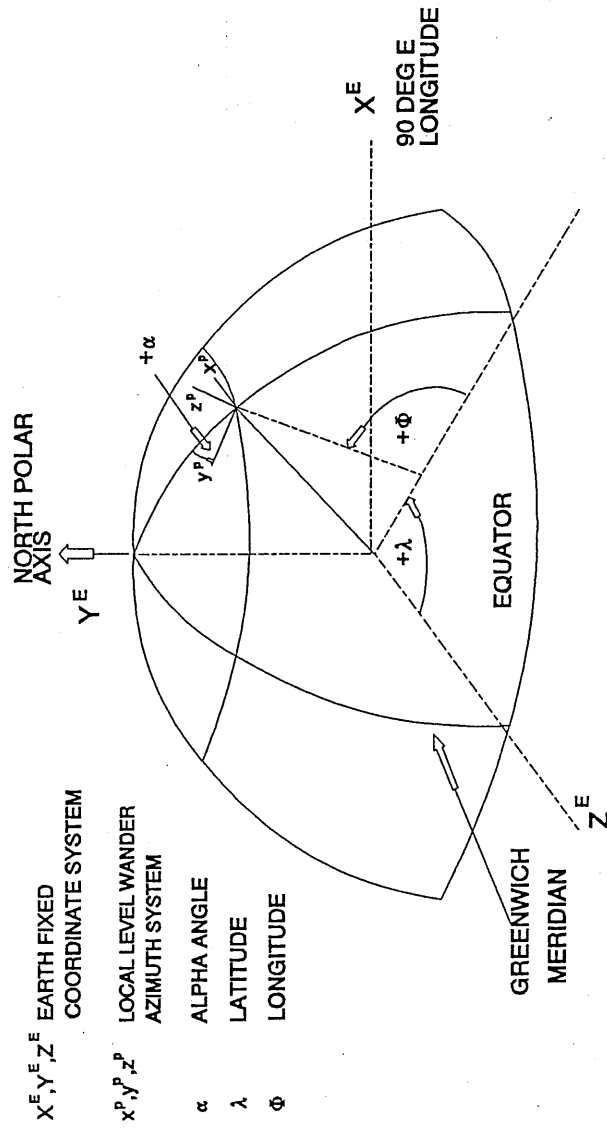


Figure 2-2

RELATIONSHIP BETWEEN BODY AXIS AND WANDER AZIMUTH AXIS

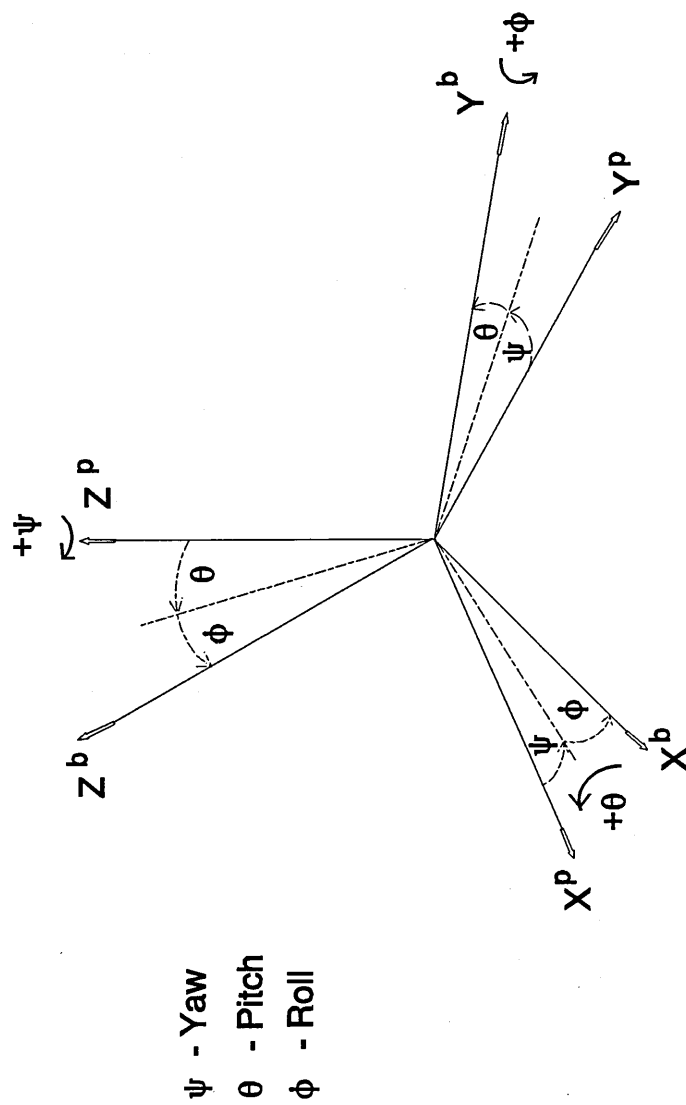


Figure 2-3

BARO INERTIAL LOOP

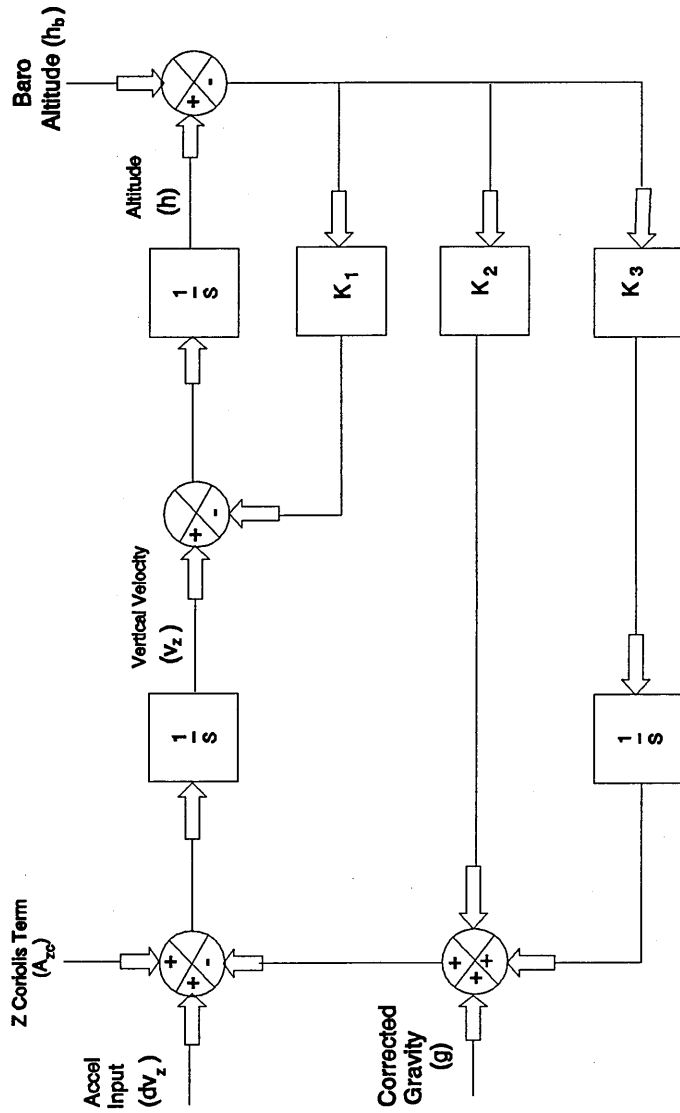


Figure 2-4

BARO INERTIAL LOOP ERROR MODEL

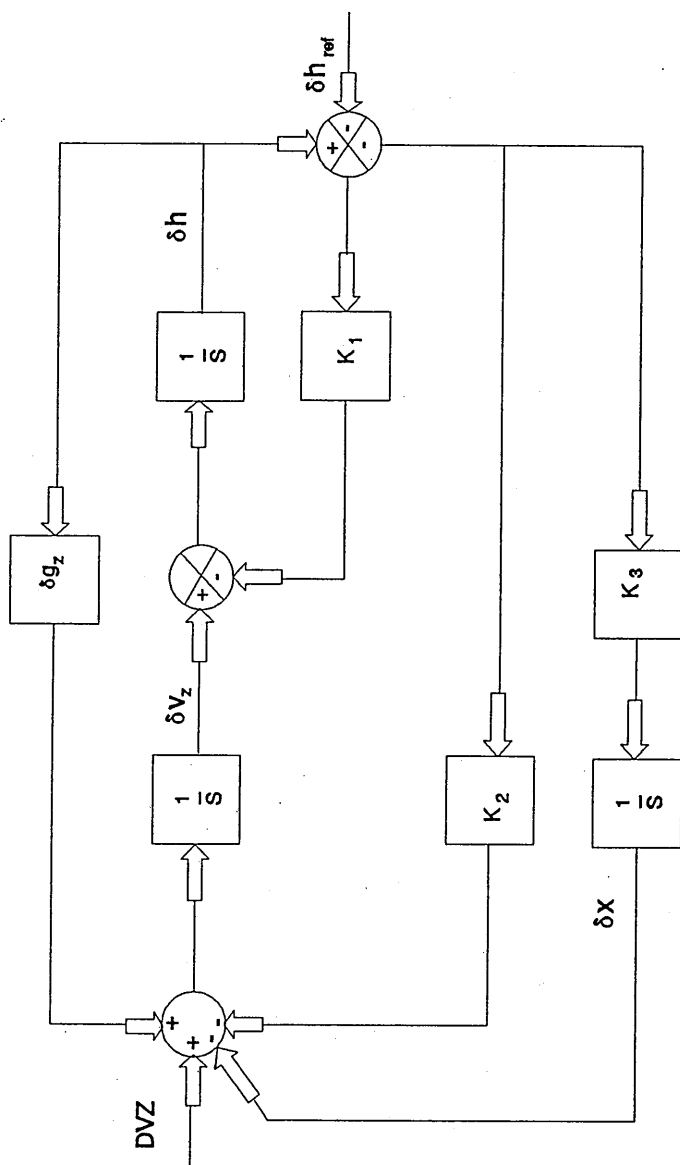


Figure 2-5

GLOBAL POSITIONING SYSTEM

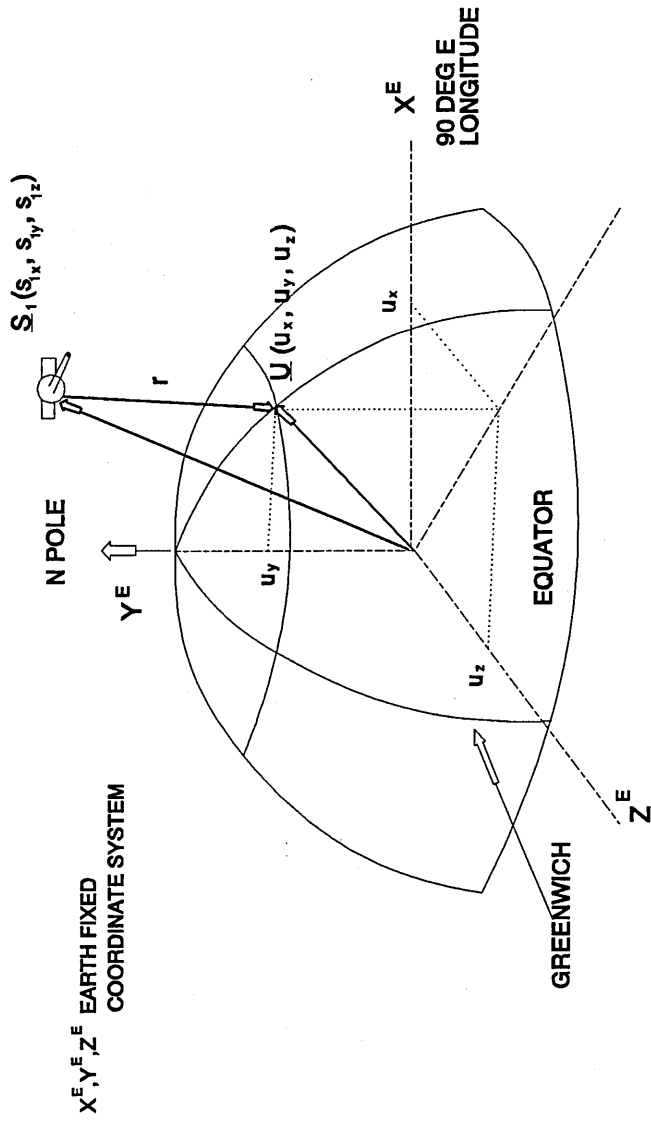


Figure 3-1

KALMAN FILTER BLOCK DIAGRAM

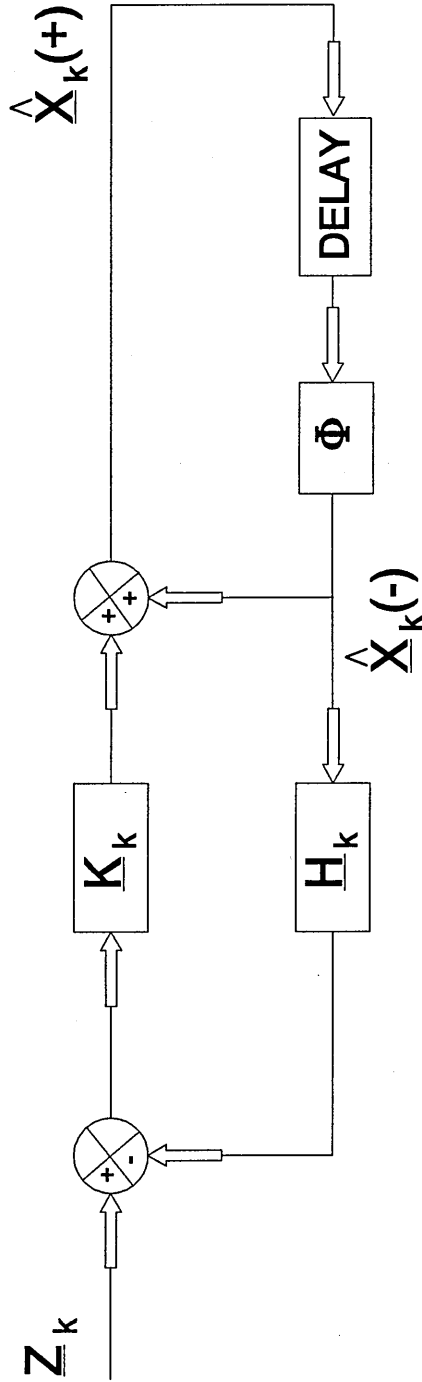


Figure 4-1

KALMAN FILTER SYSTEM MATRIX

The 12 state sub optimal Kalman filter system matrix is given below :

$$\begin{bmatrix} \delta \dot{\theta}_x \\ \delta \dot{\theta}_y \\ \delta \dot{v}_x \\ \delta \dot{v}_y \\ \dot{\phi}_x \\ \dot{\phi}_y \\ \dot{\phi}_z \\ \dot{\epsilon}_x \\ \dot{\epsilon}_y \\ \dot{\epsilon}_z \\ \dot{\nabla}_x \\ \dot{\nabla}_y \end{bmatrix} = \begin{bmatrix} 0 & 0 & 0 & -\frac{1}{R_0} & 0 & 0 & 0 & 0 & 0 & 0 & 0 & 0 \\ 0 & 0 & \frac{1}{R_0} & 0 & 0 & 0 & 0 & 0 & 0 & 0 & 0 & 0 \\ 0 & 0 & 0 & 0 & 0 & -g & 0 & 0 & 0 & 0 & C_{11} & C_{12} \\ 0 & 0 & 0 & 0 & -g & 0 & 0 & 0 & 0 & 0 & C_{21} & C_{22} \\ 0 & -\Omega_z & 0 & -\frac{1}{R_0} & 0 & W_z & -W_y & C_{11} & C_{12} & C_{13} & 0 & 0 \\ \Omega_z & 0 & \frac{1}{R_0} & 0 & -W_z & 0 & W_x & C_{21} & C_{22} & C_{23} & 0 & 0 \\ -\Omega_y & \Omega_x & 0 & 0 & W_y & -W_x & 0 & C_{31} & C_{32} & C_{33} & 0 & 0 \\ 0 & 0 & 0 & 0 & 0 & 0 & 0 & 0 & 0 & 0 & 0 & 0 \\ 0 & 0 & 0 & 0 & 0 & 0 & 0 & 0 & 0 & 0 & 0 & 0 \\ 0 & 0 & 0 & 0 & 0 & 0 & 0 & 0 & 0 & 0 & 0 & 0 \\ 0 & 0 & 0 & 0 & 0 & 0 & 0 & 0 & 0 & 0 & 0 & 0 \\ 0 & 0 & 0 & 0 & 0 & 0 & 0 & 0 & 0 & 0 & 0 & 0 \end{bmatrix} \begin{bmatrix} \delta \theta_x \\ \delta \theta_y \\ \delta v_x \\ \delta v_y \\ \phi_x \\ \phi_y \\ \phi_z \\ \epsilon_x \\ \epsilon_y \\ \epsilon_z \\ \nabla_x \\ \nabla_y \end{bmatrix}$$

Figure 4-2

OPTIMAL v SUB OPTIMAL IRS STATE VECTORS

$$\begin{array}{l}
 \mathbf{x}_{optimal} = \begin{bmatrix}
 \delta\theta_x \\
 \delta\theta_y \\
 \delta h \\
 \delta v_x \\
 \delta v_y \\
 \delta v_z \\
 \phi_x \\
 \phi_y \\
 \phi_z \\
 \epsilon_x \\
 \epsilon_y \\
 \epsilon_z \\
 \nabla_x \\
 \nabla_y \\
 \nabla_z \\
 \delta x \\
 \delta h_{ref}
 \end{bmatrix}
 \end{array}
 \qquad
 \begin{array}{l}
 \mathbf{x}_{subopt} = \begin{bmatrix}
 \delta\theta_x \\
 \delta\theta_y \\
 \delta v_x \\
 \delta v_y \\
 \phi_x \\
 \phi_y \\
 \phi_z \\
 \epsilon_x \\
 \epsilon_y \\
 \epsilon_z \\
 \nabla_x \\
 \nabla_y
 \end{bmatrix}
 \end{array}$$

Figure 4-3

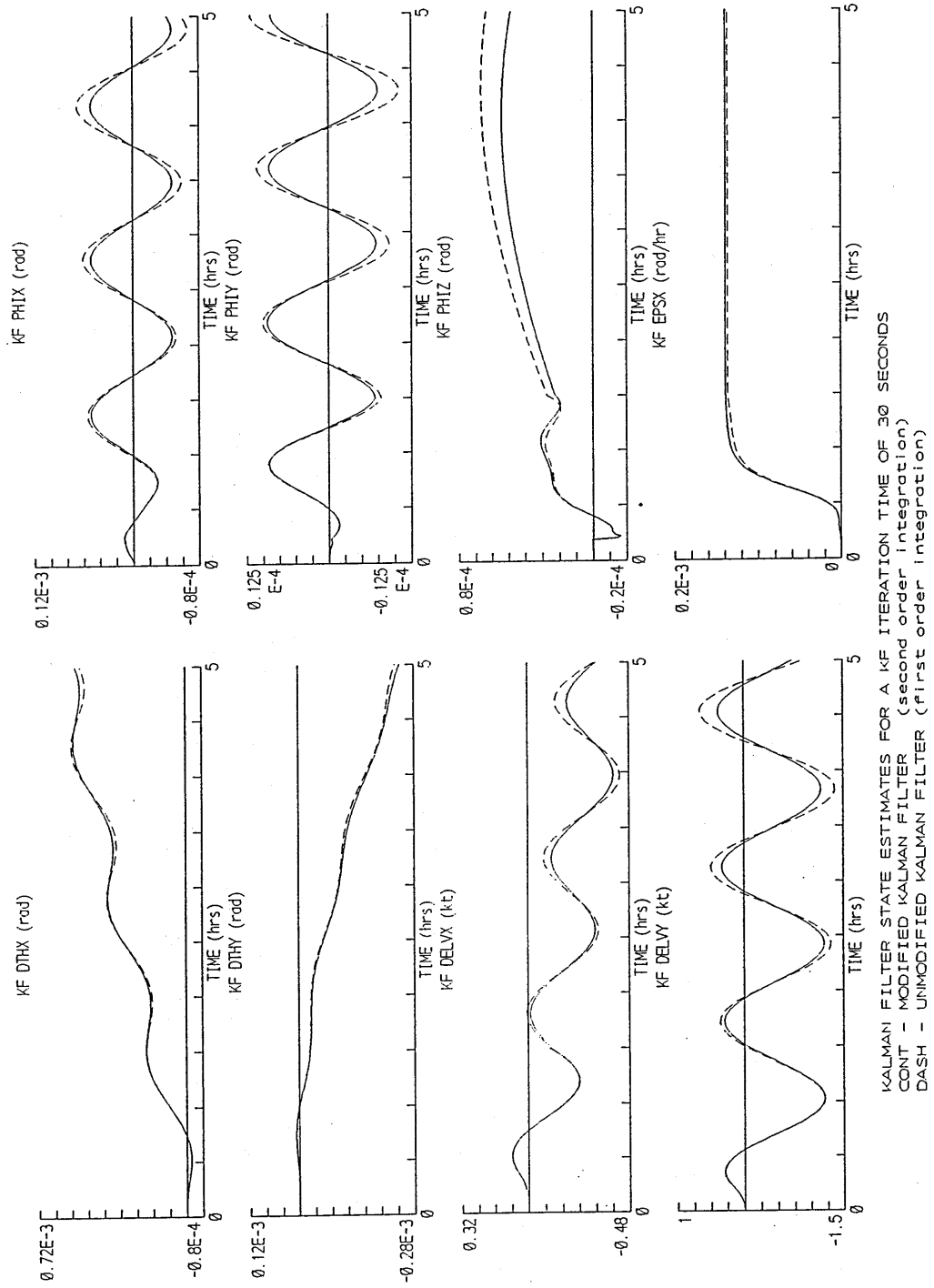


Figure 4-4

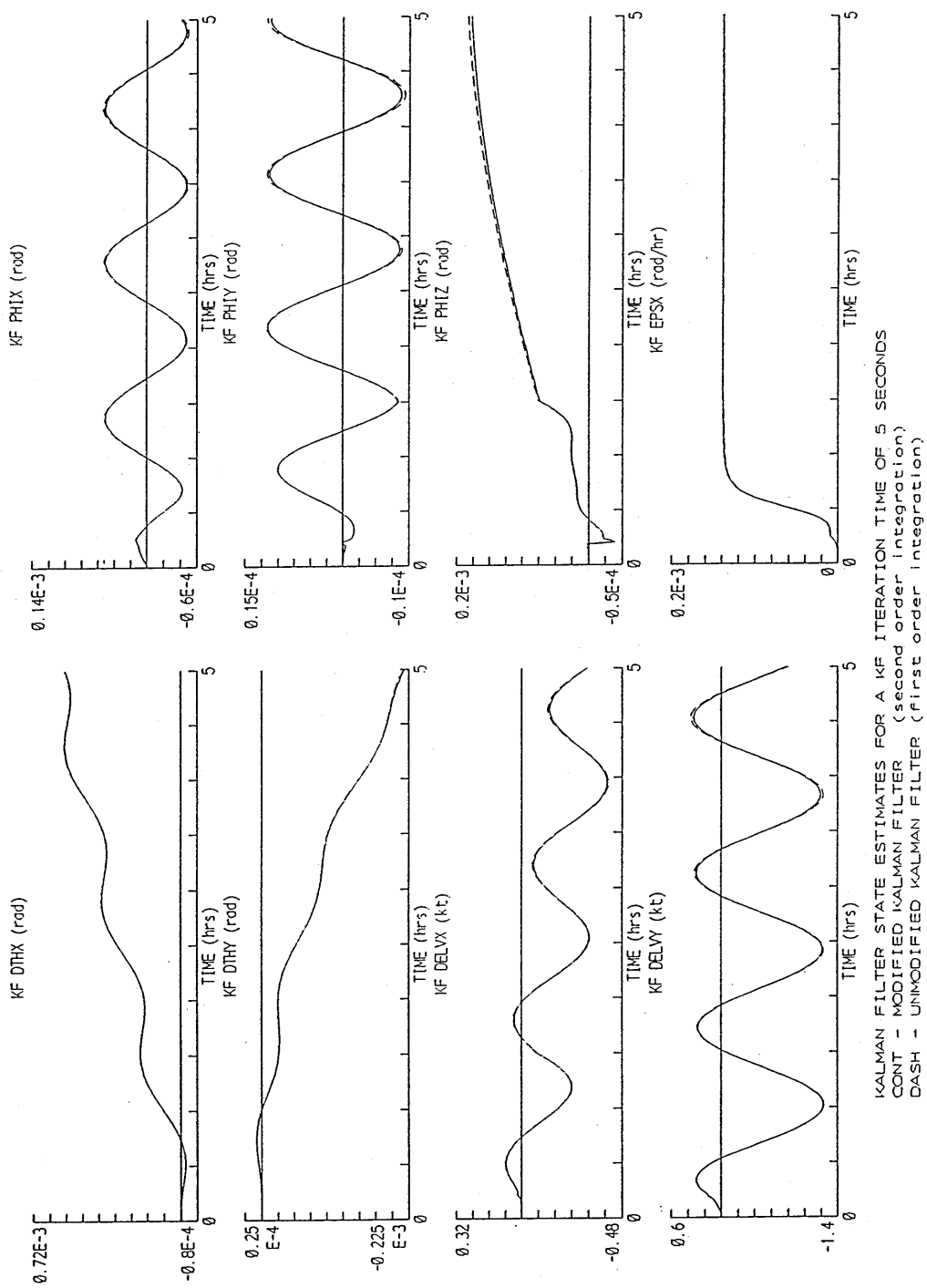


Figure 4-5

ACCELEROMETER NOISE POWER SPECTRAL DENSITY PLOT

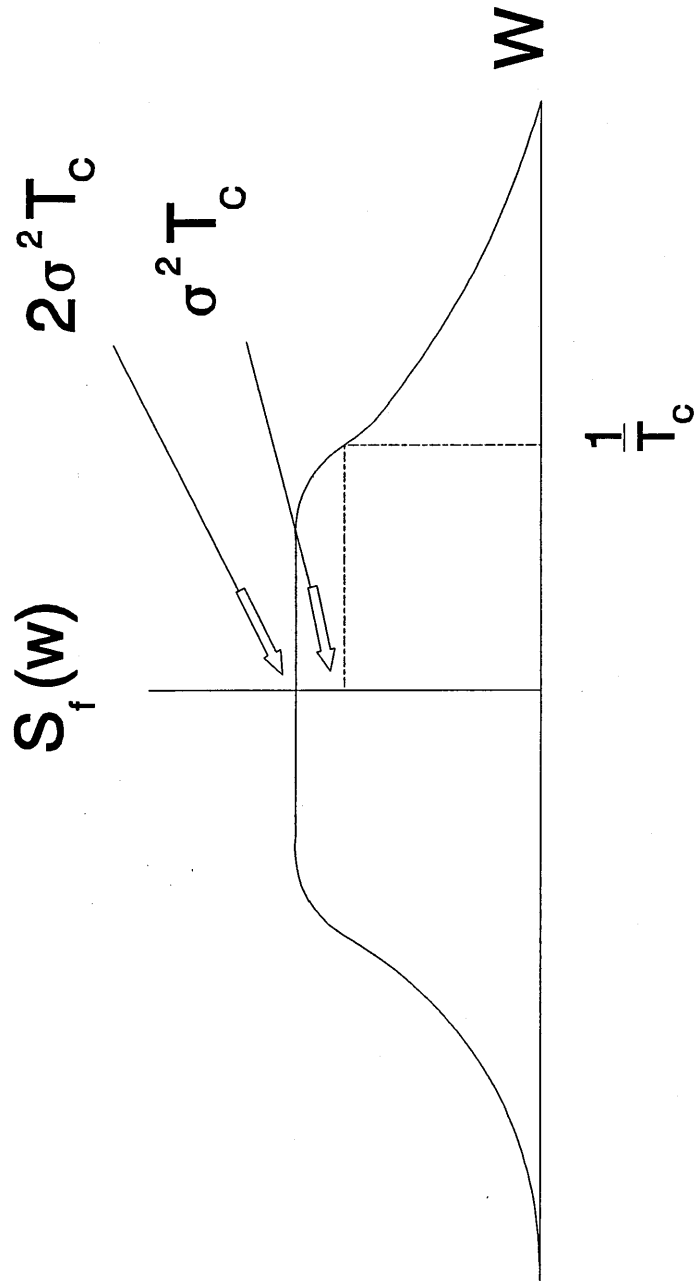


Figure 4-6

SIMULATION PROGRAM MODULES

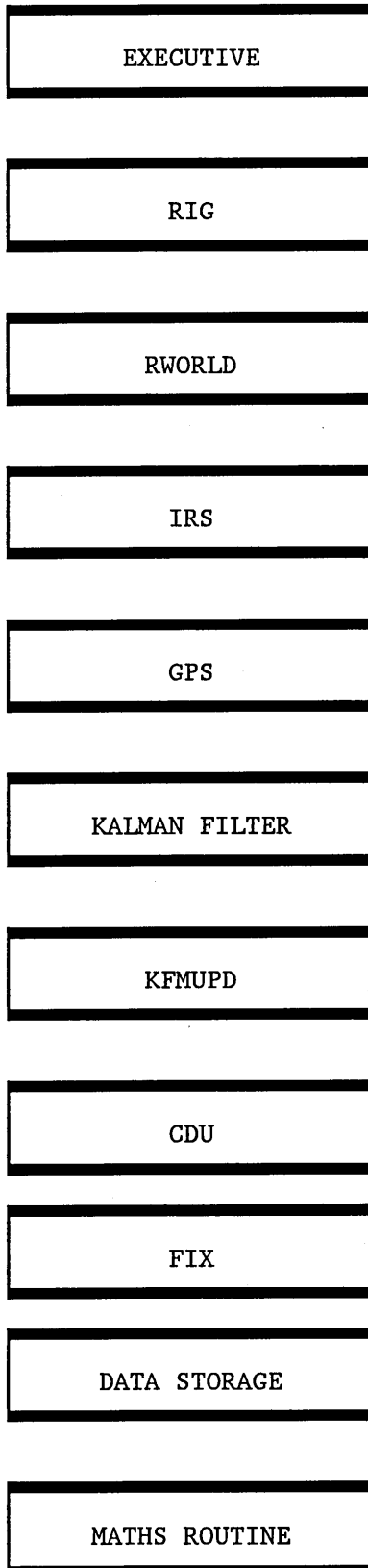


Figure 5-1

SIMULATION PROGRAM EXECUTIVE CALLING ROUTINES

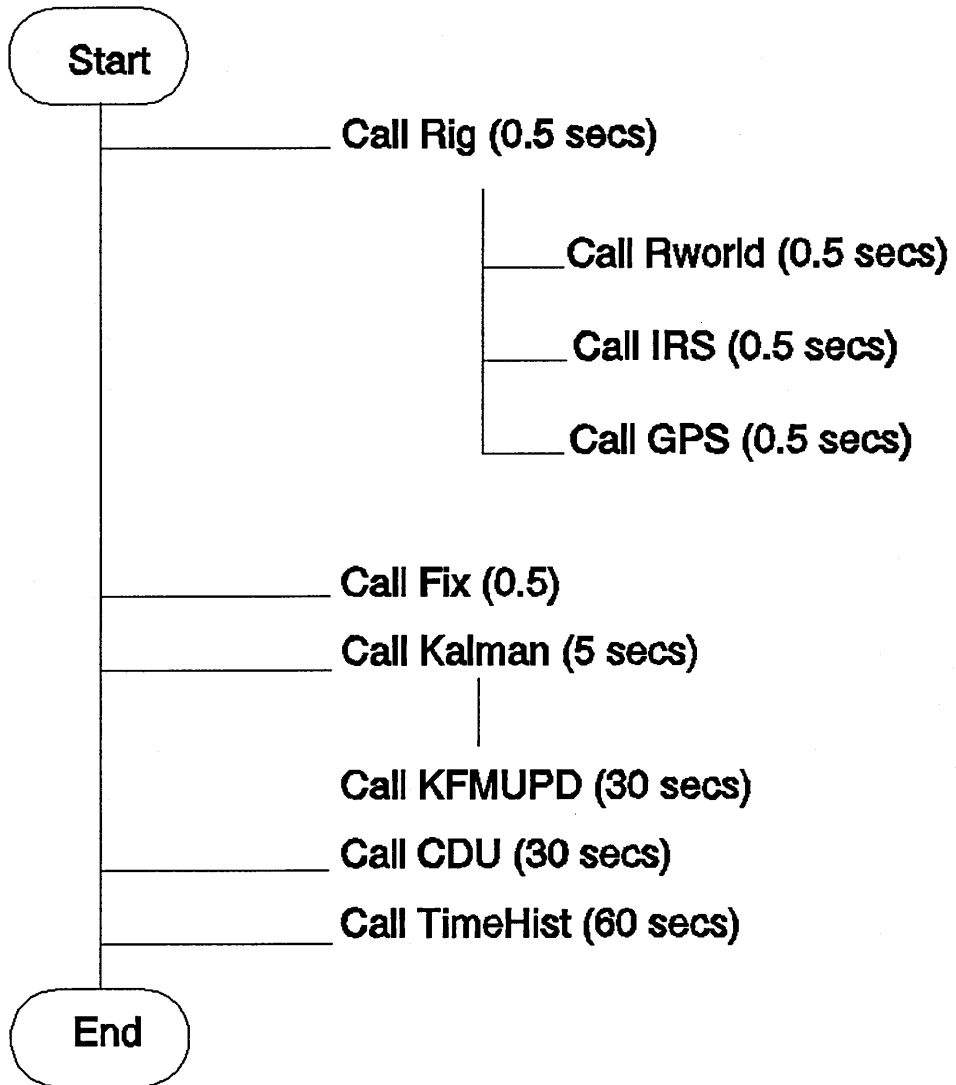


Figure 5-2

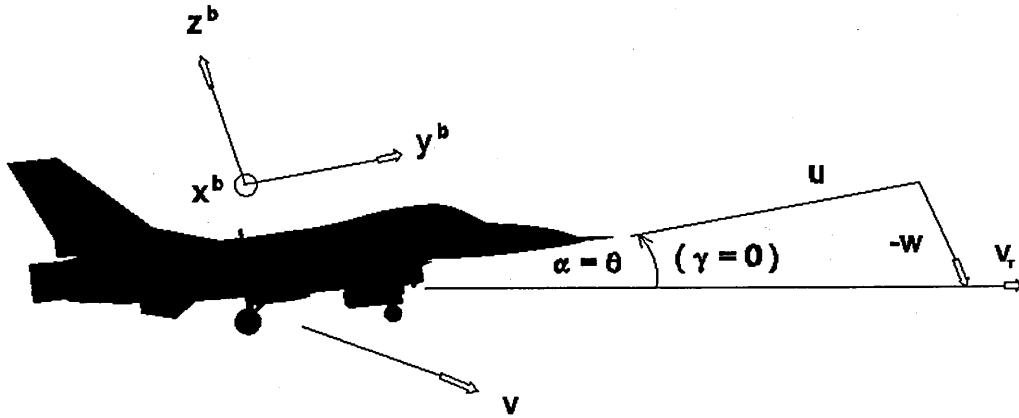
LEVEL FLIGHT

Figure 5-3a

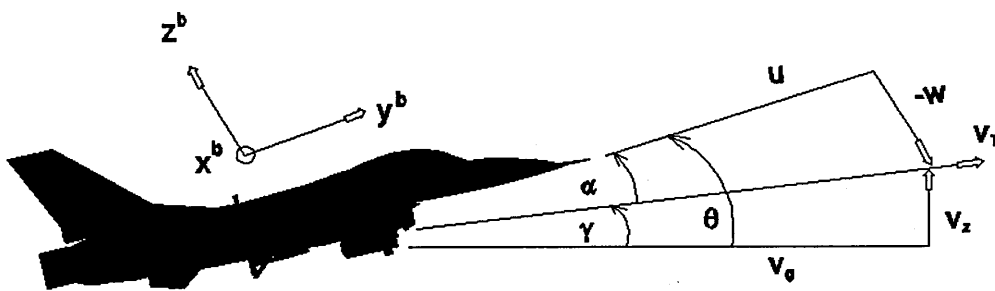
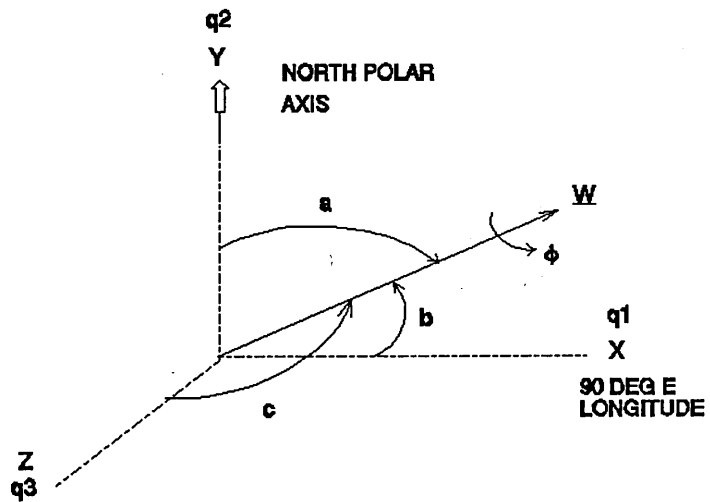
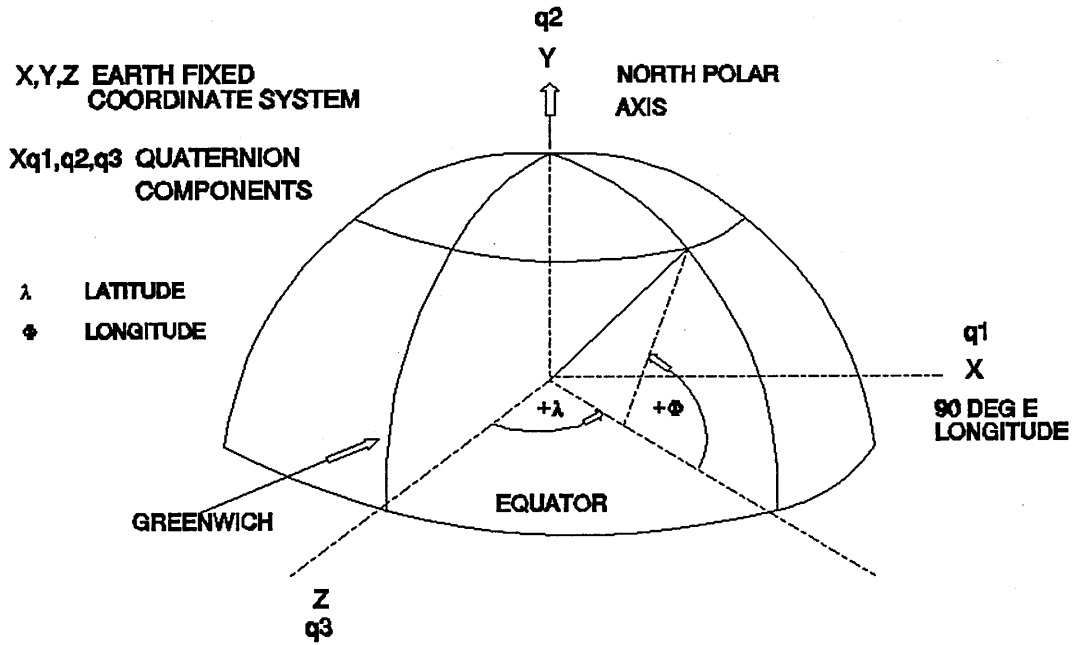
NON LEVEL FLIGHT

Figure 5-3b

QUATERNION REPRESENTATION OF POSITION



$$Q = (\cos\phi/2, \sin\phi/2\cos a, \sin\phi/2\cos b, \sin\phi/2\cos c)$$

Figure 5-4

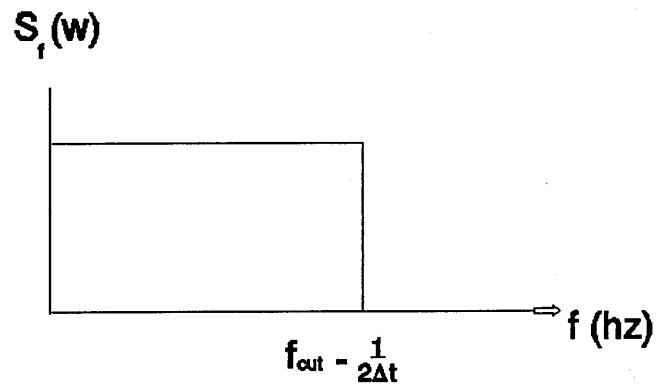
SINGLE SIDED POWER SPECTRAL DENSITY PLOT

Figure 5-5a

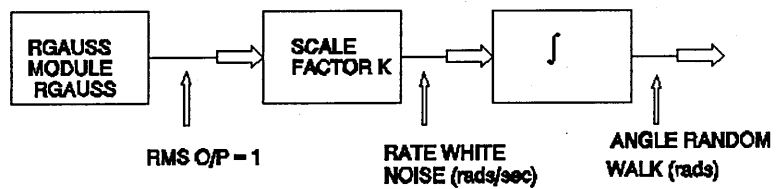
GYRO RANDOM WALK SIMULATION MODULE

Figure 5-5b

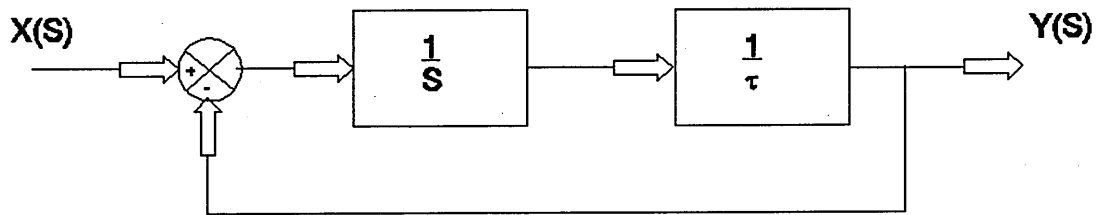
CORRELATED NOISE MODELS

Figure 5-6a

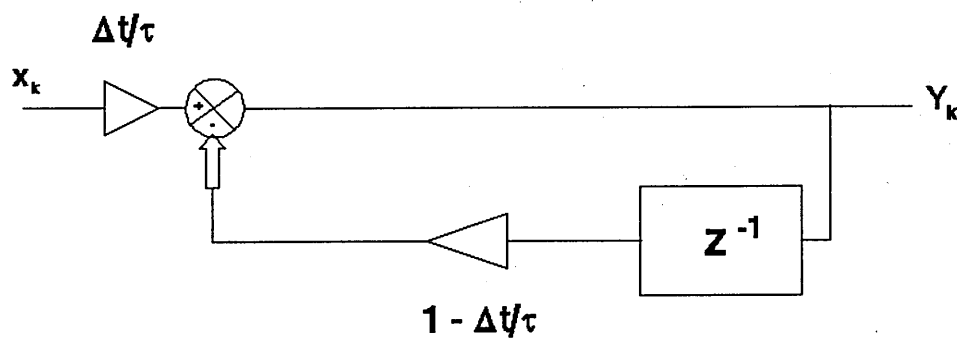


Figure 5-6b

ACCELEROMETER CORRELATED NOISE SIMULATION MODEL

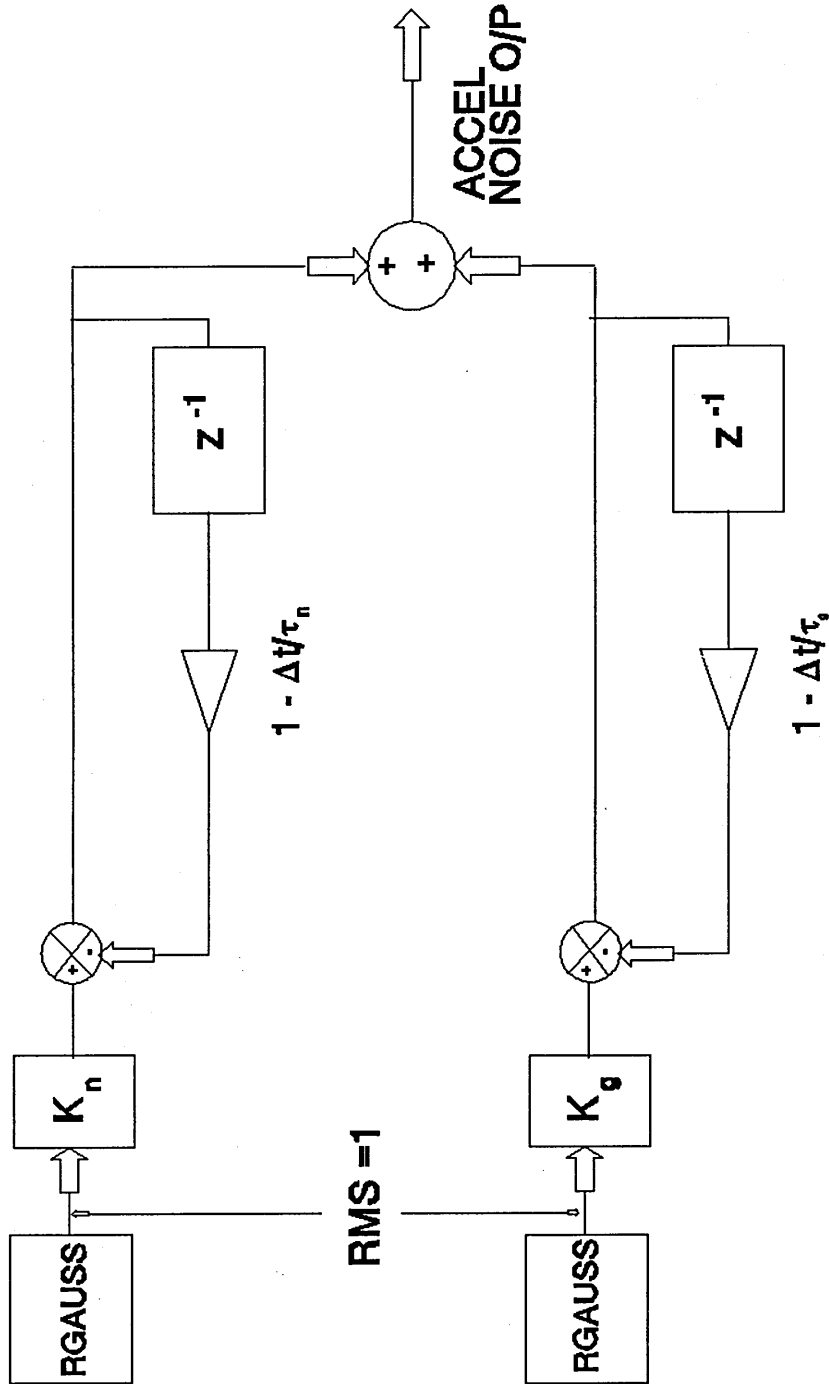


Figure 5-7

KALMAN FILTER IMPLEMENTATION

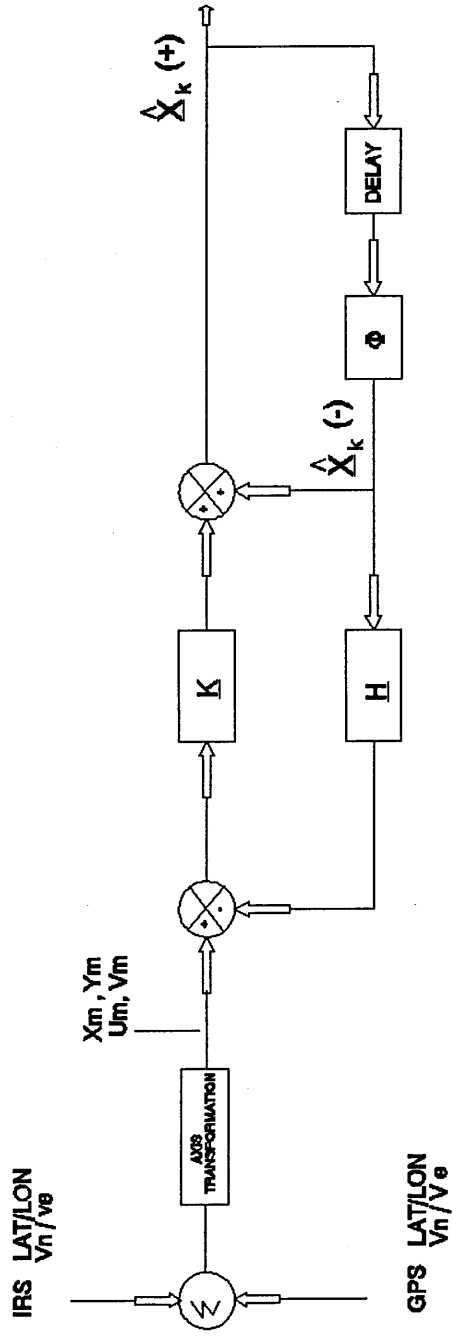


Figure 5-8

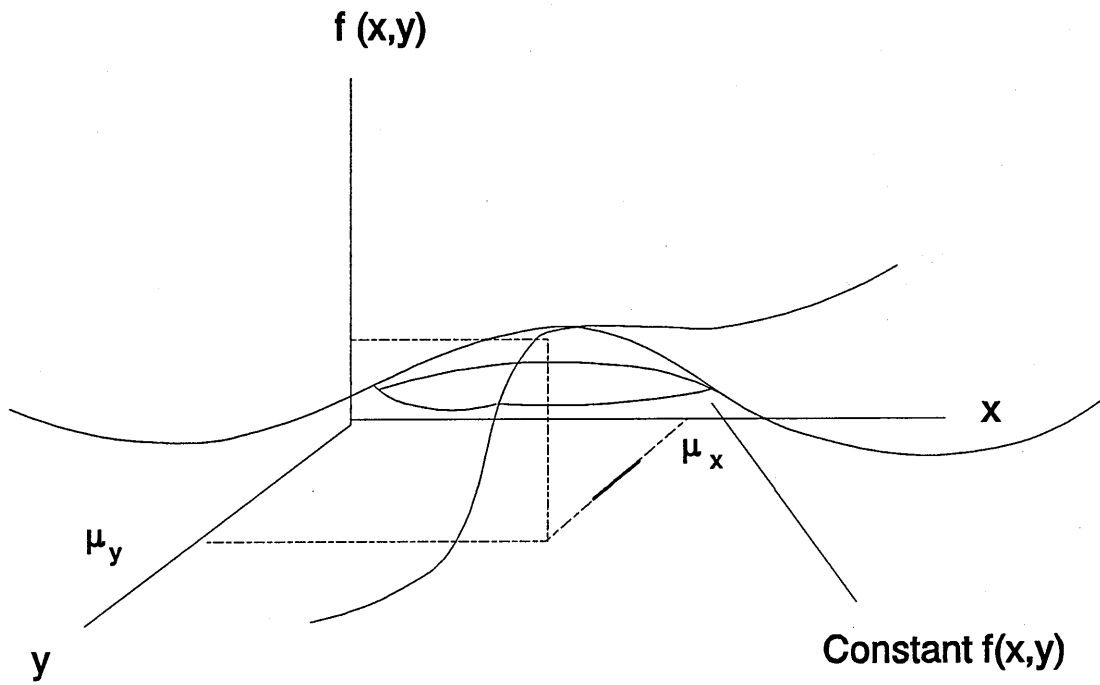
BIVARIATE NORMAL DISTRIBUTION

Figure 6-1

FLIGHT PROFILE 1

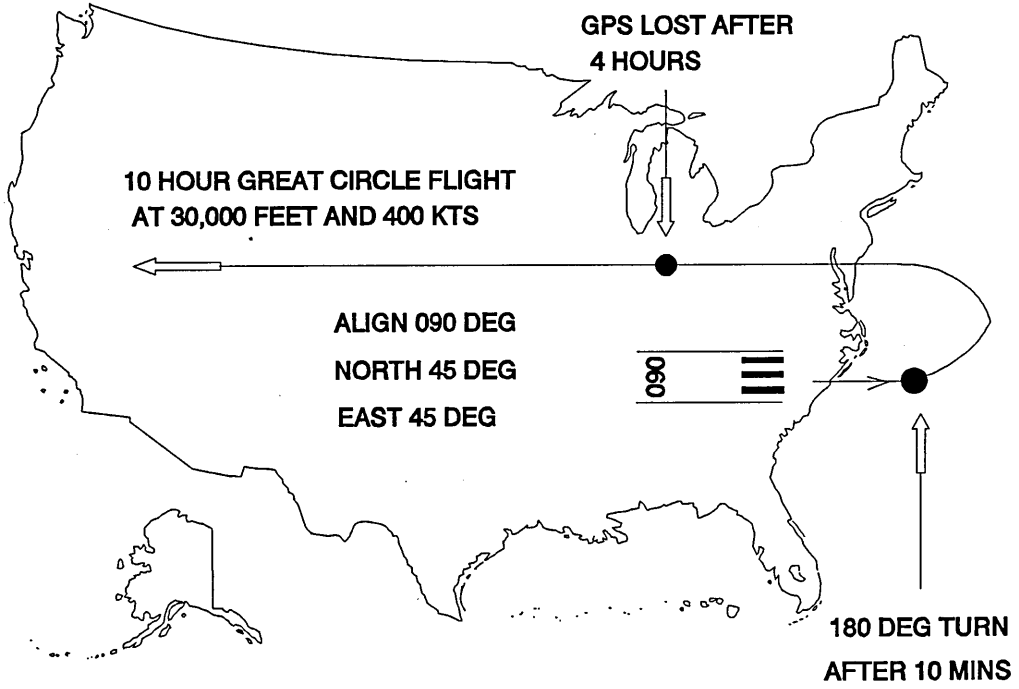
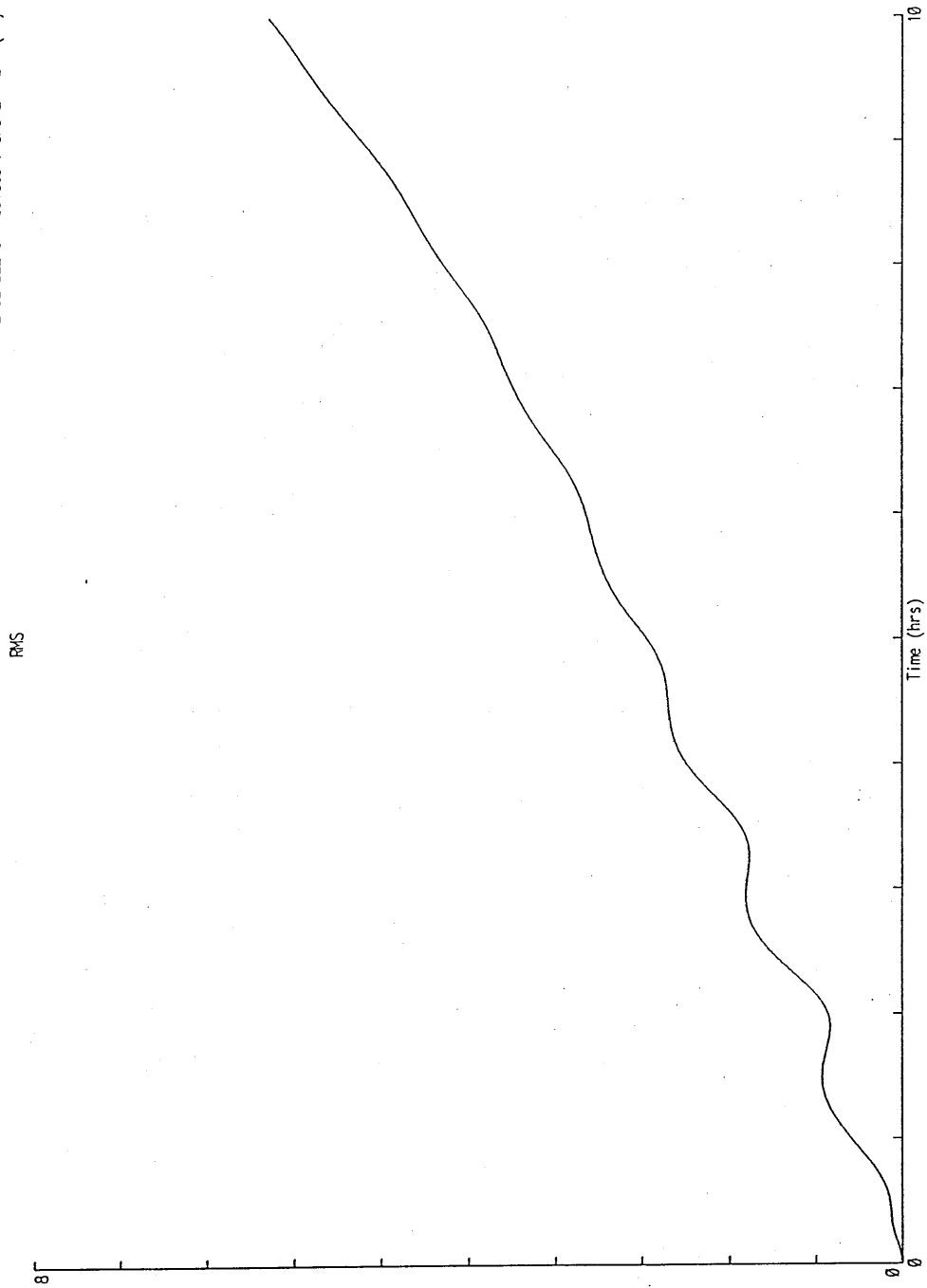


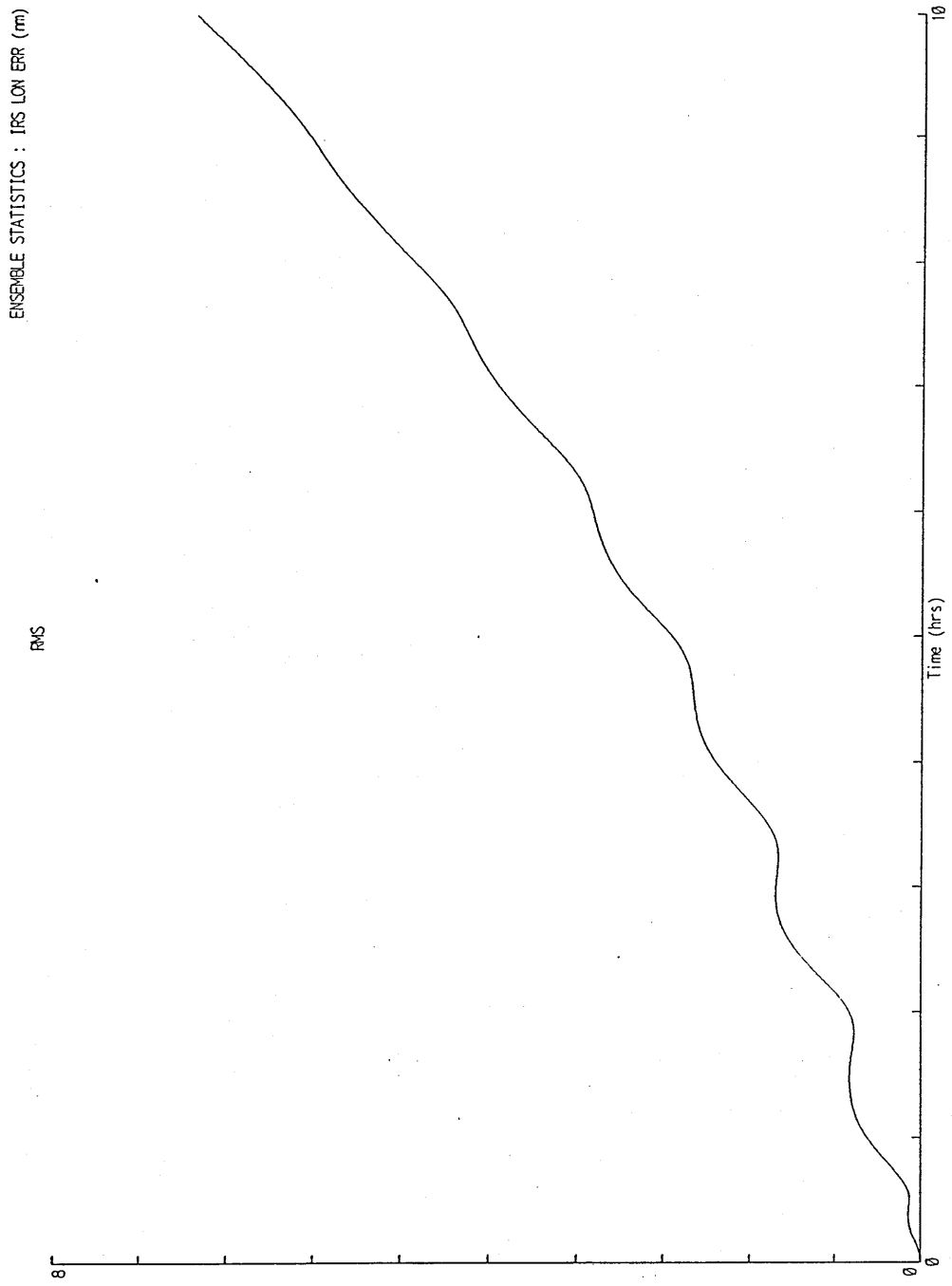
Figure 6-2

ENSEMBLE STATISTICS : IRS LAT ERR (nm)



Ensemble RMS for IRS Latitude error. Monte Carlo simulation.

Figure 6-3



Ensemble RMS for IRS Longitude error. Monte Carlo simulation.

Figure 6-4

METHOD TO COMBINE RESULTS FOR SENSITIVITY ANALYSIS

RANDOM TIME SERIES ERRORS

Random sample for x,y,z gyro bias
and x,y,z accelerometer noise.

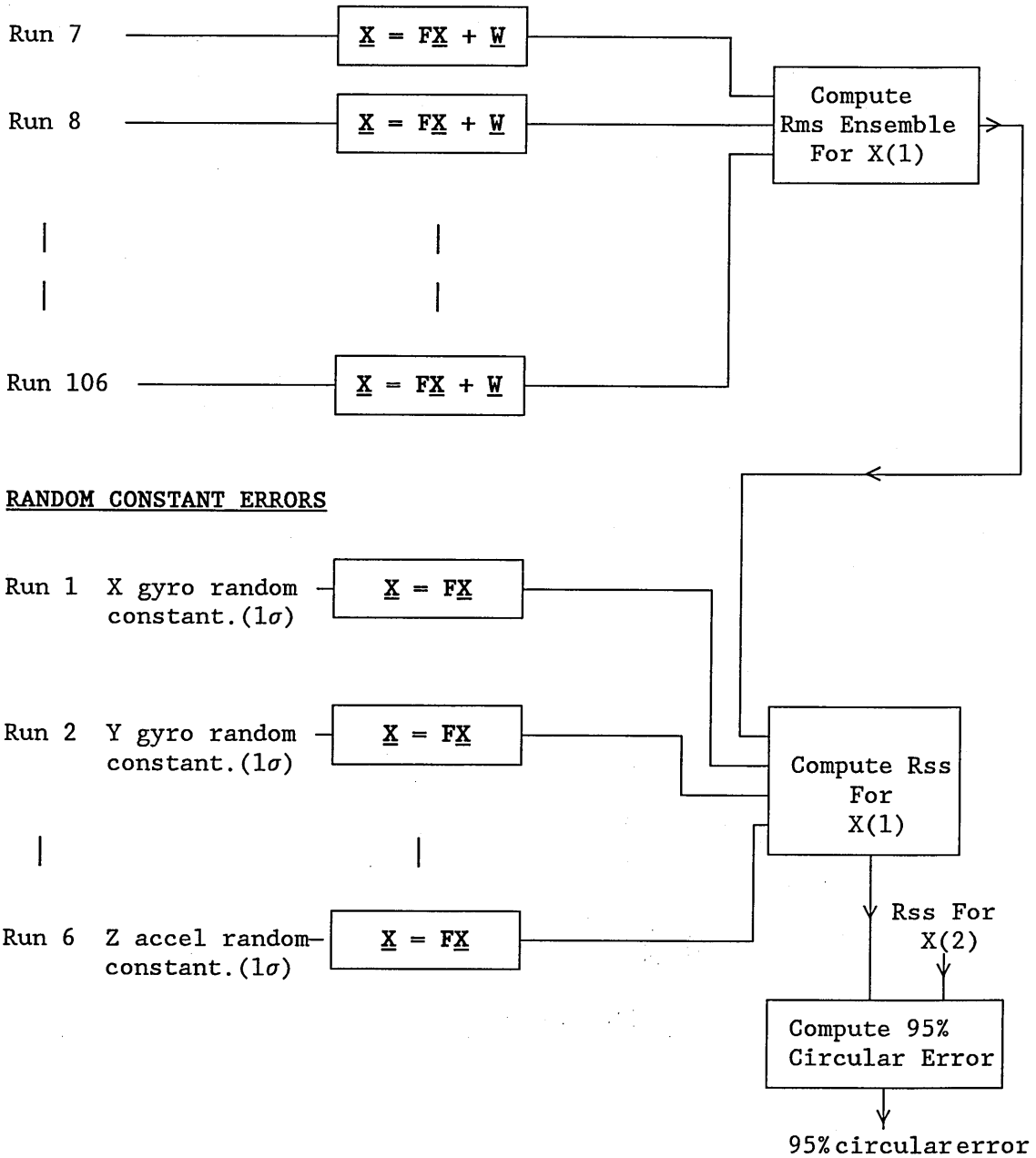


Figure 6-5

METHOD TO COMBINE RESULTS FOR COVARIANCE ANALYSIS

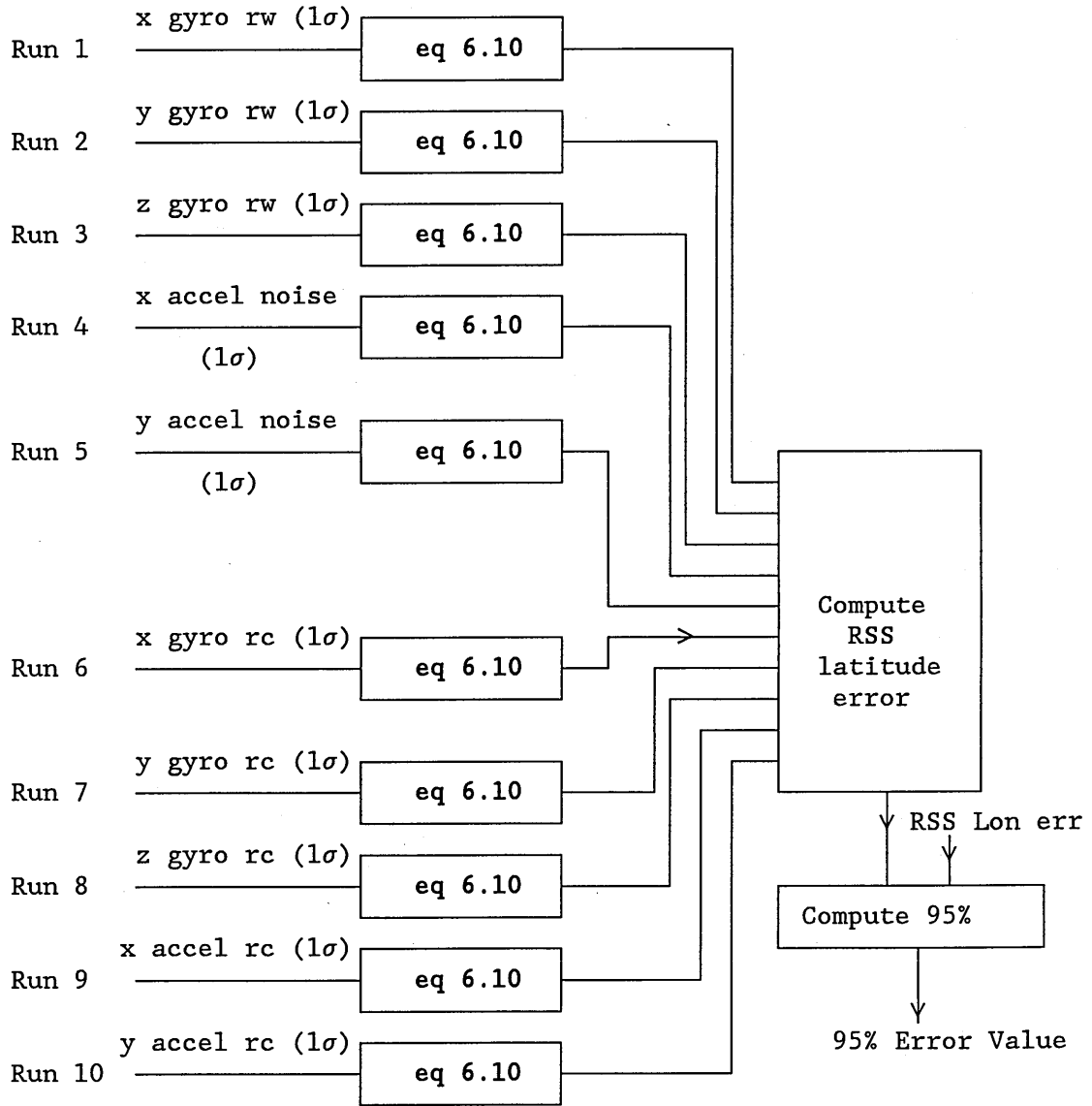
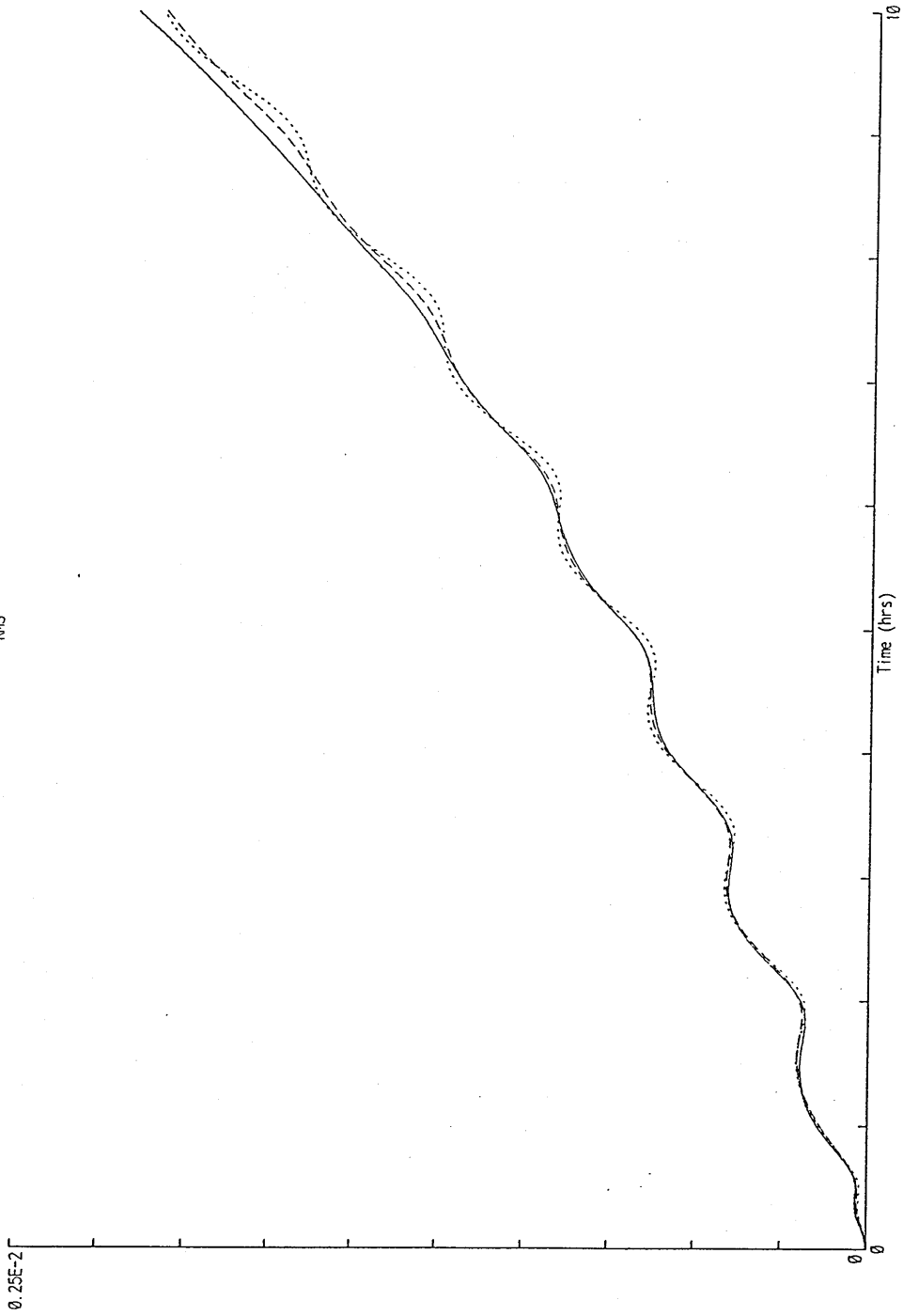


Figure 6-6

ENSEMBLE STATISTICS : DTHX (rod)

RMS



Monte Carlo V Sensitivity analysis V covariance analysis
for IRS error state dthx. ALL IRS Error sources considered.
Continuous - Rms Monte Carlo Dashed Line - Rss Sensitivity Dotted Covariance.

Figure 6-7

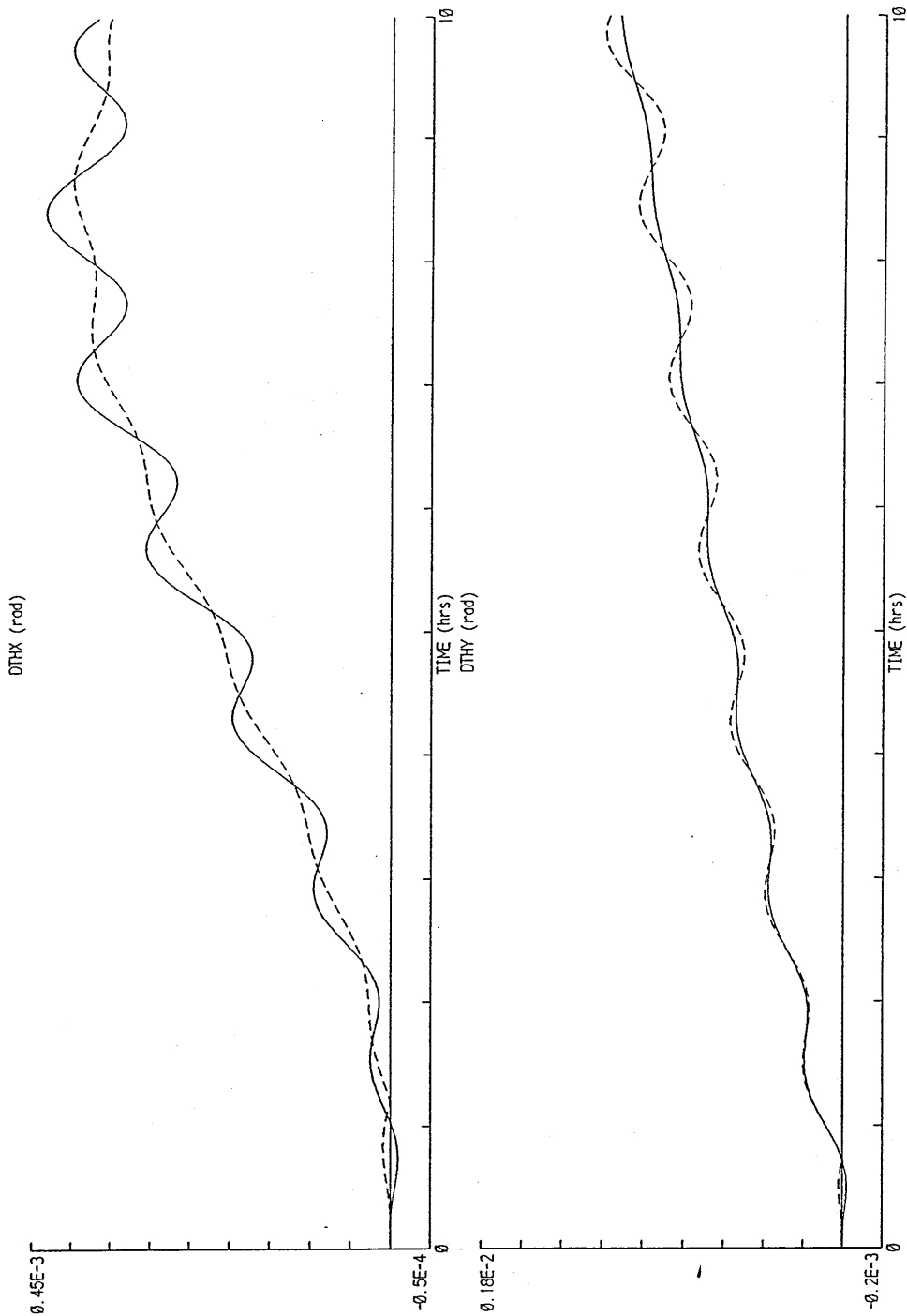
ENSEMBLE STATISTICS : DTHY (rad)

RMS



Monte Carlo V Sensitivity analysis V covariance analysis
For IRS error state dthy. ALL IRS Error sources considered.
Continuous - Rms Monte Carlo Dashed Line - Rss Sensitivity Dotted Covariance.

Figure 6-8



Sensitivity analysis V covariance analysis for IRS error states dthx and dthy.
IRS Error source Y gyro bias of 1 sigma.
Continuous Line - Rms Sensitivity ; Dashed Line - Rms Covariance .

Figure 6-9

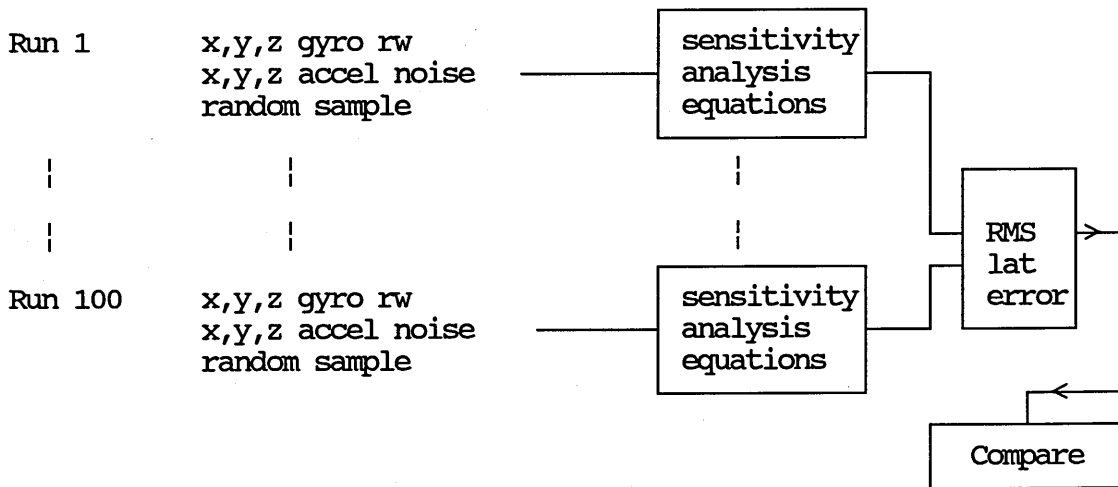


Sensitivity analysis V covariance analysis for IRS error states dthx and dthy. .
IRS Error source Z gyro bias of 1 sigma.
Continuous Line - Rms Sensitivity : Dashed Line - Rms Covariance .

Figure 6-10

**METHOD TO COMPARE SENSITIVITY ANALYSIS AND COVARIANCE RESULTS
FOR TIME SERIES ERRORS ONLY**

SENSITIVITY ANALYSIS



COVARIANCE ANALYSIS

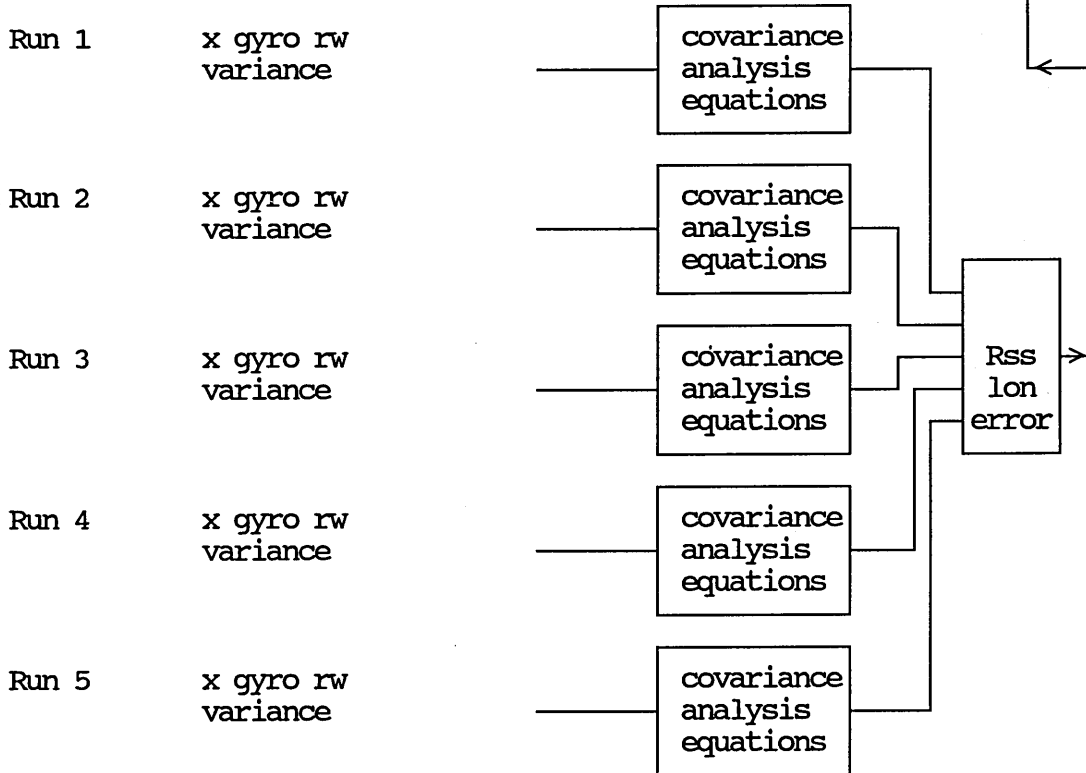
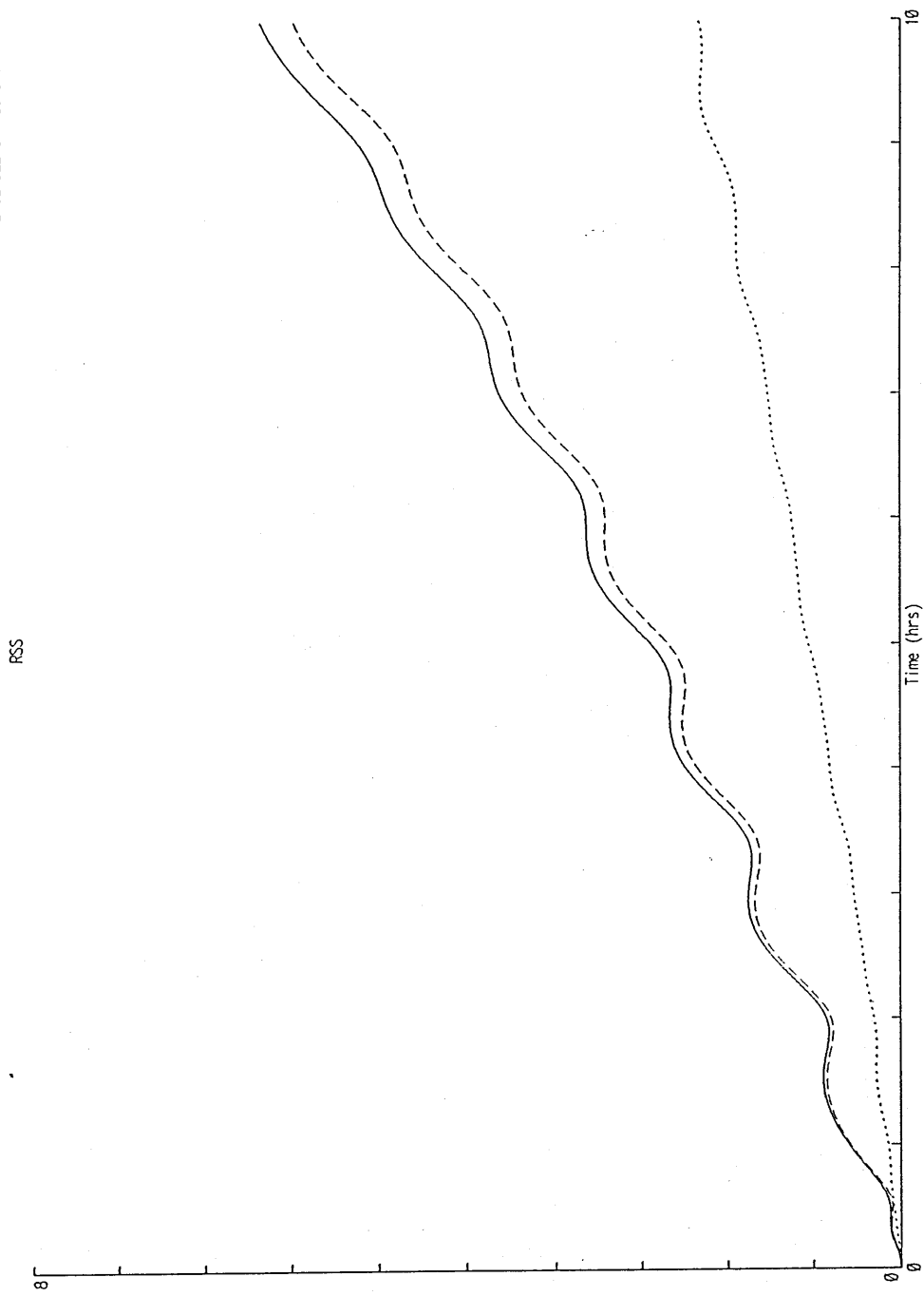


Figure 6-11

ENSEMBLE STATISTICS : RMS

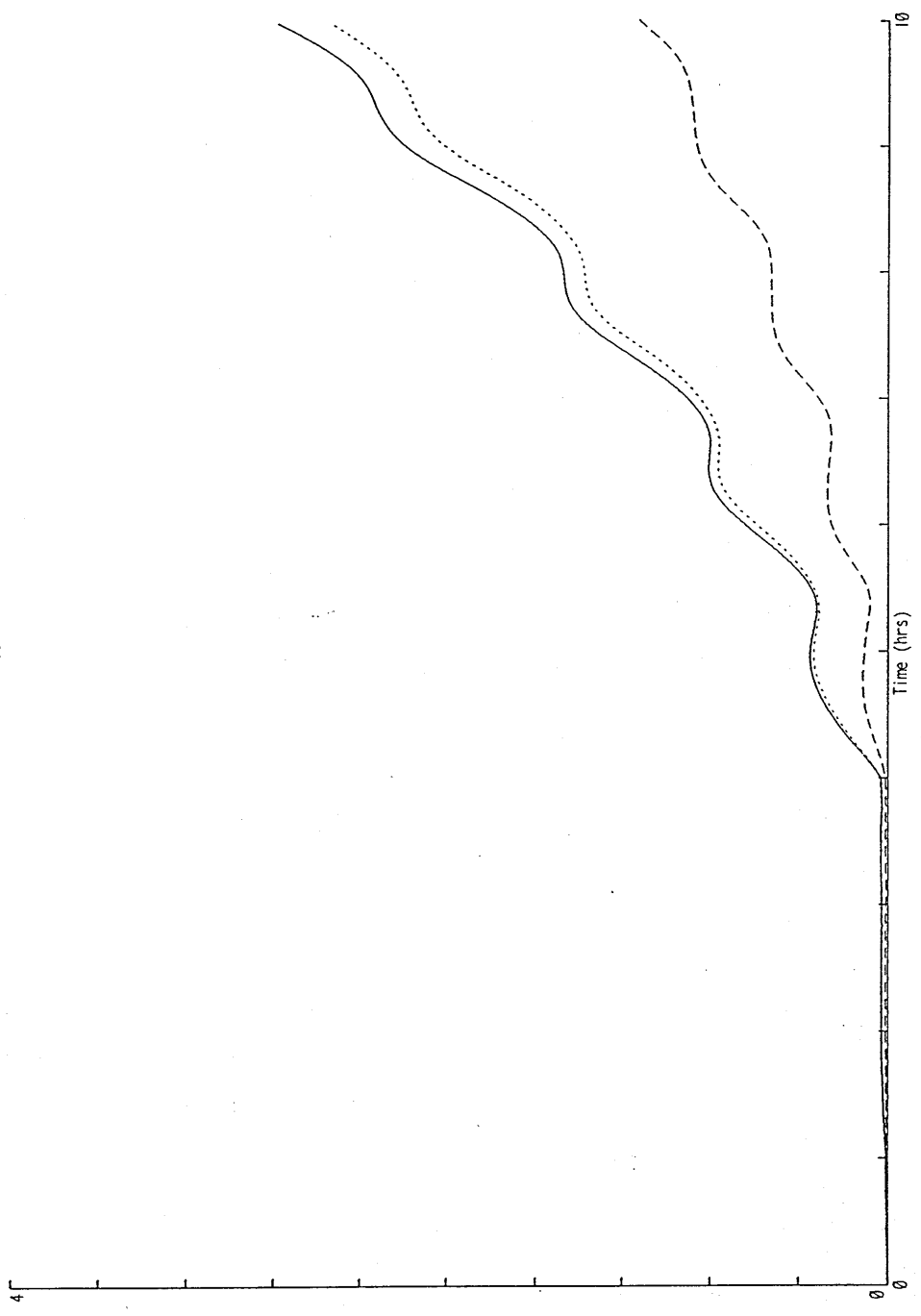


CASE : Overlay of Irs Latitude errors.
: Continuous Line - Noise and Rc. Dashed - Rc. Dotted - Noise

Figure 7-1

ENSEMBLE STATISTICS : RMS

RSS

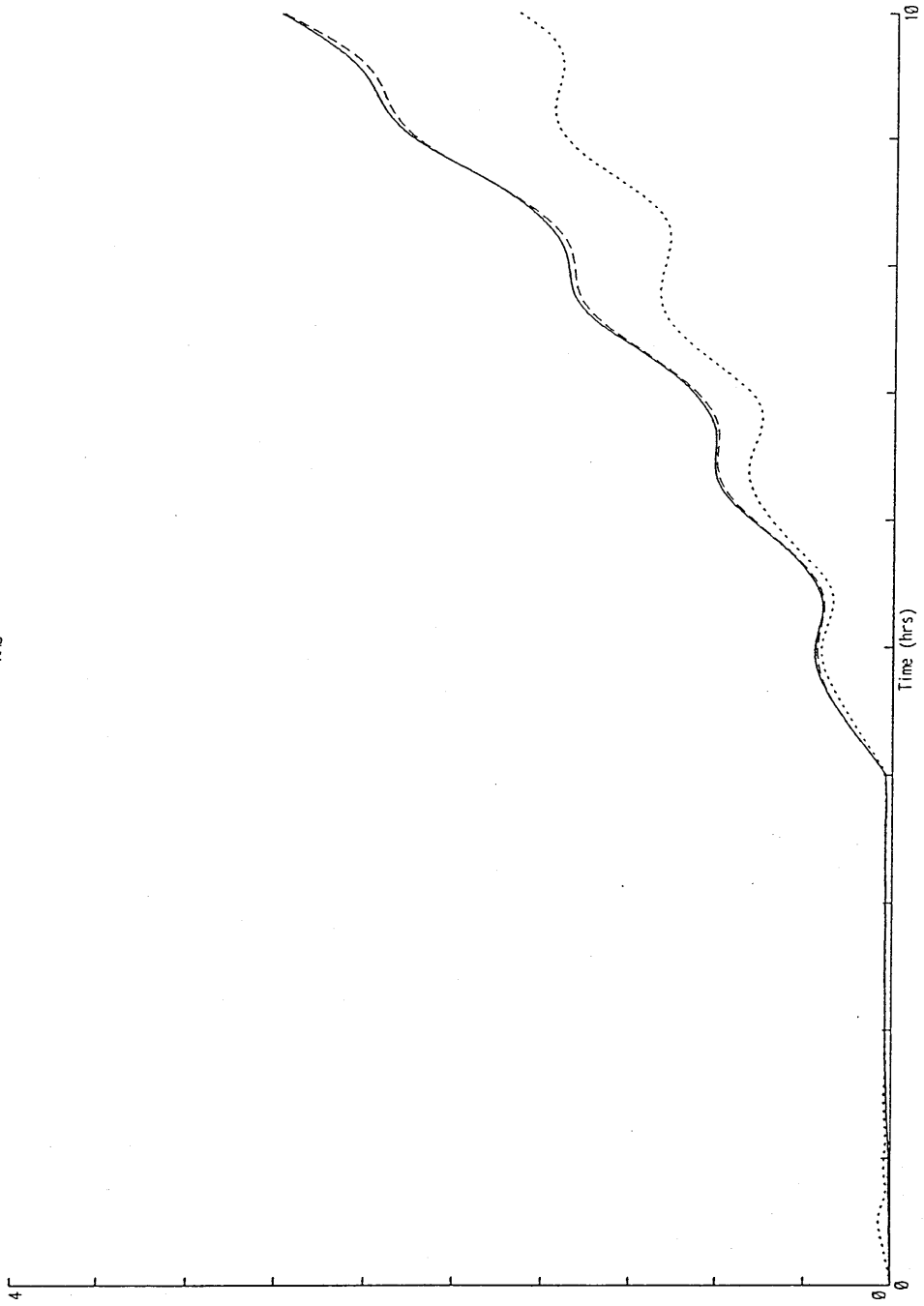


CASE : Overlay of Kalman Filter Latitude errors.
: Continuous Line - Noise and Rc. Dashed - Noise. Dotted - Noise

Figure 7-2

ENSEMBLE STATISTICS : RMC LAT ERR (m)

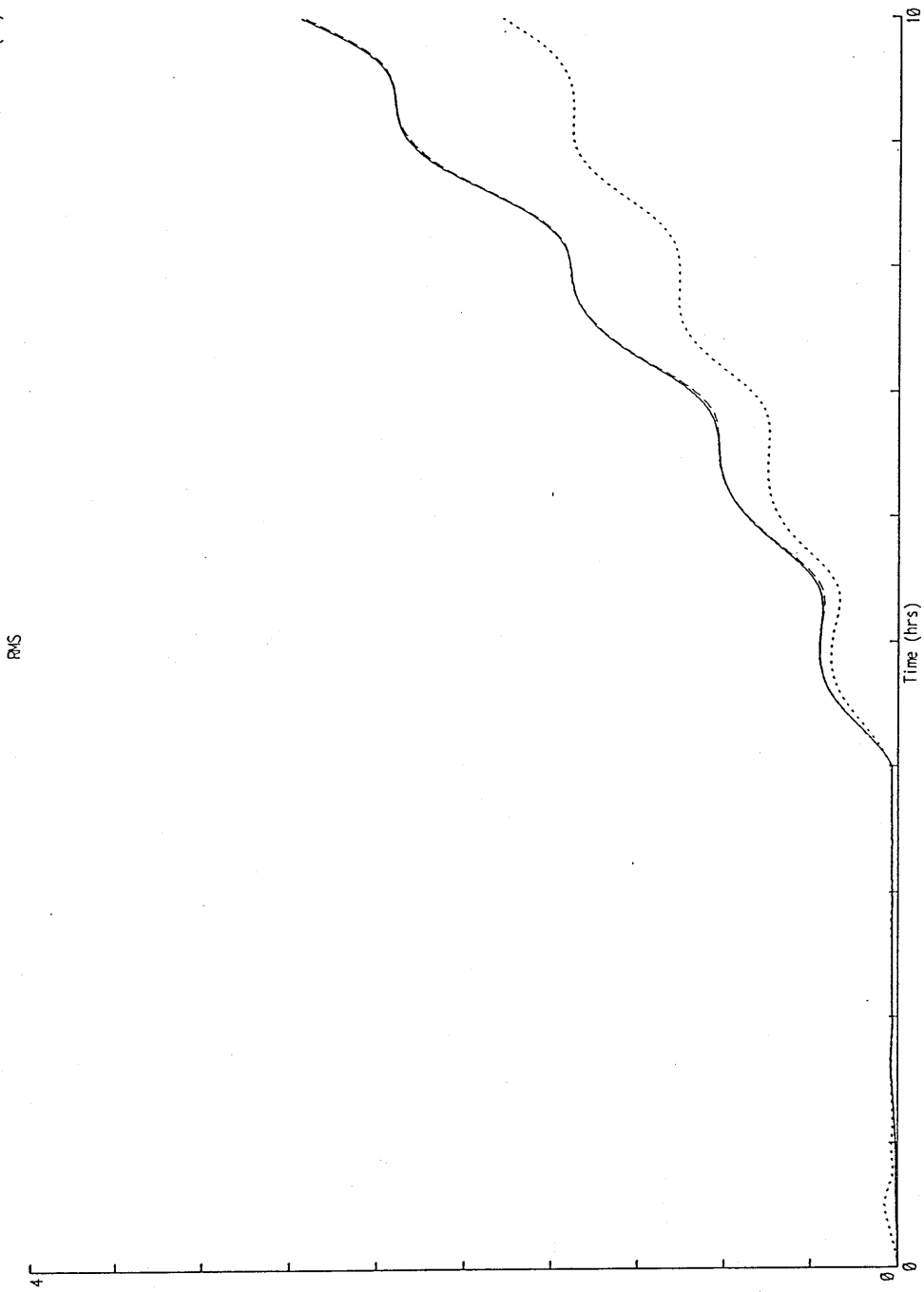
RMS



Monte Carlo simulation v Sensitivity analysis for KF Latitude error.
Continuous Line - Monte Carlo Dashed Line - Sensitivity Analysis (unmodified).
Dotted Line - Sensitivity analysis (modified).

Figure 7-3

ENSEMBLE STATISTICS : RMSE LONG ERR (m)



Monte Carlo simulation v Sensitivity analysis for KF Longitude error.
Continuous Line - Monte Carlo Dashed Line - Sensitivity Analysis (unmodified).
Dotted Line - Sensitivity analysis (modified).

Figure 7-4

FLIGHT PROFILE 2

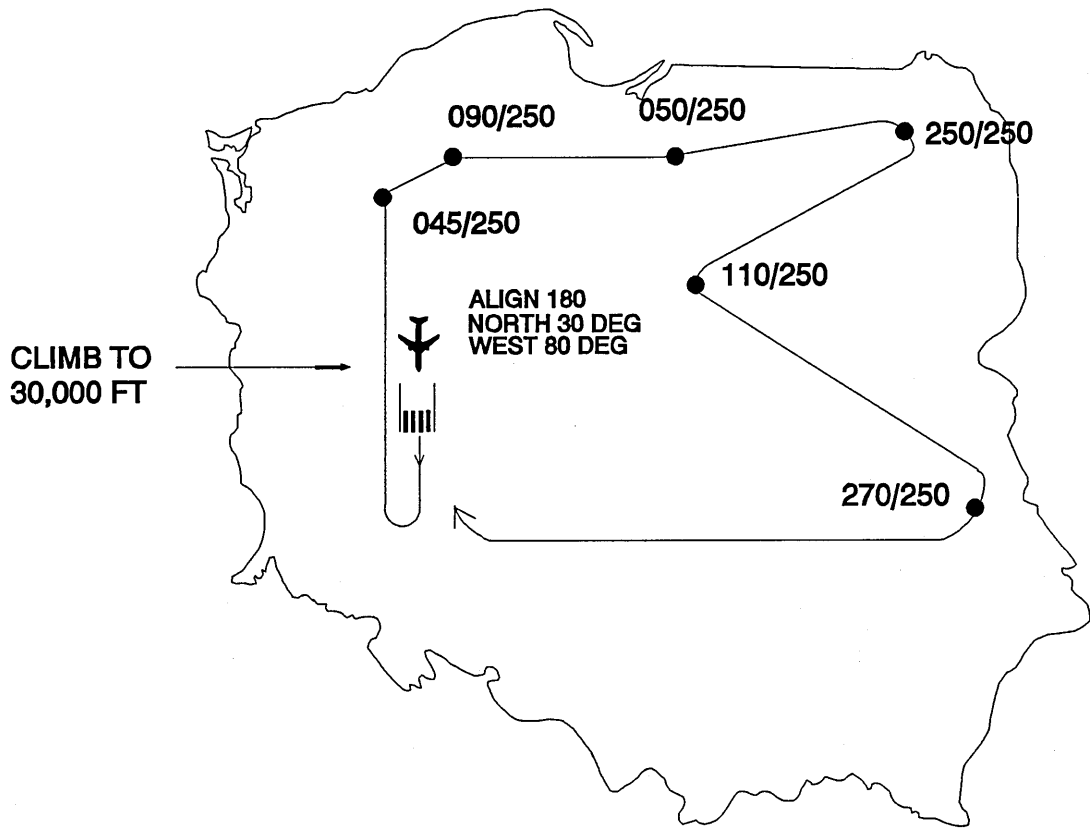
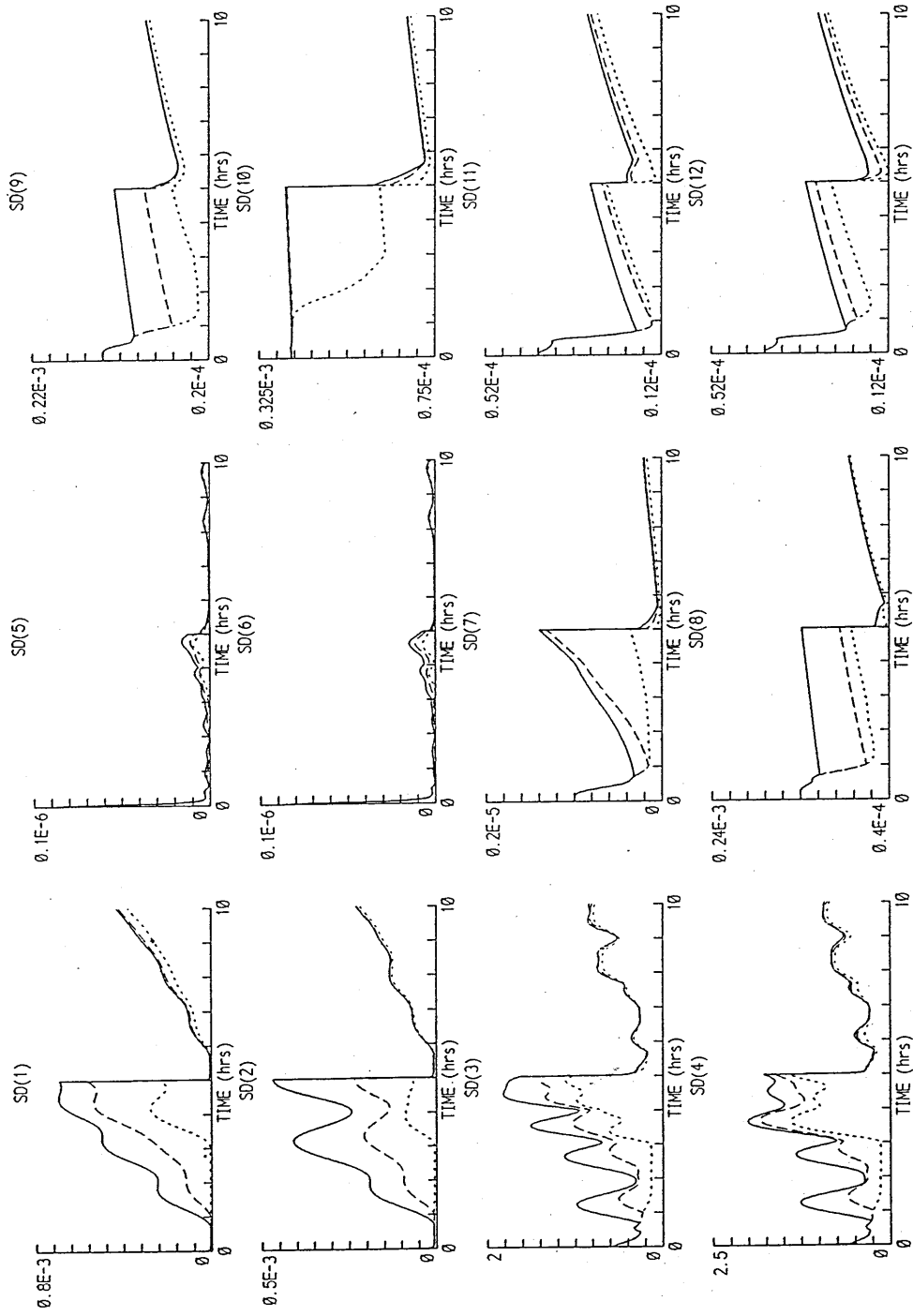


Figure 7-5

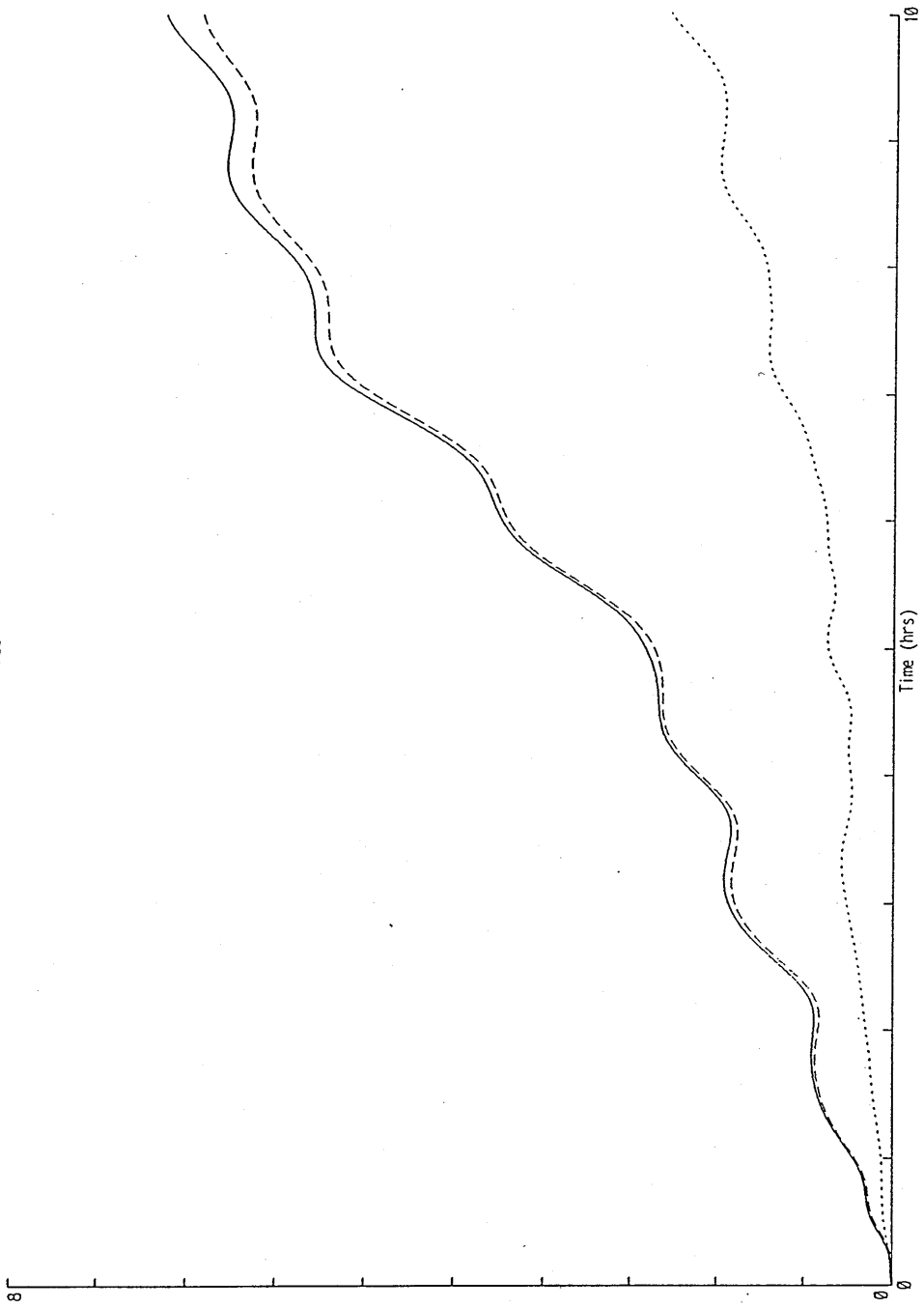


12 STATE KALMAN FILTER COVARIANCE PLOTS FOR DIFFERENT GPS COVERAGE.
 CONTINUOUS LINE 42 MINUTE DASHED LINE 60 MINUTE. DOTTED LINE 3 HRS

Figure 7-6

ENSEMBLE STATISTICS : RMS

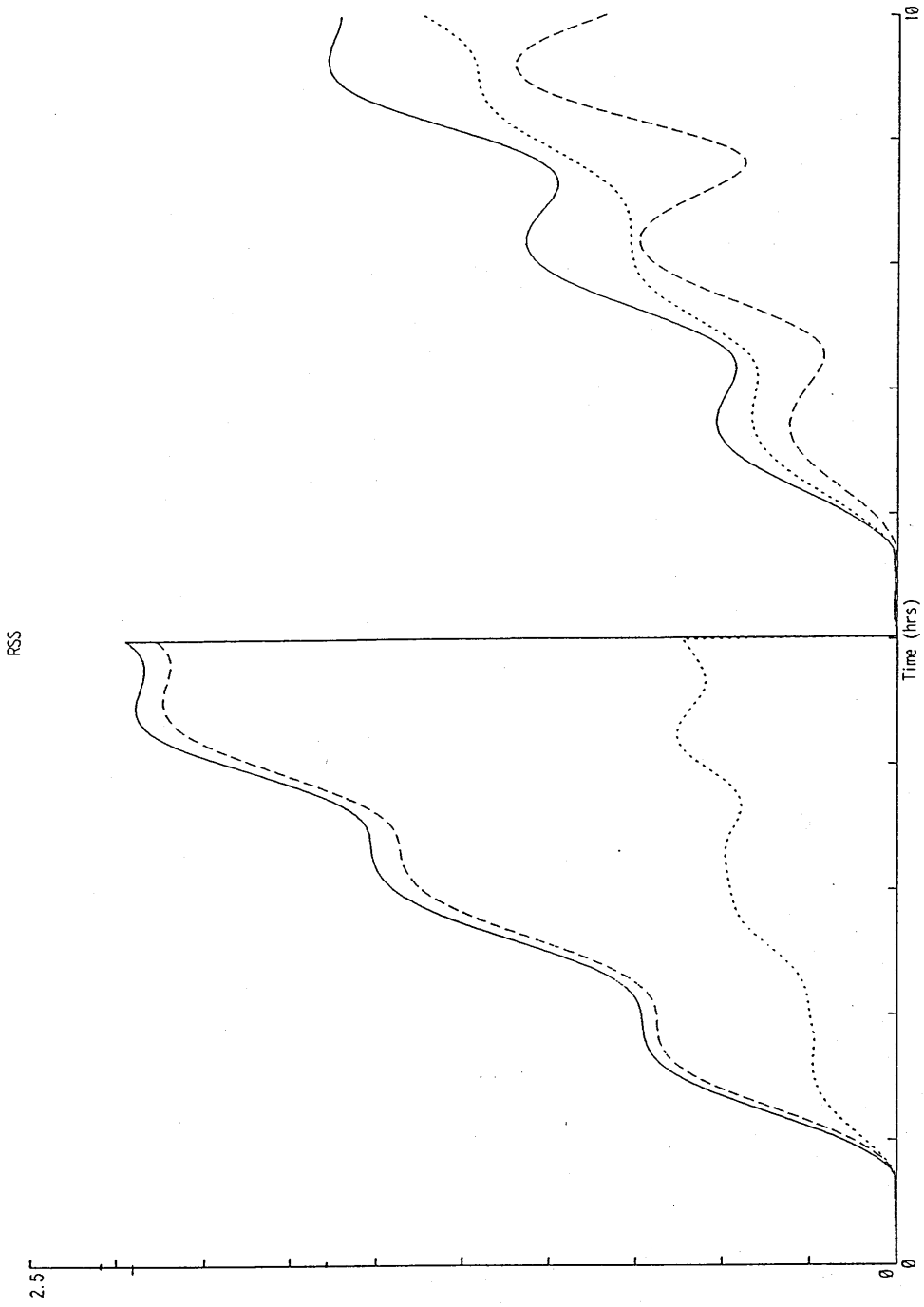
RSS



CASE : Overlay of Irs Latitude errors.
: Continuous Line - Noise and Rc. Dashed - Rc. Dotted - Noise

Figure 7-7

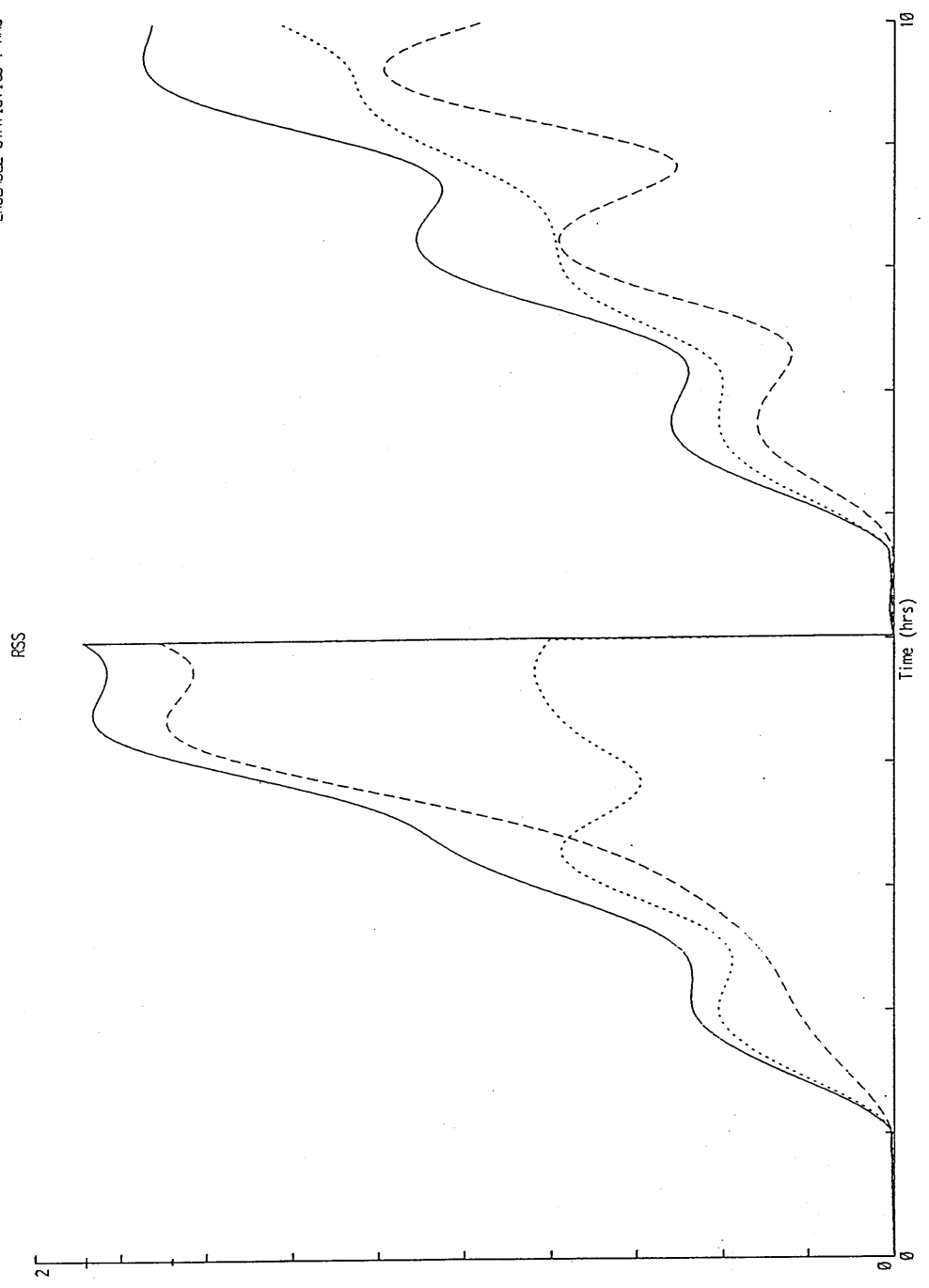
ENSEMBLE STATISTICS : RMS



CASE : Overlay of Kalman Filter Latitude errors.
: Continuous Line - Noise and Rc. Dashed - Rc. Dotted - Noise

Figure 7-8

ENSEMBLE STATISTICS : RMS

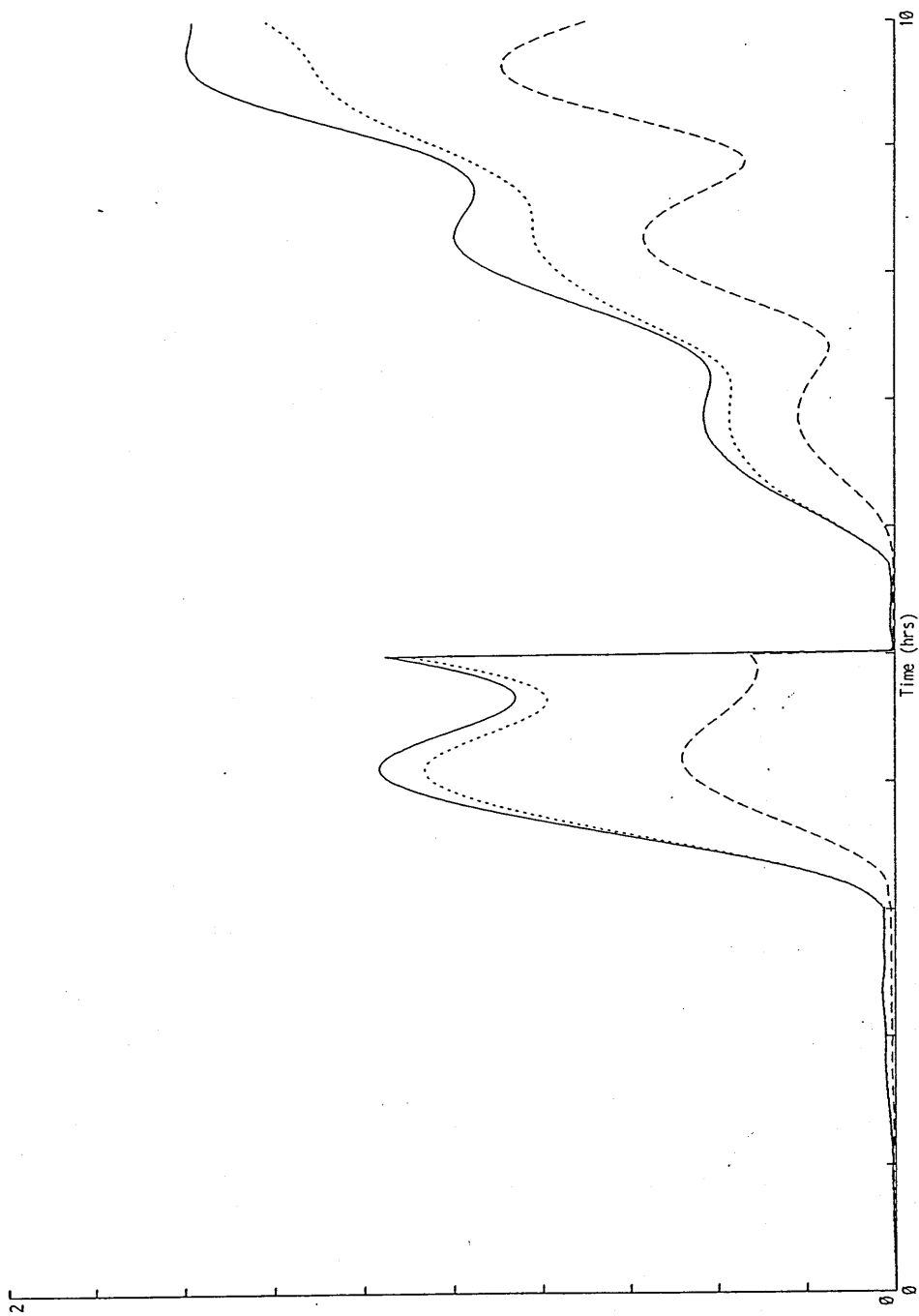


CASE : Overlay of Kalman Filter Latitude errors.
: Continuous Line - Noise and Rc. Dashed - Rc. Dotted - Noise

Figure 7-9

ENSEMBLE STATISTICS : RMS

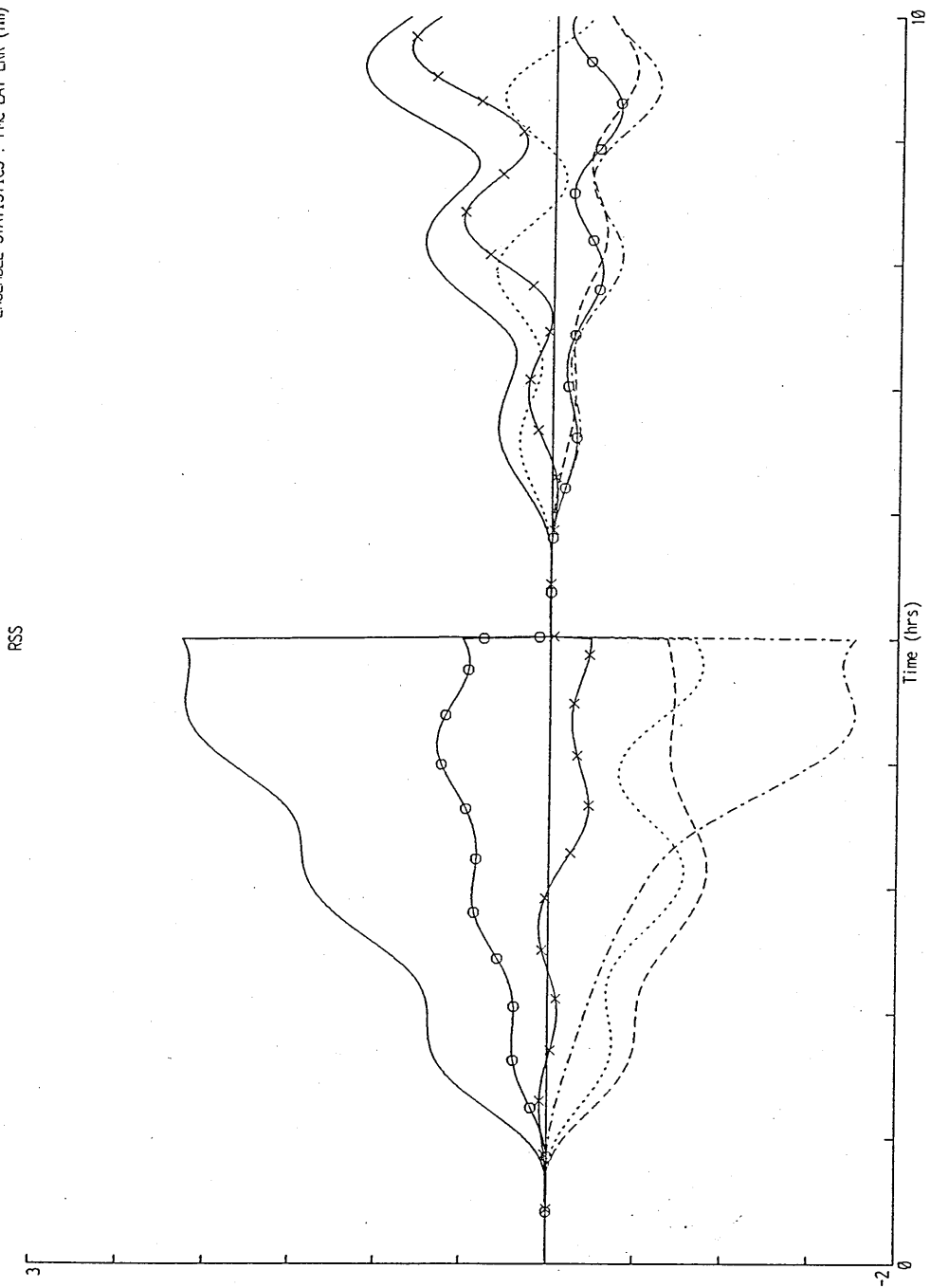
RSS



CASE : Overlay of Kalman Filter Latitude errors.
: Continuous Line - Noise and Rc. Dashed - Noise. Dotted - Noise

Figure 7-10

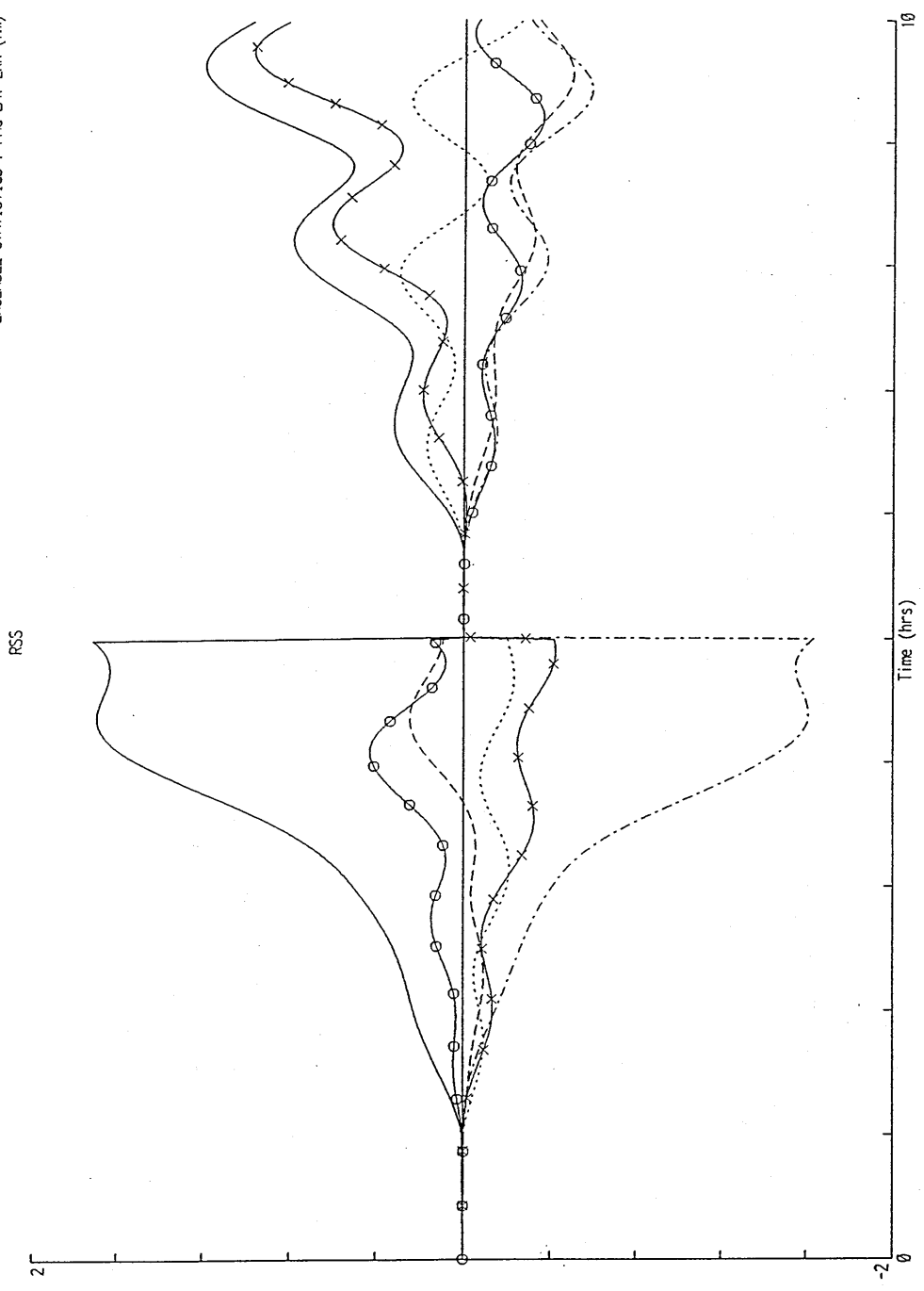
ENSEMBLE STATISTICS : RMC LAT ERR (m)



CONTRIBUTION OF RANDOM CONSTANTS TO OVERALL RANDOM CONSTANT LATITUDE ERROR.

Figure 7-11

ENSEMBLE STATISTICS : RMC LAT ERR (m)



CONTRIBUTION OF RANDOM CONSTANTS TO OVERALL RANDOM CONSTANT LATITUDE ERROR.

Figure 7-12

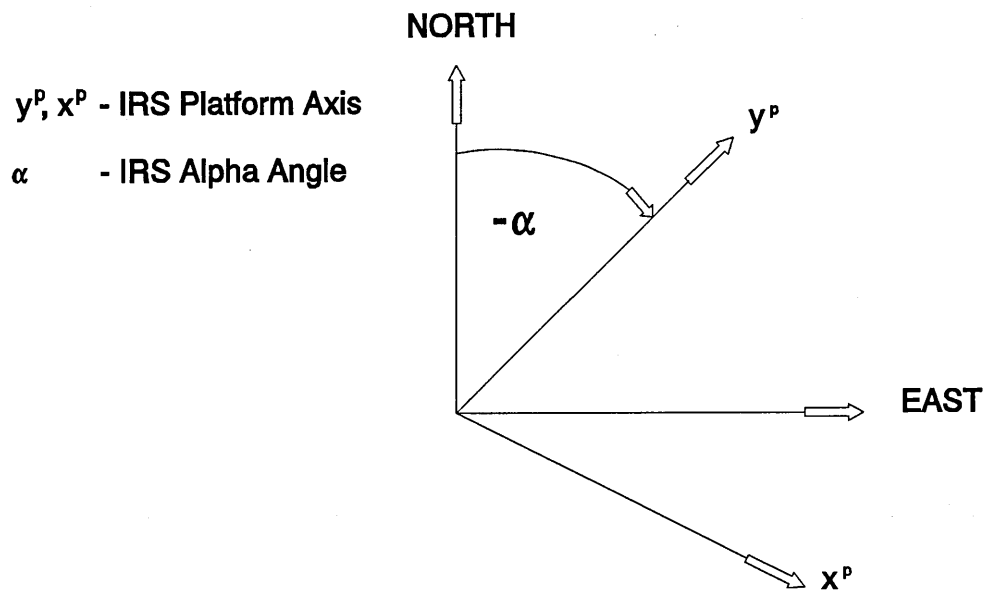
EXTENDED ALIGNMENT AXIS SET

Figure 8-1

SINGLE CHANNEL INERTIAL SYSTEM GYRO MODEL

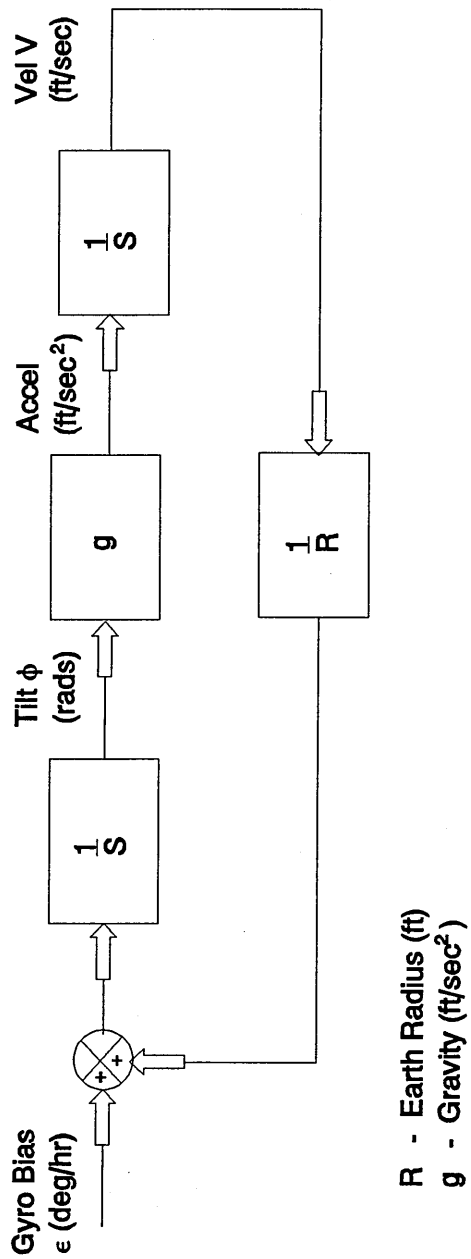


Figure 8-2

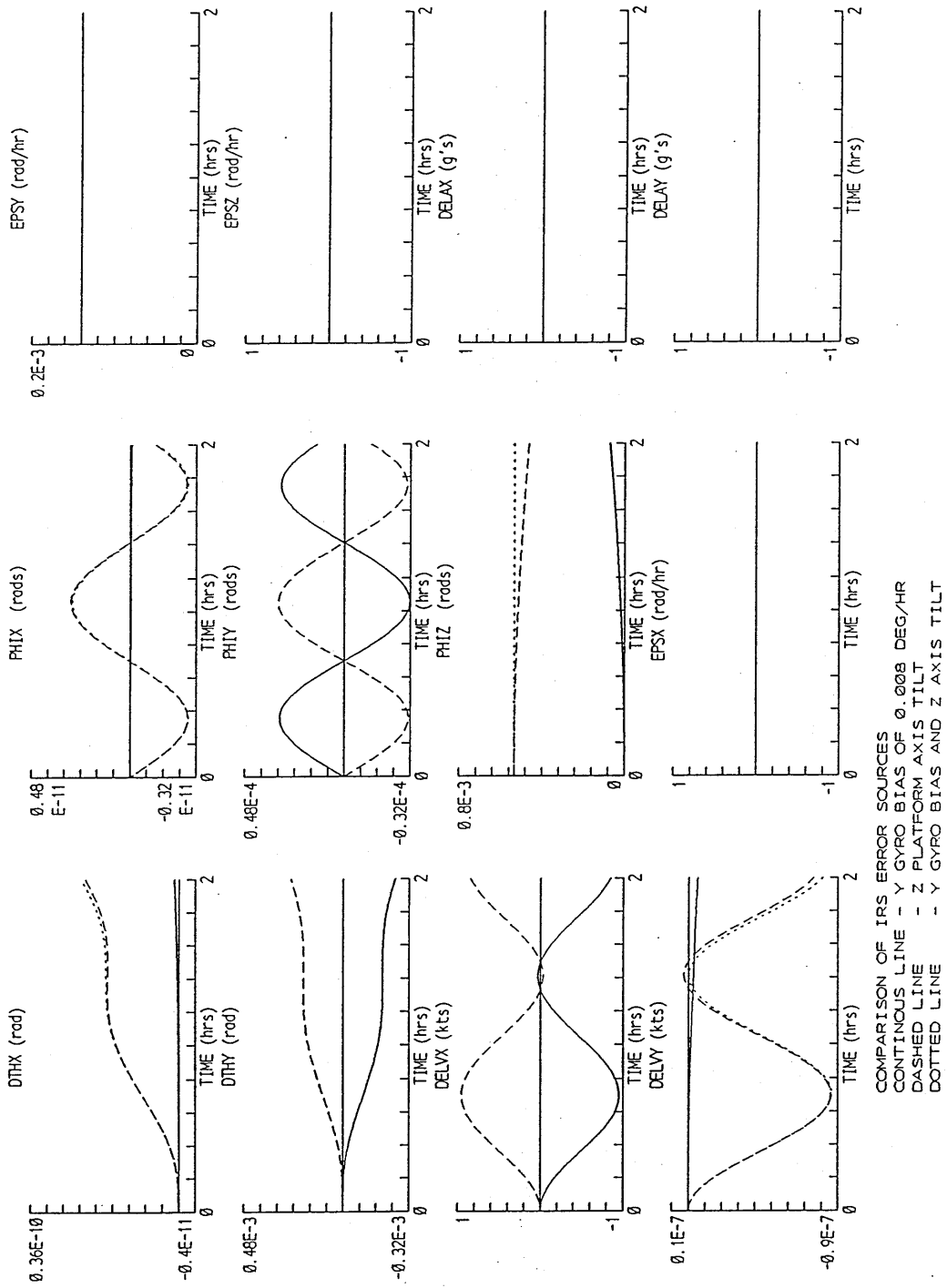


Figure 8-3

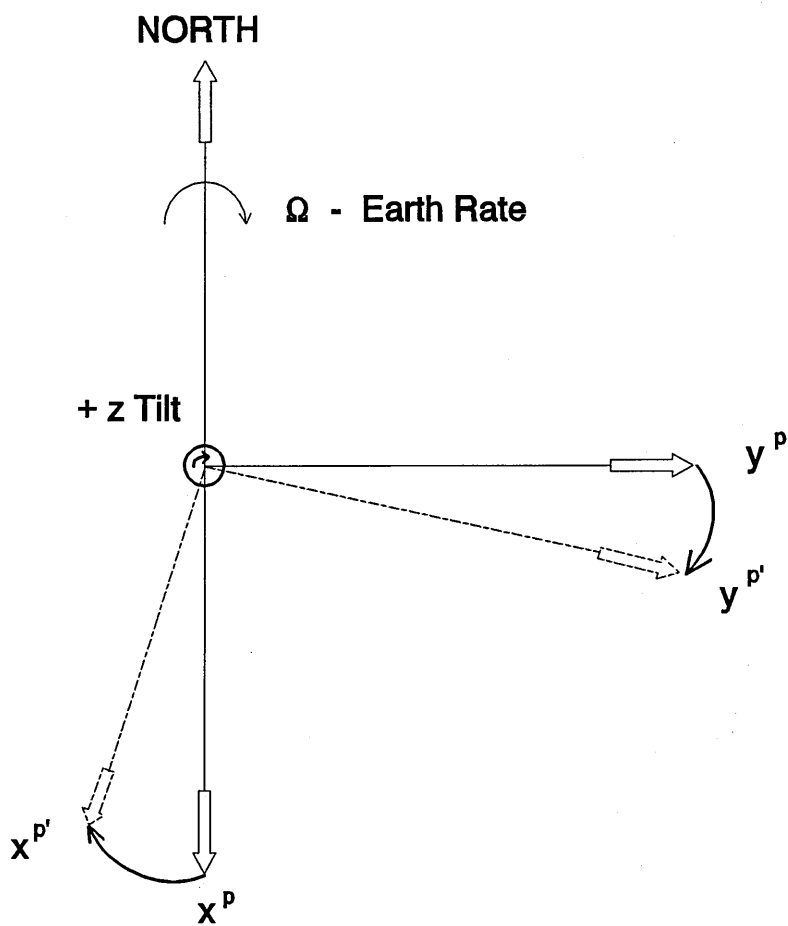
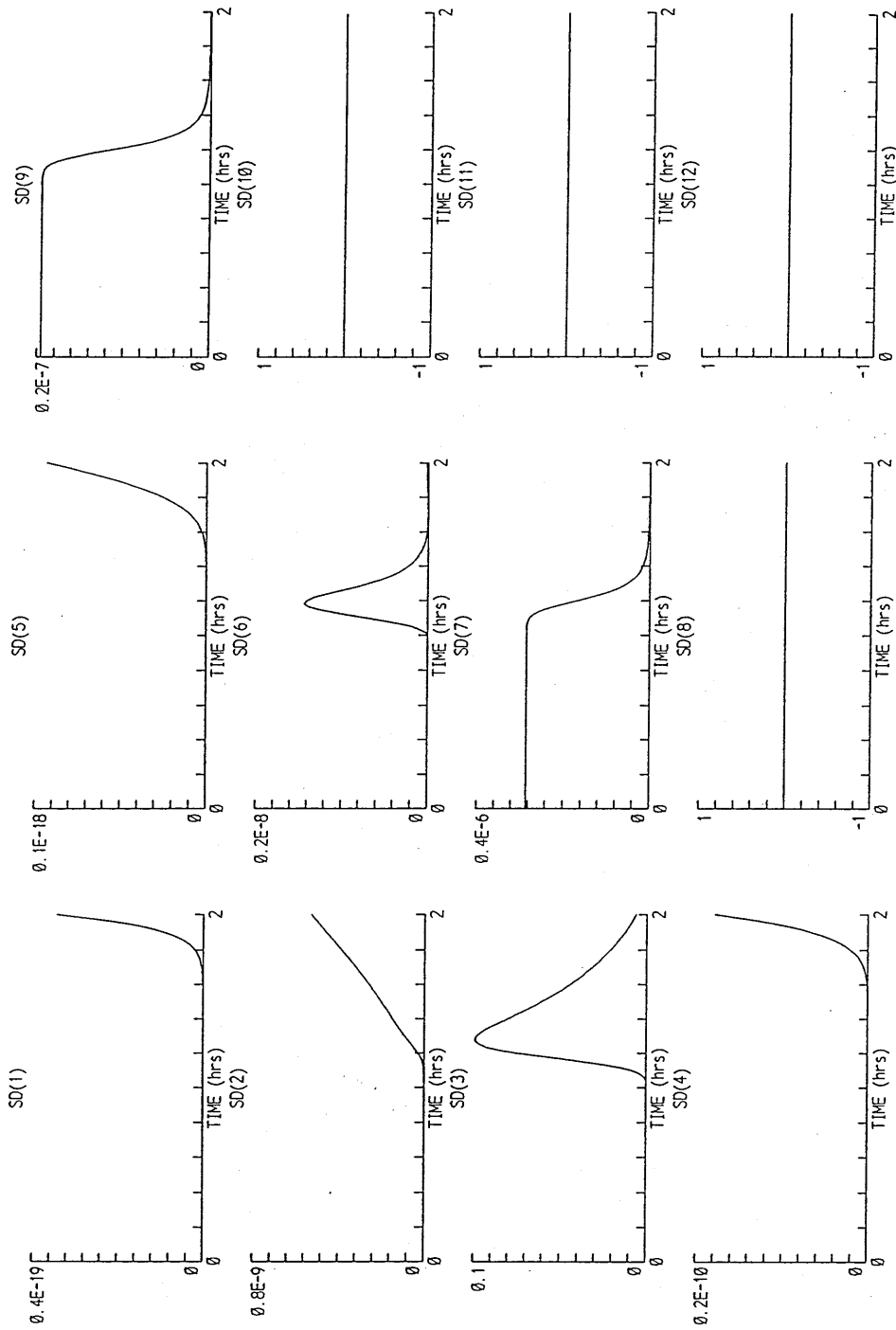
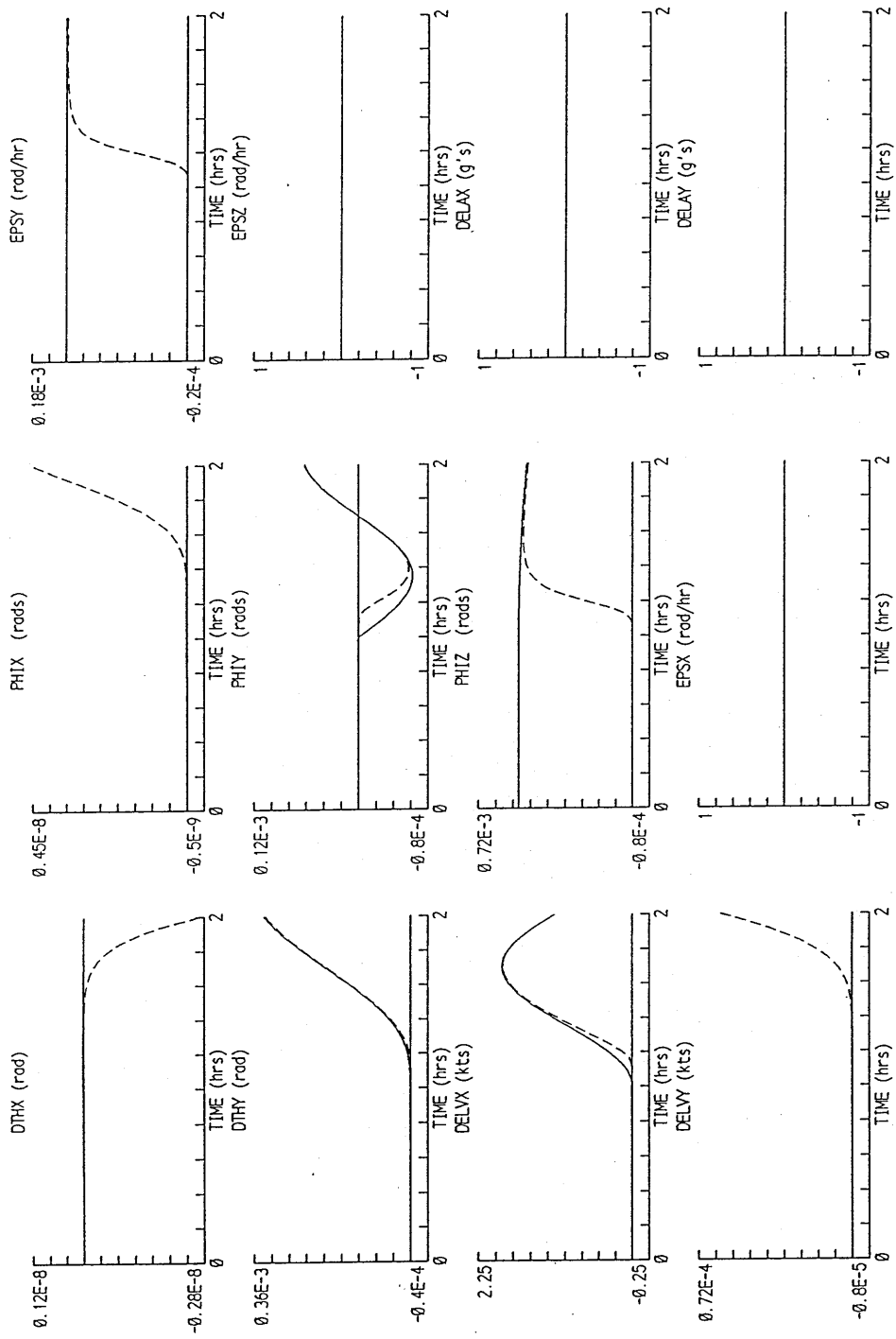
Z PLATFORM AXIS TILT AFFECT ON LOCAL LEVEL AXIS

Figure 8-4



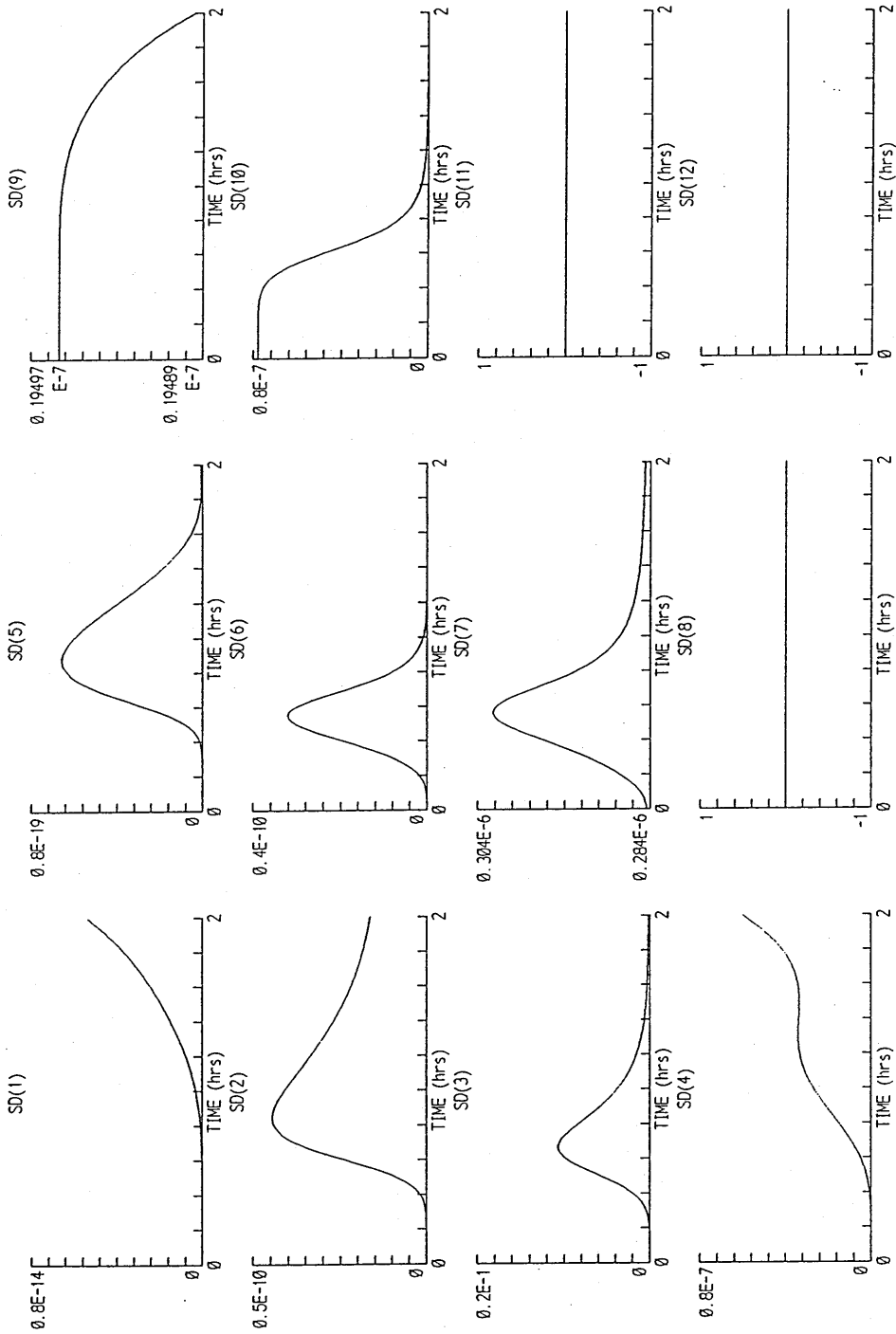
12 STATE SUB OPTIMAL KALMAN FILTER COVARIANCE PLOTS (Fast/slow version)
FOR ALIGNMENT/OBSERVABILITY INVESTIGATION.

Figure 8-5



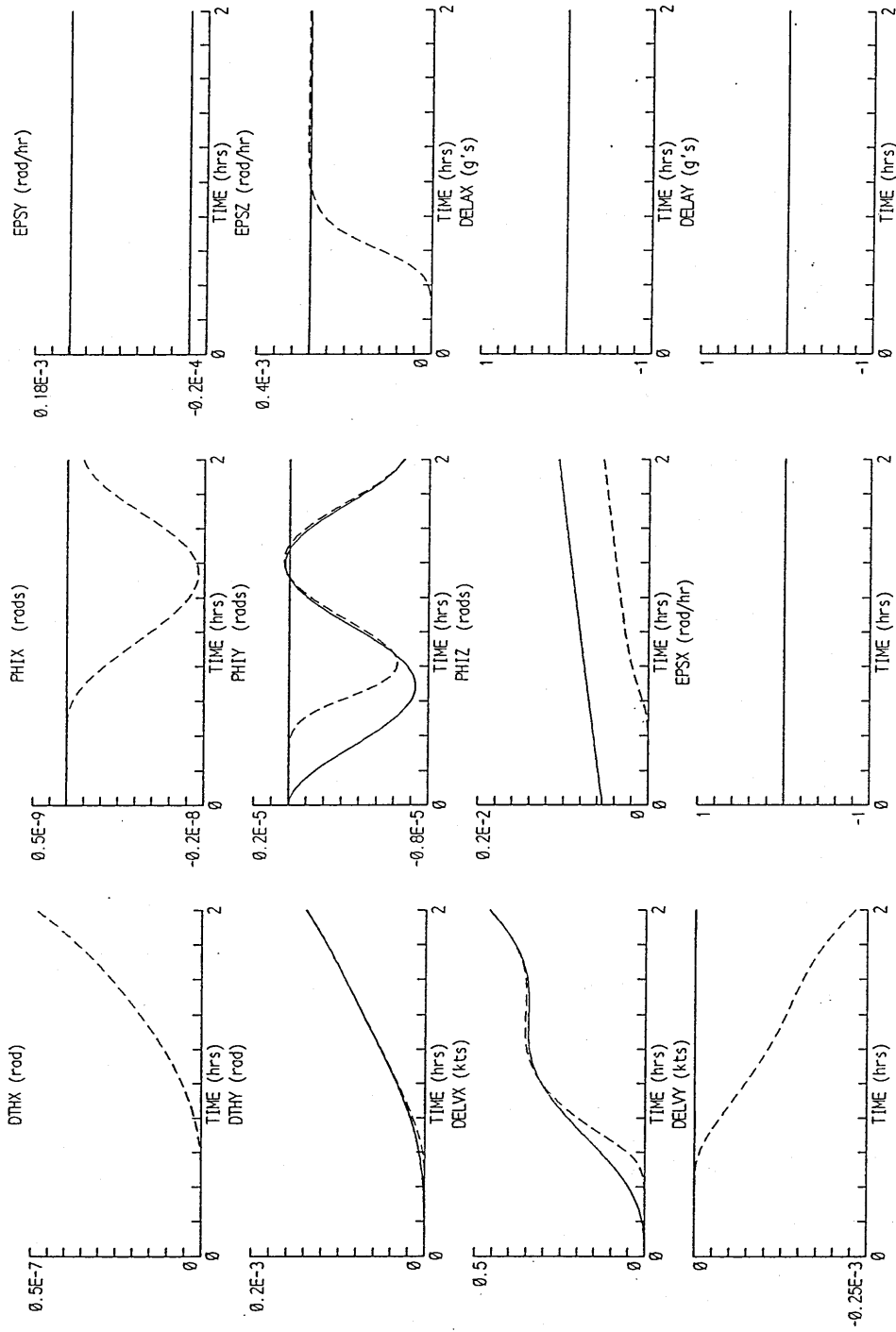
CASE: OPTIMAL STATE IRS v SUB OPTIMAL KF (fast/slow version called at 5 secs)
 CONTINUOUS LINE - IRS. DASHED LINE - KALMAN FILTER ESTIMATES OF IRS STATES.

Figure 8-6



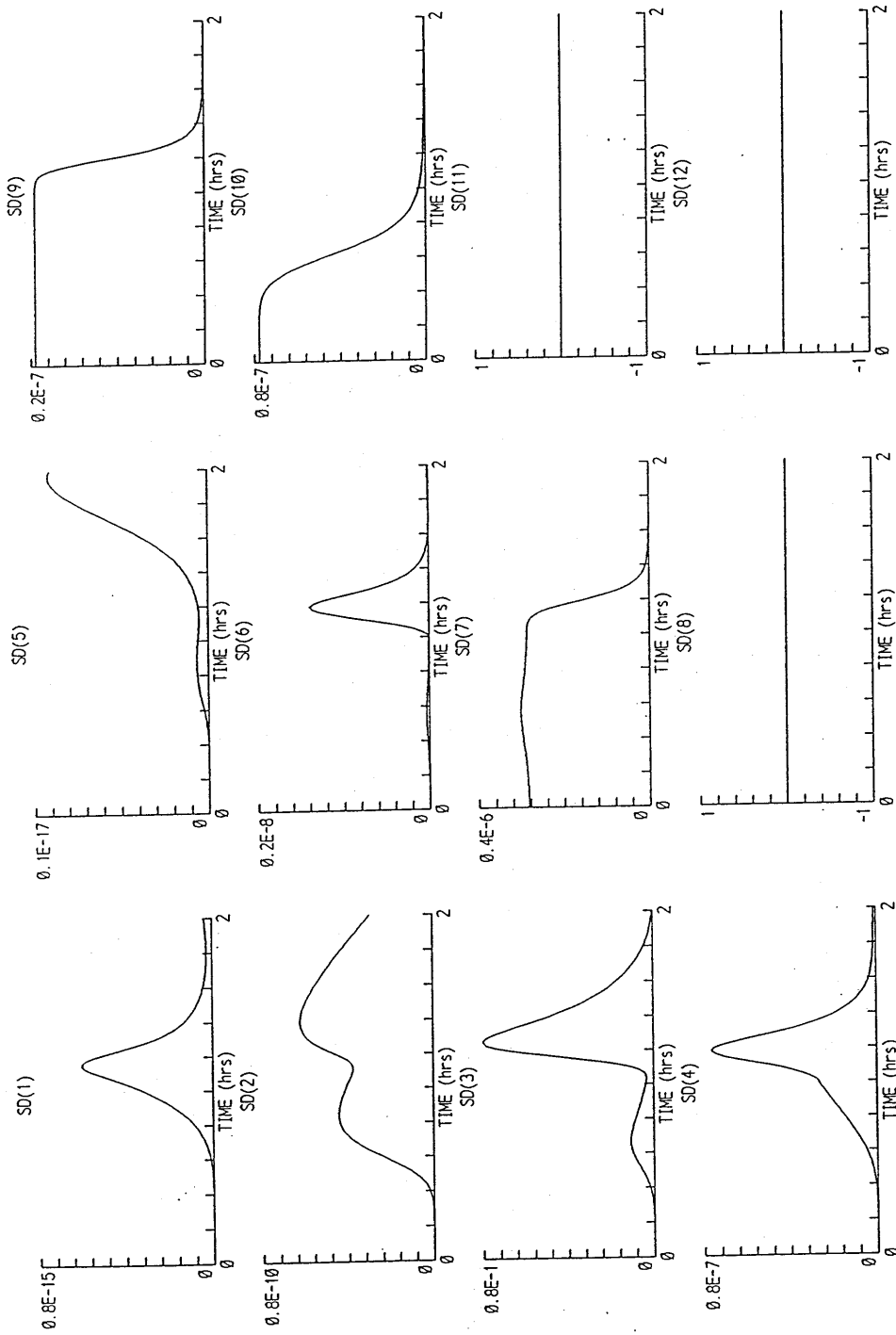
12 STATE SUB OPTIMAL KALMAN FILTER COVARIANCE PLOTS (fast/slow version)
FOR ALIGNMENT-OBSERVABILITY INVESTIGATION.

Figure 8-8



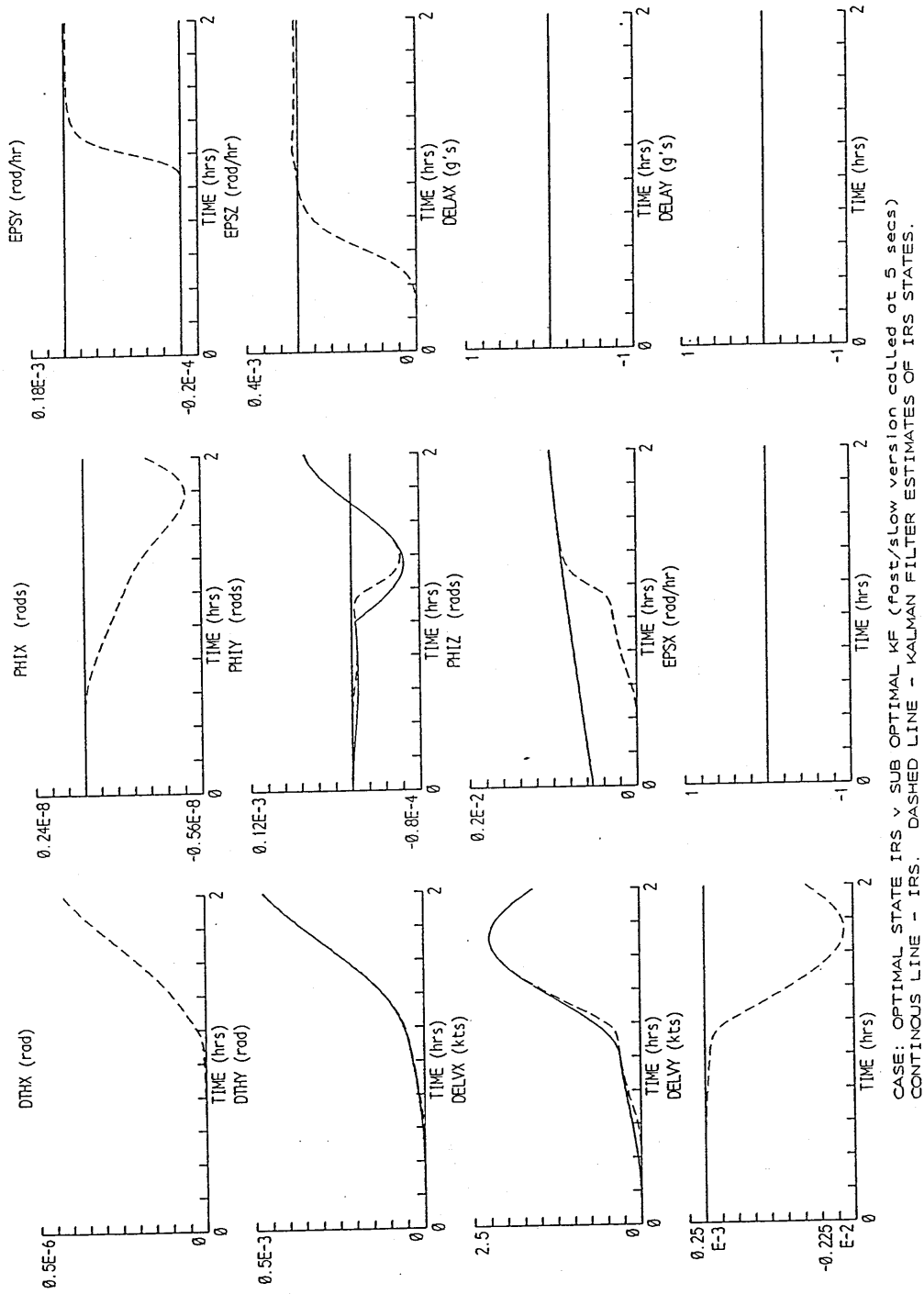
CASE: OPTIMAL STATE IRS v SUB OPTIMAL KF (fast/slow version called at 5 secs)
 CONTINUOUS LINE - IRS. DASHED LINE - KALMAN FILTER ESTIMATES OF IRS STATES.

Figure 8-9



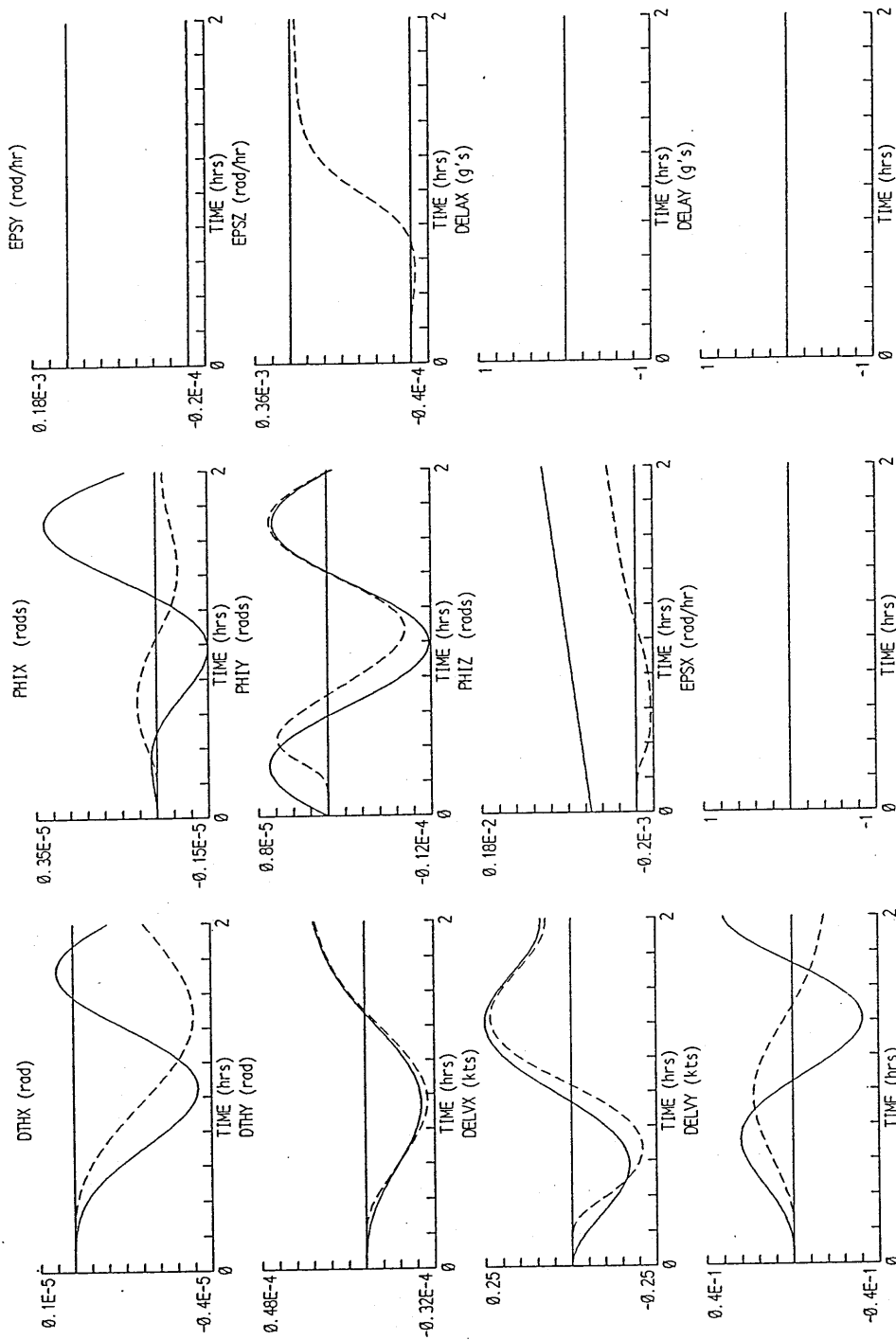
12 STATE SUB OPTIMAL KALMAN FILTER COVARIANCE PLOTS (fast/slow version)
FOR ALIGNMENT/OBSERVABILITY INVESTIGATION.

Figure 8-10



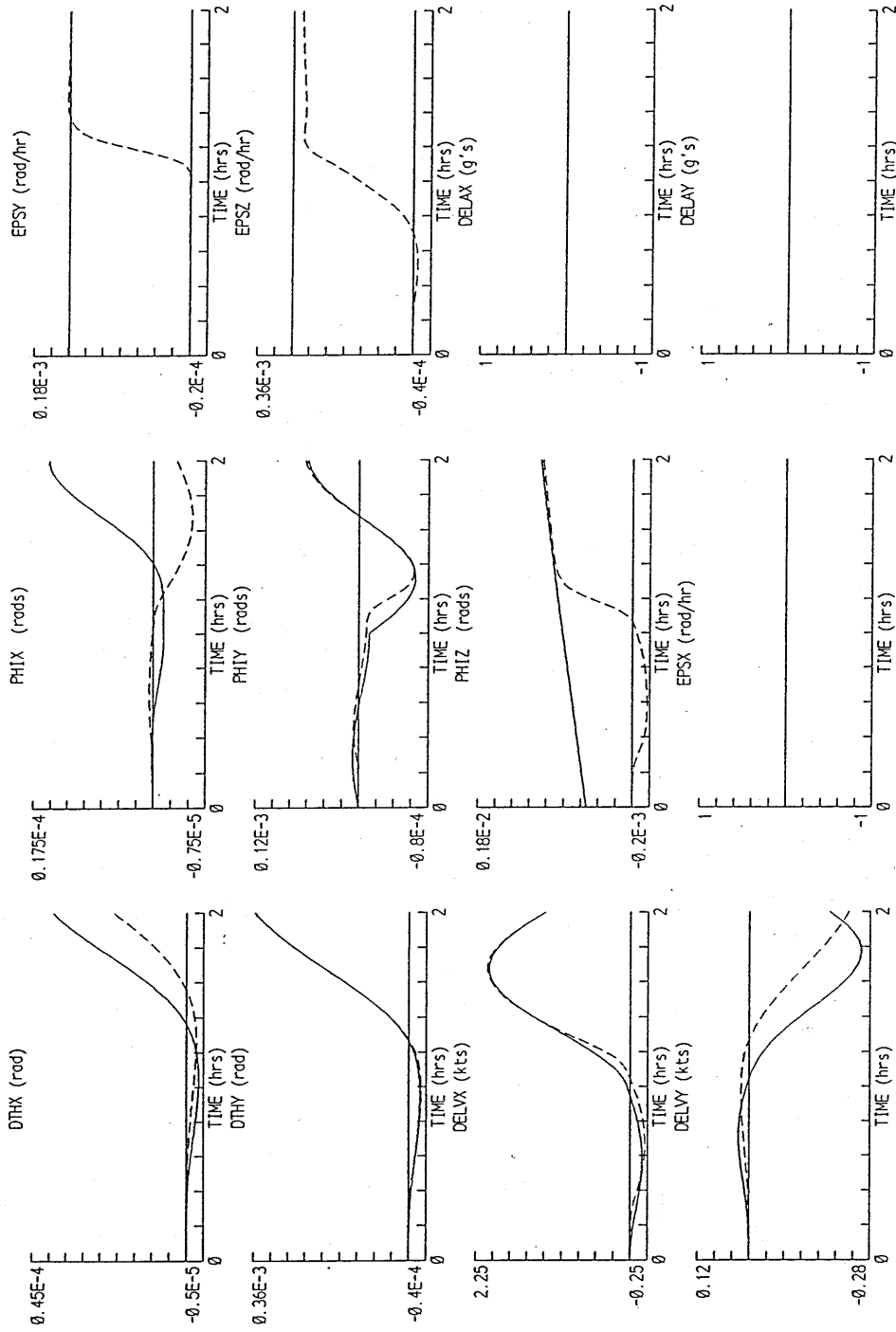
CASE: OPTIMAL STATE IRS v SUB OPTIMAL KF (FAST/SLOW VERSION CALLED AT 5 SECS)
 CONTINUOUS LINE - IRS. DASHED LINE - KALMAN FILTER ESTIMATES OF IRS STATES.

Figure 8-11



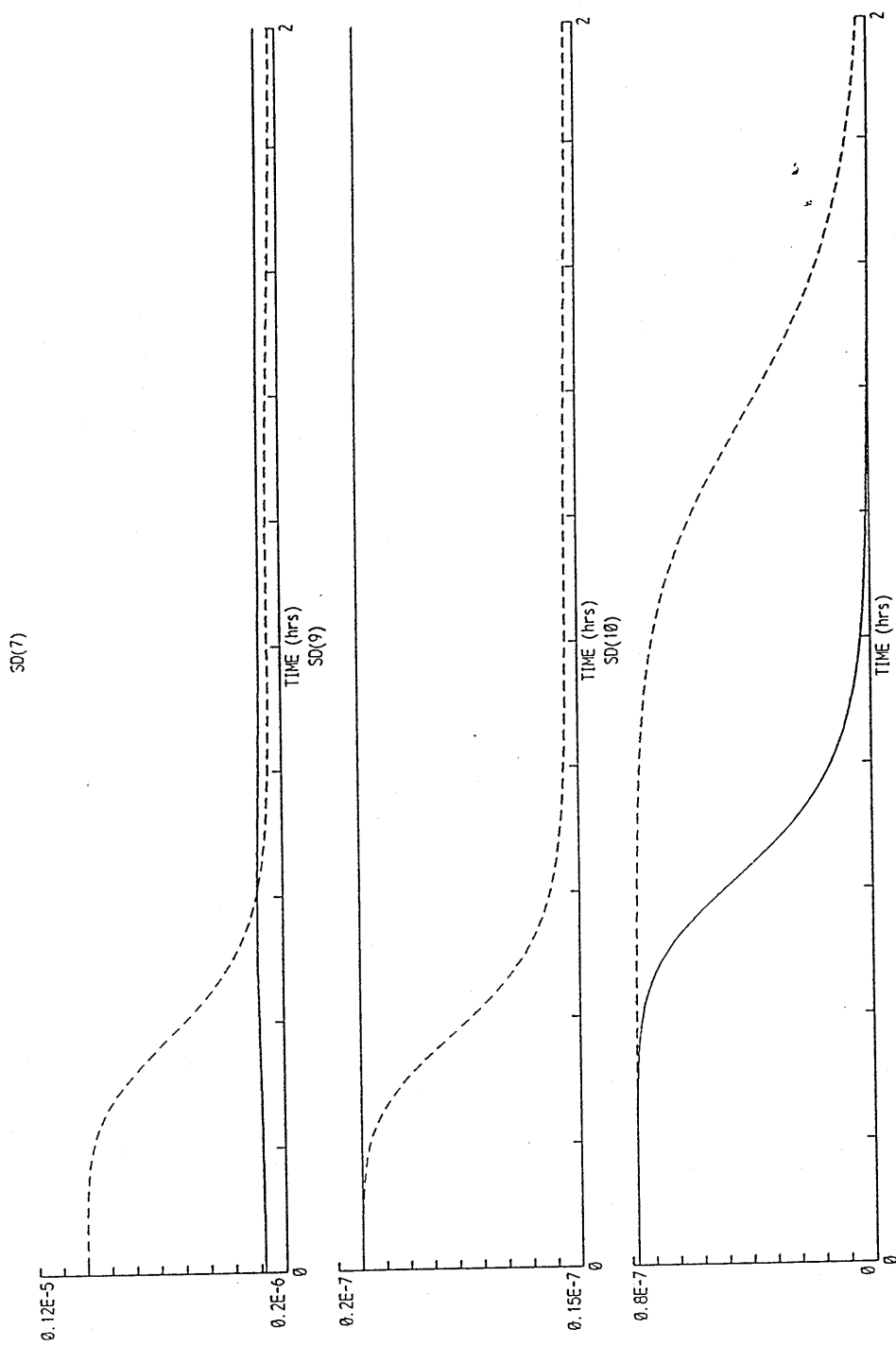
CASE: OPTIMAL STATE IRS v SUB OPTIMAL KF (fast/slow version called at 5 secs)
 CONTINUOUS LINE - IRS. DASHED LINE - KALMAN FILTER ESTIMATES OF IRS STATES.

Figure 8-12



CASE: OPTIMAL STATE IRS v SUB OPTIMAL KF (fast/slow version called at 5 secs)
 CONTINUOUS LINE - IRS, DASHED LINE - KALMAN FILTER ESTIMATES OF IRS STATES.

Figure 8-13



COMPARISON OF KALMAN FILTER COVARIANCE PLOTS.
 CONTINUOUS LINE - MODIFIED KALMAN FILTER CONTAINS CROSS CORRELATION TERMS
 DASHED LINE - UNMODIFIED KALMAN FILTER CONTAINS DIAGONAL TERMS ONLY

Figure 8-14

SEATTLE BASED FLIGHT PROFILE

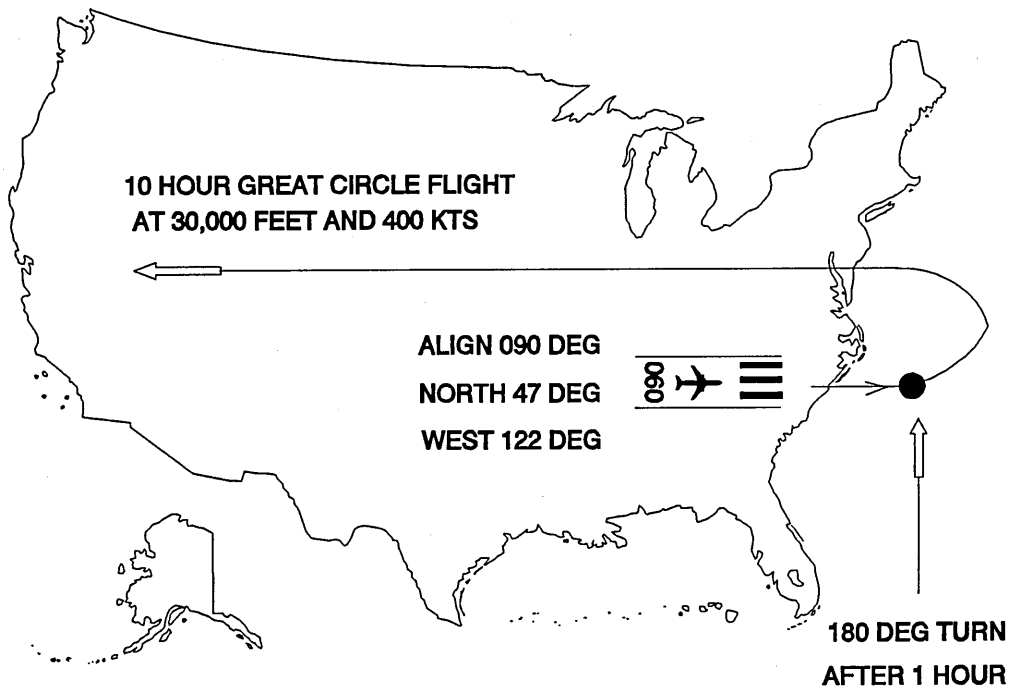


Figure 8-15

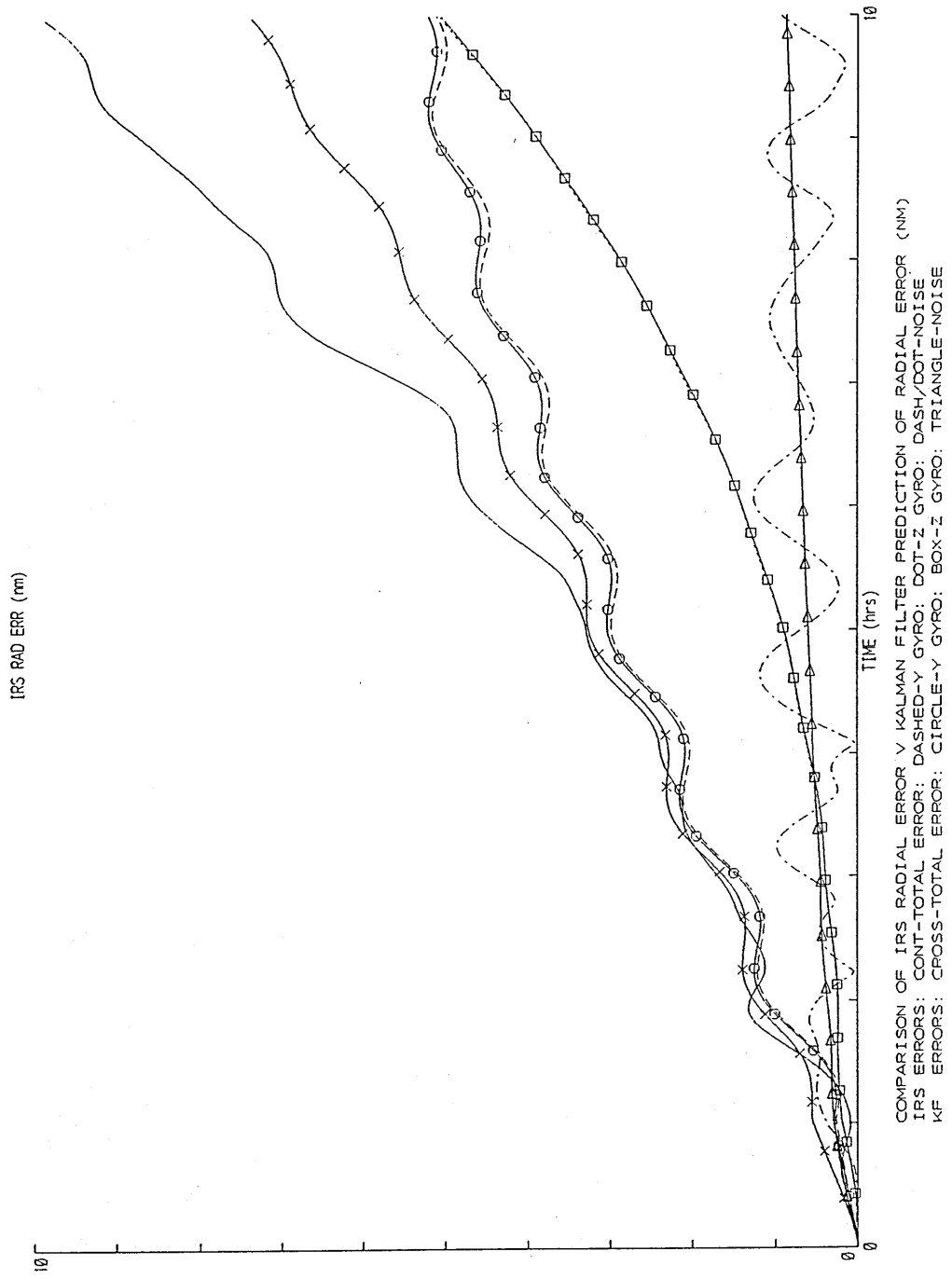


Figure 8-16

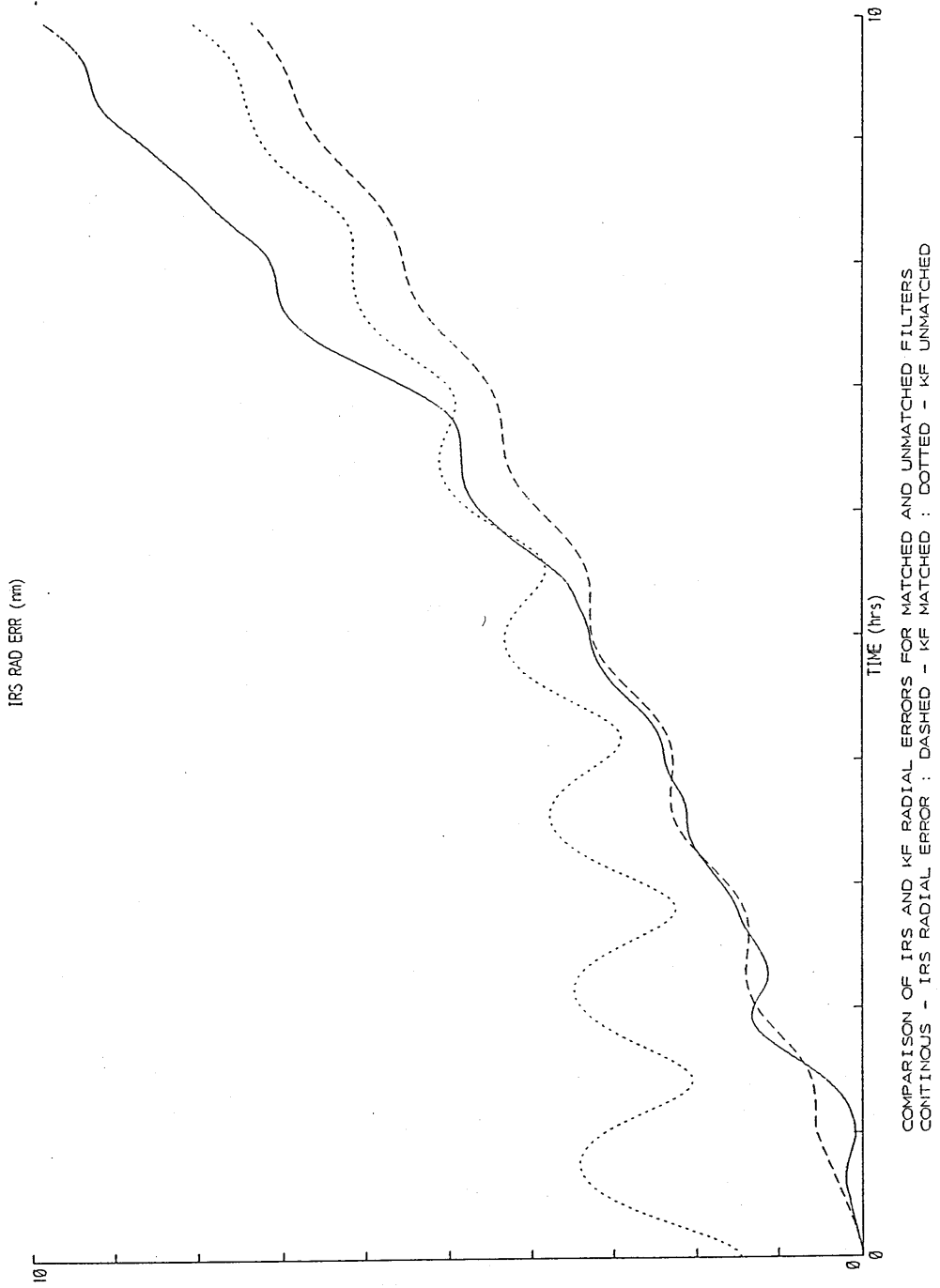


Figure 8-17

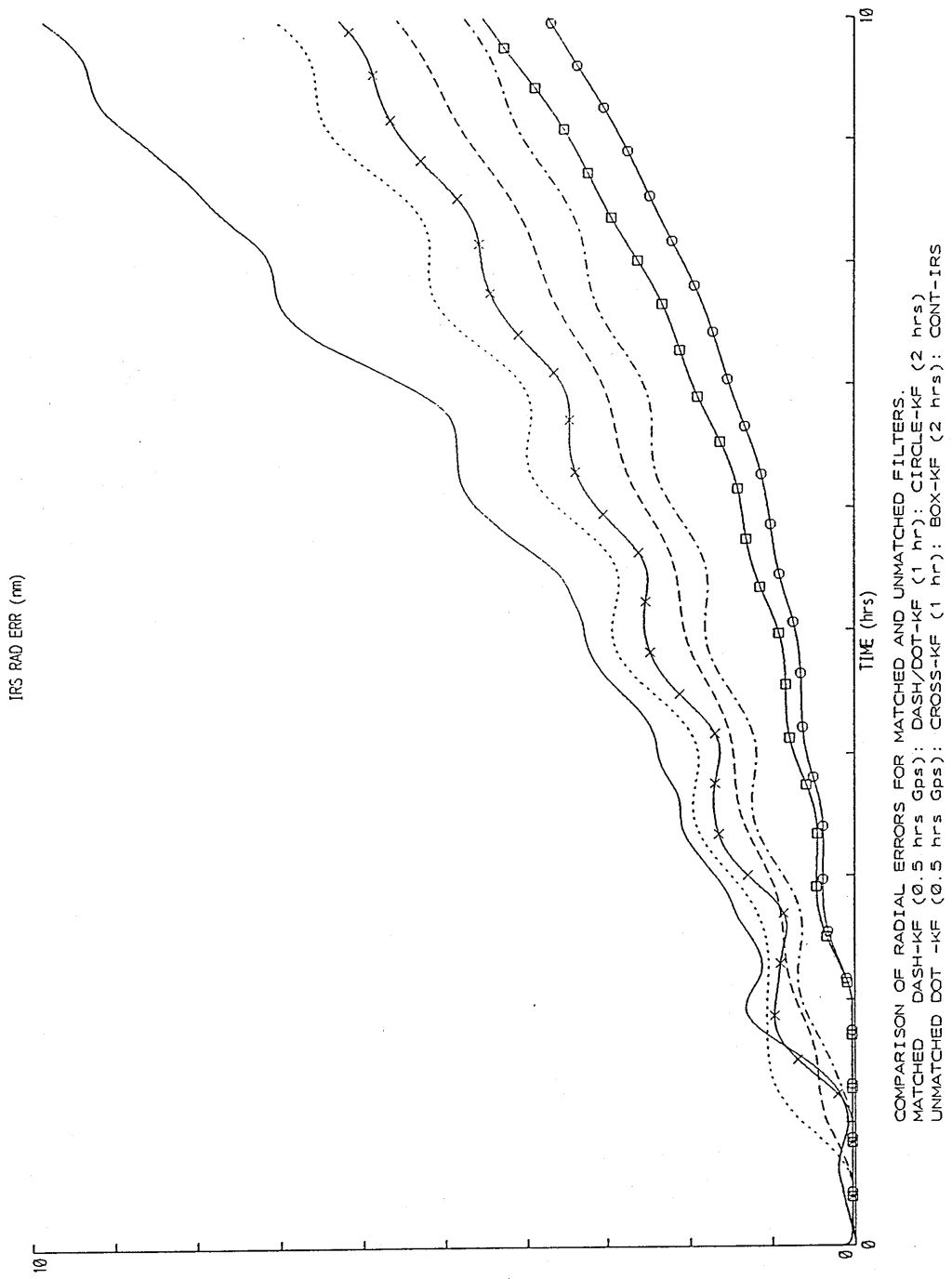
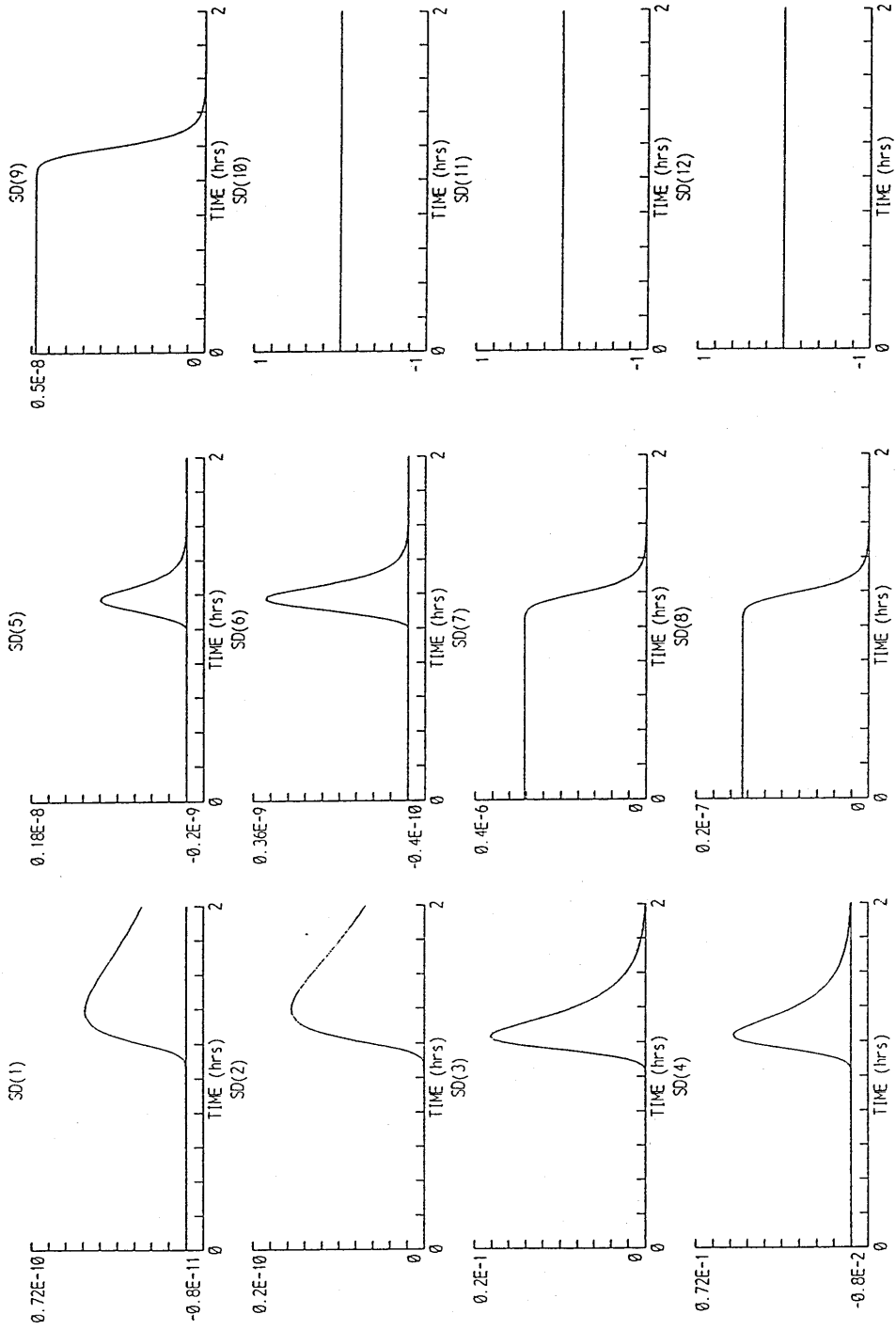
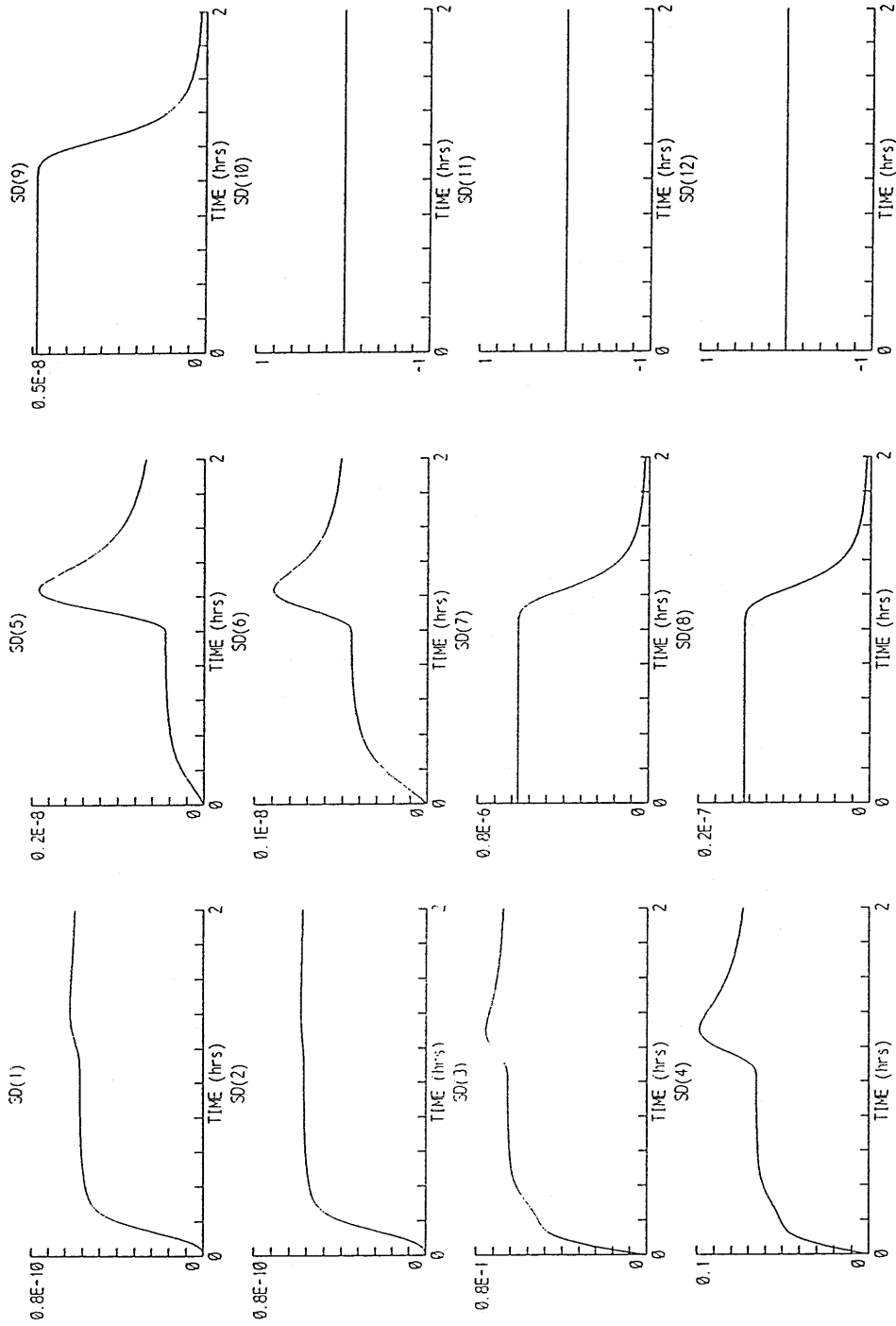


Figure 8-18



12 STATE SUB OPTIMAL KALMAN FILTER COVARIANCE PLOTS (fast,slow version)
 FOR ALIGNMENT,OBSERVABILITY INVESTIGATION.

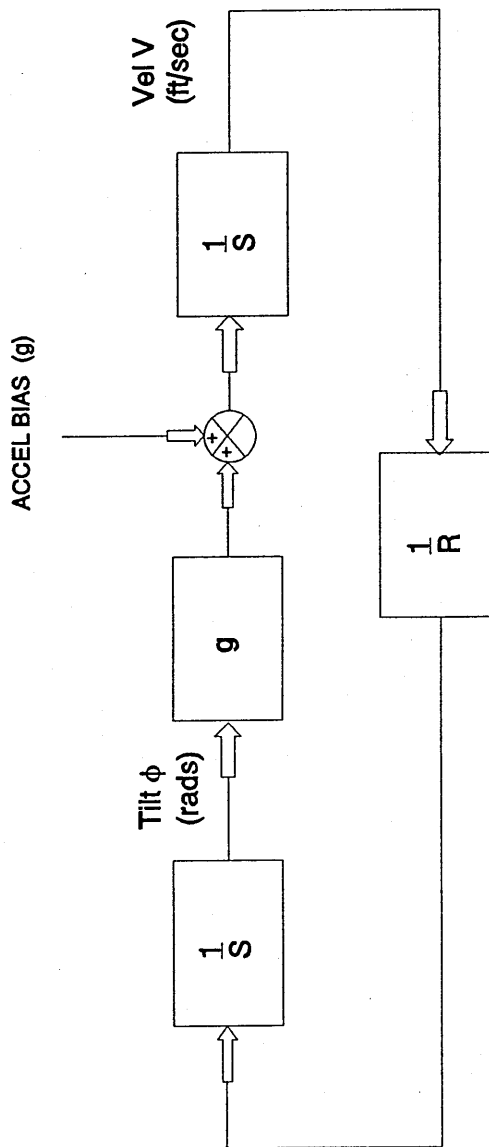
Figure 8-19



12 STATE SUB OPTIMAL KALMAN FILTER COVARIANCE PLOTS (fast/slow version)
FOR ALIGNMENT/OBSERVABILITY INVESTIGATION.

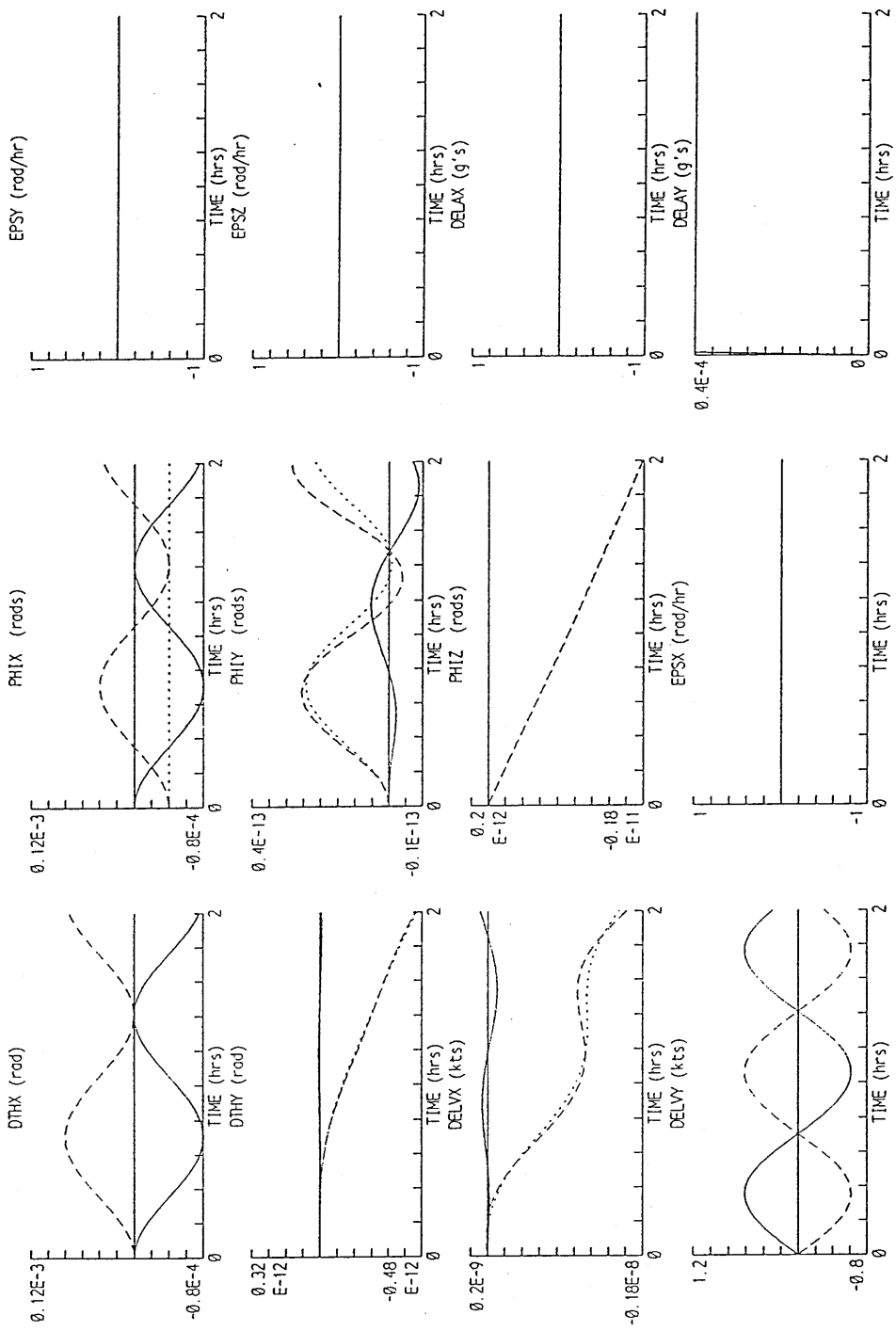
Figure 8-20

ACCELEROMETER SINGLE CHANNEL INERTIAL SYSTEM MODEL



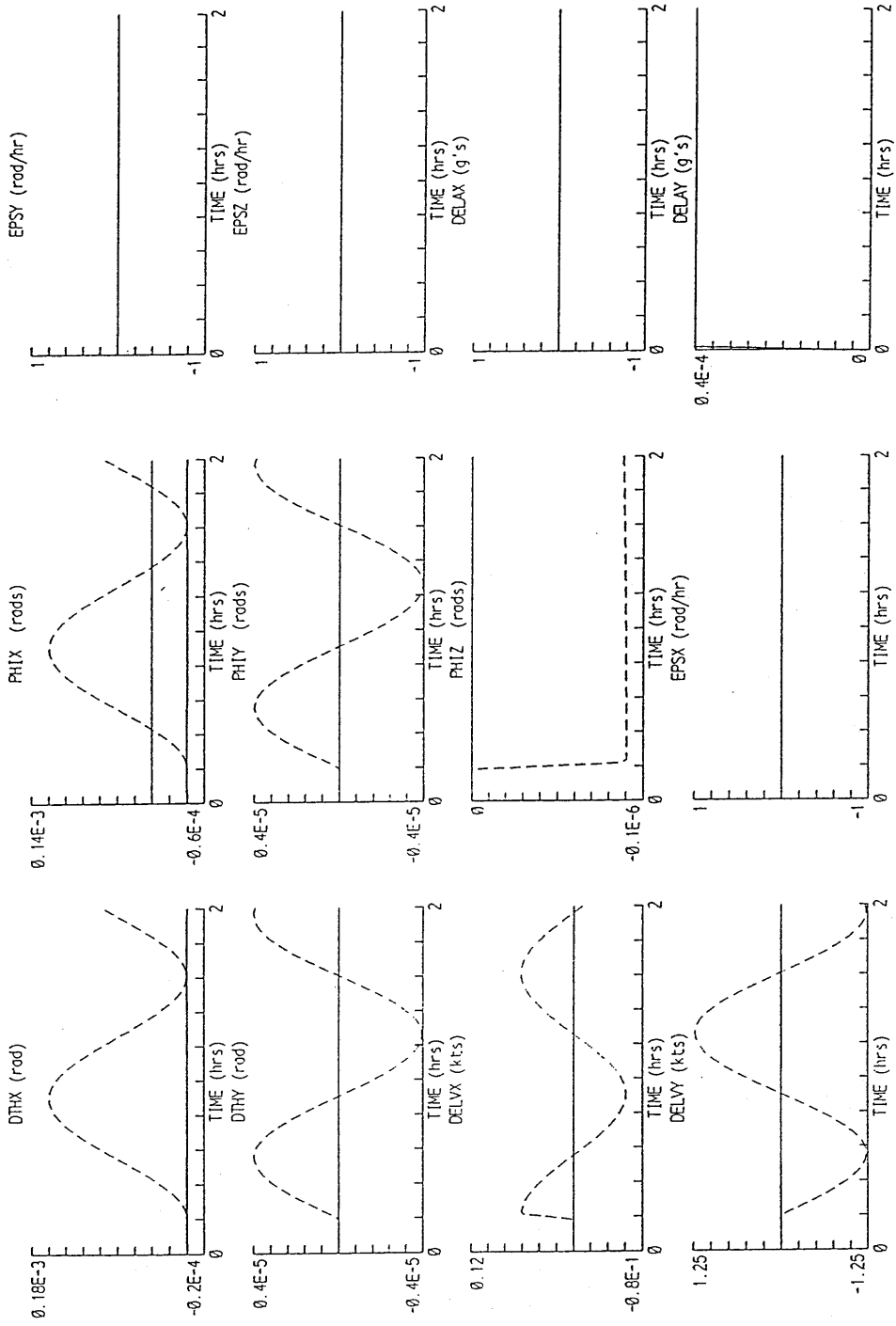
R - Earth Radius (ft)
 g - Gravity (ft/sec²)

Figure 8-21



COMPARISON OF IRS ERROR SOURCES
 CONTINUOUS LINE - Y AXIS ACCEL BIAS OF 40 UG
 DASHED LINE - X PLATFORM AXIS TILT EQUIVALENT TO Y ACCEL BIAS
 DOTTED LINE - Y ACCEL BIAS AND X AXIS TILT

Figure 8-22



COMPARISON OF IPS ERRORS
 CONTINUOUS LINE - Y ACCEL BIAS AND X AXIS TILT NON STATIONARY
 DASHED LINE - Y ACCEL BIAS AND X AXIS TILT NON STATIONARY WITH 180 DEG TURN

Figure 8-23

Y CHANNEL INERTIAL SYSTEM MODEL

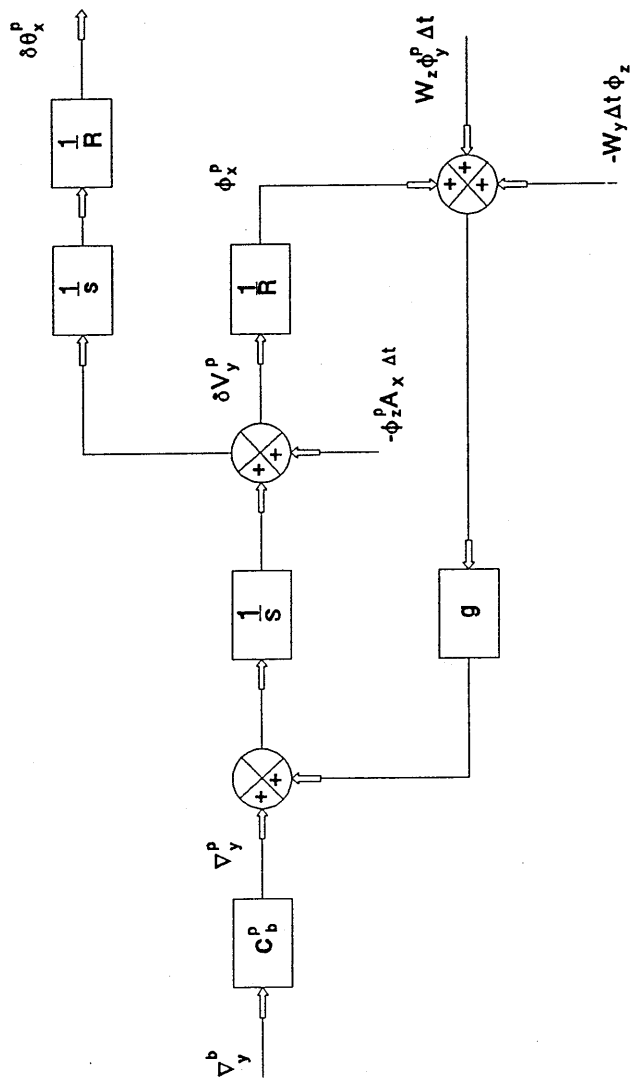
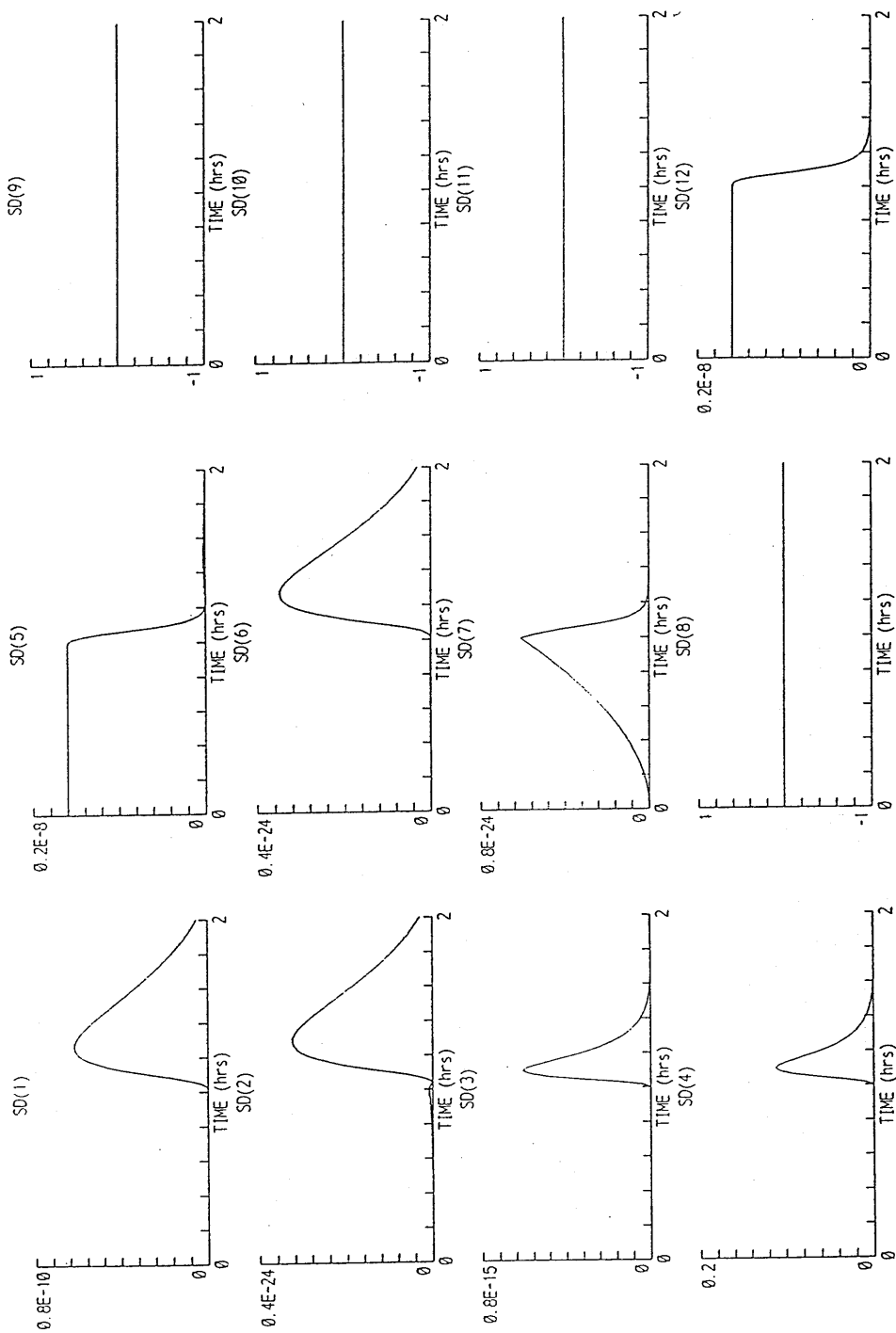
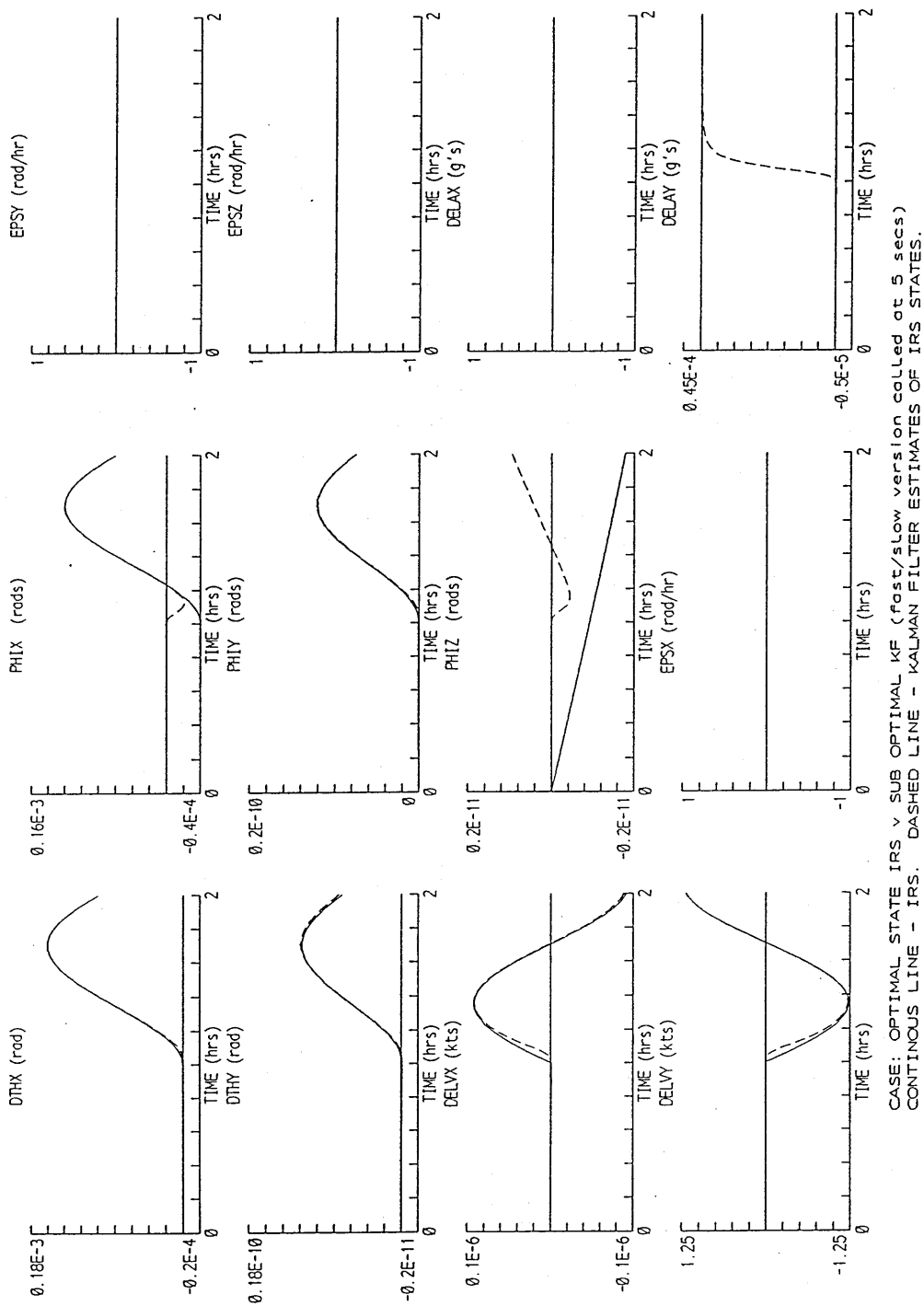


Figure 8-24



12 STATE SUB OPTIMAL KALMAN FILTER COVARIANCE PLOTS (fast/slow version)
FOR ALIGNMENT/OBSERVABILITY INVESTIGATION.

Figure 8-25



CASE: OPTIMAL STATE IRS v SUB OPTIMAL KF (fast/slow version colled at 5 secs)
 CONTINUOUS LINE - IRS. DASHED LINE - KALMAN FILTER ESTIMATES OF IRS STATES.

Figure 8-26